DRAG REDUCTION IN OIL-WATER FLOWS

Ph.D Thesis

Department of Chemical Engineering

University College London

Lawrence Chukwuka Edomwonyi-Otu

2015

DECLARATION

I, Lawrence Chukwuka Edomwonyi-Otu, declare and confirm that the work presented in this Thesis is my own

Whenever information provided has been consciously taken from other sources, as to show previous work, present other author's result or make comparison or a point for discussion, etc…. It has been so indicated in the texts.

_____

Signature

Lawrence Chukwuka Edomwonyi-Otu

June 2015

ACKNOWLEDGEMENT

accommodating, responding to those questions when they do arise and those lovely postcards from around the world as we proclaimed UCL to the world.

The high speed cameras and PIV system loan facilities and technical support from members of the Engineering and Physical Sciences Research Council (EPSRC) as well as the TSI team are acknowledged. Without these equipment, this work would be impossible. All the hydrolysed polyacrylamide (Magnafloc 1011) used in these experiments were freely supplied by BASF Chemicals UK/Germany.

I deeply appreciate the moral, intellectual and spiritual support of my family members (biological and marital); Our parents; Mr and Mrs David Edomwonyi-Otu, Prof and Mrs Andrew Ozo, and Prof and Dr (Mrs) P.I. Ozo-Eson. Our Siblings; Mr Nosakhare and Mr Lucky Edomwonyi-Otu, Mrs Ekinadose Idehen, Mrs Juliet Imade, Barr Osarodion Ozo, Engr Ehigiegbamen Ozo, Engr Ikhuoria & Dr (Mrs) Osarhiemen Aimiewanu, Barr (Mrs) Oghogho Ewere, Mr Omosigho Ozo-Eson, Mrs Osarhiemen Jatto. Our friends: Dr Chris Emokaro, Dr Sylvester Uwadiae and Dr Ebenezer Ojo who have been brothers to me.

The support of my former supervisor and senior colleague Prof Benjamin Aderemi and family, is deeply appreciated. He is like a father to me and has been deeply concerned with constant encouragements and his continuous support back home is unprecedented. I must acknowledge Prof A.S. Ahmed for his encouragement to embark on this program. My colleagues in the Department of Chemical Engineering, Ahmadu Bello University, Zaria are appreciated for standing in the gap for us.

I deeply appreciate the support and patience of my dear wife, Osarense (who actually became the unofficial second supervisor of this project) on whose shoulders I fell, in those frustrating moments of this program. You left everything to accompany me to London for this program and thank God you came along. My lovely children, John, David, and James (Jamusu) suffered my absence and sometimes my frustrations. My wife and children are the driving force behind my pursuit in this project. Looking into their eyes, I could not afford to fail. The journey has been long from the initial PhD in catalysis which I had to abandon, after almost 3 years because of funding issues, to take up this current one in fluid dynamics. 7 toil-full years in all!   I am grateful and will remain a role model to you. Words fail me to appreciate you.

Above all, I am eternally grateful to the Almighty God for life, His mercy and help through Jesus Christ my Lord and Saviour, to whom I owe my existence both now and in the world to come, Amen. It was through His help and mercy that I secured this studentship to fulfil my ambition. He always assured me that He will help me get to the end successfully, and He sure did!

LIST OF PUBLICATIONS

Journals Papers

1. **Edomwonyi-Otu, L.C**; Angeli, P. (2014). Effects of Polymer Addition on Pressure Drop and Interfacial Waves in Horizontal Oil-Water Flows. Petroleum Technology Development Journal (PTDJ) 4 (2) 5-18

2. **Edomwonyi-Otu, L.C**; Angeli, P. (2015). Pressure Drop and Holdup Predictions in Horizontal Oil-Water Flows for Curved and Wavy Interfaces. Chemical Engineering Research and Design (ChERD) journal 93 (Jan 2015), 55-65.

3. **Edomwonyi-Otu, L.C**., Chinaud, M., Angeli, P. (2015). Effect of drag reducing polymer on horizontal liquid-liquid flows. Exp. Therm. Fluid Sci. 64, 164 – 174**.**

4. **Edomwonyi-Otu, L.C**., Angeli, P. (2015). PIV measurements in drag-reduced oil-water flows. International Journal fo Multiphase Flows (Submitted).

Peer reviewed conference papers

1. **Edomwonyi-Otu, L.C;** Simeoni, M; Angeli, P; Campolo, M. (2015). Polymer-Fiber Laden Flows in Pipes of Different Diameters. Book of proceedings, COST Action FP1005 Final Conference, Trondheim, Norway.

2. **Edomwonyi-Otu, L.C**; Chinaud, M; Angeli, P. (2014). Drag Reduction in Oil-Water Flows. Proceedings of the 9th North American Conference of Multiphase Flows, Banff, Canada. Pp165-173.

3. **Edomwonyi- Otu, L.C**; Barral, A.H; Angeli, P. (2013). Influence of Drag Reducing Agent on Interfacial Waves Characteristics in Horizontal Oil-Water Flows. Proceedings of 16th International Multiphase Production Technology Conference, Cannes, France, pp353-362

4. Barral, A.H; **Edomwonyi- Otu, L.C**; Angeli, P. (2013). Interfacial Waves Characteristics in Stratified Oil-Water Flows in Pipes of Different Diameter. Proceedings of International Conference on Multiphase Flow, Jeju, South Korea, ICMF2013-712, pp1-6.

Other presentations at conferences and technical meetings

5. **Edomwonyi-Otu, L.C**; Chinaud, M; Angeli, P. (2015). Effect of Drag Reducing Polymers on Velocity Profiles in Stratified Oil-water Flows. Paper presentation at MEMPHIS-TMF Consortium Sponsors technical meeting (April 2015). Imperial College London, UK.

6. **Edomwonyi-Otu, L.C.** and Angeli, P. (2015). Drag Reduction in liquid-liquid Flows. Seminar presentation at the Department of Chemistry, Physics and Environment, University of Udine, Udine, Italy

7. Park H.K; **Edomwonyi- Otu, L.C**; Angeli, P. (2014). Oil-Water flows in Pipelines of Different Diameter. Abstracts/poster for Chemical Engineering Day (ChemEngDayUK2014) University of Manchester, UK

8. **Edomwonyi-Otu, L.C**; Chinaud, M; Angeli, P. (2014). Velocity measurements in Oil-Water flow with Drag Reducing Agents. Paper presentation at MEMPHIS-TMF Consortium Sponsors technical meeting (April 2014). Imperial College London, UK.

9. **Edomwonyi- Otu, L.C**; Angeli, P. (2013). Effect of Drag Reducing Agents on Stratified Liquid-liquid Flows. Paper presentation at MEMPHIS-TMF Consortium Sponsors technical meeting (September 2013). Imperial College London, UK

10. **Edomwonyi- Otu, L.C**; Barral, A.H; Angeli, P. (2013). Oil-Water flows in Pipes of Different Diameters. Abstracts/poster for Chemical Engineering Day (ChemEngDayUK2013) Imperial College London, UK.

Workshops and Technical meetings attended

1. COST Action FP1005 Training School. 27 – 29 May 2015. Regular and Irregular Non-Spherical Particles in Laminar and Turbulent Flows. Zentrum fur Ingenieurwissenschaften Verfahrenstechnik (TVT) Martin-Luther-Universitat Halle-Wittenberg (Halle, Germany).

2. Departmental seminar on Fiber modelling in multiphase flows. 18th March 2015. Department of Chemistry, Physics and Environment, University of Udine, Udine, Italy

ABSTRACT

Liquid-liquid flows occur in many chemical and process industries including the petroleum industry where crude oil and its derivatives are transported over long distances often in mixtures with water. Depending on flow conditions and pipe geometry different flow patterns can appear ranging from fully separated to dispersed ones. The addition of small amounts of some polymeric materials to one of the phases has been found to change the flow patterns and their boundaries and reduce the frictional pressure drop. Understanding these changes and the underlying physical mechanisms is necessary for the design of pipelines for the transport of oil-water mixtures.

In this thesis, the effects of a drag reducing polymer (Magnafloc 1011; hydrolysed copolymer of polyacrylamide and sodium acrylate, HPAM, mol. wt. = 10×10^6 g/mol) added in the water phase of an oil-water mixture were studied experimentally in a horizontal 14 mmID acrylic test section. The test fluids were a distillate oil (Exxsol D140: viscosity 5.5 mPas, density 828 kg/m^3) and tap water. For some measurements two different molecular weights; 5×10^6 g/mol and 8×10^6 g/mol polyethylene oxide (PEO) polymers were also used. Flow patterns and pressure drop were investigated for a wide range of fluid velocities ranging from 0.052 m/s to 3.620 m/s for single phase water flows while oil and water superficial velocities ranged from 0.008 m/s to 0.580 m/s, and from 0.052 m/s to 0.80 m/s respectively. Both before and after the addition of polymer. Detailed studies of interface height and velocity fields were then carried out in stratified flows. Two types of conductivity probes, a wire probe and a ring probe, were used to measure interface heights in the middle and the wall of the pipe respectively. The velocity profiles and turbulence properties of the water phase were studied with particle image velocimetry (PIV) within the stratified flow regimes of the oil-water flows.

The addition of 20 ppm of polymer solution to the water phase resulted in drag reduction of 80 % in single phase water flows and 52 % in oil-water flows. In addition, flow patterns were changed while the region of stratified flows was extended to higher superficial oil and water velocities. In stratified flows with the addition of polymer the in-situ average water velocity, interfacial wave celerity, and wavelength increased while the interface height, amplitude, and power spectrum were decreased. The conductivity probe measurements revealed a curved interface in stratified flows which with the addition of the polymer remained relatively unaffected. A relationship was developed between the two interface heights. The velocity

profiles in the water phase became more parabolic compared to the flow without polymer. In addition, the axial component of velocity fluctuations decreased close to the interface and the wall but increased in the middle of the flow, while the Reynolds stresses and radial component of velocity fluctuations reduced throughout the water phase. From the two types of PEO tested, drag reduction was found to increase with polymer molecular weight but also depended on the mechanical degradation of the polymers at high Reynolds numbers and their ionic strength. A two-fluid model was developed that took into account the interface shape and waviness. To calculate its length, the interface was considered circular and the correlation between the two interface heights in the middle and the wall of the pipe was used. The interface waviness was included as roughness in the interfacial friction factor correlation, equal to the average wave amplitude found experimentally. Results showed when both interface curvature and waviness were included; the model predicted better the experimental pressure drop data compared to the two-fluid model with other interfacial shear stress correlations found in the literature. The friction factor correlation in the two-fluid model was also modified to account for drag reduction and it was able to predict the drag reduction in oil-water flows better than correlation available in the literature. The combination of polymer and fibers in single phase water flows resulted in a synergistic effect with drag reduction higher than when either polymer or fibers were used alone.

TABLE OF CONTENTS

LIST OF FIGURES

LIST OF TABLES

LIST OF APPENDIX FIGURES

NOMENCLATURE

Roman symbols

A   cross sectional area (m^2)

API   American Petroleum Index

A_o area occupied by oil phase (m^2)

A_w area occupied by water phase (m^2)

B   constant in Equation 2-24

C   constant in Equation 2-24

C   centre of circle in Figure 4-9

cP   centipoise

$\dfrac{dp}{dz}$ pressure gradient (Pa/m)

D   pipe diameter (m)

D_o hydraulic diameter of oil phase (m)

D_w hydraulic diameter of water phase (m)

d_p particle diameter (m)

Dpo   pressure drop of oil phase (Pa)

Dpw   pressure drop of water phase (Pa)

Do/w   dispersed oil in water flow

Dw/o   dispersed water in oil flow

DR   drag reduction (%)

DRA   drag reducing agent

C_f Fanning friction factor

Eo   Eötvös number

g   grams

g acceleration due to gravity (m/s)

H_o	hold-up of oil phase
H_w	hold-up of water phase
Hz	hertz (Hz)
h_w	interface height (m)
kg	kilogram
ID	internal diameter (m)
m	flow regime constant
mol	mole
MDRA	maximum drag reduction asymptote
MW	molecular weight (g/mol)
n	flow regime constant
^oC	degree Celsius
Pa	Pascal
Pa s	Pascal second (unit of viscosity)
PAM	polyacrylamide
HPAM	partially hydrolysed polyacrylamide
PEO	polyethylene oxide
5MPEO	PEO of molecular weight 5×10^6 g/mol
8MPEO	PEO of molecular weight 8×10^6 g/mol
ppm	parts per million
Q	flow rate (m^3/s)
R	radius in Figure 5-2
Re	Reynolds number
S	slip ratio
St	Stokes number
S_i	interfacial perimeter/length (m)

S_o	wetted perimeter of oil phase (m)
S_w	wetted perimeter of water phase (m)
St/ST	stratified flow
t_p	particle relaxation time (s)
Uso	superficial oil velocity (m/s)
Usw	superficial water velocity (m/s)
Uo	in-situ oil velocity (m/s)
Uw	in-situ water velocity (m/s)
U	bulk velocity (m/s)
u_o	fluid velocity (m/s)
u_f	friction velocity (m/s)
u'	axial velocity fluctuation
v'	radial velocity fluctuation
u'v'	Reynolds shear stress
W^o	polymer solution constant
X	half interfacial perimeter (Figure 5-2) (m)

Greek symbols

δ	constant in Equation 2-2
%	percent
β	angle in Figure 5-2
Δ	delta
γ	proportionality constant in Equation 2-26
μ	viscosity
π	pi
α	pipe inclination angle (^{O})
ρ	density

ρ_p particle density

τ shear stress

θ   angle in Figure 5-2

Subscripts

c   annular core

i   interfacial

p   polymer

pol   polymer added

o   oil

s   solvent

w   water

CHAPTER 1

1   INTRODUCTION

In this chapter, a brief introduction to the current state of crude oil and water mixtures as well as the challenges in the oil industry is presented. In addition, a brief introduction into the relevant researches in oil-water flows particularly with regards to drag reduction, including the motivation and objectives of this current investigation are also presented.

1.1   Current State of Oil-Water Flows

The increasing global demand for energy means that energy sources must be transferred from areas of production to regions of consumption. Crude oil and its derivatives which are still a main source of energy are in many cases transported over long distances and mostly in pipes of varying sizes and inclinations. Also, the maturing nature of oil wells increases the amount of water extracted with water often added to the down-hole to enhance production. Hence, the flow of crude oil is often in mixtures with water, and results in different flow patterns depending on pipe size and fluid properties and flow rates. Flows of aqueous-organic two-phase mixtures are also very common in the process industries (Abubakar et al., 2015b; Ahmed, 2014; Barral and Angeli, 2013).

It has been found that the addition of very small amounts (parts per million) of some polymeric materials can significantly reduce frictional pressure drop in pipes and associated pumping requirements. This phenomenon is called drag reduction and has found wide applications in industrial processes such as crude oil transportation over long distances, well drilling and hydrofracking operations and settling and filtration of oil-sand tailings. Other applications include domestic heating and cooling, suppression of atherosclerosis and prevention of lethality from haemorrhagic shock, waste water treatment and in firefighting (Abubakar et al., 2014b; Al-Sarkhi, 2010; Wang et al., 2011).

Drag reducing additives are of three major types, namely polymers, surfactants and fibers. Examples of polymers and biopolymers commonly used as drag reducing agents (DRA), include polyethylene oxides (PEO), polyacrylamides (PAM), hydrolysed polyacrylamides (HPAM), polystyrene (PS), polyisobutylene (PIB), guar gum, carboxymethylcellulose (CMC) and xanthan gum amongst others (Abdulbari et al., 2014). Examples of surfactants include

sodium dodecyl-benzene sulfonate (SDBS), sodium lauryl cetyl trimethyl ammonium chloride (CTAC)/ sodium salicylate, cetyl trimethyl ammonium bromide (CTAB). Pulp, asbestos, and some nylon fibers are commonly used fibers for drag reduction, although asbestos is now restricted because of health concerns. Drag reduction can also result from the modifications of the channel/pipe walls (Abdulbari et al., 2013)

The effectiveness of the drag reducing additive is usually given in terms of DR (%);

$$DR(\%) = \frac{\Delta P - \Delta P_p}{\Delta P} \times 100 \qquad \textbf{1-1}$$

where ΔP is the pressure drop of flow without polymer and ΔP_p is the pressure drop of the flow with the drag reducing agents added.

Addition of polymers has been found to affect multiphase flows, where changes in flow patterns occur in addition to frictional pressure drop reduction. This is true for both gas-liquid and liquid-liquid flows. When polymer solution was added in the liquid phase of gas-liquid flows, the region of stratified flows was significantly extended, with annular and slug flows changing to stratified ones. In addition, slug frequencies were significantly reduced while disturbance waves were dampened and the liquid hold-up increased (Al-Sarkhi and Soleimani, 2004; Al-Sarkhi, 2010; Al-Sarkhi et al., 2006; Baik and Hanratty, 2003; Hanratty and Al-Sarkhi, 2001; Mowla and Naderi, 2006). The delayed transition to slug flow as well reduction in the slug frequencies resulted in over 50 % reduction in corrosion in pipelines (Kang et al., 1998a).

In oil-water flows, the addition of polymer has been mainly in the water phase and extended the stratified flow region, similar to gas-liquid flows. Patterns such as rivulet, dual continuous and annular changed in many cases to stratified flows. Dispersed flows changed to dual continuous ones while in some oil in water dispersed flows the drop size increased. In stratified flows the interface height changed while interfacial wave characteristics were affected (Abubakar et al., 2015a; Al-Wahaibi et al., 2012, 2007; Al-Yaari et al., 2012, 2009). According to their studies, the effectiveness of polymeric additives was mainly dependent on the fluid velocities, while the changes in flow patterns were attributed to the dampening of the disturbance waves, reduction in turbulent mixing and increased drop coalescence. There are also some models for the prediction of drag reduction in multiphase phase flows that compare well with experimental data (Al-Sarkhi et al., 2011; Al-Wahaibi et al., 2012).

Despite the many studies available, the mechanism of drag reduction is still not entirely understood while different theories have been suggested (Al-Sarkhi, 2010; Manfield et al., 1999; Mowla and Naderi, 2006; White and Mungal, 2008). The proposed mechanisms involve thickening of the buffer layer, turbulence suppression and redistribution, vortex dissipation, and reduction in Reynolds stresses. According to some works, the DRA interferes with the momentum and vorticity transport in the radial flow direction and re-distribution of the turbulent kinetic energy in the axial direction, which modify the logarithmic velocity profile. The changes in the velocity field with polymer addition have been studied both experimentally (Den Toonder et al., 1997; Hoyer et al., 1996; Lumley, 1973; Virk, 1975; Vleggaar and Tels, 1973; White et al., 2004; Yu et al., 2004), using laser doppler velocimetry (LDV) and particle image velocimetry (PIV) (Den Toonder et al., 1997; Li et al., 2008; Warholic et al., 2001, 1999; Wei and Willmarth, 1992; White et al., 2004; Zadrazil et al., 2012), and numerically (Den Toonder et al., 1997; Yu et al., 2004). Mechanistic models have also been suggested (Sharma et al., 1979; Sher and Hetsroni, 2008).

1.2 Challenges in Oil-Water Flows

The prediction of the two-phase flow properties poses a challenging task because of their dependence on several interrelated factors such as fluid properties and flowrates, pipe diameter and inclination among others. An accurate prediction of the pressure drop and hold up is needed for an effective design and maintenance of the fluid transport systems (Ahmed, 2014; Hadžiabdić and Oliemans, 2007; Rodriguez and Baldani, 2012).
In most of the cited literature, the focus has been on large pipes of greater than 20 mm internal diameter while in recent years there is a growing number of papers on liquid-liquid flows in very small pipes driven by process intensification requirements (Kim and Mudawar, 2012; Tsaoulidis et al., 2013). However, reported data on intermediate pipe sizes (10 mmID to 20 mmID) are very few in the open literature (Jin et al., 2013; Xu et al., 2010). The flow properties and geometry at these intermediate sizes are known to be greatly influenced by surface and interfacial forces, which become more significant as the diameter reduces, particularly for Eötvös number (Eo, ratio of buoyancy to surface tension forces) greater than 1.0 (Brauner and Moalem, 1992; Das et al., 2010).

One of the main patterns in liquid-liquid flows is the stratified including stratified wavy flows. The waves that develop at the interface have been linked to drop formation, transition to dispersed patterns (Al-Wahaibi and Angeli, 2008, 2007) and transfer of mechanical energy

between phases (Cheung and Street, 1988; Cohen and Hanratty, 1968). However, there is very limited information available on how the added polymer influences the wave characteristics in stratified and stratified wavy flows. There are also no current studies on the effect of these additives on the turbulent properties of oil-water flows. This is despite the significant drag reduction found in these systems and the interesting changes in flow patterns when polymers are added. Also, the reported mechanisms of drag reduction are based on experiments in single phase flows without a consideration for the complexities that exist in multiphase flows particularly at the interface after polymer addition.

1.3 Research Objectives

The aim of these current investigations were to study the effect of polymer addition in oil-water flows and particularly in the stratified and stratified wavy regimes and to develop models that can predict pressure drop and hold up. Detailed experimental studies were carried out using a variety of instruments including conductance probes, high-speed cameras, as well as particle image velocimetry (PIV) technique. Preliminary investigations into the drag reduction effects of polymer and fiber combined systems in larger diameter water flows were also carried out.

In particular, the following objectives were addressed;

- ❖ Acquire experimental data of interface curvature and waviness for separated oil-water flows in a 14 mmID horizontal acrylic pipe. Develop a one-dimensional two-fluid model that takes into account interface waviness and curvature.
- ❖ Study the effect of polymer addition in horizontal oil-water flows with emphasis on the interfacial wave characteristics.
- ❖ Investigate the effect of polymer addition in water on the velocity profiles and turbulence properties of separated oil-water flows.
- ❖ Study the synergistic effects of polymer and fibers in water flows for pipes of larger diameter

CHAPTER 2

2   LITERATURE REVIEW

In this chapter, the relevant literature in the study of oil-water flows and drag reduction both in single and multiphase flows is presented.

2.1   Drag Reduction

Drag reduction is an 'engineering intervention whereby the frictional pressure drop occurring in a flow system is deliberately reduced or minimized' (Manfield et al., 1999). The aim is to enhance the energy efficiency of the flow system with the aid of active ingredients called drag reduction agents (DRA), or by implementing certain pipe design techniques such as baffles, riblets, dimples, oscillating walls, and compliant surfaces (Abdulbari et al., 2014).

The pressure drop (drag) occurring in a flow system is the contribution of three components, namely friction, gravitation and acceleration. The frictional drag results from energy losses by viscous forces within the fluid and is dependent on the properties of the fluid, the velocity and the flow regime. The gravitational pressure drop, also called the hydrostatic head, is the result of action of the force of gravity on the flowing fluid, while the accelerational pressure drop is caused by the acceleration of the fluid as a result of expansion. The contribution of each of these parts to the total pressure drop is dependent on the flow arrangement in a particular process. Nieuwenhuys, (2003) in inclined gas-liquid flow showed that the contribution of the accelerational part was negligible and concluded that the viscous and gravity forces were far more significant. However, Rosehart et al., (1972) observed that the contribution of the acceleration component in slug flow exceeded the frictional component of the axial pressure gradient.

2.1.1 Benefits and Applications of Drag Reduction

The benefits that accrue from the use of drag reducing techniques (including DRAs) in flow systems are enormous and include the following;

- Increased pipeline capacity (throughput).
- Reduction in pipe diameter in the design phase as well as the number and/or size of pumping facilities
- Savings in pumping power resulting from minimization of energy loss in flow.

- Reduction of heat transfer rates because of reduction in turbulent mixing. This can be used to conserve heat and maintain temperature in the pipelines, and hence reduce insulation costs.
- Reduction in turbulence leads to reduction in the pressure exerted by the fluid on the wall of the pipeline, with the associated reduction in pipeline thickness and pressure surge.
- Minimization of waiting time for oil tankers loading/offloading because of improved fluid flow.
- Increase region of stratified flows and reduce that of dispersed flows that reduces requirements for separation in liquid-liquid systems.
- Reduction in pipe erosion and corrosion rates

The above advantages leads to reduced overall costs and also high operational flexibility (Al-Sarkhi, 2010; Deslouis, 2003; Manfield et al., 1999; Mowla and Naderi, 2006; Sedahmed et al., 1999; Sellin et al., 1982; Vleggaar and Tels, 1973; Wang et al., 2011).

As a result of these benefits, drag reduction has found applications in various fields including;

- Long distance fluid transport in pipeline
- Domestic heating and cooling
- Petroleum loading and offloading as well as in refineries
- Pipeline corrosion inhibition
- Well drilling and hydraulic fracturing operations
- Settling and filtration of oil-sand tailings
- Firefighting
- Suppression of atherosclerosis and prevention of lethality from haemorrhagic shock
- Water supply, Irrigation and hydropower systems
- As anti-misting agents in jet fuels and tanks
- Sewage systems and in the transportation of suspensions and slurries
- Paper making

A notable application is the addition of 10 ppm of an oil-soluble polymeric additive to the 1.25 m diameter and 1,300 km long Trans-Alaskan pipeline in 1979, which led to 50 % reduction in pressure drop and eliminated the need for 2 additional pumping stations. The crude oil throughput was also increased by up to 30 %. A 1 ppm solution of the same

polymer was later reported to result in 33 % drag reduction in the same pipeline system (Gyr and Bewersdorff, 1995). Since then, drag reducing polymers have found applications in the Bass Strait in Australia, Mumbai Offshore, Iraq-Turkey oil pipeline and in the Oseberg Field in the North Sea amongst others. (Abdulbari et al., 2014; Jubran et al., 2005)

2.1.2 Drag Reduction Determination

Drag reduction (DR) is defined as the reduction of skin friction in turbulent flow below that of the solvent and is given by the friction factor ratio or by the ratio of the wall shear stress τ_w for the polymeric solution and the solvent. The friction factor is found from:

$$f = \frac{\Delta PD}{2U^2 l \rho} \qquad \textbf{2-1}$$

where ΔP is the measured pressure drop, l is the pipe length, U is the bulk fluid velocity, D is pipe diameter and ρ is the fluid density. The velocity, U can be obtained from:

$$U = \frac{Q}{A} \qquad \textbf{2-2}$$

Q is the flow rate and A is the cross sectional area of the pipe given as;

$$A = \frac{\pi D^2}{4} \qquad \textbf{2-3}$$

The wall shear stress τ_w is related to the friction factor by;

$$\tau_w = \frac{f \rho U^2}{2} \qquad \textbf{2-4}$$

Drag reduction is then found as:

$$\% DR = \frac{\tau_{ws} - \tau_{ws}}{\tau_{ws}} \times 100 \qquad \textbf{2-5}$$

However, drag reduction is most commonly shown as;

$$DR = 1 - \frac{f_{wp}}{f_{ws}} \times 100 \qquad\qquad 2\text{-}6$$

$$DR = 1 - \frac{\Delta P_p}{\Delta P_s} \times 100 \qquad\qquad 2\text{-}7$$

Virk (Virk, 1975) showed that three distinct regions are exhibited by dilute polymeric solutions in a fully developed turbulent pipe flow, and the representative equation for the friction factor, *f* are shown below in order of increasing flow rate or Reynolds number (Re). These regions are the Newtonian, polymeric and maximum drag reduction regimes (Equations 2-8 to 2-10), as shown in the friction factor vs Reynolds number plots on the Prandtl-Karman coordinates (see Figure 2-1).

Newtonian line (a):

$$f^{-1/2} = 4.0 \log_{10} \mathrm{Re} f^{1/2} - 0.4 \qquad\qquad \mathbf{2\text{-}8}$$

Along this line, there is no drag reduction and the friction factor (*f*) relation is the same as for the solvent. That is the usual Prandtl-Karman (or Blasius) law for Newtonian turbulent flow.

Drag reduction line (b):

$$f^{-1/2} = (4.0 + \delta) \log_{10} \mathrm{Re} f^{1/2} - 0.4 - \delta \log_{10} \sqrt{2W^o \mathrm{D}} \qquad\qquad \mathbf{2\text{-}9}$$

Equation 2-9 is an approximate relation for the polymeric region which starts at point P, in Figure 2-1, the onset point, which is dependent on the polymer specie, concentration and solvent pair. The friction factor relation is dependent on the nature of the polymeric solutions. Here δ (slope increment) is the difference between the slopes of the Newtonian (a) and polymeric line (b). Its value also depends on the polymer type and concentration in a given solvent. W^o represents the drag reduction onset wave number (Virk, 1975) and D is pipe diameter.
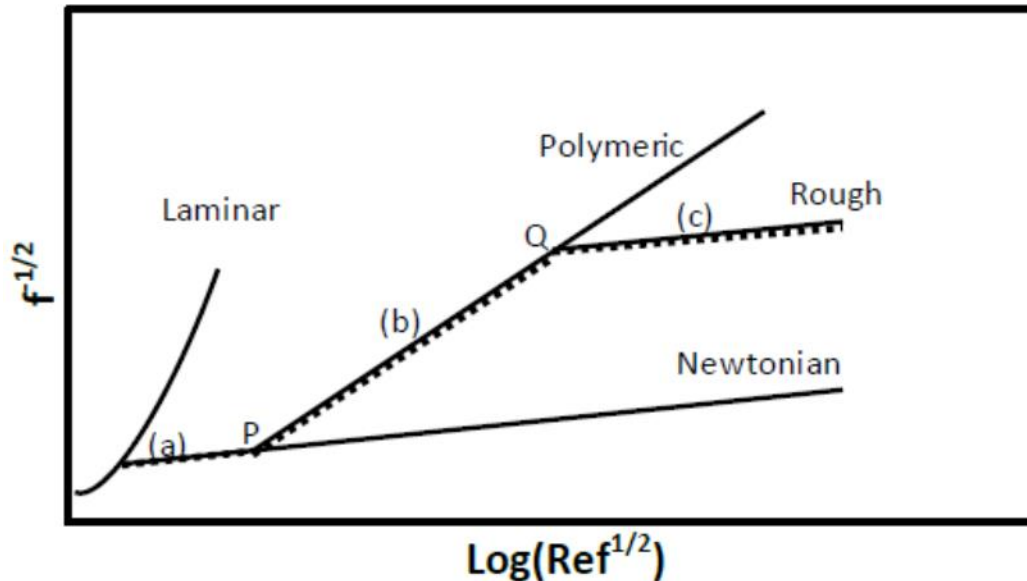
Figure 2-1 Friction factor vs Reynolds number plots on Prandtl-Karman coordinates showing the regions of polymeric solution (culled from (Gómez Cuenca et al., 2008)

Maximum drag reduction line (c)

$$f^{-1/2} = 19.0\log_{10}\text{Re}f^{1/2} - 32.4$$ **2-10**

This region starts from point Q (Figure 2-1) and its line is most times almost parallel to the Newtonian line. The region between this line and the Newtonian is called the Newtonian plug. The friction factor is independent of the Reynolds number and polymer solution. Equation 2-10 is also called the maximum drag reduction asymptote (Virk, 1975).

2.1.3 Types of Drag Reduction by DRA

Drag reduction is either heterogeneous or homogenous in terms of the mode of addition of polymeric materials to the fluid system. Heterogeneous occurs when the additive is not soluble in the fluid or is in a different phase from the fluid. It involves the presence of threads of a concentrated solution of the additive in the flow system (Hanratty and Al-Sarkhi, 2001; Hoyer and Gyr, 1998; Hoyer et al., 1996; Kim and Sirviente, 2005; Vleggaar and Tels, 1973; Warholic et al., 1999). In these studies, the highly concentrated solutions of the additive were injected into the centreline of the pipe flow while considerably high drag reduction was found. In homogenous drag reduction a certain amount of the soluble additive, which will give the desired concentration, is dissolved in the fluid system in a holding tank. The solution is mixed for a long time in the tank to allow for proper homogenization and hydration before it is pumped into the test section (Al-Sarkhi, 2012; Gyr and Bewersdorff, 1995). Based on

these, Gyr and Tsinober, (1997) concluded that the phenomenon of drag reduction in a number of fluid systems is of rheological nature, because the effective viscosity of the polymeric solution is qualitatively and quantitatively different from that of the Newtonian fluid. In general, higher drag reduction is found in heterogeneous systems than in homogeneous ones for both polymer and surfactant additives (Baik et al., 2005; Tamano et al., 2014; Vlachogiannis et al., 2003).

2.2 Drag Reducing Agents

Drag reducing additives are of three major types, namely polymers, surfactants and fibers. A review of some non-additive means of drag reduction including the use of riblets and compliant surfaces was recently reported (Abdulbari et al., 2013).

2.2.1 Polymers

These are high molecular weight (MW > 10^6 g/mol) long chain polymers, also called flow improvers. Common ones are polyisobutylene (PIB, with Oppanol as main trade name) which is known to be soluble in most oil phases, Poly dimethylsiloxane (PDMS), polyethylene oxide (PEO, with Polyox as main trade name) known to be the best single polymer, polymethacrylate (PMMA), polystyrene (PS), polyacrylamide (PAM, with Separan as main trade name), partially hydrolysed polyacrylamide (HPAM; a copolymer of polyacrylamide and sodium acrylate, with Magnafloc as main trade name) (Abubakar et al., 2014b).
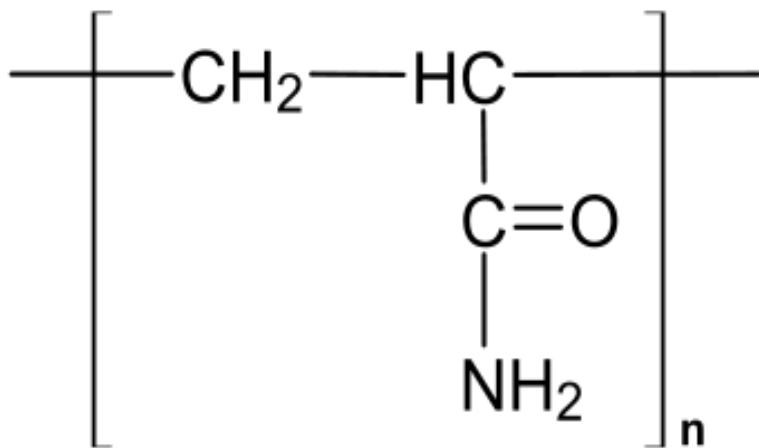
Figure 2-2 structure of polyacrylamide (PAM) monomer unit
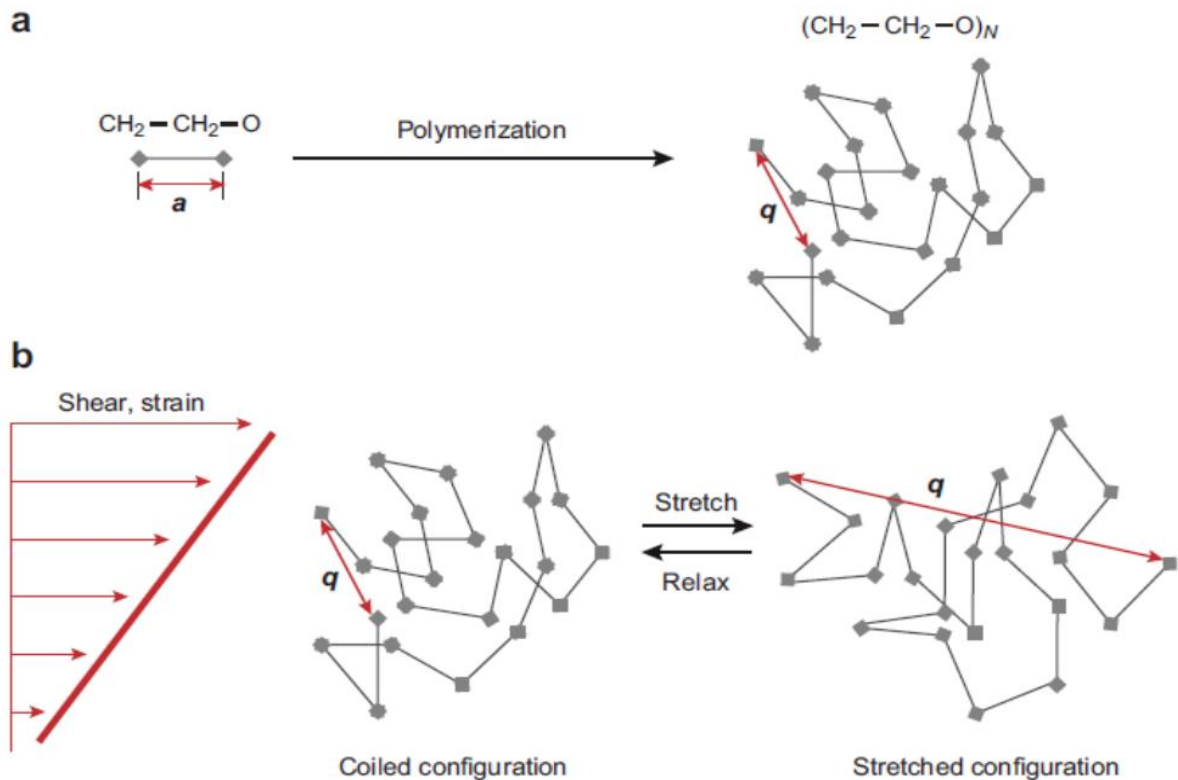
Figure 2-3 Schematics of PEO formation from monomer units and its behavior under shear flow. The flexibility of the molecular chain is evident as well as the extent of stretching (q) (White and Mungal, 2008)

They belong to the group of synthetic polymers and are known to be more effective drag reducers than biopolymers such as guar gum (GG), Xanthan gum, carboxymethylcellulose (CMC), Arthrobacter viscosus, locust bean, tragacanth, karaya, aloe vera, amylopectin, chitosan and okra among others (Abdulbari et al., 2014; Gyr and Bewersdorff, 1995; Hong et al., 2015; Kulicke et al., 1989; Virk, 1975). These biopolymers have been suggested as likely replacements for current synthetic high molecular weight polymers for drag reduction applications because they are more biodegradable and environmentally friendly and can also give high drag reduction.

Polymers can also be classified as ionic (e.g. PAM) or non-ionic (e.g. PEO) depending on the side bonding between its own chains. The chemical structure of PAM is shown in Figure 2-2 while a schematics showing the formation of PEO from monomer units and its subsequent behaviour under shear stress is shown in Figure 2-3

The polymers have good linear structures with excellent extensivity and solubility in the fluid of choice, though elasticity can have an adverse effect on drag reduction when added to a

viscous anisotropic fluid (Den Toonder et al., 1997; Gyr and Bewersdorff, 1995). These polymers do not affect the surface tension of fluids. Nieuwenhuys (2003) reported a negative influence of polymers on experiments in vertical air-water flows.

The choice of polymer used in any particular application is guided by the phase it will be applied to since some of the polymers are only soluble in certain phases. An example is poly-isobutylene (PIB) that is soluble in most oil phases and insoluble in water, while polyacrylamides (PAM & HPAM) are soluble only in water phase and hence retained within this phase even in an oil-water flow system. The qualities and criteria for the selection of a good drag reducing polymer include the following, among others:

- Molecular weight $>10^6$ g/mol
- Shear degradation resistance
- High solubility in the fluid
- Heat, light, chemical and biological degradation resistance
- Ionic structure
- Nature and flexibility of polymer chain (linear or branched).
- Retainability within the fluid of choice in multiphase systems

(Abdulbari et al., 2014; Den Toonder et al., 1997, 1995; Kulicke et al., 1989; Manfield et al., 1999).

Sellin et al. (1982) and Al-Yaari et al. (2009), based on their experimental observations, concluded that polymers with molecular weight < 10^6 g/mol are ineffective in drag reduction. The following factors have been known to affect the effectiveness of these polymers in drag reduction. They are:

- Method of addition and injection into flowing fluid, including nature of mixing point in multiphase systems (homogenous or heterogeneous addition)
- Concentration (also of master solution)
- Pipe diameter and inclination
- Pipe roughness
- Temperature and pH
- Presence of turbulent flow
- Fluid viscosity (including its hydrodynamic viscosity)
- Presence of paraffin and or saline water
- Less likely by pipe length

(Al-Sarkhi, 2010; Al-Wahaibi et al., 2012; Al-Yaari et al., 2012; Bewersdorff et al., 1993; Gyr and Bewersdorff, 1995; Hanratty and Al-Sarkhi, 2001; Jubran et al., 2005; Nieuwenhuys, 2003; Vleggaar and Tels, 1973; Yusuf et al., 2011).

Since very small polymer concentrations (in ppm) are required in drag reduction, it may imply that the higher the molecular weight the lower the required concentration. At high polymer concentrations, polymers form aggregates and in turbulent flow they are stretched and hence attain very high aspect ratio (ratio of length to width), which is required in drag reduction (Den Toonder et al., 1997; Dunlop and Cox, 1977; Kim and Sirviente, 2005; Vlachogiannis and Hanratty, 2004). This is the principle behind the injection of high concentration master solution even when low in-situ concentrations are needed. The absence of this extensional force makes drag reduction almost impossible in laminar flows (White and Mungal, 2008).

However, polymers can degrade easily mainly from turbulence, chemical, thermal, and mechanical action. Under these conditions and in line with results from molecular weight distribution measurements (Kulicke et al., 1989; Liberatore et al., 2004; Tiu et al., 1993; Vlachogiannis et al., 2003), the molecules are stretched beyond limit leading to chain scission of covalent bonds almost midway along the polymer molecule. The rate of polymer degradation is proportional to the molecular weight of the polymer and inversely proportional to the pipe diameter at constant wall shear stress and concentration (Manfield et al., 1999). The use of high stress inducing pumps such as centrifugal pumps for polymer transport is therefore discouraged in favour of positive displacement pumps. This is why polymers are usually added after pumping stations in the Trans-Alaskan Pipeline System as well as other similar applications. To avoid degradation, 'once-through' experiments are often carried out (Al-Sarkhi and Soleimani, 2004; Al-Sarkhi, 2012; Al-Yaari et al., 2012; Hanratty and Al-Sarkhi, 2001; Kim and Sirviente, 2005; Manfield et al., 1999; Otten and Fayed, 1976; Pollert and Sellin, 1989; Tiu et al., 1993).

Amongst the commonly used water soluble polymers, polyacrylamides and more specifically hydrolysed polyacrylamide has been reported to be more resistant to degradation. They are also ionic in structure which enables them to form better hydrodynamic volumes than their non-ionic counterparts, such as PEOs, of similar molecular weight. For this reason, it has found more applications particularly in areas where high shear is unavoidable (Abubakar et al., 2014a; Den Toonder et al., 1995; Hoyt, 1986).

In an air-water system, injecting the polymer solution in the water before the air inlet can result in the breakup of some polymer molecules when the high velocity of the air phase impacts the water (Al-Sarkhi and Soleimani, 2004). Gyr and Bewersdorff (1995) as well as Hanratty and co-workers (Hanratty and Al-Sarkhi, 2001; Liberatore et al., 2004; Vlachogiannis et al., 2003; Warholic et al., 1999), based on their experimental observations, suggested the deliberate preparation of polymeric solutions to promote polymer entanglements which increase drag reduction. They concluded that apart from molecular scission, breakup of polymer aggregates was a dominant mechanism in polymer degradation. Vlachogiannis et al. (2003) further suggested that an understanding of the formation and structure of the aggregates would be useful in the design and modelling of both mixing and delivery of polymer solutions in practical systems.

2.2.2 Surfactants

These are low molecular-weight alkali-metal and ammonium soap molecules which have the ability to reduce the surface tension of a liquid, the interfacial tension between two liquids, or that between a liquid and a solid. Examples include Sodium dodecyl-benzene sulfonate (SDBS), Sodiumlauryl cetyltrimethyl ammonium chloride (CTAC)/ sodium salicylate, cetyltrimethyl ammonium bromide (CTAB), Sodium lauryl sulfate (SLS), cetylpyridinium chloride/sodium salicylate (CPCl/NaSal) amongst others. The surfactant molecules are amphiphilic, which means they consist of a hydrophilic head (water-loving) and a hydrophobic tail (oil-loving, water-hating). These makes it possible for them to be partly soluble in oil and also in water and hence enables them to modify the surface properties of oil-water interfaces (Gyr and Bewersdorff, 1995; Hadri and Guillou, 2010).

Surfactants are classified as anionic, cationic, non-ionic or amphoteric. The anionic surfactants are relatively inexpensive, can precipitate in the presence of calcium, and are quite effective at low temperatures in non-aqueous systems. On the other hand, cationic surfactants are quite expensive but do not precipitate in the presence of calcium. They are chemically degraded in an aqueous system within a few days and though they are mechanically stable they possess a thermal instability and thus a limited applicability. The non-ionic surfactants possess chemical, mechanical and thermal stability and do not precipitate in the presence of calcium ions in solution. There are also the set of amphoteric surfactants with both anionic and cationic heads but these are not as common as others (Kulicke et al., 1989; Zakin et al., 1998).

The structure of surfactants enhances their resistance to degradation because of the reversible degradation of their aggregates (micelles). Hence, they are more suitable industrially and possess excellent potential for drag reduction at high temperatures when compared to polymers (Abdul-hadi and Khadom, 2013; Kulicke et al., 1989; Zakin et al., 1998). However, one of the major drawbacks is the need to use much higher concentrations of surfactants to achieve similar drag reduction achievable with a few tens parts per million of polymer solution.

2.2.3 Fibers

Fibers are sometimes referred to as rigid polymers. The orientation of the fiber molecules parallel to their axis results in high aspect ratios (as high as 10^5) while the bindings of the molecules determines their flexibility. These properties are highly desirable for drag reduction applications. Examples include nylon fibers, cotton, rayon and glass fibers. In fact the first known drag reducer was paper pulp. Of these, asbestos fibers are known to yield up to 85 % drag reduction at concentrations between 25-2000 ppm (Gyr and Bewersdorff, 1995). Although fibers are not as effective as polymer solutions, they are not easily degraded like polymers, and are easily separated from the flow, a property that makes them desirable in drag reduction applications (Kulicke et al., 1989). Sharma et al., (1978) reported that the method of injection of the fiber suspensions greatly influences their effectiveness. It is believed that the interaction between fibers and eddies of turbulent flow results in drag reduction (Roy and Larson, 2005).

Some investigators have reported that the combination of polymers and fibers has a synergistic effect that surpasses the drag reduction if either is used alone (Doulah, 1981; Kale and Metzner, 1976; Metzner, 1977). Delfos et al. (2011) showed that maximum drag reduction decreases with fiber length and is not dependent on fiber diameter. Recently, Ogata et al. (2011) used a bio-fiber (bacterial cellulose) and obtained an appreciable drag reduction of about 11 %. They observed that drag reduction increased with bio-fiber concentration but decreased with increasing mechanical shear, unlike the regular fibers. The bacterial cellulose is environmentally friendly because it is produced via a natural process from acetic bacteria which are able to form complex networks.

Figure 2-4 Images of fiber particles (not actual sizes; courtesy of (Delfos et al., 2011)**)**

Fibers can cause problems by plugging pipelines because high concentrations are usually required for appreciable drag reduction to be obtained (Wang et al., 2011).

It is also worth noting that while other operational conditions are kept fixed, drag reducing agents are effective to a certain dose after which drag reduction remains constant (Manfield et al., 1999). This observation has been made by several investigators (Al-Sarkhi, 2010; Hanratty and Al-Sarkhi, 2001) who reported that the DRA concentration and the method of its introduction to the flowing liquid in the pipe determine the minimum threshold concentration for drag reduction onset as well as the maximum drag reduction asymptote (MDRA; (Virk, 1975)).

2.3 Drag Reduction by Additives

Since Toms' (1948) pioneering publication, the effect of DRA in single phase flows has been well reported. Manfield et al. (1999) and Abubakar et al. (2014b) gave a compendium of works in both single phase and multiphase flows. They concluded that more work is needed to have a fundamental understanding of the mechanism of drag reduction by additives, based on experimental and theoretical evidence.

2.3.1 Drag Reduction by Additives in Single Phase Flows

Vleggaar and Tels (1973) in their experiments on heat transfer in heterogeneous drag reducing systems reported that heat transfer is reduced in a similar way as radial momentum and that in homogeneous systems, heat transfer values tend to be lower than drag reduction. They also observed that, since at low Reynolds number homogeneous drag reduction is negligible, heat transfer is not affected. Mansour et al. (1998) studied the effect on pressure and heat transfer reduction in a crude oil system (API = 21.31) of a heterogeneous surfactant (MDR-2000). They reported that the surfactant (MDR-2000) loses

its drag reducing ability when the solution temperature reaches about 82°C. They also reported that in smaller pipe diameters the critical wall shear stress is reached at lower Reynolds number than for larger pipe diameters. This suggested that degradation of the surfactant was higher and occurred at lower Reynolds number in smaller pipes than in larger ones. This may explain the observation by Fadhl (2011) and later by Yusuf et al. (2011) that higher concentration of polymer is required in smaller pipe diameter than in larger pipes. Drag reduction of 60 % and 50 % were found in 2.54 cm and 1.9 cm pipes respectively. The maximum heat and drag reduction achieved in the experiment by Mansour et al. (1998) were 77 % and 57.5 % respectively at a temperature of about 62°C. Jubran et al., (2005) suggested areas that need further investigations in single and multiphase flows which included the role of drag reducing agent as flow conditioners at large pipe inclinations, high water cuts, heat and hydrodynamic processes.

2.3.2 Drag Reduction by Additives in Gas-Liquid Flows

In a recent paper, Al-Sarkhi (2010) reviewed works on drag reduction in the area of gas-liquid and liquid-liquid flows with polymers. He showed that the molecular weight of polymers greatly affects their effectiveness as drag reducers, which is in agreement with the earlier findings by Sellin et al. (1982) although only one polymer (polyethylene oxide) was tested. The author recommended that more work is needed specifically on the effects of pipe length, temperature, and pressure on DRA degradation. There is also a need to determine DRA effects in inclined pipes and bubbly flows.

More recently, Al-Sarkhi (2012) argued that the introduction method of the fluids in the test section in gas-liquid flows influence the effectiveness of DRA in the system. Air impinging at the fluids mixing point is capable of breaking up or at least changing the structural arrangements of the polymer aggregates. This was however not supported by his experimental studies. In the other method, the polymer solution is injected after the gas-liquid mixing point. It may be argued that the only difference between the two injection methods is the fact that the entering air actually impinges on the flowing water that contains the polymer in one case. It is questionable whether the air has enough energy to break the aggregates, since the polymer fibers and aggregates are not located at the air-water interface.

Negative effects of DRA on gas-liquid flows have also been reported. Nieuwenhuys (2003) attributed it to the fact that flows were not fully developed and the polymers (polyacrylamide

based) were not fully mixed with the fluid. On the other hand, Parimal et al. (2008) observed that with the addition of an oil soluble polymer to their CO_2-oil system, an emulsion with high apparent viscosity was formed. This increased viscosity may have resulted in increased drag in the system. The polymers were not fully mixed with in the oil phase. Fernandes et al., (2009), in a vertical air-water flow system, observed an appreciable drag reduction of 74 % in the frictional component of the pressure drop. This was later reduced because of the increase in the hydrostatic component of the pressure gradient as a result of 27 % increase in liquid hold-up in the vertical system.

In general, several researchers have agreed that any condition, such as increased Reynolds number or pipe roughness which increases turbulence in a system actually enhances drag reduction (Al-Sarkhi and Hanratty, 2001; Baik and Hanratty, 2003; Mowla and Naderi, 2006). It has also been generally agreed from experimental observations that the drag reduction in two phase flows surpasses that of single phase flows for the same operational conditions of flowrate, temperature etc. (Al-Sarkhi, 2010; Rosehart et al., 1972), though Saether et al., (1989) reported a contrary observation.

2.3.3 Drag Reduction by Additives in Liquid-Liquid Flows

Though many works have been done in the area of liquid-liquid flows, it has comparatively received far less attention than gas-liquid flows.

The first documented report on the effect of drag reducing agents on a horizontal oil-water flow was by Al-Wahaibi et al. (2007) in a small diameter 14 mm ID acrylic pipe using a co-polymer (Magnafloc 1011; of polyacrylamide and sodium acrylate) solution in water and oil (viscosity; 5.5 mPa s, density; 828 kg/m3). Using a 1000 ppm master solution, and with the aid of a two-fluid model, they found that there was a decrease in both the interfacial and water wall shear stresses when the polymer was added to the water phase.

They observed a maximum 50 % drag reduction after the addition of the polymer to annular flow, while no significant differences in drag reduction were found between 50 ppm and 20 ppm polymer concentrations. They noted that flow patterns and their transitions were strongly influenced by the presence of the drag reducing agent, whereby annular flow was changed to dual continuous or stratified flow and, in most cases, slug flow to stratified flow. The addition of the polymer led to an increase in the water hold-up and dampened the

interfacial waves in stratified and stratified wavy flows in agreement with findings in gas-liquid flows (Al-Sarkhi and Soleimani, 2004; Hanratty and Al-Sarkhi, 2001).

Abdullah et al. (2008) studied the effect of polymer concentration and hydration period on horizontal oil-water flows using the same test system. It was found that drag reduction reduced with longer hydration periods, which were attributed to a reduced solution and intrinsic viscosity because of the reduction in the hydrodynamic volume of the polymer with time. They also found that drag reduction increased and then decreased with polymer concentration probably due to the increase of fluid viscosity at higher polymer concentration. This contradicted the findings of other investigations and some recent reports that drag reduction increases to a maximum and then remains constant with increase in polymer concentration (Abubakar et al., 2015a, 2014a; Hanratty and Al-Sarkhi, 2001).

Al-Yaari et al. (2009) also found that DRA influenced flow patterns, in a 25.4 mm acrylic pipe, with water and oil (viscosity = 0.0016 Pa.s; and density = 780 kg/m^3) as test fluids. They observed that phase inversion in the dispersed flow regime, at a water fraction range of 0.33 – 0.35, disappeared after the addition of 5 ppm polymer. 65 % drag reduction was obtained with the addition of 10-15 ppm polymer. The drag reduction decreased when 5 % salt solution was added to the water phase. In electrolytic saline water the ionic polymer molecules form coils due to the electrostatic interaction between different parts of the same polymer, which inhibits the formation of aggregates essential for drag reduction. They also found that polymers with molecular weight less than 10^6 g/mol are ineffective and that drag reduction increases with the molecular weight of polymers, in agreement with a previous report (Sellin et al., 1982).

Al-Yaari et al. (2012) also found increase in water hold up and flow pattern changes using the same test fluids and system as in (Al-Yaari et al., 2009). The addition of polymers into the water phase of dispersed flow (oil in water and water in oil) reduces the turbulent mixing forces and increases the droplet coalescence rate which eventually leads to stratification and increased water hold up.

Al-Sarkhi et al. (2011) presented correlations for predicting drag reduction in both gas-liquid and liquid-liquid systems, suitable for a wide variety of pipe diameters and flow patterns. In gas-liquid flows, the mixture friction factor of the drag reduced flow is given as:

$$f_m = 3.36 \times 10^{-7} \frac{D_r}{D} \left(Re_m \left(\frac{Usg}{Usl} \right)^{0.5} \right)^{0.595} \qquad \textbf{2-11}$$

where D is the experimental pipe diameter, Re_m is the mixture Reynolds number ($Re_m = U_m D / \nu$, U_m is sum of superficial fluid velocities and ν is kinematic viscosity of water), D_r is the reference pipe diameter, Usg and Usl are respectively the superficial gas and liquid velocities. In liquid-liquid flows, the drag-reduced friction factor is given as;

$$f_m = 0.614 \left(Re_m \left(\frac{Usw}{Uso} \right)^{0.5} \right)^{-0.5} \qquad \textbf{2-12}$$

here Uso and Usw are the superficial oil and water velocities respectively. The model predicted experimental data from literature with reasonable accuracies.

Recently, Al-Wahaibi and co-workers (Al-Wahaibi et al., 2012; Yusuf et al., 2011) used Magnafloc (1035) a copolymer as a drag reducing agent (DRA) in oil–water flow in a horizontal 25.4 mmID acrylic pipe. They reported that the addition of 2 ppm of polymer solution to the oil-water flow induced significant drag reduction with a maximum drag reduction attained at 10 ppm polymer concentration. They also found that concentration of polymer master solution beyond 1000 ppm (i.e. 2000 and 3000 ppm) did not significantly improve the drag reduction. Previously, 1000 ppm master solution had been found to give the optimum drag reduction (Abdullah et al., 2008; Al-Sarkhi, 2012; Al-Wahaibi et al., 2007; Hanratty and Al-Sarkhi, 2001). A strong influence of pipe diameter on drag reduction was found in agreement with findings in air-water (Al-Sarkhi and Hanratty, 2001) and air-oil (Mowla and Naderi, 2006) systems. DRA addition to oil-water flows extended the region of stratified flows to higher fluid velocities in agreement with earlier reports (Al-Wahaibi et al., 2007; Al-Yaari et al., 2012, 2009). Their result also showed that drag reduction increased with water velocity to a maximum of 60 % and 45 % at oil velocities of Uso = 0.14 m/s and Uso = 0.52 m/s respectively, with no significant influence of pipe length.

Abubakar et al. (2015) studied the effects of a drag reducing polymer on oil (Viscosity; 24 mPa s, density; 872 kg/m^3)–water flow patterns, pressure drops, phase inversion and slip ratio in a horizontal acrylic pipe of 30.6-mm ID. They used a concentration of 40 ppm from 2000 ppm master solution of a water soluble high molecular weight (12×10^6 g/mol) anionic copolymer of polyacrylamide and 2-Acrylamido-2-Methylpropane Sulfonic acid (AMPS). Changes to flow patterns were found but only in water continuous regimes. The regions of

stratified, dual continuous and water continuous flow patterns were extended to higher superficial oil and water velocities. The addition of polymer to the water phase resulted in an increase in the water hold up and slip ratio while maximum drag reduction of 64 % was obtained at the highest mixture velocity in the water continuous flow region. The increase in pressure drop at the phase inversion point was eliminated by the polymer addition. However, their experiments were limited to a maximum mixture velocity of 1.6 m/s and input oil volume fraction of between 0.05 and 0.9.

A summary showing the drag reduction agents (DRAs) that has so far been used in liquid-liquid flow experiments is shown in Table 2-1

Table 2-1 Studies on the effect of DRA in oil-water flows

Author(s) name/year	Fluid types /properties	Pipe material(s) /geometry	Polymer type/ concentration	Investigated parameters	Measurement technique(s)	Max. DR %
(Al-Wahaibi et al., 2007)	Water and oil (μ_o=5.5cP, ρ_o=828kg/m^3)	Acrylic/ horizontal ID=14mm L=3.5m	Magnafloc 1011+/ 20, 50ppm	Effect of DRA on the flow patterns, hold-up, pressure drop	Visual observation, Differential manometer	50
(Al-Yaari et al., 2009)	Water-SAFRA D60 (μ_o=1.57cP, ρ_o=780kg/m^3)	Acrylic/ horizontal ID=25.4mm L=10m	Magnafloc 1011+/ 10–15ppm	Effect of DRA on flow, pressure drop; Effect of DRP Conc.,MW; Salt content	Visual observation, Pressure transducer	65
(Omer and Pal, 2010)	3 water-in-oil emulsions/ μ_o =2.5, 6, 5.4cP, ρ_o =753, 785, 816kg/m^3	4 stainless steel pipes/ horizontal ID=8.9, 12.6, 15.8, 26.5mm and 1 PVC pipe/ horizontal ID=23.7mm	Polyethylene oxide (PEO) and carboxymethyl cellulose/ 0–1wt%	Effect of DRAs on dispersed aqueous phase of the water-in-oil emulsion	Pressure transducers	Not stated
(Al-Yaari et al., 2012)	Water-SAFRA D60 (μ_o=1.57cP, ρ_o=780kg/m^3)	Plexiglas/ horizontal ID=25.4mm L=10m	Magnafloc 1011+/ 50ppm	Effect of DRA on water hold up	Conductivity probe, Pressure transducer	42
(Langsholt, 2012)	Water-ExxsolD80- μ_o =1.8cP, ρ_o=22.5kg/m^3	Near horizontal, ID=100mm L=25m	Acrylic copolymer, poly α-olefin*/ 120,80* ppm	Effect of DRA on the hold-up, Pressure drop, diameter scaling	Beam, gamma densitometers, Pressure transducer	30, 10
(Yusuf et al., 2011)	Water-Mineral oil (μ_o=12cP, ρ_o=875kg/m^3)	Acrylic/ horizontal ID=25.4mm L=8m	Magnafloc 1035+/2–10ppm	Effect of DRA on flow patterns, drag reduction	Visual observation, Dywer 490DDM	60
(Al-Wahaibi et al., 2012)	Water-Mineral oil (μ_o=12cP, ρ_o=875kg/m^3)	2 Acrylic pipes/ horizontal ID=19, 25.4mm L=8m each	Magnafloc 1035+/ 2–30ppm	Effect of pipe diameter on the performance of DRA	High-speed camera, Visual observation, Dywer 490DDM	45 for 19mm, 60 for 25.4mm
(Abubakar et al., 2015)	Water-mineral oil (μ_o=24cP, ρ_o=872kg/m^3)	Acrylic/ horizontal ID=30.6mm L=12m	polyacrylamide and 2-Acrylamido-2-Methylpropane Sulfonic acid (AMPS)	Effect of DRA on flow patterns, pressure drops, phase inversion and slip ratio	High-speed camera, Visual observation, pressure transducer	64

*oil-soluble polymer, + copolymer of polyacrylamide and sodium sulfate.

2.3.4 Drag Reduction in Three Phase Systems

Three phase flow system are common in chemical processes and particularly in oil production systems where, most times, water is injected into wells to improve its productivity. During drilling operations, mixtures of solid, liquid and gas are also very common and the need to reduce the energy requirements by using drag reducing agents particularly during their transportation is a welcome development. However, very few works have been published on drag-reduction in 3 phase systems. The earliest studies were on a solid-liquid-liquid system by Sifferman and Greenkorn, (1981) using white oil and tap water and two concentrations (5 & 10 %) of silica sand in tap water and in the oil. Three different water soluble polymers were used namely; sodium carboxymethylcellulose (CMC), polyethylene oxide (Polyox), and guar gum (Jaguar) at different concentrations. Very similar drag reduction was found in both the two phase and three phase systems. Kang et al. (1998) carried out drag reduction experiments in CO_2–oil-water system in a 10-cm ID plexiglass system using polymer concentrations up to 75 ppm and found drag reduction of 81 % and 35 % for stratified and annular flows respectively in horizontal flows. Transition to slug flow was shifted to higher superficial liquid velocities after polymer addition. They concluded that the polymer was more effective for lower superficial liquid and gas velocities for both single and multiphase flows.

Using two partially degraded polymers; a water-soluble acrylic copolymer and an oil-soluble poly α-olefin, Langsholt, (2012) studied drag reduction in a 100-mmID horizontal pipe for gas-oil-water system. Under the conditions tested, drag reduction was obtained in the dispersed flows when the polymers were in the continuous phase. The addition of polymer also dampened the interfacial waves, while the boundaries of the flow patterns remain unaltered. A maximum drag reduction of over 50 % was obtained while drag reduction increased with the inlet fraction of the liquid that carries the polymers.

2.4 Mechanism of Drag Reduction by Additives

It is widely accepted that drag reduction in fluid flows is a result of suppression of turbulent activity. This implies that a complex interaction exists between the turbulence dynamics and the polymer dynamics which depends on the number of monomers (of the polymer) available in the flow system at a particular time (White and Mungal, 2008). The dissipative nature of turbulent flows results in energy exchange which normally involves a loss of the mean flow (pressure drop) to the turbulence. Gyr and Bewersdorff, (1995) defined drag

reduction as the product of the change in energy balance resulting from the interaction of the flow with the additives.

Kinetic energy of the flowing fluid is transferred from the mean flow via vortex motion of an ever decreasing scale until it is finally dissipated by viscosity. The small scale motions rearrange their length scales and intensities until all the energy from the larger scales are completely dissipated, in a process called the energy cascade. The process is independent of viscosity: this is known to cause dissipation, but does not control the rate (Gyr and Bewersdorff, 1995). This dissipation results in an increased pressure drop in the system. DRAs are more effective in the near wall region at the boundary layer where the no-slip condition exists and the velocity gradients are large (Scharnowski et al., 2010; Schmitt, 2008). Turbulent eddies originate from the near wall region as streaks which then rise through the buffer zone and are ejected as bursts in the turbulent core (Den Toonder et al., 1997; Gyr and Bewersdorff, 1995; Zadrazil et al., 2012). The DRA absorb the energy of the streaks from the near wall region and prevent the bursting phenomenon, and because they are of a small scale, they introduce an orientation in the fluid that leads to a modification of the logarithmic velocity profile of the flow. This leads to the limitation of momentum and vorticity transport. Thus the DRA suppresses high turbulent activities (vortex stretching and dissipation) by causing a major reduction and/or redistribution to the turbulent motion in the axial flow direction (Vleggaar and Tels, 1973; White and Mungal, 2008). These makes the distribution of DRA molecules in the turbulent flow intermittent, resulting in high local concentrations in regions of strong turbulent activities leading to a suppression of vortex stretching and dissipation (Hoyer et al., 1996).

At the onset of drag reduction, polymer molecules are stretched by the turbulence stresses (strain rate and vorticity fields associated with the buffer layer) generated in the flow. The resulting increase in the elongational viscosity leads to an increase in the thickness of the buffer layer and subsequent reduction in the wall friction (Gyr and Bewersdorff, 1995; Lumley, 1973; Mowla and Naderi, 2006; White and Mungal, 2008). The elongated molecules with an elastic energy comparable to the kinetic energy in the buffer layer then interfere with the energy cascade and cause its premature termination. This leads to a reduction of the Reynolds shear stresses and the velocity fluctuations in a direction normal to the wall (White and Mungal, 2008). This agrees well with the mechanistic model of Sher and Hetsroni (2008) who suggested a turbulent kinetic energy dissipation mechanism in polymer

suspensions. They postulated that rotational flow kinetic energy is converted to polymer elastic energy when the initially coiled polymer is rotated and stretched in the turbulent eddies. The elastic energy is subsequently dampened when the polymer relaxes in the surrounding viscous fluid. In their model, the polymer fibers are represented by a dumbbell (spring with masses at their ends) influenced by elastic and centrifugal forces from the surrounding turbulent fluid flow. The polymer alignment, extent of stretching and subsequent relaxation in the surrounding fluid determines its drag reduction effectiveness. The cumulative elastic energy of the polymer molecules that enables them to induce drag reduction by the processes already described is a function of the concentration of the polymer (Den Toonder et al., 1997; Dubief et al., 2004; Lumley, 1973; Min et al., 2003; Tabor and De Gennes, 1986).

Maximum drag reduction (MDR) is obtained when the vortices are saturated with the DRA molecules. Hence an increase in the concentration of the DRA beyond the saturation level will yield no further increase in drag reduction (Al-Sarkhi, 2012; Al-Wahaibi et al., 2012, 2007; Den Toonder et al., 1997; Doulah, 1981; Gyr and Bewersdorff, 1995; Hoyer et al., 1996; Katepalli and Christopher, 2000; Manfield et al., 1999; Warholic et al., 1999).

For polymer molecules already stretched by other means before been introduced into the flow, onset and maximum drag reduction are expected to occur earlier. The ability of polymer molecules to be extended and attain higher aspect ratios, compared to fibers and surfactants, can explain why they are more effective in drag reduction (Den Toonder et al., 1997; Hanratty and Al-Sarkhi, 2001; White and Mungal, 2008).

The formation of aggregates in polymer solutions of high concentrations, which are stretched at the injection point also enhances drag reduction (Kim and Sirviente, 2005; Vlachogiannis and Hanratty, 2004; Warholic et al., 1999). This may explain why higher drag reduction are obtained in heterogeneous systems than in homogeneous ones (Al-Sarkhi, 2012; Den Toonder et al., 1997; Dunlop and Cox, 1977; Gyr and Bewersdorff, 1995; Virk, 1975; Wei and Willmarth, 1992).

Paschkewitz et al. (2005) presented a quantitative analysis of the microstructural dynamics during the generation of fiber stress fluctuations associated with turbulent drag reduction. They showed that when fibers confined within some planes in the flow are rotated, there is generation of span-wise shear stress, which oppose vorticity leading to the weakening of a

vortex. As in the case of polymers, there is a modification of the logarithmic velocity profile of the flow field. The fibers are then realigned leading to further weakening of the vortex and suppression of the bursting phenomenon.

Despite the volume of work available, investigators still consider that there is not full understanding of the mechanism of drag reduction and the changes in the buffer layer. White and Mungal (2008) pointed out that a predictive model for the process is desperately required particularly at low and moderate Reynolds numbers. Also challenging is the incorporation of polymer concentration inhomogeneities as well as polymer degradation into the models. It should be noted that the mechanism of the interaction between polymer molecules and turbulence is applicable to both single phase and multiphase flows, although the presence of interfaces increases the complexities of the multiphase flows.

Some investigators have suggested that the combination of drag reducing agents could lead to higher drag reduction in multiphase systems. Such combinations include polymer-fiber, polymer-surfactants and surfactants-fiber systems, since it was reported to give higher yield in single phase water flows than when the individual additives were used alone (Doulah, 1981; Kale and Metzner, 1976, 1974; Langsholt, 2012; Metzner, 1977).

2.5 Flow Patterns in Multiphase Flows

When two or more fluids flow in a pipe, different flow patterns (the geometric/spatial distribution of a phase in a system) form depending on the velocity, density, viscosity, interfacial tension of the respective fluids, pipe roughness, diameter and inclination as well as surface wettability. The main flow patterns that have been observed in liquid-liquid flows are briefly described below (Al-Wahaibi et al., 2007; Chakrabarti and Das, 2006; Das et al., 2010; Pietro, 2007).

2.5.1 Stratified Flows (including Stratified-Wavy)

Here both phases flow in layers under the influence of gravitational force with the less dense phase flowing at the top while more dense phase flows at the bottom of the pipe respectively (see Figure 2-5). As the superficial velocity increases, the inertial forces become greater than the gravity force and create instability at the interface, which becomes wavy. The Kelvin-Hemoltz instability equation is used to predict the onset of the drop entrainment from

the wavy interface (Al-Wahaibi and Angeli, 2009, 2007). This flow pattern is desired in many processes particularly when the phases are required to be separated.
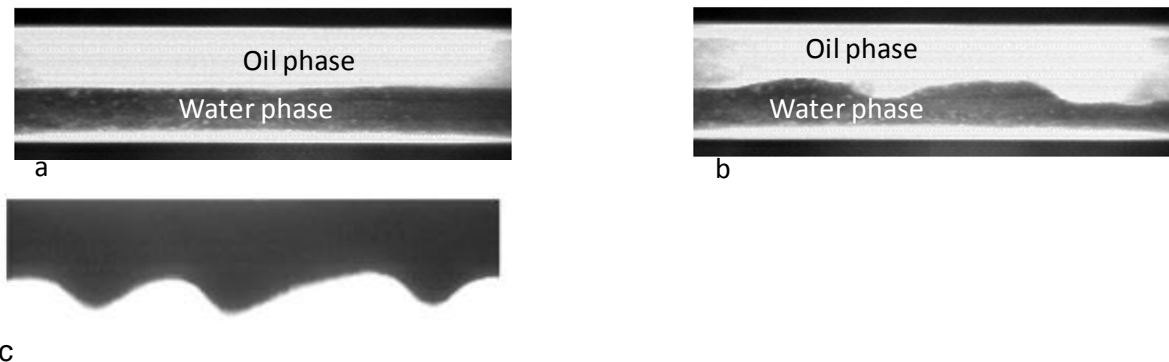
Figure 2-5 Stratified flows (a), stratified-wavy flows (b & c) (Al-Wahaibi et al., 2007; Rodriguez and Baldani, 2012)

2.5.2 Dual Continuous Flow

Here both phases form continuous layers as in stratified flow but drops of each phase are seen in the continuum of the other phase (see Figure 2-6). The drops of either or both phases detaching from the interfacial waves are mostly uniform in size. Some reporters refer to this pattern as stratified with mixing at the interface (ST & MI) or three layer flow (Al-Yaari et al., 2009).
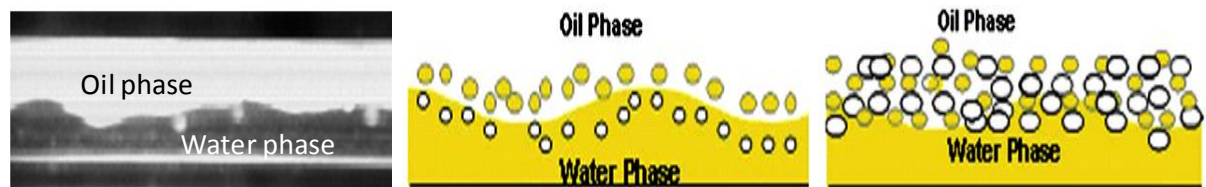
Figure 2-6 Dual continuous flows (Al-Wahaibi et al., 2007; Al-Yaari et al., 2012)**.**

2.5.3 Annular Flow

This flow pattern exists at higher fluid velocities compared to stratified flows and consists of an annulus formed by one phase surrounding the core of the other phase (see Figure 2-7). The interface is mostly circular and can be wavy depending on the relative velocity of the flow. The denser phase usually forms the annulus and occurs both in low viscous (Al-Wahaibi et al., 2007) and high viscous (Colombo et al., 2014; Rodriguez and Bannwart, 2006; Rodriguez and Baldani, 2012) oil-water flows.

Figure 2-7 Different types of annular flow

2.5.4 Slug Flow

Slug flow is characterized by its intermittence. It consists of sequence of slugs of the dense phase containing dispersed bubbles of the less dense phase alternating with sections of separated flow within long bubbles (see Figure 2-8). In some cases, droplets of the dense phase are seen within the large bubbles of the less dense phase. The slugs can be several pipe diameters long, and alongside the frequency, is dependent on the difference between the velocities of both phases (Al-Wahaibi et al., 2007; Fabre and Line, 2010).
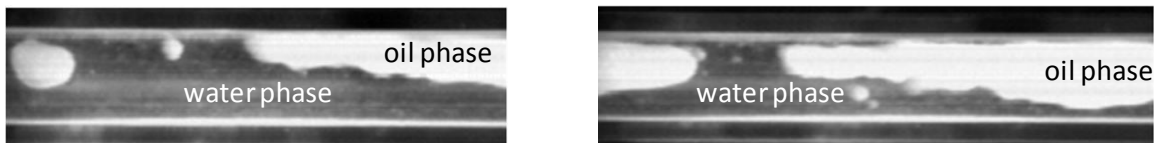
Figure 2-8 slug flow

2.5.5 Plug Flow

In this flow, small plugs/drops of the less dense phase (oil) are seen in the continuum of the denser phase (water), with the plugs touching the upper and lower parts of the pipe. The plugs can be of regular shapes (like pistons) moving at same velocity. In some cases, part of the oil plugs is seen to touch the upper pipe wall while the other part is surrounded by the water phase (see Figure 2-9). It occurs in all fluid flows and predominant in small diameter pipe/micro channel flows. In gas-liquid flows, the pattern is known as Taylor flow (Dore et al., 2012; Janes et al., 2010; Lee and Lee, 2008; Tsaoulidis et al., 2013).
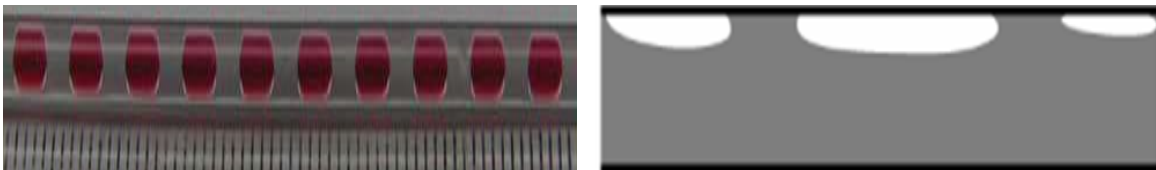
Figure 2-9 Plug flow

2.5.6 Rivulet Flow

This flow pattern, is not common but has been seen in both gas-liquid and liquid-liquid flows (Das et al., 2010; Moore, 2013). It can be categorized as a stratified flow because of the presence of a clear interface. It consists of one phase flowing as a continuous stream throughout the length of the tube in a tortuous or meandering manner while the other phase occupies the space not filled by the first phase (see Figure 2-10). In some instances, both phases are observed to follow the tortuous path with very clear interface and the frequency depends on the fluid velocities. Pressure drop fluctuations are a common phenomenon with this flow pattern. The pattern has mainly been seen in small tubes where interfacial phenomenon are significant and prevail over inertial forces (Das et al., 2010).
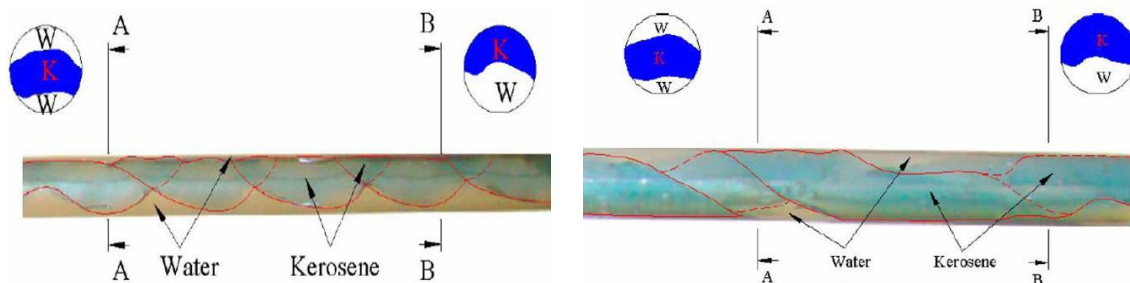
Figure 2-10 Rivulet flow pattern (Das et al., 2010)

2.5.7 Dispersed Flow

This flow consists of drops that are dispersed in a continuous liquid phase (see Figure 2-11). The drops are in continuous motion with deformable and complex interacting interfaces (Kataoka and Serizawa, 2010). It appears when the velocity of one of the phases is high compared to the other (Al-Wahaibi et al., 2007). At certain phase fractions the dispersed phase can change to become continuous and vice versa (phase inversion; (Abubakar et al., 2015a; Al-Wahaibi and Angeli, 2009; Ngan, 2010; Ngan et al., 2009)). Different types of dispersed flows have been seen depending on the continuous phase and the distribution of the drops. These include dispersion of oil in water (Do/w), dispersion of water in oil (Dw/o), dispersion of oil in water and water (Do/w&w) and dispersion of water in oil and oil (Dw/o&o). Due to gravity stratification, the dense fluid and droplets flows at the bottom portion of the pipe while the less dense fluid drops flow at the upper part of the pipe.

Do/w&w

Dw/o

Dw/o&o

Dw/o & Do/w
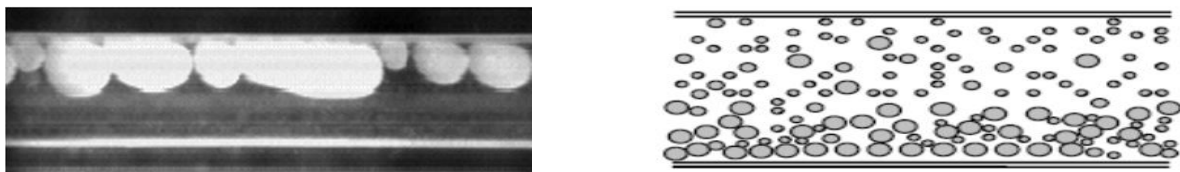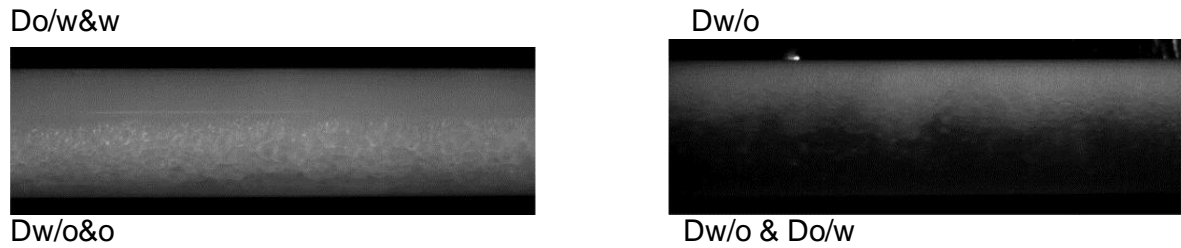
Figure 2-11 Dispersed flow patterns (Abubakar et al., 2015b; Al-Wahaibi et al., 2007)

The above flow patterns are usually shown in flow pattern maps. These are two-dimensional representation of the observed flow patterns with coordinates such as superficial gas and liquid velocities, mixture velocities or input oil ratio or fractions. An example is shown in Figure 2-12 to Figure 2-14. Flow pattern maps are constructed by identifying sets of flow conditions common to a particular flow pattern, while the continuous lines represent boundaries between the different patterns.
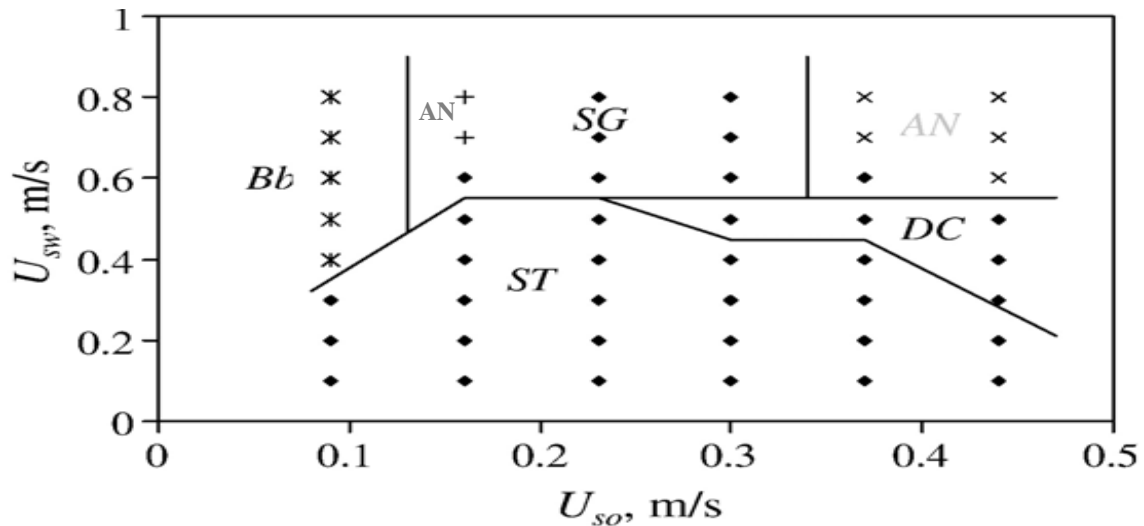
Figure 2-12 Flow pattern map for horizontal oil-water flow in a 14mmID acrylic pipe (ST-stratified, DC-dual continuous, SG-slug, Bb-bubble, AN-annular flows. Uso=superficial oil velocity, Usw-superficial water velocity (Al-Wahaibi et al., 2007)**)**
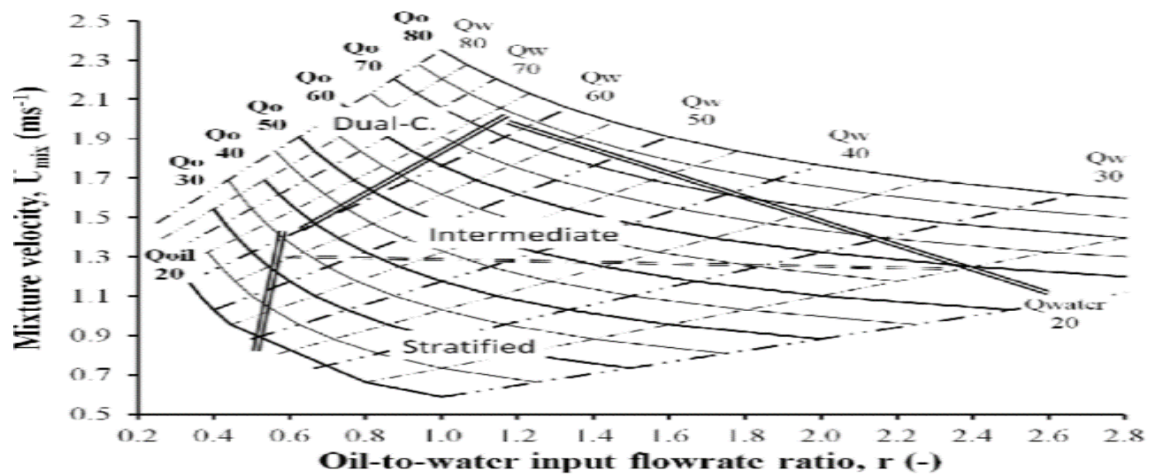
Figure 2-13 Flow pattern map for oil-water flows in a 38mmID pipe (Qo & Qw are oil and water flow rates respectively) (Barral, 2014)
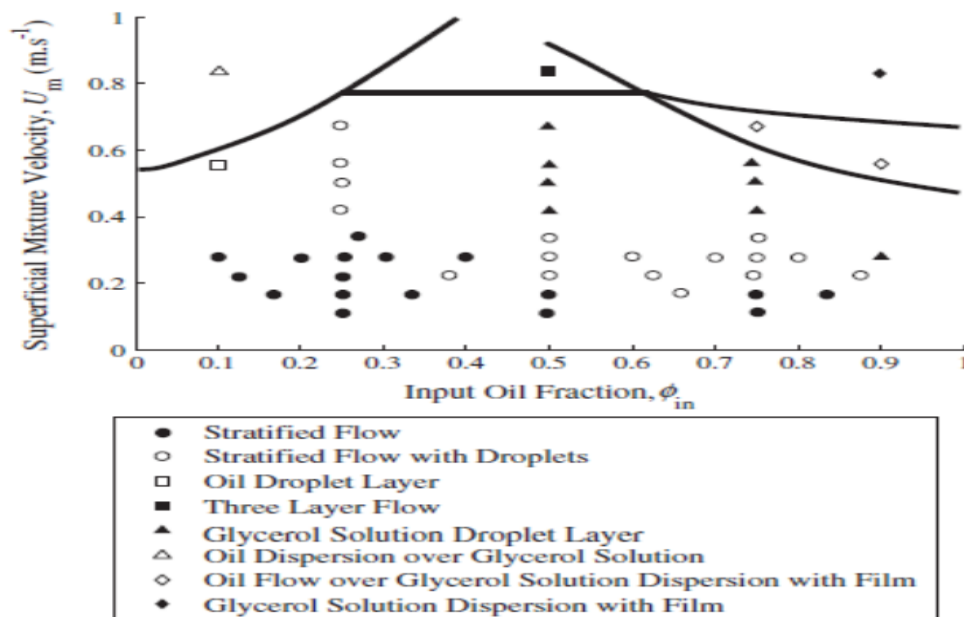
Figure 2-14 Flow pattern map for oil-glycerol solution flow in a horizontal pipe (Morgan et al., 2013)

2.6 Pressure Drop and Liquid Holdup Modelling in Multiphase Flows

An accurate prediction of the pressure drop and holdup is needed for an effective design and maintenance of the fluid transport systems (Hadžiabdić and Oliemans, 2007; Rodriguez and Baldani, 2012). For separated flows the one-dimensional two-fluid model (Al-Wahaibi and Angeli, 2007; Al-Wahaibi et al., 2007; Brauner and Moalem, 1992a; Taitel and Dukler, 1976) has been used to predict the pressure drop and liquid holdup. Its effectiveness has

been found to depend on the closure relations for the wall (oil and water) and interfacial shear stresses as well as the nature of the interface geometry.

The one-dimensional two-fluid model (2FM) is based on momentum balance equations. Two continuous fluids are considered to flow in layers in a circular pipe according to their density and assumed to be separated by a smooth and flat interface. For a fully developed steady state flow, the integral forms of the one-dimensional momentum equations for the two phases are given by:

$$- A_o \left(\frac{dp}{dz}\right) - \tau_o S_o \mp \tau_i S_i + \rho_o A_o g \sin \alpha = 0 \qquad \textbf{2-13}$$

$$- A_w \left(\frac{dp}{dz}\right) - \tau_w S_w \pm \tau_i S_i + \rho_w A_w g \sin \alpha = 0 \qquad \textbf{2-14}$$

The subscripts *i, o and w* stand for interfacial, oil and water respectively. S_i, S_o, S_w, A_o and A_w are the perimeters and areas of the respective phases. By equating the pressure drop in the two phases, the following equation is derived where *α* (the pipe inclination) is zero for horizontal flow:

$$- \frac{\tau_w S_w}{A_w} + \frac{\tau_o S_o}{A_o} + \tau_i S_i \left(\frac{1}{A_w} + \frac{1}{A_o}\right) = 0 \qquad \textbf{2-15}$$

τ_w, τ_o, τ_i are the water wall, oil wall and interfacial shear stresses respectively. Table 2-2 shows the geometric parameters used in the two-fluid model. The wall shear stresses, τ_w and τ_o are expressed in terms of the corresponding fluid friction factors; f_w and f_o:

$$\tau_w = f_w \frac{\rho_w U_w^2}{2}; \; f_w = m \, \mathrm{Re}_w^{-n} = m \left(\frac{D_w U_w \rho_w}{\mu_w}\right)^{-n} \qquad \textbf{2-16}$$

$$\tau_o = f_o \frac{\rho_o U_o^2}{2}; \; f_o = m \, \mathrm{Re}_o^{-n} = m \left(\frac{D_o U_o \rho_o}{\mu_o}\right)^{-n} \qquad \textbf{2-17}$$

The friction factors are Fanning type and the pipes are considered smooth. The coefficient m and the exponent *n* are equal to 0.046 and 0.2 respectively for turbulent flow, while 16 and 1.0 are used for laminar flow. D_w and D_o are the hydraulic diameters. Their values are based on the relative velocities of the two phases, which unlike gas-liquid flows are not necessarily different.
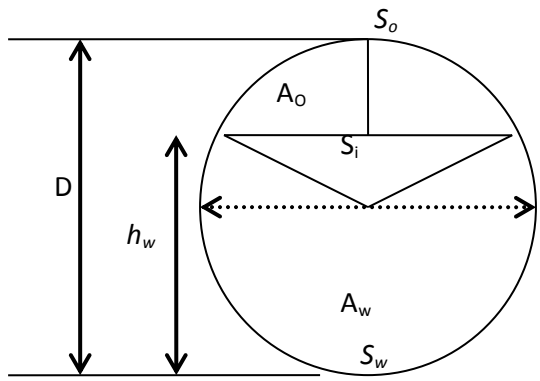
$$D_w = \frac{4A_w}{(S_w + S_i)}; \quad D_o = \frac{4A_o}{(S_o)} \quad for \quad U_w > U_o \qquad \textbf{2-18}$$

$$D_o = \frac{4A_o}{(S_o + S_i)}; \quad D_w = \frac{4A_w}{(S_w)} \quad for \quad U_w < U_o \qquad \textbf{2-19}$$

$$D_o = \frac{4A_o}{(S_o)}; \quad D_w = \frac{4A_w}{(S_w)} \quad for \quad U_w \approx U_o \qquad \textbf{2-20}$$

The parameters S_i, S_o, S_w, A_o and A_w are defined in Table 2-2

Table 2-2 Geometric parameters used in the two-fluid model (Al-Wahaibi et al., 2007)

Parameter	
Interfacial length (S_i)	$D \times \left(1 - \left(2\dfrac{h_w}{D} - 1\right)^2\right)^{0.5}$
Wall perimeter of oil phase (S_o)	$D \times \cos^{-1}\left(2\dfrac{h_w}{D} - 1\right)$
Wall perimeter of water phase (S_w)	$\pi D - S_o$
Cross sectional area of the pipe (A)	$\dfrac{\pi}{4}D^2$
Area oil phase (A_o)	$\dfrac{D}{4} \times (S_o - S_i \times (2\dfrac{h_w}{D} - 1))$
Area water phase (A_w)	$A_w = A - A_o$
Oil hold-up (H_o)	A_o/A
Water hold-up (H_w)	A_w/A
In-situ oil velocity (U_o)	U_{so}/H_o
In-situ water velocity (U_w)	U_{sw}/H_w

The interfacial shear stress is given by:

$$\tau_i = f_i \frac{\rho_i (U_o - U_w)|U_o - U_w|}{2}; \quad f_i = m Re_i^{-n} = m\left(\left(\frac{S_i}{\pi}\right)\frac{U_i \rho_i}{\mu_i}\right)^{-n} \qquad \text{2-21}$$

$$\text{where } \rho_i, U_i, \mu_i = \begin{cases} \rho_w, U_w, \mu_w & \text{if } U_w > U_o \\ \rho_o, U_o, \mu_o & \text{if } U_w < U_o \end{cases} \qquad \text{2-22}$$

When the ratio of the two phase velocities is between 0.98 and 1.05 (Brauner and Moalem, 1992a) then there is no interfacial shear stress and both phases are assumed to flow as in an open channel. In this case the hydraulic diameters are calculated by Equation 2-20. By substituting Equations 2-16 and 2-17 in Equation 2-13 or 2-14, and eliminating $\tau_i S_{i,}$ an expression for the pressure drop of the liquid-liquid system in a horizontal pipe is obtained;

$$\frac{dp}{dz} = \frac{(-\tau_w S_w - \tau_o S_o)}{A} \qquad \text{2-23}$$

where A is the cross sectional area of the pipe as defined in Table 2-2, $A = (A_w + A_o)$. The model is usually solved iteratively for different interface heights. Iterations stop when the pressure drops of the two layers becomes equal.

The inclusion of an appropriate interfacial shear stress correlation in the two-fluid model is expected to improve the predictions of pressure drop and water holdup compared to the experimental results. Arirachakaran et al. (1989) suggested that pressure gradient could be obtained from the sum of the single phase water and oil wall shear stresses averaged over the wall perimeter wetted by each phase. This procedure yielded pressure gradients that were in good agreement with experimental data at low oil and water superficial velocities where the flow was stratified with smooth interface and no slip between the phases existed. This implied that the interfacial shear stress (τ_i) could be neglected. Brauner (1991) proposed the following correlation for the interfacial friction factor f_i, for annular liquid-liquid flows where the faster flowing phase forms the core:

$$f_i = BC\left(\frac{D_c U_c \rho_c}{\mu_c}\right)^{-n} \qquad \text{2-24}$$

The interfacial shear stress τ_i is obtained by;

$$\tau_i = f_i \left(\frac{\rho_c \mathrm{U}_c^{\ 2}}{2} \right)$$

2-25

Here, D_c, μ_c, ρ_c, U_c are respectively the diameter, viscosity, density and average velocity of the core phase, B is an augmentation factor that accounts for interfacial waviness, while n and m are the constants in the friction factor-Reynolds number correlation. The value of B varies between 0.8 and 1 (Neogi et al., 1994), although Brauner (1991) suggested that B should be taken equal to 1as a result of the slight waviness of the liquid-liquid interface. Hall (1992) suggested that for flow between parallel plates, the oil wall shear stress is related to the interfacial shear stress by a proportionality factor γ, closely related to the water/oil viscosity ratio. This factor was calculated from the analytical solution of the one-dimensional momentum equations for oil–water stratified laminar flow between parallel plates. The factor γ should be less than unity since the oil phase is almost always more viscous than the water phase. According to Hall (1992) τ_i is given by:

$$\tau_i = \gamma \tau_o$$

2-26

where τ_o is the oil wall shear stress.

According to Taitel et al (1995), the interfacial friction factor should be equal to 0.0142, unless the wall friction factor of any of the phases becomes larger than this value, in which case the larger value should be used.

In the above model, interfacial waves which are known to contribute to pressure drop are not considered (Andritsos and Hanratty, 1987; Andritsos et al., 2008; Brauner and Moalem, 1993; Brauner et al., 1998; Brauner, 2002; Hadžiabdić and Oliemans, 2007). Although the use of the one-dimensional two-fluid model has yielded some success even in commercial simulators, its ineffectiveness has also been well documented. Rodriguez and Baldani, (2012) gave a detailed compendium of the works done so far. Their two-fluid model which included a correlation for the interface curvature and a modified interfacial friction factor based on experimental liquid-liquid flow and computational fluid dynamic simulations, was able to predict well their experimental results with heavy oil (viscosity of 280 mPas) and water as well as data from other works.

In most of the cited literature, the focus has been on large pipes of greater than 20 mm internal diameter while in recent years there is a growing number of papers on liquid-liquid

flows in very small pipes driven by process intensification requirements (Kim and Mudawar, 2012; Tsaoulidis et al., 2013). However, reported data on intermediate pipe sizes (10 mmID to 20 mmID) are very few in the open literature (Jin et al., 2013; Xu et al., 2010). The flow properties and geometry at these intermediate sizes are known to be greatly influenced by surface and interfacial forces, which become more significant as the diameter reduces, particularly for Eötvös number (Eo, ratio of buoyancy to surface tension forces) greater than 1.0 (Brauner and Moalem, 1992; Das et al., 2010).

2.7 Application of Laser Based Diagnostic Techniques in Fluid Flows

The study of the velocity profiles and turbulence properties of fluid flows can give more insight into the dynamics of the flow and its response to changes in flow conditions. In particular, the changes that occur when drag reducing agents are added to flow can be better understood based on the proposed mechanism of drag reduction.

Experimentally, the velocity profiles and turbulence nature in single and multiphase flows have been studied using techniques such as particle image velocimetry (PIV), particle tracking velocimetry (PTV), and laser Doppler velocimetry/anemometry (LDV/LDA). Particle image velocimetry in particular offers whole field, instantaneous velocity measurements and has been used extensively in single and in some cases in two phase flows (Adrian and Westerweel, 2011; Birvalski et al., 2014, 2013; Chaouki et al., 1997; Westerweel, 1997; Zhou et al., 2013). These techniques have also been applied in some cases to the investigation of velocity profile and turbulence properties in flows with drag reducing polymers (Gyr and Bewersdorff, 1995; Virk, 1975; Zadrazil et al., 2012).

Wei and Willmarth (1992) used LDV to study velocity fields in channel flows with PEO added in water. They found that the polymer changed the turbulence structure with the radial turbulence intensity decreasing and the axial one increasing. The authors argued that while the energy in the radial direction is suppressed over all frequencies, in the axial flow direction it is redistributed from the high to the low frequencies. Den Toonder et al. (1997) studied drag reduction, when with 20 ppm of Superfloc A110 was added in water, both numerically (DNS simulations) and experimentally using LDV. It was found that the radial root mean square (RMS) velocity decreased while the peak of the axial RMS velocity profile increased and shifted away from the wall. The turbulent energy in the axial direction redistributed from small to large scales, while in the radial direction it was dampened over

the whole pipe cross section particularly in the near-wall region. A mechanism was proposed for drag reduction based on the viscous anisotropic effects introduced by the extended polymeric chains on the turbulence structure. From their numerical simulations, they found that the elasticity of the polymeric chains also seemed to be important, with large elasticity increasing the drag reduction and vice versa.

Warholic et al. (2001) studied drag reduction in water flows with Percol 727 (a copolymer of polyacrylamide and sodium acrylate) using PIV. In the polymeric flows, there was drastic reduction or even elimination of the ejections of low momentum fluid close to the wall to the bulk flow which is characteristic of Newtonian flows. They also found a reduction of both the Reynolds and radial stresses when polymer was added. At maximum drag reduction, it was possible to have turbulent flows with zero Reynolds stresses. Zadrazil et al. (2012) used 3 different molecular weight polyethylene oxide (PEO) polymers in water in a 25.4 mmID pipe to study drag reduction with PIV. They observed that drag reduction is accompanied by the appearance of randomly formed and non-stationary thin filament-like regions of high velocity gradients that act as interfaces separating low-momentum flow regions near the pipe wall and high-momentum regions close to the pipe centre, where they eventually disappear. The thickness of the filaments was related to the level of drag reduction and increased with polymer concentration. They also reported that at a fixed polymer concentration, the thickness of the buffer layer increased with increasing polymer molecular weight which consequently increased drag reduction.

The applications of PIV to oil-water flows are very limited (Kumara et al., 2010a, 2010b, 2009; Morgan et al., 2013, 2012). There are no current studies on the effect of drag reducing polymers on the turbulent properties of oil-water flows. This is despite the significant drag reduction found in these systems and the interesting changes in flow patterns when polymers are added.

Kumara et al. (2010a) carried out measurements in a 15 m long, 56 mmID stainless steel pipe, at 0° and 5° pipe inclinations, using water and Exxsol D60 oil (density 790 kg/m^3 and viscosity 1.64 mPa s) and found good agreement between LDA and PIV measurements. Mean velocities and turbulent intensity profiles were found to depend on pipe inclination. Kumara et al. (2010b) reported that while the presence of interfacial waves enhanced turbulence fluctuations, a damping effect on the Reynolds stress was observed near the interface due to density stratification. They concluded that the high axial velocity gradients in

the near-wall region resulted in high values of the stress tensors in that region. Except for the slight distortions close the interface, the reported profiles were similar to those obtained for single phase flows. Morgan et al. (2013, 2012) studied the flow of a water/glycerol solution (density 1205 kg/m^3 and viscosity 47 mPa s) with Exxsol D80 oil (density 796 kg/m^3 and viscosity 2.3 mPa s) in a 25.4 mmID stainless steel pipe using PLIF, PTV and PIV techniques and obtained data on flow patterns, phase distribution, velocity profiles, interface level and droplet size distribution. The velocity profiles showed that the flow of the heavier and more viscous aqueous solution was always laminar while, depending on flowrates, the oil phase was either laminar or turbulent. Their experimental measurements of in-situ phase fractions and interface levels were well predicted by the two-fluid model.

2.8 Particle Image Velocimetry (PIV)

PIV belongs to a class of laser based diagnostic technique used in experimental fluid mechanics to determine instantaneous fields of the velocity vector by measuring the displacements of fine particles that accurately follow the motion of the fluid (Adrian and Westerweel, 2011). It enables optical flow visualizations and whole flow field instantaneous velocity measurements.

When it is possible to follow an individual particle because of the low concentration of the tracer particles, the method is called particle tracking velocimetry (PTV), while laser speckle velocimetry (LSV) is used when the concentration is so high that an individual particle cannot be observed in a flow image. One major advantage of PIV over other laser based flow diagnostic techniques is the ability to obtain two and three-dimensional velocity vector fields while the other techniques measure the velocity at a point. The method is non-intrusive while the added tracer particles cause negligible distortion to fluid flow.

The technique is based on taking two flow images (see Figure 2-15) in quick succession and calculating the distance particles travelled within this time. The images, with the particles, are divided into several square boxes called interrogation windows whose sizes are chosen based on processing needs. From the set time difference (Δt) between the successive images and the measured displacement the velocity of the grey scales of the particles within the interrogation windows are calculated (see Equation 2-27). This procedure is accomplished for every window in the image so as to obtain a full field velocity vector.

From Figure 2-15, if x is the displacement of particles between successive frames and Δt is the time difference (($t_o + \Delta t$) - t_o), then;

$$\text{Velocity (unit/s)} = \frac{X}{\Delta t} \qquad \textbf{2-27}$$
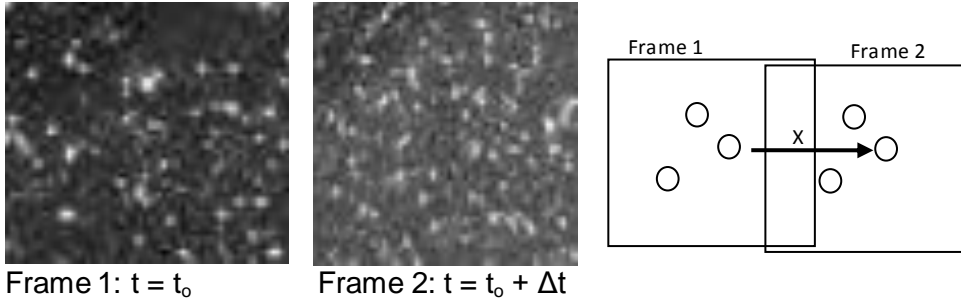
Frame 1: t = t_o Frame 2: t = t_o + Δt
Figure 2-15 PIV image frames of a single capture

The choice of the type of seeding for a particular PIV application is important to the quality and reliability of the results obtained. The particles must be able to follow the fluid flow. This is determined by the Stokes number (St) defined as follows;

$$St = \frac{u t_p}{D} \qquad \textbf{2-28}$$

Where, u is the fluid velocity of the flow well away from the wall, t_p is the time constant (or relaxation time) in the exponential decay of the particle velocity due to drag on the particle, and D is the characteristic diameter of the flow channel/pipe. The particle response time should be faster than the smallest time scale of the flow. Smaller Stokes numbers represent better tracing accuracy; for $St \gg 1$, particles will detach from a flow especially where the flow decelerates abruptly; for $St \ll 1$, particles follow fluid streamlines closely. For $St \ll 1$, tracing accuracy errors are below 1% (Brennen, 2005; Tropea et al., 2007). The particle relaxation time t_P is greatly influenced by its Reynolds number, and it is given as:

$$t_p = \frac{d_p^2 \rho_p}{18 \mu} \qquad \textbf{2-29}$$

Where μ is fluid dynamic viscosity, d_p is the particle diameter, and ρ_p is the particle density.

2.9 Conclusion

The few literature reviewed in this chapter has highlighted some of the current state of research in multiphase flows particularly in oil-water related research which is vital in improving the productive capacity of the oil and gas industry that is a main stay to the global economy. The design and operations of efficient transportation systems for oil-water

mixtures is dependent on the knowledge and understanding of the prevailing flow geometries, pressure drop and holdup as well as the mechanism by which the pressure drop is been reduced in order to minimize pumping and associated costs. Current predictive tools for pressure drop and holdup needs to be updated to improve accuracy, while an understanding of the mechanism of pressure drop reduction will enhance process design, optimization and efficiency. The experiments conducted in this current study were aimed at providing more insight and data for oil-water flows as well as the influence of high molecular weight polymeric materials on the flow and turbulence properties.

CHAPTER 3

3 INSTRUMENTATION AND EXPERIMENTAL METHODS

In this chapter the experimental flow facility, instrumentations and methods used to achieve the above objectives are described in detail. Section 3.1 describes the testing fluids used in this work. Section 3.2 shows the detailed description of the experimental flow facility while a description of the instrumentation and techniques used for flow observations and study of pressure drop and its reduction by polymer addition is given in Section 3.3. The experimental procedure for single phase water and two phase oil-water flows are presented in Section 3.4.

3.1 Working Fluids

The test fluids used in this study are tap water and a model oil EXXSOL D140 by Exxon Chemicals. The average properties of the fluids are shown in Table 3-1

Table 3-1 Properties of test fluids

	Water	Oil
Density	ρ_w =1000 kg/m^3 at 23 $^\circ$C	ρ_o= 828 kg/m^3 at 23 $^\circ$C
Viscosity	μ_w = 1 mPa s at 23 $^\circ$C	μ_o = 5.5 mPa s at 23 $^\circ$C
Surface tension	σ_w = 71.35 mN/m at 23 $^\circ$C	σ_o =21.5 mN/m at 23 $^\circ$C
Oil-water interfacial tension	39.6 mN/m at 23 $^\circ$C	

The viscosity of the oil was measured using a Contraves 155 rheometer over a range of temperatures. The surface and interfacial tension were measured using a Kruss DSA 100 tensiometer. This equipment will be described later.

3.2 Experimental Flow Facility

The experimental flow facility that was used in this investigation is located in the Multiphase Flow Laboratory in the Department of Chemical Engineering, University College London.

Figure 3-1 and Figure 3-2 show a schematic diagram and photograph respectively of the facility. The design allows for both horizontal and inclined flow operations. The flow facility is made up of three main parts: the fluid handling system, the separator and the test section. The fluid handling system consists of two tanks each with a volume of 160 litres for oil and water respectively. The separator is a gravity settler and has a capacity of about 220 litres.

Water is normally drained from the separator in most cases while the oil is recycled to the oil handling tank. The fluids from their respective storage tanks are fed separately to the test section via fixed flowrate centrifugal pumps (Procon, Sandtex; 12 l/min, 300kPa). Recycle loops and valves are used to regulate the flowrates which are measured with variable area flowmeters, separate for each fluid, and are located between the pumps and the test section. Each fluid line has two flowmeters with maximum flowrates of 7.5 l/min and 35 l/min and accuracies of 0.013 l/min (±0.2 %) and 0.06 l/min (±0.2 %) respectively for both oil and water flows. The flowmeters were calibrated for each fluid before the start of the experiments.
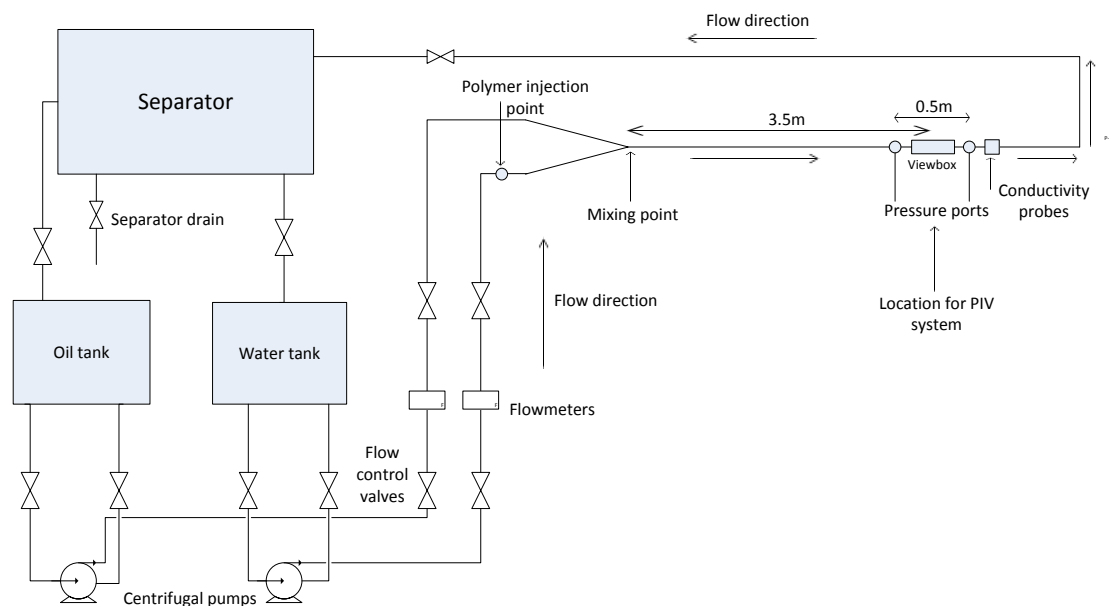
Figure 3-1 Schematics of experimental flow facility

The fluids are brought together at the beginning of the test section via a smooth Y-junction with a very small angle (30°) that ensures minimum mixing (see Figure 3-3) of the fluids at the inlet. The design is such that the oil enters from the top while the water enters from the bottom inlet. This inlet section (see Figure 3-3) is enclosed in an acrylic structure and it is mid-way between the UPVC piping from the flow meters and the acrylic test section. The structure has two 14 mm ID groves, one for either fluid (oil and water). Before the fluid mixing point, there is an acrylic mesh within the grove that acts as a filter for the fluid from the flow meters and it serves the other purpose of helping with the polymer mixing because of the jets created when the polymer carried by the water impinges on and passes through the filter. Also, the joining of the two 14 mm ID groves into a single 14 mm ID pipe section

creates flow constriction with a venturi effect and this further helps in mixing the water-soluble polymer in the water phase, before entrance to the test section.
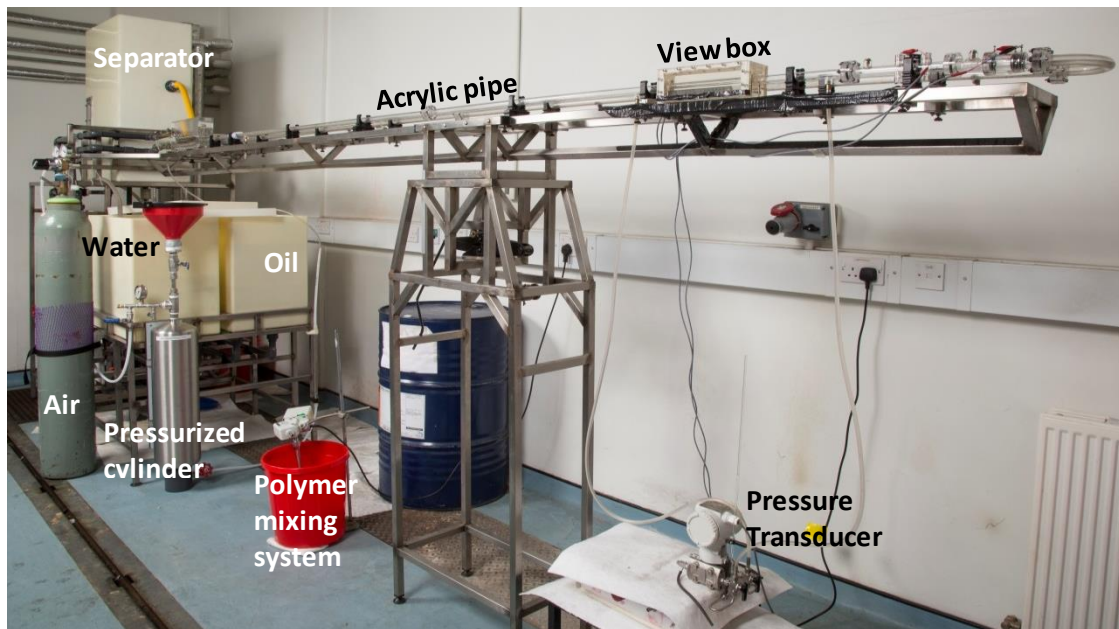
Figure 3-2 Photograph of experimental flow facility showing the test section, view box fluid handling system, separator and polymer mixing and injection systems.

The test section is a 14 mmID, 4 m long acrylic pipe made up of shorter lengths joined together with flanges that allow instrumentation to be placed at different distances from the inlet. The design of the flanges ensures a smooth joint of the pipe with no interruption to the fluid flow. After the test section the fluids return via an acrylic pipe with 14 mmID to the separator. The water holding tank was continuously filled with water. An acrylic (n = 1.489 @ 632.8 nm) view box, (Figure 3-4) filled with glycerol (n = 1.46 @ 23°C), was placed 3.5 m downstream the inlet for flow visualization and the PIV measurements. A ruler inserted in the box is used for calibration purposes.

Pressure drop was measured by a differential pressure transducer (ABB 266MST; max pressure 6.0 kPa, 0.04 % base scale accuracy) through two pressure taps, 1 mm diameter and 0.5m apart, located at 3.25 m and 3.75 m respectively from the point where the two fluids join and situated before and after the viewing box.
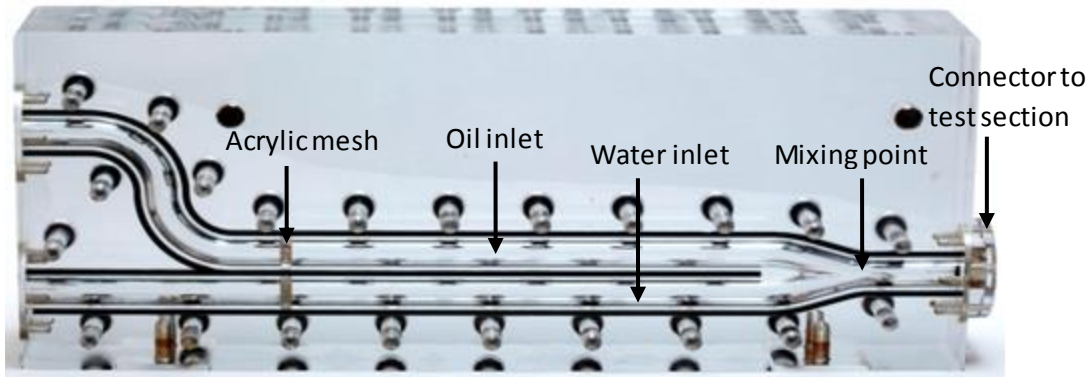
Figure 3-3 Inlet section with small Y-junction mixing point
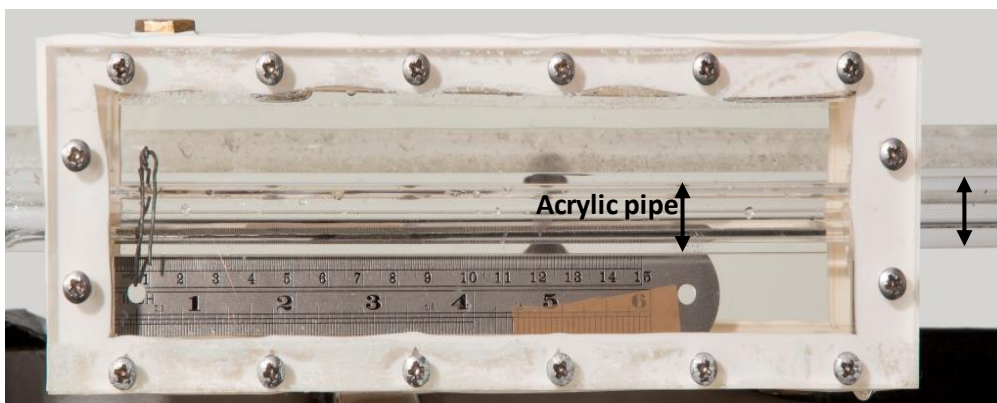
Figure 3-4 View box filled with glycerol

3.3 Instrumentation and Procedure

Different instruments were used to investigate the oil-water flows in this study without and with polymers present in water. These are described below in detail.

3.3.1 High Speed Imaging

The main objective of the high speed imaging was to identify the different flow patterns obtained under certain superficial water and oil velocities (Usw & Uso) in the flow facility. The observations were carried out with a high-speed video camera (Photron Ultima APX) loaned from the Engineering and Physical Sciences Research Council (EPSRC) Equipment Pool.

The Photron Ultima APX camera system, uses CMOS sensors with a maximum resolution of 1024 x 1024 (17µ) pixels. Flows were recorded at 2,000 fps giving about 3 seconds of recording time. The system is controlled via a Dell Optiplex 790 PC. APX processor is connected to the PC via a 1394 firewire interface. The stored images can be processed

using the Photron Ultima software with video playing capability installed in the computer. The camera was positioned opposite the view box and flow patterns were recorded for superficial oil (Uso) and water (Usw) velocities ranging from 0.008 m/s to 0.58 m/s and from 0.05 m/s to 0.80 m/s respectively. The camera was automatically calibrated, by covering the lens to obtain a black background, before image acquisition. Images were taken after about 10 minutes once the flow was started to avoid any start up effects. From the images, flow patterns, wave and characteristics in stratified flows were determined.

3.3.2 Conductivity Probes

Two conductivity probes (see Figure 3-5), a ring and wire, were located 0.1 m after the viewing box. They were used to measure the oil-water interface heights. The wire probe consists of two parallel wires 4 mm apart, stretched along a vertical pipe diameter. This probe provides a measurement of interface height over time in the middle of the pipe cross section. The ring probe consists of two metallic rings which are embedded at the circumference of the pipe, flush with the internal wall and in contact with the fluids. The rings are 0.5 mm thick, 3 mm wide and 10 mm apart. This probe measures the interface height next to the wall over time (see Figure 3-5). For each set of conditions, data were collected from the two probes at a frequency of 512 Hz and for 240 s and then averaged. The probe signals were calibrated and processed to give average interface heights following the procedure given in Barral and Angeli (2013).

3.3.2.1 Calibration of Conductivity Probes

The objective of the calibration was to develop a correlation between the conductivity signals and the interface height. The calibration was carried out using a conductivity probe system which consists of a transmitter, the two probes and the cable which connect the probes to the computer using the Labview data logging software. Both probes are part of a detachable section of the test pipe which enables cleaning and allows offline calibration. Two correlations were developed separately for the parallel wires and for the ring conductor. The electrical conductance varied with the thickness of the water layer; the thicker the film, the higher the conductance. The calibration of the probes was carried out offline using water and air, instead of oil, as air is non-conductive and easier to use. The detachable section filled with water (100 % water) was closed airtight at both ends and was placed horizontally. The signals were then read at a frequency of 512 Hz. The procedure was repeated for test section empty (0 % water). Thereafter, signals were obtained for known volumes of water

while the water height for each of the volume was easily calculated from geometric correlations. Calibration curves are shown in Figure 3-6 for both probes.
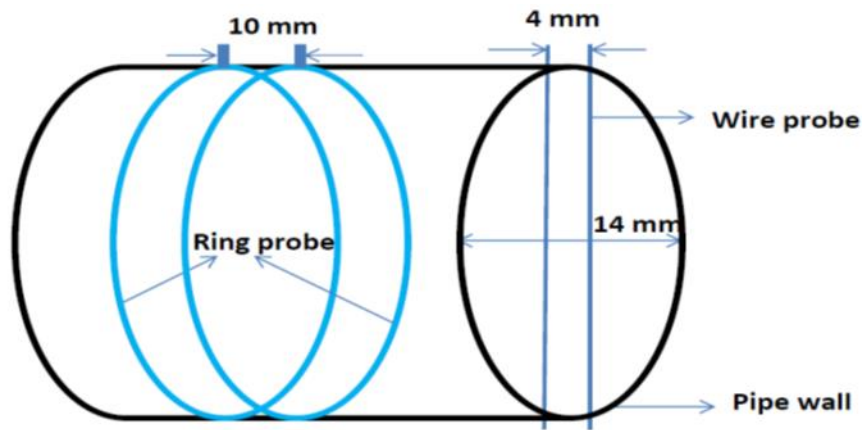
Figure 3-5 Schematics of conductivity probes

3.3.2.2   *Determination of Probe Data Collection Frequency*

The quality of comparison of experimental and predicted values of water hold-up is dependent on the accuracy of the measured interfacial heights. To this end a procedure was recently developed by Barral and Angeli (2013) for calculating the interfacial heights in oil-water flows. According to the methodology, the signals are tested for stationarity and ergodicity in order to ensure that the obtained average signals are consistent and have very small deviations. A matlab code is then used for de-trending (removing trends) the signals if trends are observed. The most appropriate frequency for collecting the signals was also determined from a test of all the possible frequencies with this system that are a power of 2, since fast Fourier transform (FFT) was to be used for further analysis of the data obtained from the probe.

Some data were obtained from the parallel probe at frequencies of 64 Hz, 128 Hz, 256 Hz, and 512 Hz for 2 minutes and oil and water superficial velocities Uso = 0.022 m/s and Usw = 0.222 m/s (see Figure 3-7). It was found that the signals were stationary but there were trends in all cases apart from 512 Hz (blue signal). This frequency was therefore selected for collection of signals. Although the signals can undergo de-trending before further analysis, it is still better to use one with little or no trend in the original data, and in most cases de-trending was not necessary.
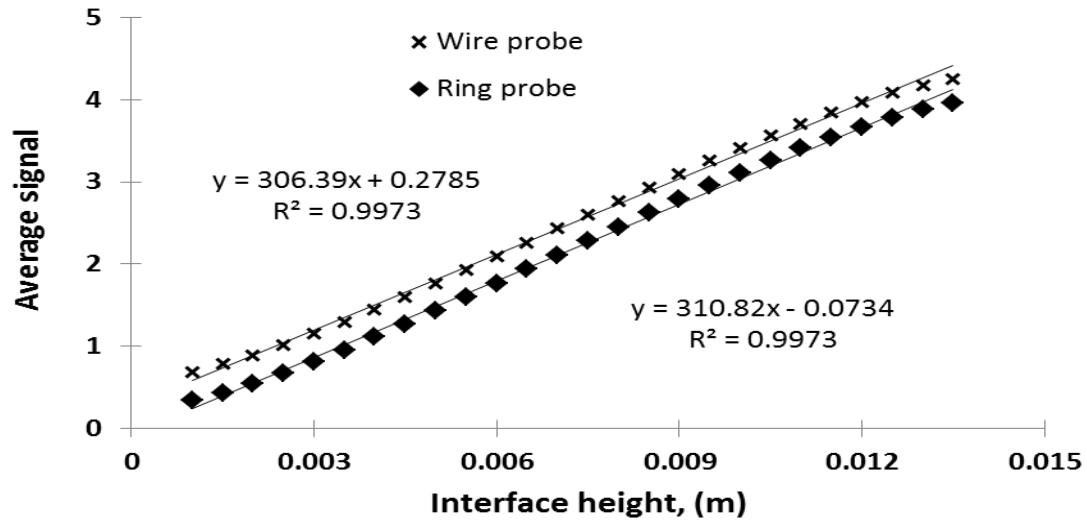
Figure 3-6 Calibration curves for conductivity probes
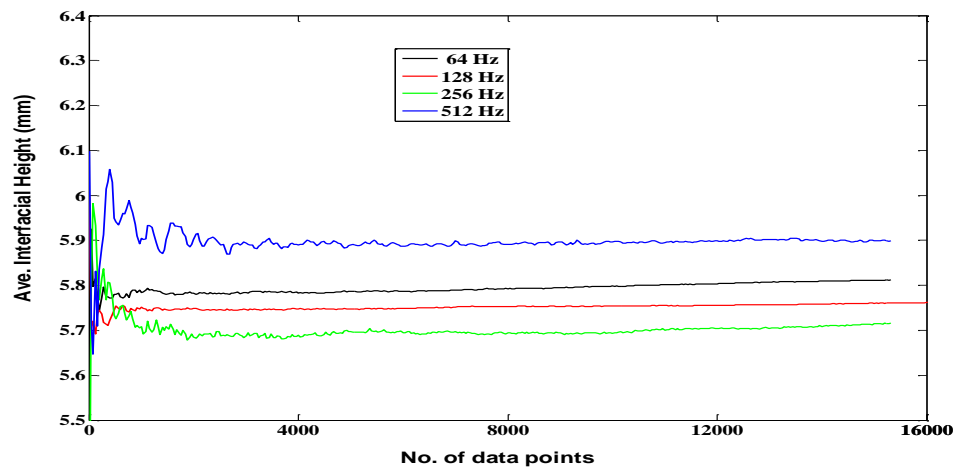
Figure 3-7 Signals obtained at different frequencies from parallel probe (Uso = 0.022m/s, Usw = 0.222m/s)

3.3.3 Polymer Preparation and Injection System

The polymers used are Magnafloc 1011, a partially hydrolysed polyacrylamide (HPAM) manufactured by BASF Chemicals and two different molecular weight (5×10^6 and 8×10^6 g/mol) polyethylene oxide (PEO) (Sigma Aldrich). All polymers were used as received without further purification. 1000 ppm of the polymer was prepared as follows. 10 g of the polymer was weighed and gently sprinkled into 10 litres of water in a vessel. The mixture was stirred at low speed (40 rpm), to minimize shear effect from the blades, for about 4 hours by a powered mechanical stirrer (Heildolph, D-91126; Figure 3-8**).** This was to ensure

uniform distribution of the polymer particles in the solution, and to avoid the formation of any lumps. The stirred solution was left for at least 12 hours (mostly overnight), before use for degassing and for proper hydration of the polymer particles. This resulted in a very clear solution (see inset, Figure 3-8) like water, with no trapped bubbles seen. It should be noted that the polymer is not soluble in the oil phase and hence it was expected to remain within the water phase in which it is very soluble.

Figure 3-8 Heildolph Mechanical stirrer for preparation of polymer solution

The polymer is introduced in the test section via a polymer injection system. Initially, a diaphragm pump (Masterflex-Model No. 07090-42 by Cole-Parmer) was used (see Figure 3-9) to deliver the polymer solution from the reservoir into the inlet section. The pump can work continuously against back pressure up to 50 psig with accuracy better than 1 % of dispensed volume. A Masterflex L/S variable speed drive controlled the flow rate of the injected polymer solution. To minimize pulsation, the outlet tube of the pump was connected to a pulse dampener (Masterflex L/S pulse dampener). The polymer reservoir is a 20 litre tank used to store the 1000 ppm master solution after preparation for a maximum of 2 days.

The calibration curve for the dosing pump with the polymer is shown in Figure 3-10. Using polymer mass balance, Equation 3-1 gives the relation for calculating the polymer injection rate for a required polymer concentration in the flow system.

Polymer flowrate, Q_p (cm³/s) = $\dfrac{C_1 \times Q_w}{C_m - C_1}$ **3-1**

where C_1 is the required in-situ polymer concentration in the test section, C_m is the concentration of the polymer master solution and Q_w is the water inlet flowrate.

Figure 3-9 Diaphragm pump for polymer injection
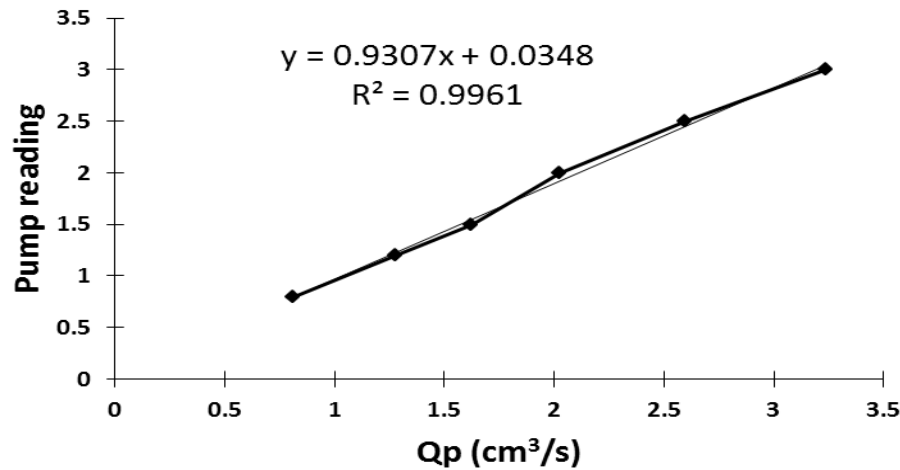
Figure 3-10 Calibration curve for polymer injection using a dosing pump

3.3.3.1 Influence of Polymer Injection Method on Interfacial Waves Characteristics

The use of the dosing pump described in the previous section was found to introduce pulsation and interfacial waves in stratified flow. These waves had the same frequency as the dosing pump and interfere with the accurate determination of the changes that occur at the interface after the addition of polymer to the flow. The frequency of the pulsation increased with polymer concentration (see Figure 3-11).
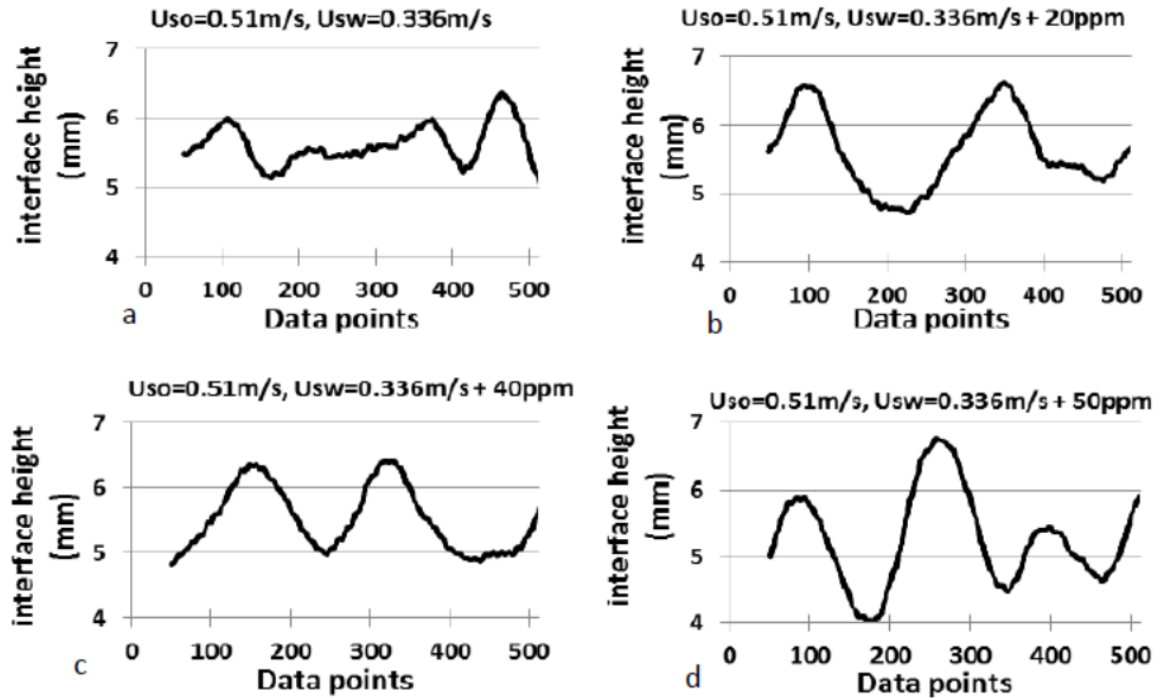
Figure 3-11 Interfacial wave structures (a–d) with single pulse dampener at different polymer concentrations

For example, the wave frequency at 50 ppm polymer concentration (obtained from the wave structure) was about 3.05 Hz while that of the pump was found to be 2.96 Hz. This observation was supported by the rise in average wave amplitude with increase in polymer concentration (see Figure 3-12), which is calculated as the standard deviation of the time-series data obtained from the wire probe. These observations are contrary to previous findings that the addition of polymer dampens the interfacial waves (Al-Wahaibi et al., 2007) and leads to reduction in wave amplitude. The results suggest that the polymer injection method affects the interfacial wave characteristics.

Two extra pulse dampeners were added in series to the single dampener of the polymer pump to minimize the pulses introduced during polymer injection. The wave amplitude was observed to reduce with the addition of polymer. Pulses, however, were still noticeable at high polymer concentrations as well as at high flow rates of the water phase, which requires higher dosing frequencies to achieve the desirable polymer concentration. The introduced pulses from the injection system do not allow the changes in wave characteristics to be studied accurately after polymer is added. Consequently, a pulseless system that uses pressurized air to push the polymer into the water flow line and with minimal shear was

designed and implemented (see Figure 3-13 and Figure 3-14). The resulting wave form was free of the pulses.
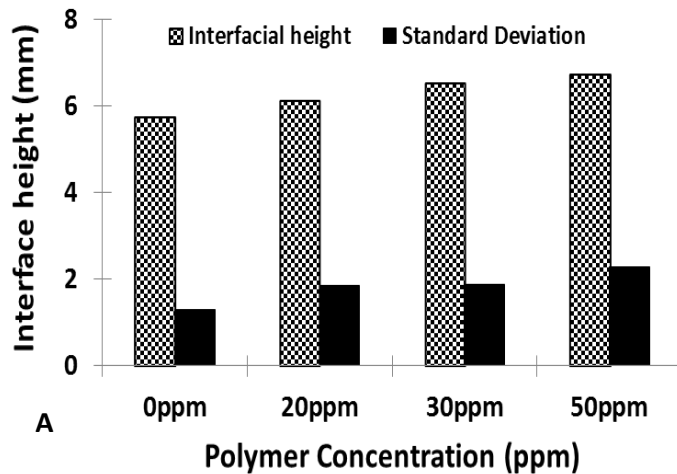
Figure 3-12 Interface height and standard deviation of data obtained from conductivity probe for a single pulse dampener

In the air-pressurized polymer injection system (Figure 3-13 and Figure 3-14), the polymer master solution is poured into an air-tight stainless steel cylindrical vessel and pressurized air from a gas cylinder at 2 bars is used to push the polymer from the cylinder into the water flow line. In this way, the pulsation from the pump dosing is eliminated. The polymer flowrate is controlled via the air flow and was measured with a flowmeter.
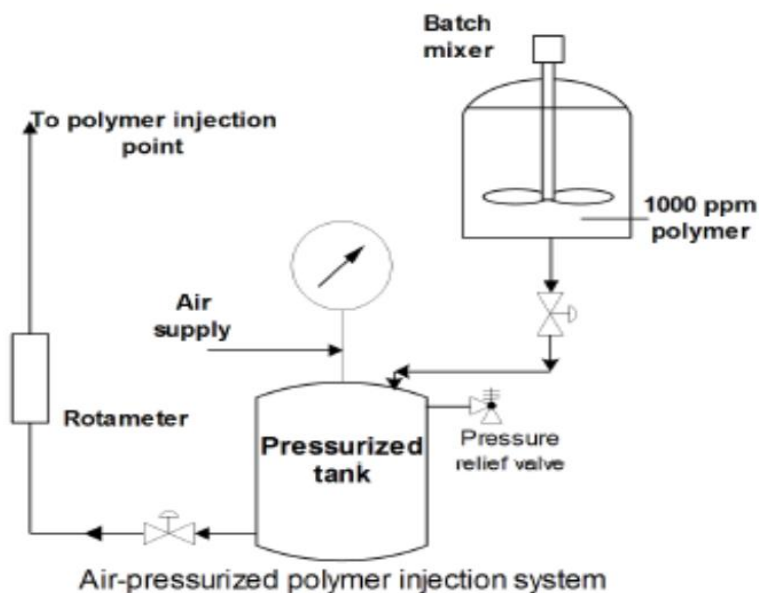
Figure 3-13 Schematics of air-pressurized polymer injection system

Figure 3-14 Photograph of pressurized polymer injection system

The water phase then flows through the acrylic mesh in the water inlet of the Y-junction (see Figure 3-3) which ensured further mixing. The location of the measurements downstream the inlet and the turbulence further enhances mixing of the highly soluble polymer with water.

The flow rate of the polymer is controlled with the use of valves and a flowmeter. The calibration of the polymer flowrate was carried out when the polymer line was not connected to the main test section but at the same vertical position where the online injection point is situated. The injection point was a single hole, 1.5 mm diameter, located at the bottom of the water inlet pipe, 0.5 m upstream the mixing point of the two fluids. The calibration was performed by measuring the volume of polymer that flows for a certain time at a particular graduation mark on the flowmeter. The calibration curve obtained is shown in Figure 3-15

The graph shows:
$y = 0.0583x^3 - 0.8557x^2 + 5.7518x - 0.1798$
$R^2 = 0.9991$

with y-axis labeled "Rotameter Reading" and x-axis labeled "Polymer Flowrate (cm^3/s)"
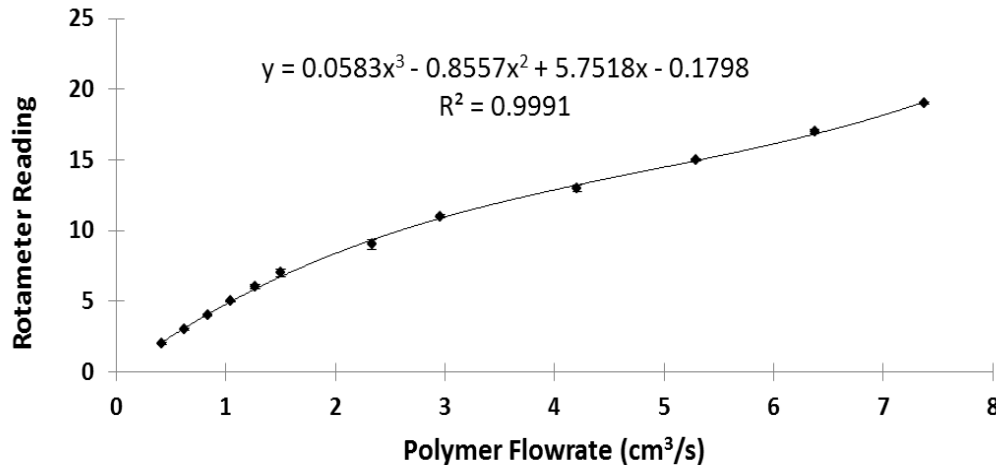
Figure 3-15 Calibration curve for polymer injection using air-pressurized system

3.3.4 Particle Image Velocimetry (PIV)

PIV was implemented in this investigation to observe the changes to the velocity and turbulences properties of water with the addition of polymer. The schematic of the setup is shown in Figure 3-16.

3.3.4.1   PIV Image Acquisition

The PIV system consists of a CCD camera, computer systems, a synchronizer and a high power (400mJ), double-pulsed, Nd:YAG (neodymium-doped yttrium aluminium garnet; Nd:Y$_3$Al$_5$O$_{12}$) laser (Litron: S65-15PIV) that generates green light (532 nm) at a frequency of 7.25 Hz.
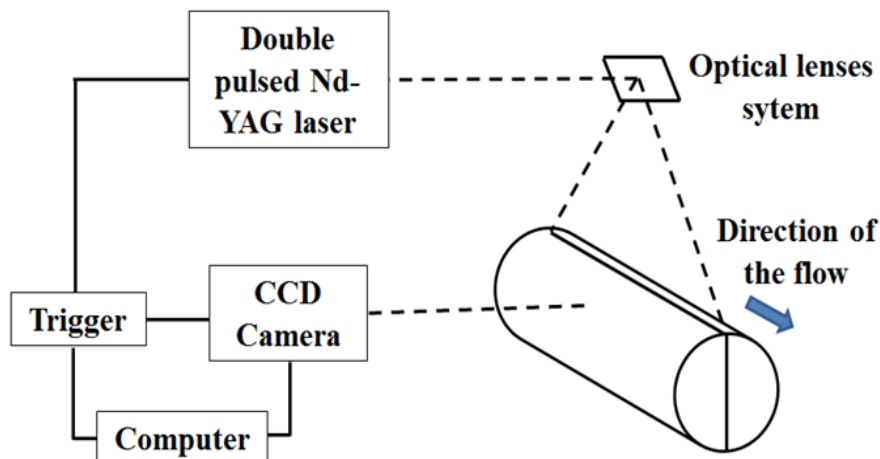
Figure 3-16 Schematics of PIV setup showing components of PIV system

The synchronizer (TSI: 610035) controls the timing of the laser pulses and image acquisition. A laser arm, which contains a set of convex and concave lenses, was used to guide the light and generate a sheet with thickness of about 1mm that illuminated the pipe exactly in the middle along the flow direction. The laser arm was fixed above the pipe (see Figure 3-16). The tracer particles needed in the PIV measurements were added in the water tank. Silver-coated glass particles (TSI: 10089-SLVR) with 12 μm diameter and density of 1220 kg/m^3 were used. Their properties are such that they can follow the flow dynamics. The Stokes number for the particles used for the conditions studied varied from 0.00012 to 0.0014 and it shows that particles followed the flow (Adrian and Westerweel, 2011; Westerweel, 1997). To obtain homogenous seeding, several trials were made until a satisfactory particle concentration of 0.02g/l was obtained and used for the rest of the experiments.

A high-resolution 4 megapixel (1024 x 1024) CCD frame straddling PowerView PIV camera (TSI) was used to visualize the flow and to acquire images at 8 fps from the view box (see Figure 3-16). The camera was equipped with a 60 mm Nikon lens, set at f/16 aperture. The time difference between laser pulses (Δt), based on flow conditions, was varied between 20 to 500 μs. Measurements were made for single phase water flow, stratified and slightly stratified wavy oil-water flows and about 400 image pairs were captured for each flow condition.

A commercial software (Insight 3G, TSI) was used for data acquisition and data analysis to obtain some turbulence properties of the flow. Further data analysis and generation of velocity and turbulence profiles was carried out using Matlab codes (see Appendix 5) developed in-house.

3.3.4.2   *PIV Image Processing*
The captured images of the flow field were cleaned by first generating a background image at minimum intensity and then subtracting it from the raw images. This procedure removes unwanted intensities and noise from the images. A rectangular mask was applied afterwards to isolate the area of interest. It should be noted that in the experiments only the water phase was seeded and the mask was placed a little distance from the interface to account for waviness. The images were then divided into a large number of interrogation windows of size 32 by 32 pixels a 50 % overlap which corresponded to 0.21 mm spatial resolution.

The pipe diameter was used for the spatial calibration of the images in order to obtain a pixel to millimetre conversion. The displacement over a set time (Δt) and the actual size of each pixel on the camera was converted to particle velocity field represented by velocity vectors. For any flow condition, the velocity field and turbulence properties were averaged over the total number of captured frames (400) (Adrian and Westerweel, 2011).

Post-processing techniques were implemented in the cases where there are zero or spurious vectors. Zero vectors can be the result of absence or blurring of tracer particles, while spurious vectors are the result of insufficient particle-image pairs, in-plane and out-of-plane loss-of-pairs as well as gradients. A median filter was used to remove the spurious vectors while interpolation from neighbouring vectors (e.g. 5 by 5) is used to fill the mixing vector spaces. A brief flow sheet for the PIV data processing is shown in Figure 3-17.
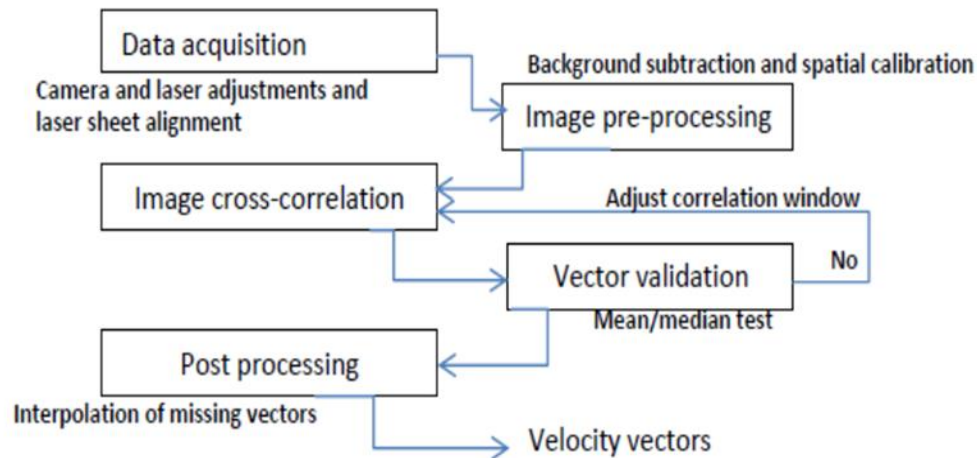
Figure 3-17 Brief flow sheet for the PIV technique

From the velocity fields generated, velocity and turbulence profiles were calculated based on established models in the literature (Adrian and Westerweel, 2011; Jahanmiri, 2011; Westerweel, 1997). The mean velocity components in the axial (U) and radial (V) direction of flow were estimated as follows:

$$U = \frac{1}{N}\sum_{i=1}^{N} u_i \qquad\qquad \textbf{3-2}$$

$$V = \frac{1}{N}\sum_{i=1}^{N} v_i \qquad\qquad \textbf{3-3}$$

Here, u_i and v_i are respectively the instantaneous velocity components in the axial and radial directions and N is the number of sample. The axial, radial and Reynolds stress components are given by:

$$\overline{u'^2} = \frac{1}{N} \sum_{i=1}^{N} (u_i - U)^2 \qquad \textbf{3-4}$$

$$\overline{v'^2} = \frac{1}{N} \sum_{i=1}^{N} (v_i - V)^2 \qquad \textbf{3-5}$$

$$\overline{u'v'} = \frac{1}{N} \sum_{i=1}^{N} (u_i - U)(v_i - V) \qquad \textbf{3-6}$$

where $\overline{u'^2}$, $\overline{v'^2}$, and $\overline{u'v'}$ are respectively the time-averaged axial, radial and Reynolds stress (or cross moments) components, while u' and v' represent the fluctuating velocity components in the axial and radial directions respectively.

3.3.5 Surface Tension

In this section, the measurement of the surface tension of the test fluids (oil and water) as well as the oil-water interfacial tension is briefly described. The surface tension obtained helps us to determine the Bond number or Eötvös number (Eo, ratio of buoyancy to surface tension forces) for the current fluid system.

3.3.5.1 Surface Tension Measurement

Surface tension measurements were performed in a Drop Shape Analyzer (KRUSS DSA100S). The DSA100S (Figure 3-18) features x, y and z axis and manual lift table, viewing angle adjuster, zoom lens, camera and different software that control dosing, illumination and shape analysis. These controls are implemented via software. It also has the capability to measure contact angle and the surface free energy of a solid. It measures the surface tension of a liquid by using Pendant Drop method which involves the determination of the profile of a drop of one liquid suspended from a needle in the bulk of another fluid at mechanical equilibrium. The profile of the drop depends on the balance between gravity and surface tension (Arashiro and Demarquette, 1999; Drelich et al., 2002).

After the drop dosing, the software automatically starts and records the raw images captured by the camera. The surface tension (or interfacial tension of a liquid in air) is calculated from the shadow image of the drop. To measure the oil-water interfacial tension, a water drop is

formed in an oil medium but not the other way round. This is due to the difficulty of having an oil drop in water as the later will always push upwards due to density/gravity effects. 4 measurements were made to improve accuracy to (±0.5 %).
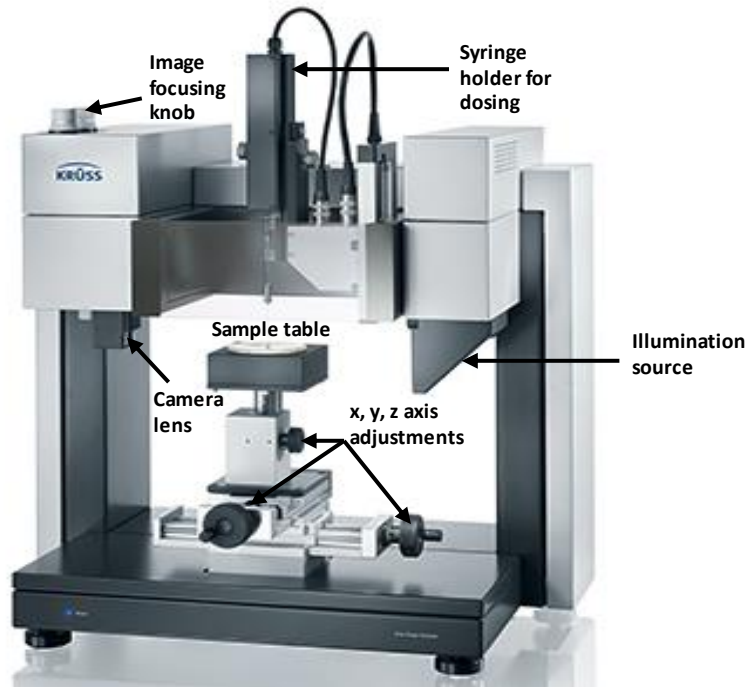
Figure 3-18 Drop shape analyzer (KRUSS DSA100S)

3.4 Pressure Drop, Flow Pattern, Drag Reduction Determination and Turbulence Measurements

This section gives the details of the experiments in single phase oil, water and two phase oil-water flows conducted in the 14mm ID acrylic pipe.

3.4.1 Single Phase Flow Experiments

Pressure drop for single phase water and oil flows were measured. The results were compared with the Blasius equation for smooth pipes. They were also used to obtain a correlation for single phase friction factor and Reynolds number. The correlation was applied in the two-fluid model for comparison between experimental and theoretical pressure drop and interfacial heights. Drag reduction experiments were also carried out in single phase water using polymer (Magnafloc 1011) concentrations of 2.5 ppm to 100 ppm from an initial master solution of 1000 ppm (Abdullah et al., 2008; Al-Wahaibi et al., 2007; Hanratty and Al-Sarkhi, 2001) and for Reynolds number from 730 to 50500. An optimal polymer concentration of 20 ppm was obtained from these test experiments. Some experiments were later conducted using the 20 ppm of two different molecular weights of PEO. PIV

measurements were also made, at selected velocities of 0.40 m/s, 0.80 m/s and 1.81 m/s, to obtain the velocity profiles and turbulence properties of water flows before and after the addition of solutions of the different polymers.

3.4.2 Experiments with Polymers and Fibers in 30 mm and 50 mm Pipes

This work was part of a short term scientific mission (STSM) funded by the European Cooperation for Science and Technology (COST) Action FP 1005 and titled "Fiber Suspension Flow Modelling". These experiments were carried out with the help of Dr Mattia Simeoni and under the supervision of Prof Marina Campolo at the Department of Chemistry, Physics and Environment of the University of Udine, Udine, Italy.

The purpose of the STSM was to perform experiments on drag reduction according to the scheduling proposed in the cooperative benchmark proposal. The study was to provide data of pressure drop versus flow rate for a significant number of test conditions in two pipe diameters (30 mm and 50 mm) which include:

1. PEO solutions at three different concentrations,
2. Fiber suspensions at three different concentrations,
3. PEO solutions with Nylon fibers at three different concentrations.

Due to instrument limitations, only polymer concentrations of 5 ppm and less were investigated. Also further tests were carried out to compare the effectiveness of polyethylene oxide (PEO) and hydrolysed polyacrylamide (HPAM) at same concentrations, water flowrates and in the different pipe sizes. However, only the PEO was added to the nylon fibers for the tests on the synergistic effects of polymers and fibers in water flows. The concentrated polymer injection method was adopted over the homogenous method (Vlachogiannis and Hanratty, 2004; Vleggaar and Tels, 1973; Wei and Willmarth, 1992) owing to its proven drag reduction efficacy. 2000 ppm master solutions of each polymer were prepared with the help of a mechanical stirrer, and injected into the water flows using a Medrad EnVision CT injector system at pre-determined flowrates to attain the required in-situ polymer concentrations. The fibers were added homogenously because they are known to be resistant to shear effect of centrifugal pumps. The tested Reynolds number ranged from 15000 to 150000 for the 30 mm pipe while it ranged from 25000 to 150000 for the 50 mm pipe. Table 3-2 shows the test materials and conditions in the course of these experiments. The pressure drop for each condition was measured with the aid of Müeller differential pressure transmitter, measuring range 0-700 mbar with adjustable span, and

error of 0.075 % of the set span. For the purpose of validation, confidence and reproducibility, measurements were first made for single phase water flows while the pressure drop was compared with theory using the Blasius correlation for turbulent friction factor determination.

Table 3-2 Flow properties and test conditions for larger pipes experiments

Test fluid	Water @ 20°C (ρ =1000 kgm^{-3}, μ = 1.0cP)
Polymers and tested concentrations	PEO; Mol. wt. 8 x10^{6} g/mol
	HPAM; Mol. wt. 10 x 10^{6} g/mol
	0.25 ppm, 0.5 ppm, 1 ppm, and 5 ppm
Fibers and tested concentrations	Polyamide nylon fibers; L/D = 120
	0.25 wt%, 0.5 wt%, and 0.75 wt%
Pipe sizes	30mm and 50mm internal diameter
Reynolds No.; 30mm	15000, 30000, 60000, 90000, 120000, and 150000
50mm	25000, 50000, 100000, and 150000

3.4.3 Two Phase Flow Experiments

Pressure drop and interface height in two-phase oil-water flows were measured before and after the addition of DRA (5 ppm to 60 ppm). The flow patterns were recorded, with the high speed camera at 1200 fps, positioned opposite the acrylic viewing box. Only the HPAM was used during flow pattern observations. Fresh water was continuously used for each run to avoid reusing of the polymer (once-through experiments) (Al-Wahaibi et al., 2012, 2007; Manfield et al., 1999). This approach prevented polymer degradation and in addition helped to keep the oil temperature low. The temperature of the oil phase was continuously monitored with a thermometer to ensure a constant temperature during the experiments. The experiments were carried out at intervals of about 50 minutes to prevent overheating of the oil phase by the centrifugal pump. The investigated superficial velocities were 0.0081 m/s to 0.58 m/s for the oil phase and 0.052 m/s to 0.80 m/s for the water phase respectively. Each of the pressure drop and interface height measurements for a particular flow condition was repeated at least 3 times and the presented results are average values with error less than 1 %.

PIV measurements were made for some selected combinations of oil-water velocities. These conditions include superficial oil velocities (Uso) of 0.11 m/s, 0.15 m/s, 0.195 m/s,

and 0.246 m/s, and superficial water velocities (Usw) from 0.166 m/s to 0.34 m/s. These velocities were restricted within the stratified and stratified-wavy flows with small amplitude waves because of difficulty of PIV measurements at highly wavy and dispersed flows (Birvalski et al., 2014; Kumara et al., 2010a). These measurements were made for all polymers and for concentration of 20 ppm.

CHAPTER 4

4 PRESSURE DROP AND HOLDUP MEASUREMENTS AND PREDICTIONS IN HORIZONTAL OIL-WATER FLOWS FOR CURVED AND WAVY INTERFACES

In this chapter, the flow geometries observed for oil-water flows in a 14 mmID pipe are reported. The corresponding measured pressure drops and interface heights for oil-water flows are presented. Modifications to the one-dimensional two-fluid model (2FM) based on the measured interface heights as well as comparisons of the modified model with available interfacial shear stress models for prediction of pressure drop and interface heights are also presented. Section 4.1 describes the observed flow patterns, while Section 4.2 presents the results of measured pressured drops and interface heights. Section 4.3 discusses the modifications to the one-dimensional two-fluid model and Section 4.4 presents the result of the prediction of the two-fluid model with different interfacial shear stress correlations. Section 4.5 shows the results of the predictions of the modified two-fluid model while the predictions of the modified two-fluid model with literature correlations on interfacial shear stress are discussed in Section 4.6. A brief summary of the chapter is given in Section 4.7.

For the purpose of validation, confidence and reproducibility, measurements were first made for single phase water flows. The experimental friction factor was compared with theory (Figure 4-1) using the Blasius correlation for turbulent friction factor determination as shown in Equations 4-1 and 4-2.

$$f = 0.0792\,\mathrm{Re}^{-0.25} \qquad\qquad \textbf{4-1}$$

$$\Delta\mathrm{P} = \frac{2f\mathrm{l}\mathrm{U}^2\rho}{\mathrm{D}} \qquad\qquad \textbf{4-2}$$

where f, ΔP, D, ρ, U, l, Re are respectively the friction factor, pressure drop, pipe diameter, fluid density, velocity, pipe length and Reynolds number. The results shows very good agreement between the measured pressure drop and those calculated from theory. The average deviation was less than 2 % of the calculated pressure drop.
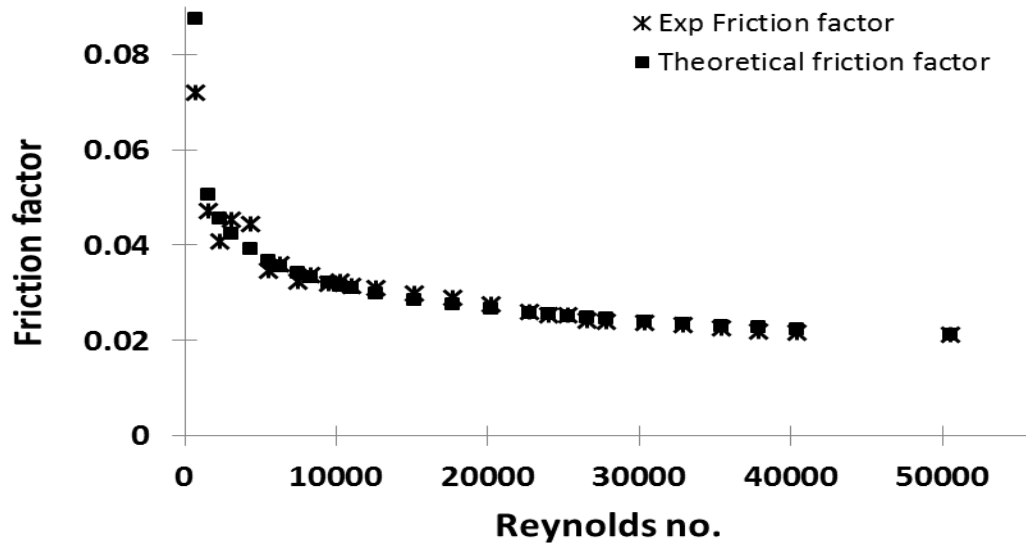
Figure 4-1 Comparison of experimental and theoretical friction factor for water flow in 14 mmID pipe.

4.1 Flow Patterns in Two Phase Flows

Here, the investigated flow conditions ranged from Uso = 0.0081 to 0.58 m/s and Usw = 0.052 to 0.80 m/s. The flow pattern map and flow patterns observed under the flow conditions studied are shown in Figure 4-2.
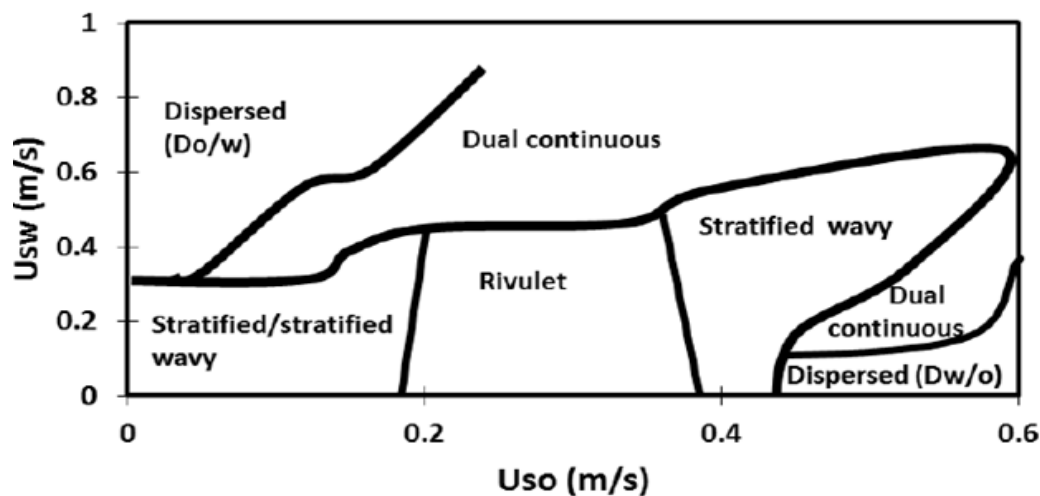
Figure 4-2 flow pattern map for oil-water flow in 14mmID acrylic pipe

Stratified and stratified-wavy flows were observed for a wide range of superficial water and oil velocities. As the phase velocities increased beyond 0.10 m/s, the interface became notably wavy, while the amplitude of the waves increased as the transition to other patterns approached (see Figure 4-2 and Figure 4-3 a&b). Results from the conductivity probe

indicate that there are always waves present at the interface, which for low velocities are very long with small amplitudes that are not easily observed visually; in these cases the flow in recordings appears as stratified smooth (see for example Figure 4-3a).
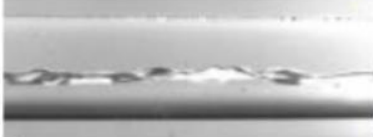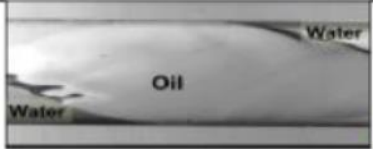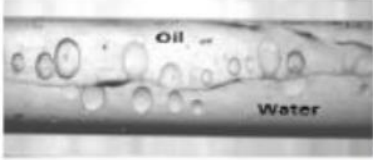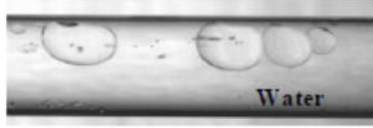
Flow patterns	Images
Stratified flow	(a)
Stratified wavy flow	(b)
Rivulet flow	(c)
Dual continuous flow	(d)
Dispersed (oil in water)	(e)
Dispersed (oil in water)	(f)
Dispersed (water in oil)	(g)

Figure 4-3 Flow patterns for oil-water flows in horizontal 14mmID acrylic pipe

At Usw < 0.34 m/s and Uso > 0.15 m/s, rivulet flow (see Figure 4-2 and Figure 4-3c) was observed. The two fluids appear to flow in a helical way along the pipe, following the path of least resistance. Sometimes at around Uso = 0.20 m/s and Usw = 0.10 m/s to 0.30 m/s, the rivulet flow would change to stratified after a long time.

These conditions are in the boundary between the two flow patterns. As the oil velocity further increased for a fixed water velocity, the rivulet flow would become disturbed and change to stratified-wavy at Uso > 0.39 m/s. The spiral frequency of the rivulets depended on the difference between the superficial oil and water velocities; for a fixed oil velocity, the frequency reduced with increasing water velocity. At Usw > 0.336 m/s and Uso > 0.07 m/s, the pattern was dual continuous (see Figure 4-2 and Figure 4-3d) with drops of each phase into the other. With increasing phase and mixture velocity the number of drops increased but their size decreased. The observed sizes ranged from around 0.1D to 0.3D (where D is the pipe internal diameter). Interestingly, when the drops were present there was no significant interfacial waviness.

Dispersed flows were seen at low oil and high water velocities, Uso < 0.20 m/s and Usw > 0.34 m/s (Dispersed oil-in-water, Do/w) (see Figure 4-2 and Figure 4-3e) and at low water and high oil velocities Uso > 0.45 m/s and Usw < 0.20 m/s (Dispersed water-in-oil, Dw/o) (see Figure 4-2 and Figure 4-3g). In both types of dispersions, the drop size decreased and their number increased as the continuous phase velocity increased which can be observed in Figure 4-2e and Figure 4-2f. It is interesting to note that within the region of velocities investigated, there were no steady annular and slug flows. They appeared for a short time in between changes in superficial fluid velocities before a new steady state flow was achieved, mainly for Usw from 0.30 m/s to 0.60 m/s and Uso from 0.15 m/s to 0.35 m/s.

The flow patterns observed in this investigation are similar to the results by Xu et al (2010), who carried out experiments in a 20 mmID horizontal acrylic resin pipe using fluids with similar properties as in this study (water and diesel oil with μ_o = 5.5 mPa s and ρ_o = 830 kg/m^3). However, they did not observe any rivulet flow pattern.

Rivulet flows are considered to be unique to pipes of small diameter where surface and interfacial phenomena become important. The Eötvös number for the system used in this work is 4.78, indicating that the pipe can be considered small (Brauner and Moalem, 1992; Panton and Barajas, 1993). Similarly, Das et al (2010), observed rivulet flow in a 12 mmID pipe. In their case the pattern was seen at higher superficial water and kerosene velocities than in this investigation, probably as a result of different fluid properties and pipe sizes. Other investigators (Al-Wahaibi et al., 2012; Al-Yaari et al., 2012) though worked with oil and water also did not observe rivulet flow while using their 25.4mmID pipes. The Eötvös

number of these systems may be beyond the range considered as small pipes and hence implies reduced nature of the surface forces present in the flow systems.

Using the same fluids and test section Al-Wahaibi et al (2007) observed stratified and dispersed oil-in-water flows at the same superficial velocity ranges as in the current work. However, the region where they observed dual continuous flow was found to be stratified wavy in this study. Al-Wahaibi et al (2007) also found annular flow at high fluid velocities (Usw > 0.60 m/s and Uso > 0.35 m/s) in the same region where dual continuous flow is seen in this work but did not report rivulet and dispersed water-in-oil flows. In addition, they recorded steady slug flow at Uso = 0.16 m/s to 0.33 m/s and Usw > 0.60 m/s where the transient slug flow and upper boundary of dispersed oil-in-water (Do/w) flow appear in the current work. The differences could be due to the inlet geometries used in the two studies; in Al-Wahaibi et al (2007) a Y-inlet was used that had a wider angle than the inlet used in the current work.

4.2 Pressure Drop Measurements in Oil-Water Flows

Some pressure drop data for the range of flowrates studied in oil-water flow are shown in Figure 4-4 and Figure 4-5. Here;

$$\text{Oil input fraction (\%)} = \frac{\text{Uso}}{\text{Usw} + \text{Uso}} \times 100 \qquad \textbf{4-3}$$

$$\text{Oil input ratio (r)} = \frac{\text{Uso}}{\text{Usw}} \qquad \textbf{4-4}$$

$$\text{Mixture velocity (Umix), m/s} = \text{Uso} + \text{Usw} \qquad \textbf{4-5}$$

As can be seen, pressure drop increases with increased oil input fractions for a constant Usw, but remains almost constant with increasing input ratio for a fixed Umix (see Figure 4-5 and Figure 4-5.). The observation suggests that the mixture velocity affects the pressure drop but the oil to water input ratio for a particular mixture velocity is not as important probably because the two phases have properties, and particularly viscosity, that are quite low (see Table 3-1). This same observation was reported in experiments conducted in a 38 mmID acrylic pipe using same test fluids (Barral, 2014; Barral et al., 2013). It can also be observed from Figure 4-4 that for oil fraction > 7 % and > 65 % at Usw = 0.052 m/s and 0.166 m/s respectively, the increase in pressure drop with Uso is more steep, while the error bars are larger. In this region, rivulet flow was observed. The flow at Usw = 0.393 m/s is outside the region of the rivulet flow hence the steady and regular increase in pressure drop.

The measured pressure gradients agree with values from previous reports (Al-Wahaibi et al., 2007; Al-Wahaibi, 2006).
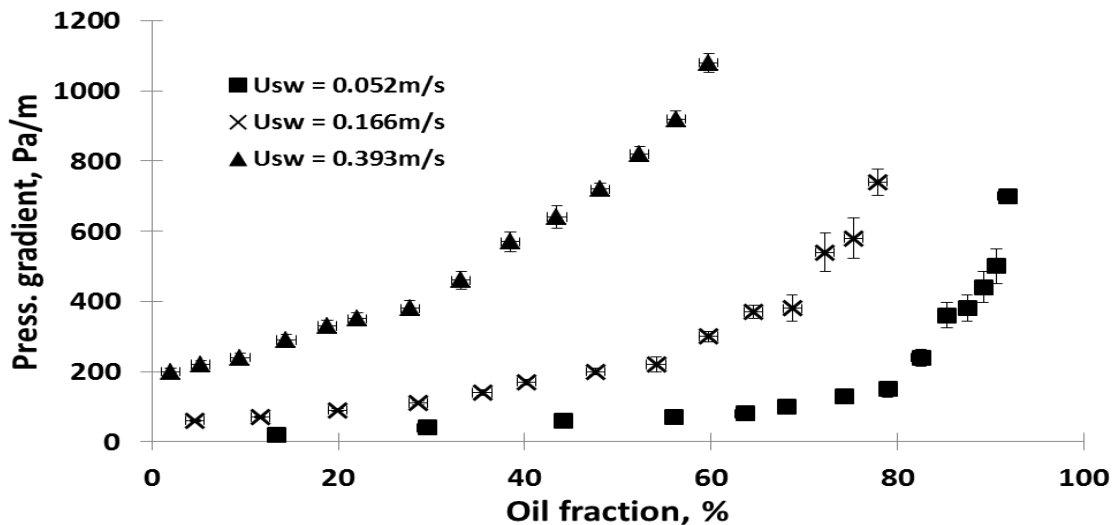
Figure 4-4 Pressure drop vs. input oil fraction for different water superficial velocities
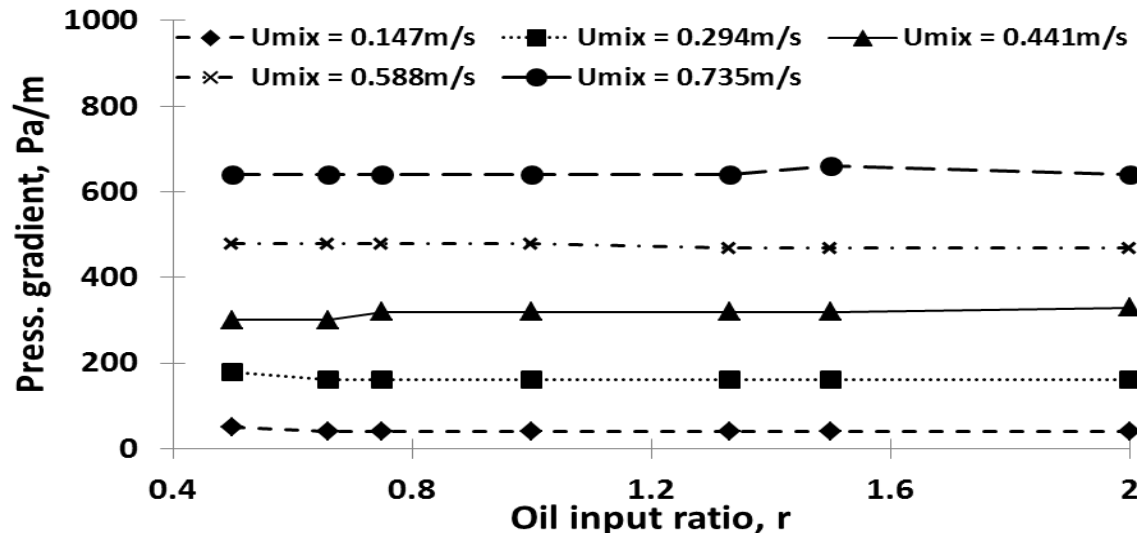
Figure 4-5 Pressure drop vs. oil input fraction for different mixture velocity (Umix)

Figure 4-6 shows the results obtained when the two-fluid model (2FM) (Brauner and Moalem, 1992a; Taitel and Duckler, 1976), developed for separated flows, was used to predict the pressure drop. Only the data points within the stratified regions (stratified, stratified wavy, rivulet and the early stages of dual continuous flow) have been included.

The pattern for water velocities Usw = 0.052 m/s and 0.166 m/s is stratified while for Usw = 0.393 m/s is at the transition boundary from stratified to mainly dual continuous flow (both phases are continuous but there is dispersion of one phase into the other).
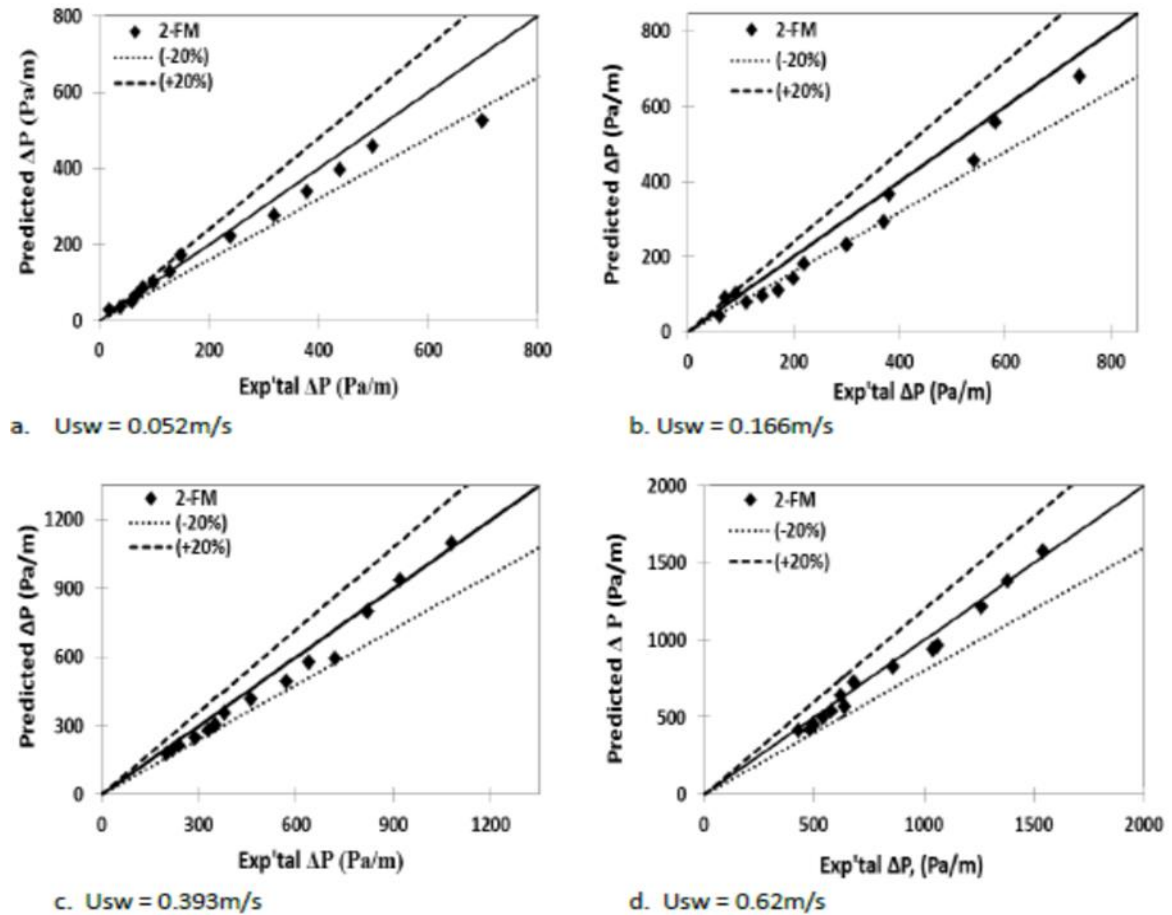
Figure 4-6 Experimental and predicted pressure drop for different water superficial velocity (a-d) and oil volume fraction

The patterns at Usw = 0.62 m/s are dispersed (oil-in-water) and mainly dual continuous flows. It can be observed that there is a good agreement (within ± 20 %) for volume fractions from 0 to 70 % particularly for Usw 0.393 m/s and 0.62 m/s (see Figure 4-6). The apparent inaccuracies of the prediction at Usw = 0.052 m/s and 0.166 m/s for volume fractions larger than 80 % and 50 % respectively, may be due to the nature of the flow. As discussed above these regions are within the rivulet flow and close to the transition boundaries to stratified wavy and dual continuous flow. The high oil fraction (low water fraction) in these regions can cause flow fluctuations and high interfacial disturbances resulting in irregular pressure drop measurements. The prediction in the dual continuous flow region was very good. Some investigators (Brauner et al., 1998) have observed that the liquid-liquid interface is curved and this can have an implication on the prediction accuracy of the two-fluid model. In addition, interfacial waves are not taken into account which would also make the predictions

less accurate (Andritsos and Hanratty, 1987; Andritsos et al., 2008; Hadžiabdić and Oliemans, 2007).

4.3 Modifications to the Two-Fluid Model

In what follows, only data within the separated regions (stratified, stratified wavy and rivulet) are used to compare against the predictions of the two-fluid model (see appendix 3a). The experimental results on average interface height from the two probes are shown in Figure 4-7.
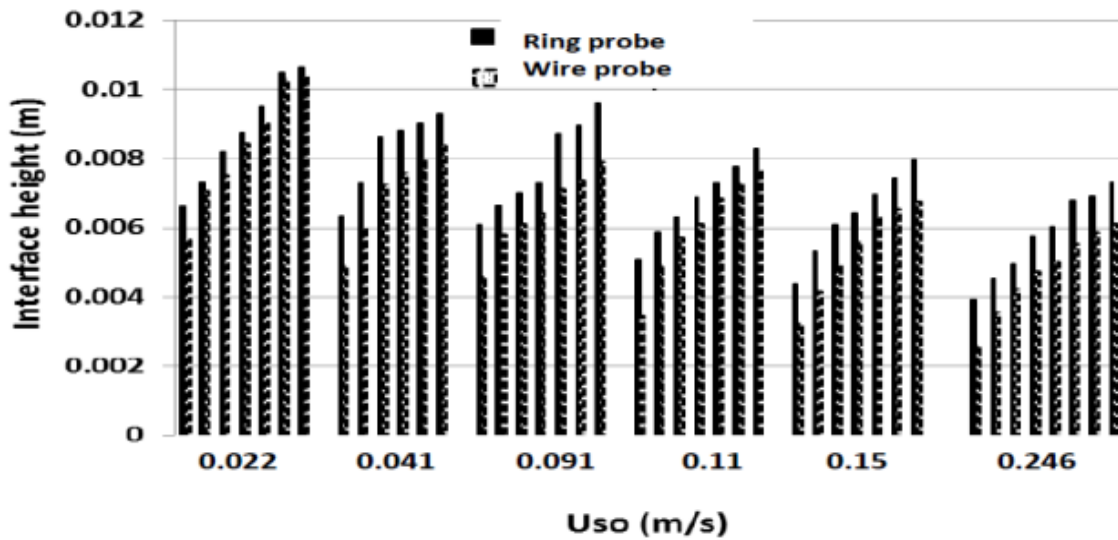
Figure 4-7 Comparison of interface height from the two conductivity probes at the different superficial oil velocities for superficial water velocities Usw = 0.052, 0.11, 0.166, 0.22, 0.28, 0.336, 0.393 and 0.45 m/s respectively from left to right

As can be seen the average interface height at the wall (given by the ring probe) is always higher than in the middle of the pipe (given by the wire probe), suggesting a curved interface shape with a concave geometry. Based on all the data collected, it was found that the interface height at the wall, h_w, and the interface height in the middle of the pipe, h_b, can be related as follows:

$$h_b = \frac{1.065 h_w \mathrm{D}}{0.014} - 0.0009 \qquad \textbf{4-6}$$

where D, h_w and h_b are measured in meter (m). Equation 4-6 is for the current pipe size and has not been tested on other pipe sizes.

The experimental interface heights from both probes are compared against the predictions of the standard two-fluid model (2FM) in Figure 4-8.
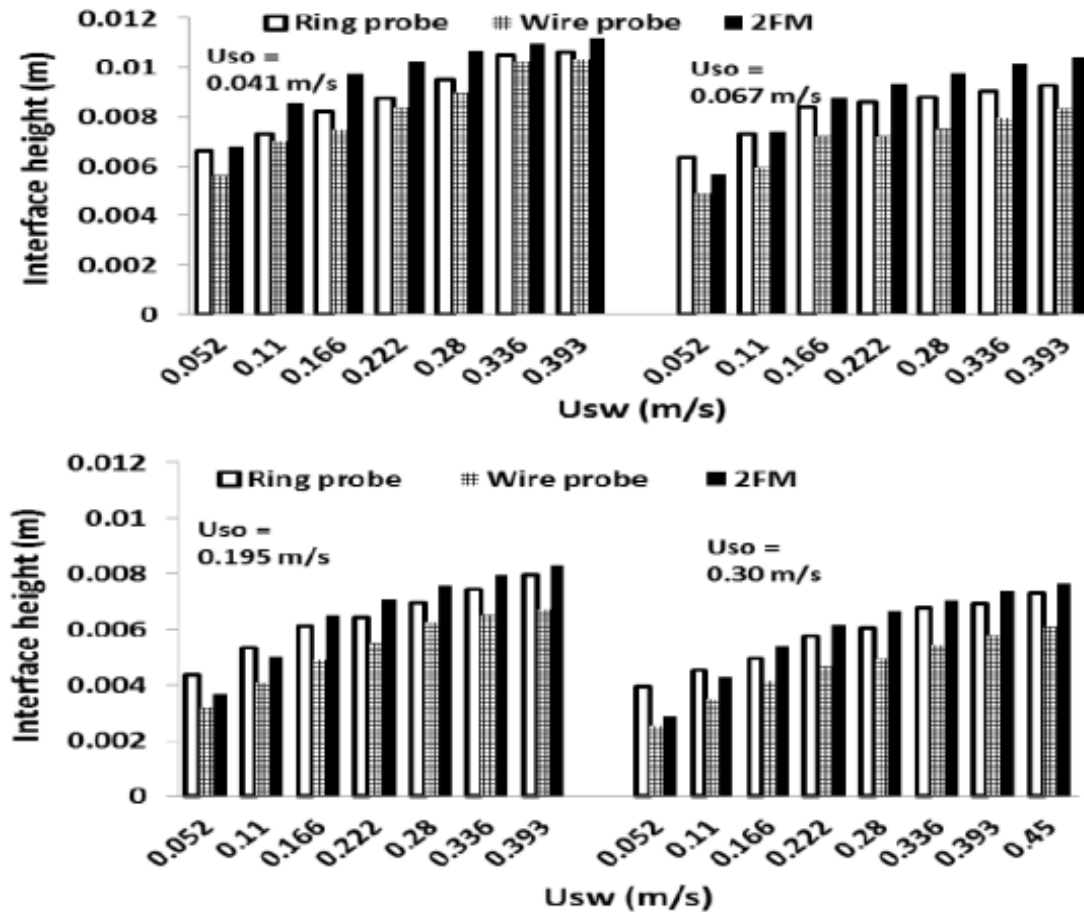
Figure 4-8 Comparison of the experimental interface heights from the two conductivity probes with the predictions of the two-fluid model

As can be seen, there is reasonable agreement between predictions and experiments, in particular for the data from the ring probe. This is reflecting the importance of the wall wetted perimeters on the calculation of shear stresses in the two-fluid model. The model gives higher interface heights than the experimental ones, apart from superficial water velocities, Usw, below 0.166 m/s; for these velocities the predictions are in fact closer to the data from the wire probe. The change from under- to over-prediction at Usw > 0.11 m/s coincides with the change in the friction factor constants used for the water phase, from the laminar to the turbulent values. At Usw < 0.166 m/s the Reynolds numbers for water lie between 1600 and 2600 but in the model the friction factor constants for laminar flow are used. In these conditions the oil phase is clearly laminar with Reynolds numbers below 1600. The model

predictions agreed better with the experimental data when a Reynolds number of 1500 instead of 2100 was used for the transition from laminar to turbulent flow.

In a similar vein, it was observed that, as expected, the interface height reduced with increase in oil input ratio for a fixed mixture velocity. Moreover, for a fixed input ratio, the interface height was observed to be lower for mixture velocities ≤ 0.441 m/s and then increased to a stable value thereafter. This observation was particularly for input ratios < 1.5 and could be attributed to the impact of the viscous forces from the more viscous oil phase at low flow rates. However, at higher mixture velocities, the inertial forces dominate the flows and the interface heights therefore attain a stable value. Note here that the viscosity of the oil phase is 5.5 times that of water.

The interface height time series data from the probes show that there are always waves at the interface even at low phase velocities. It has been suggested that waves can be considered as interfacial roughness and should be included in the interfacial shear stress term of the two-fluid model (de Castro et al., 2012; Hadžiabdić and Oliemans, 2007). From the time series data of the wire probe, the interfacial waves were found to have average amplitude of 0.0005 m ± 0.0002 m for the range of velocities studied. This value was used as roughness in the interfacial friction factor correlation proposed by Rodriguez and Baldani (2012):

$$f_i = f_k \left[1 + C_i\, \alpha/\mathrm{D}\right] \qquad\qquad \textbf{4-7}$$

where C_i is a correction factor taken as 50 (Rodriguez and Baldani, 2012), α is the interfacial wave amplitude and f_k is the wall friction factor of the faster phase.

4.3.1 Geometric Parameters of the Two-Fluid Model with Curved Interface

The two-fluid model as earlier described was modified to account for the interface curvature found experimentally. A schematic showing the geometric parameters of the stratified oil-water flow with curved interface is given in Figure 4-9. R is the radius of the circle with center C which gives the appropriate interface curvature. The various geometric parameters needed for the two-fluid model when the interface is curved are calculated as follows:

Wall wetted perimeter of the oil phase, $S_o = \mathrm{D} \times Cos^{-1}(2h_w/\mathrm{D} - 1)$ **4-8**

Wall wetted perimeter of the water phase, $S_w = \pi * \mathrm{D} - S_o$ **4-9**

Interfacial length, $Si = \beta * R$ **4-10**

Area of oil phase, $A_o = 0.5(S_i * R - R^2 Sin\beta) + 0.25D * S_o - 2X(2h_w - D)$ **4-11**

Area of water phase, $A_w = 0.25\pi * D^2 - A_o$ **4-12**

Equations 4-8 to 4-12 are used to calculate the other parameters of the two-fluid model as discussed in Section 2.6. The pressure drops for the two phases; oil (dp_o/dz) and water (dp_w/dz) are calculated for different interface heights from Equations 4-13 and 4-14 and the interface height where the difference in the two pressure drops is less than 0.0001 is taken as the solution.

$$\frac{dp_o}{dz} = \frac{\tau_o S_o + \tau i S_i}{(-A_o)}$$ **4-13**

$$\frac{dp_w}{dz} = \frac{\tau_w S_w - \tau_i S_i}{(-A_w)}$$ **4-14**

Table 4-1 shows the pressure drop data obtained experimentally in the separated flow regions. A table showing pressure gradient for all tested conditions and flowrates is shown in Appendix Table 1.

Table 4-1 Pressure gradient (Pa/m) for oil-water flow obtained in the 14 mmID acrylic pipe for stratified and stratified-wavy flow geometries

*Usw (m/s)	+Uso (m/s)						
	0.022	0.067	0.11	0.195	0.30	0.432	0.51
0.052	40	70	100	120	360	440	
0.11	60	90	140	180	300	480	
0.166	80	110	180	220	370	540	
0.222	110	150	210	280	480	620	
0.28	140	180	250	320	500	720	800
0.336	180	240	300	380	570	740	840
0.393				460	640	820	920
0.45				500	720	920	1020
0.51						1040	1160
0.563						1160	1280
0.62							1380
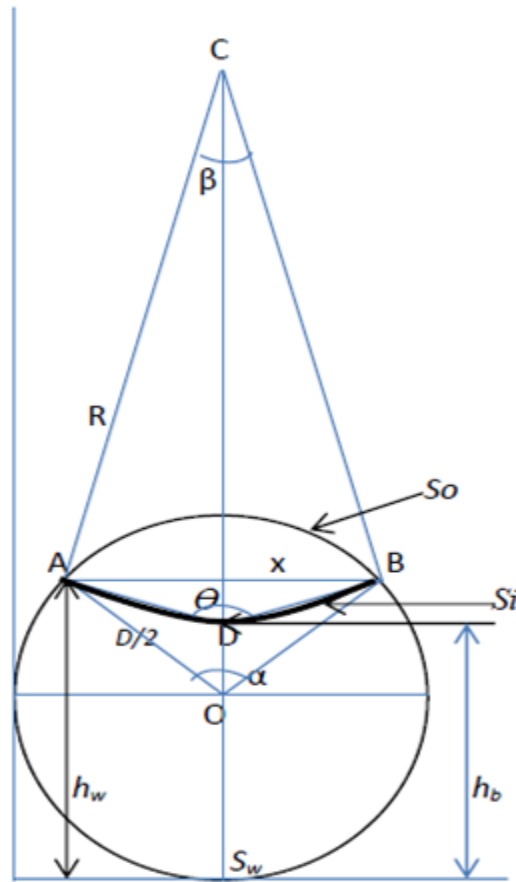
Figure 4-9 Geometric parameters used in the two-fluid model with curved interface. The thick curved line within the circle represents the curved interface in this instance

4.4 Predictions of Two-Fluid Model with Different Interfacial Shear Stress Correlations

The experimental data on pressure drop within the separated flow regions (see Table 4-1) are compared in Figure 4-10 against the predictions of the standard two-fluid model with different interfacial shear stress correlations (Brauner, 1991; Hall, 1992; Taitel et al, 1995; see section 2.6). Different values of the friction factor-Reynolds number correlation constants (Equations 2-16 and 2-17) for turbulent flow were used with m = 0.046, n = 0.2 in Figure 4-10a; and m = 0.0792, n = 0.25 (Blasius correlation) in Figure 4-10b.

As can be seen, the values of the friction factor-Reynolds number constants affect the pressure drop predictions with the Blasius constants giving better results. The constants used for Figure 4-10a are suitable for Reynolds numbers greater than 10^5, while the Blasius equation (Figure 4-10b) is recommended for Reynolds numbers between 2500 and 10^5. In fact, the phase Reynolds numbers for the conditions investigated were below 10^5. Based on

the improved predictions, the Blasius correlation will be used for further calculations. From the various interfacial stress models, the standard two-fluid model (2FM) agreed better with the experimental data in Figure 4-10a, while the models by Brauner (1991) and Taitel et al. (1995) gave better predictions in Figure 4-10b in terms of average value and standard deviation respectively.
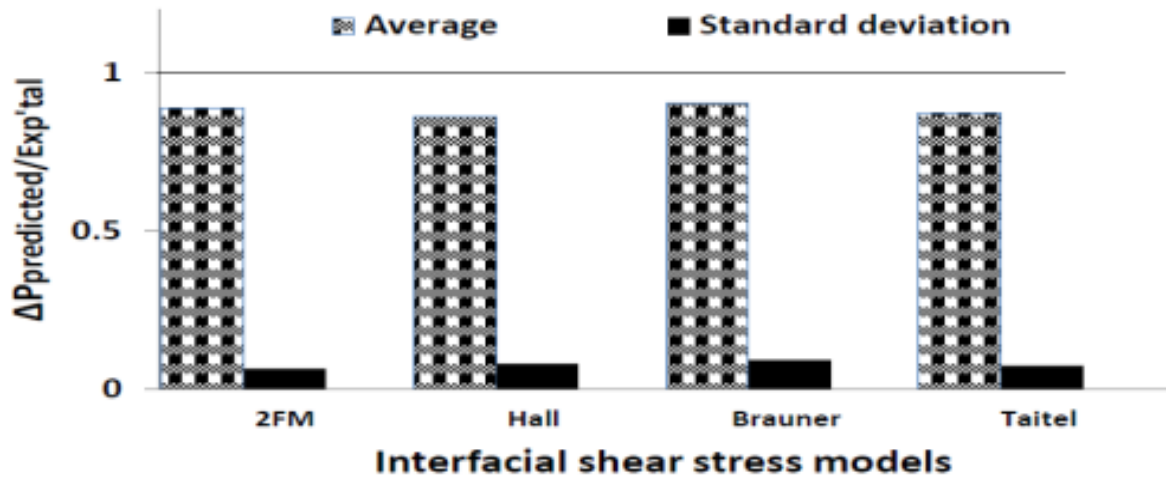
(a)
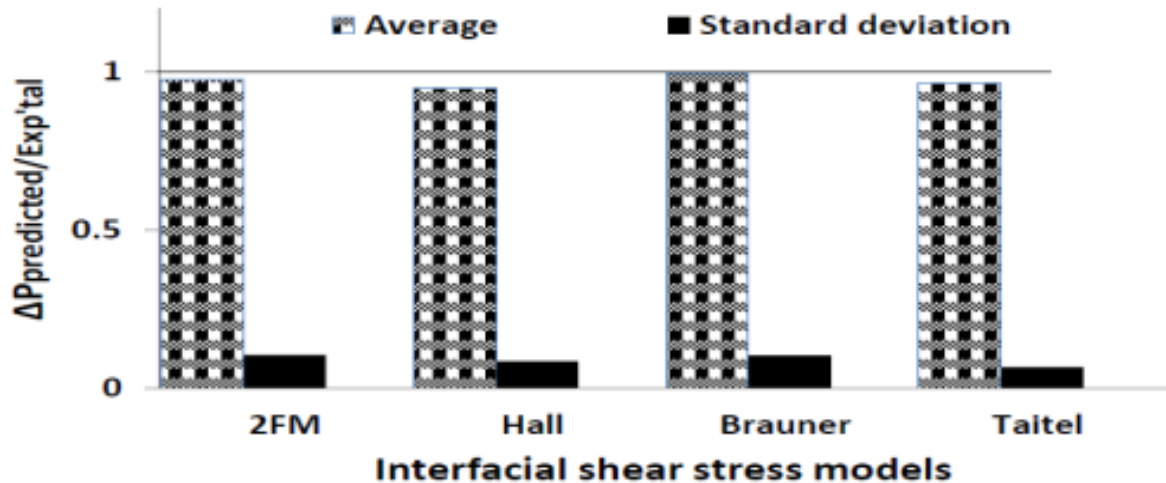
(b)

Figure 4-10 Comparison of experimental pressure drop values against the ones predicted from the two-fluid model using different interfacial shear stress correlations. Constants in Equation 2-16 are (a) m=0.046, *n*=0.2 (b) m=0.0792, *n*=0.25. The pairs of oil and water superficial velocities used for the comparison are as shown in Table 4-1

4.5 Predictions of the Modified Two-Fluid Model

The average predictions of the two-fluid model (2FM) on pressure drop, including the effects of interfacial waviness and interface curvature are shown in Figure 4-11. The effects of interface roughness (model 2FM+R) and of interface curvature (2FM+CI) are considered separately initially and are then combined in the 2FM+R+CI model
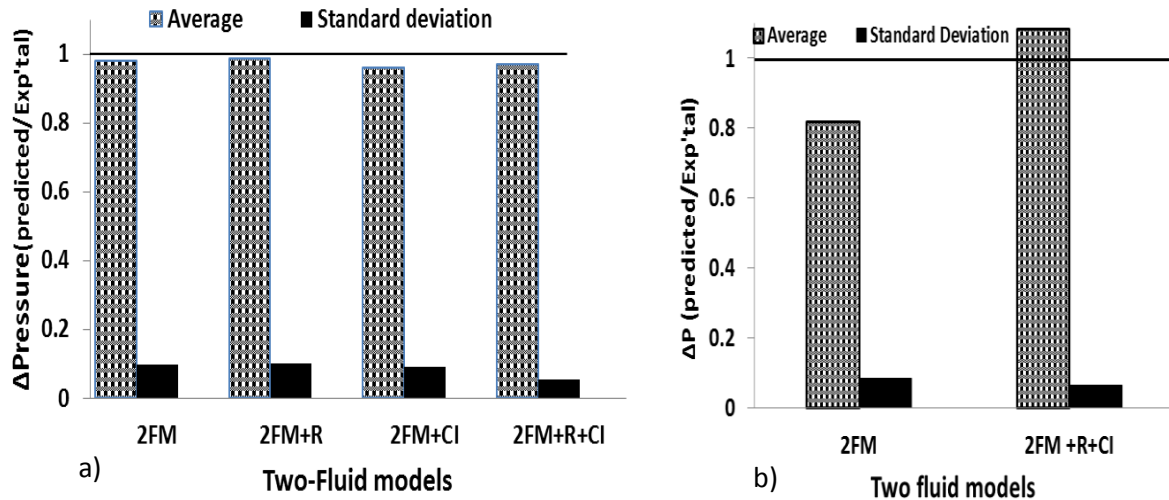
Figure 4-11 Comparison of experimental pressure drop values against the ones predicted from the two-fluid model using interface roughness and interface curvature. For a), the pairs of oil and water superficial velocities used for the comparison are as shown in Table 4-1, while b) was obtained from $U_{so}<0.25m/s$ and $U_{sw}<0.35m/s$.

As can be observed from, the interfacial roughness and curvature do not seem to improve the average pressure drop values. In the small pipe used in this work and for the range of conditions were separated flows were obtained, the amplitude of the interfacial waves was quite small (generally less than 1 mm), and their contribution to interface roughness (2FM+R model) does not seem to be significant. When the interface curvature was included (2FM+CI), the average pressure drop prediction did not improve but the standard deviation decreased, indicating that the model was able to predict the pressure drop better across all the mixture velocities compared to 2FM. By combining both effects of interface roughness and curvature (2FM+R+CI), the standard deviation reduced by almost 50 %. However, the improvements were mainly observed at low fluid velocities ($U_{so}<0.25m/s$ and $U_{sw}<0.34ms$) as can be seen in Figure 4-11b, where the interface curvature is generally more pronounced as can be seen from the experimental data (Figure 4-7 and Figure 4-8). In general, for a fixed U_{so} the relative difference between the interface heights, measured from both probes, diminishes with increasing U_{sw}.

Predicted interface heights are compared against the experimental ones in Figure 4-12 using the models described above.
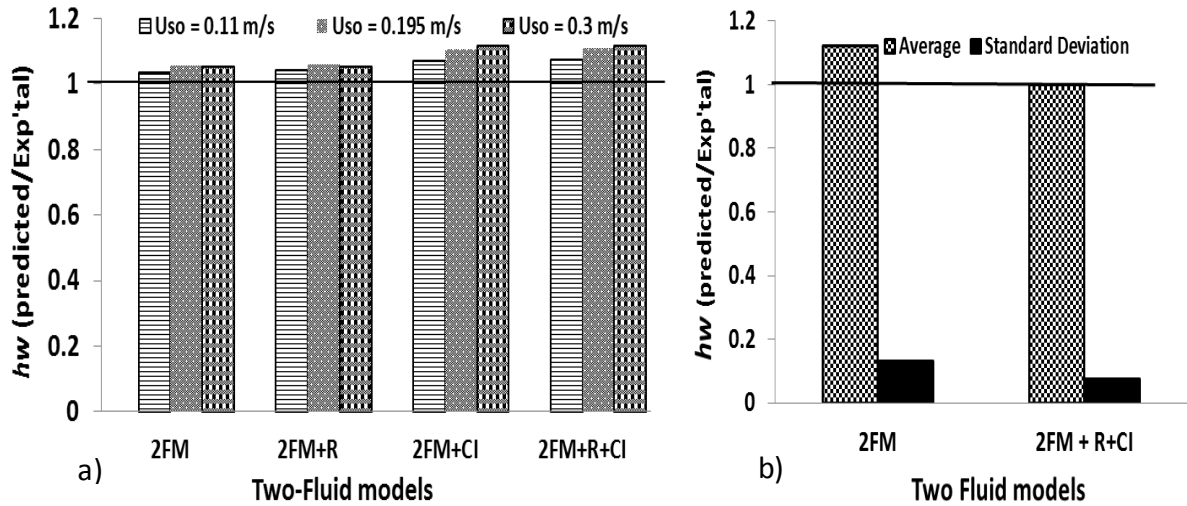
Figure 4-12 Comparison of experimental interface heights at the wall (averaged over pairs of velocities shown in Table 4-1) against the ones predicted from the two-fluid model using interface roughness and interface curvature.   b) was obtained from Uso<0.16m/s and Usw<0.34m/s.

The interface heights at the wall, h_w, are used which were found to be closer to the predictions of the standard two-fluid model than those in the middle of the pipe (see Figure 4-8). Clearly, in all cases the interface height is over-predicted and in fact the modifications of the two-fluid model either do not change significantly or even deteriorate the predictions, particularly with the inclusion of the curved interface. The prediction of the interface height (h_b) at the middle of the pipe, obtained from the model with curved interface, follows a similar trend of over-prediction. This follows from the linear relationship shown in Equation 4-6. Interestingly, the modified model performed excellently (average and standard deviation) at low fluid velocities as can be seen in Figure 4-12b for Uso< 0.16m/s and Usw<0.34ms. At higher velocities, the effect of inertial forces is dominant over surface/viscous forces and the influence of the curved surface diminishes leading to inaccurate prediction by the modified model.

4.6 Predictions of the Modified Two-Fluid Model with Literature Correlations on Interfacial Shear Stress

The effects of different interfacial shear stress correlations on the predictions of pressure drop by the two-fluid model are considered here. In all cases the interface is assumed to be curved. Interface roughness associated with waves, as given by Equation 4-7, is taken into

account in the 2FM+R+CI model. As can be seen from Figure 4-13 the model by Brauner (1991) with curved interface (Brauner+CI) gives the best absolute prediction of the average pressure drop of about 99 % ± 11 %, while the model proposed in this work (2FM+R+CI) gives a good prediction with the lowest standard deviation of 5 % (97 % ± 5 %).
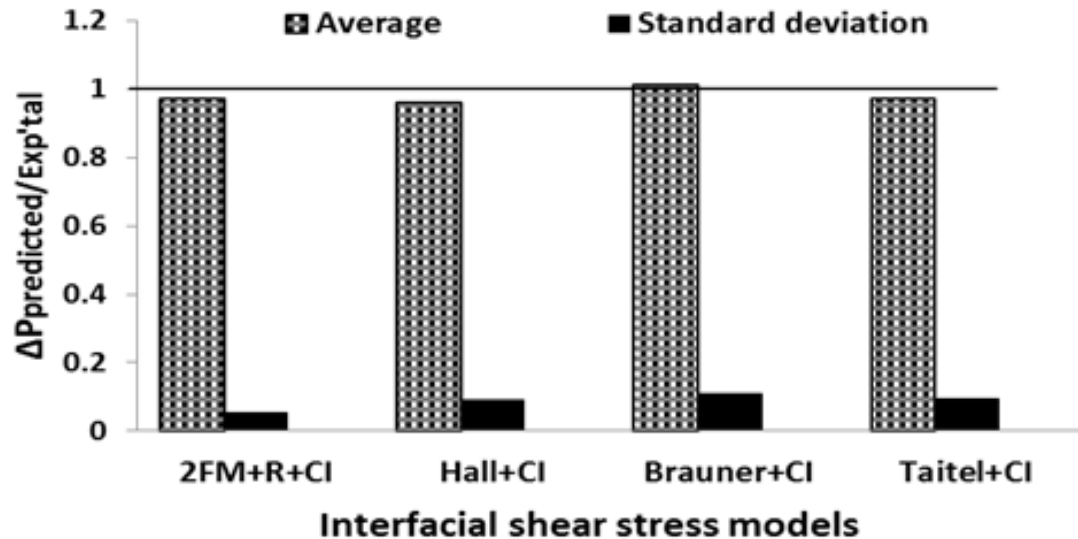
Figure 4-13 Comparison of experimental pressure drop values against the ones predicted from the two-fluid model with curved interface using different interfacial shear stress correlations. The pairs of oil and water superficial velocities used for the comparison are as shown in Table 4-1

Both these models considered interface waviness. In the current model this is included as roughness while in the Brauner (1991) model it is accounted for in the augmentation factor B. The predictions of the other two models, Hall (Hall, 1992) and Taitel (Taitel et al., 1995) are not as good. In both these models the interfacial shear stress is taken as constant (ratio of fluid viscosities for the Hall model and a constant value of 0.0142 for the Taitel model). In fact, in the Hall model the predictions improved with superficial water velocity, while in the Taitel model the predictions were better at low superficial oil velocities than at high ones. It should be noted here that considering interface curvature did not improve the predictions of the two-fluid model with the literature interfacial shear stress terms either in terms of average value or standard deviation (compare Figure 4-13 with Figure 4-10b). A curved interface, however, decreased significantly the standard deviation in our model when combined with interface roughness (Figure 4-11). Again, when the comparison is restricted to lower velocities (Uso<0.25m/s and Usw<0.34ms), the positive effect of the inclusion of the curved interface to these correlations becomes very evident as can be seen in Figure 4-14 and Figure 4-15 where over 50 % improvement in their prediction was observed.
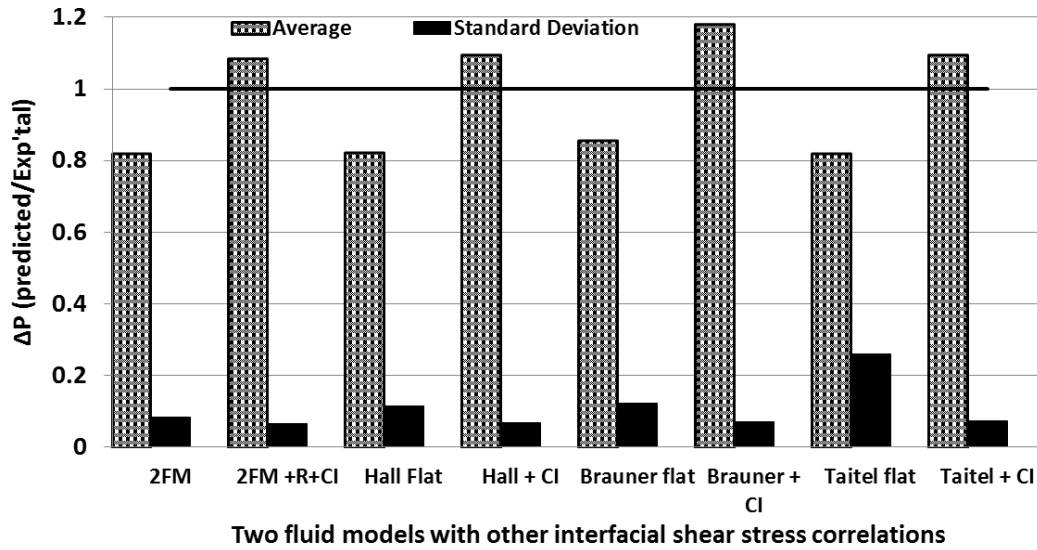
Figure 4-14 Effect of inclusion of curvature on the predictive quality of different interfacial shear stress correlations in the two fluid model at Uso<0.25m/s and Usw<0.34m/s
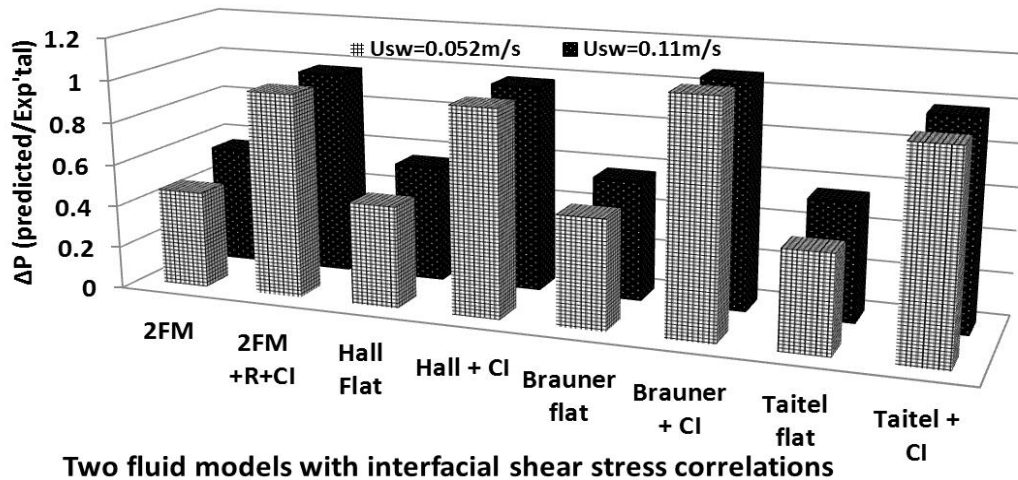
Figure 4-15 Effect of inclusion of curvature on the predictive quality of different interfacial shear stress correlations in the two fluid model at Uso<0.067m/s

Furthermore, the model proposed here was compared against the one recently proposed by (Rodriguez and Baldani, 2012), which also included interface curvature and waviness. In addition, the model suggested a modified hydraulic diameter of the slower light phase in laminar flow. The model by Rodriguez and Baldani predicted the current experimental data with an accuracy of about 66% ± 8% compared to 97 % ± 5 % of the current (2FM+R+CI) model (see Appendix Fig. 2 and Appendix Fig. 3). It was observed that the accuracy of their model increased with water velocity for a fixed oil velocity. This under-prediction by the

Rodriguez and Baldani model may be due to the modifications of most of the parameters (hydraulic diameters, friction factors and wall shear stresses) compared to those of the traditional two-fluid model (2FM). It was also found that the correlation proposed by Rodriguez and Baldani for interface curvature predicted a concave shape for most of the current data except at very low Usw (0.052 m/s) and for Uso > 0.19 m/s, where it gave a convex interface; in the current work a concave interface shape was found in all cases of stratified flow studied.

The predictions of the interfacial height (h_w) by the different interfacial stress models with and without curved interface are presented in Figure 4-16 for the conditions shown in Table 4-1. In all cases, including a curved interface resulted in an increase in the interface height values predicted. Furthermore, it was found that for all models the predicted values were lower than the experimental ones at low superficial oil velocities; as the oil velocity increased the predictions also increased and became higher than the experimental ones.
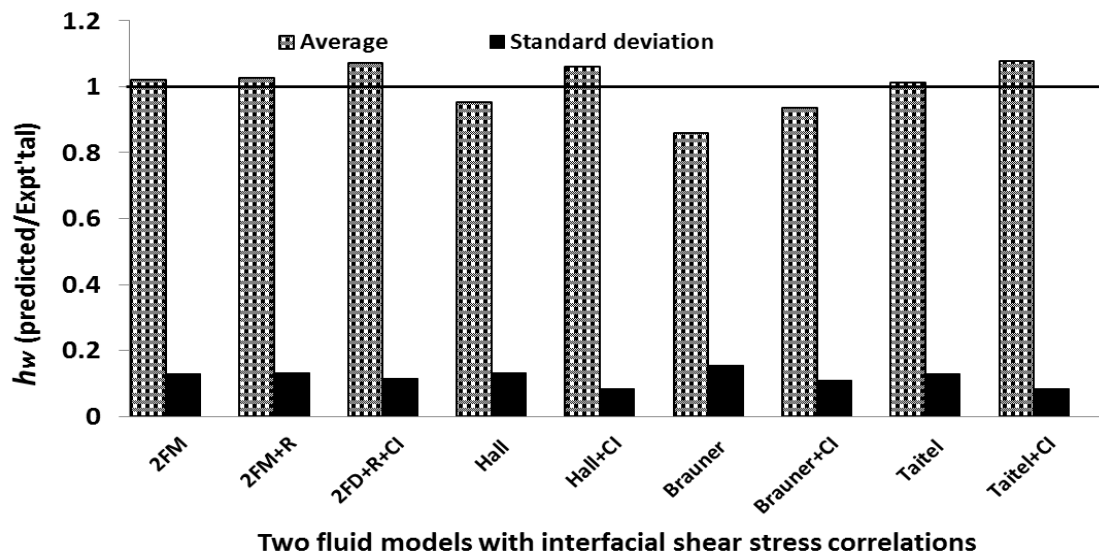
Figure 4-16 Comparison of experimental interface height at the wall (averaged over pair of velocities shown in Table 4-1) against the ones predicted from the two-fluid model using different interfacial shear stress correlations for both flat and curved interface

This was more prominent when interface curvature was included. In particular, for Usw < 0.17 m/s the Hall model under-predicted the experimental data by as much as 20 % to 25 % but this was improved to 13 % when a curved interface was used. Under the same conditions the Brauner model under-predicted the experimental data by 30 % to 35 % and was improved to 14 % with curved interface. Similarly at these conditions, the Taitel model

was improved to 11 % with the curved interface added. In general, the Hall model with curved interface was the best among the other models with 6 % over-prediction of the absolute height and a standard deviation of less than 10 %.

The two-fluid model with interfacial waviness and curvature of the oil-water interface included predicts satisfactorily both the pressure drop and the interface height with small standard deviation. These finding agree with previous reports which consider interface waviness and curvature important for improving the predictions of the two-fluid model (Andritsos and Hanratty, 1987; Andritsos et al., 2008; Brauner and Moalem, 1993; Brauner et al., 1998; Brauner, 2002; Hadžiabdić and Oliemans, 2007; De Castro et al., 2012; Rodriguez and Baldani, 2012).

4.7 Conclusions

The significance of pressure drop and holdup in designing an efficient system for oil-water transport necessitates the development of robust predictive models. One of the drawbacks has been the limited availability of experimental data for liquid-liquid flows. In this chapter, flow patterns are presented for a wide range of superficial oil and water velocities in a small diameter test section. Particularly for separated flows, new experimental data are given on the interface configuration. The data enabled modifications to the two-fluid model that account for the interface waviness through a roughness factor and for the interface curvature. The modified model showed improved predictive accuracy of over 95 % for pressure drop across the range of experimented oil and water velocities, while the interface height was predicted within 90 % accuracy. It was found that the predictions of the interface height were particularly sensitive to interface curvature, while those of pressure drop were affected by both the interface roughness and curvature. The results showed that the modified model performed better when compared against the two-fluid model that includes literature interfacial shear stress correlations particularly in predicting the pressure drop.

CHAPTER 5

5 DRAG REDUCTION IN SINGLE PHASE WATER AND IN OIL-WATER FLOWS

In this chapter, the Influence of polymeric additives on single phase water and oil-water flows in a horizontal 14 mmID acrylic pipe is reported. The changes to pressure drop (drag reduction) by the addition of partially hydrolyzed polyacrylamide (HPAM) and two different molecular weights polyethylene oxide (PEO; 5MPEO for 5×10^6 g/mol and 8MPEO for 8×10^6 g/mol) are also briefly compared for both single phase water and oil-water flows. In Section 5.1, drag reduction in single phase and comparison with the maximum drag reduction asymptote (MDRA) are presented. The influence of HPAM on oil-water flows is presented in Section 5.2. This is subdivided into Section 5.2.1 for flow patterns and flow pattern map, and Section 5.2.2 shows the influence of HPAM on pressure drop (drag reduction), including some modelling results for pressure drop prediction. The influence of polymer addition on the interfacial wave characteristics (interface height, wave celerity, wavelength, amplitude and power spectrum) of oil-water flows are presented in Sections 5.2.3 and 5.2.4. The chapter's conclusions are presented in Section 5.3.

5.1 Single-phase flows

5.1.1 Addition of Polymer to Single Phase Water Flow

The addition of polymer in single phase water flow was found to reduce significantly the pressure drop. An example is shown in Figure 5-1 where the pressure drop without polymer and with 20 ppm HPAM is plotted against the Reynolds number (Re). It can be seen that with the addition of the polymer the frictional pressure drop is reduced compared to flow without polymer and this difference increases as the Reynolds number increases. Also, at low Reynolds number (laminar flow) drag reduction is insignificant or completely absent and this agrees with previous findings (Al-Wahaibi et al., 2012, 2007; Al-Yaari et al., 2009; Virk, 1975). Onset of drag reduction was observed at a Reynolds number of about 1500 with drag reduction of 5 %. The corresponding friction factors f, were also calculated from Equation 5-1:

$$f = \frac{\Delta P D}{2 l U^2 \rho}$$

5-1

where *f*, ΔP, D, *ρ*, U and I, are respectively the friction factor, pressure drop, pipe diameter, fluid density, velocity, and pipe length.
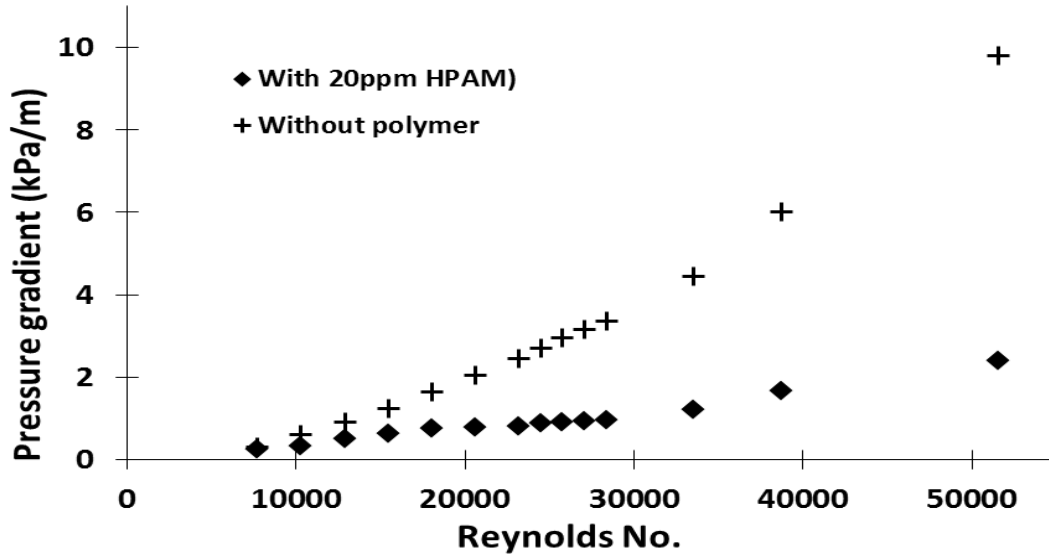
Figure 5-1 Pressure drop vs Reynolds number for drag-reduced water flows in 14 mmID pipe

Furthermore, for all velocities tested it was found that drag reduction increased initially with increasing HPAM concentration up to about 20 ppm but then reached a plateau (Figure 5-2). Interestingly, drag reduction of about 30 % can be achieved with as little as 2.5 ppm HPAM concentration. This agrees with previous findings (Al-Wahaibi et al., 2012) that a 2 ppm polymer concentration in water resulted in appreciable drag reduction during oil–water flow experiments. 1 ppm of oil-soluble polymer concentration was also reported to result in 33 % drag reduction in the Trans-Alaskan pipeline system (Gyr and Bewersdorff, 1995). The relationship between friction factor and Reynolds number for drag-reduced single phase water flows using HPAM in the current system can be described by Equations 5-2 and 5-3 for normal and Von-Karman coordinates respectively with errors less than 1 %. This will be inserted in the two-fluid model for the prediction of drag reduction in oil-water flows.

$$f = 1.2022\,\mathrm{Re}^{-0.651} \qquad\qquad \textbf{5-2}$$

$$f^{-\frac{1}{2}} = 0.858\left(\mathrm{Re}\,\sqrt{f}\right)^{0.4833} \qquad\qquad \textbf{5-3}$$
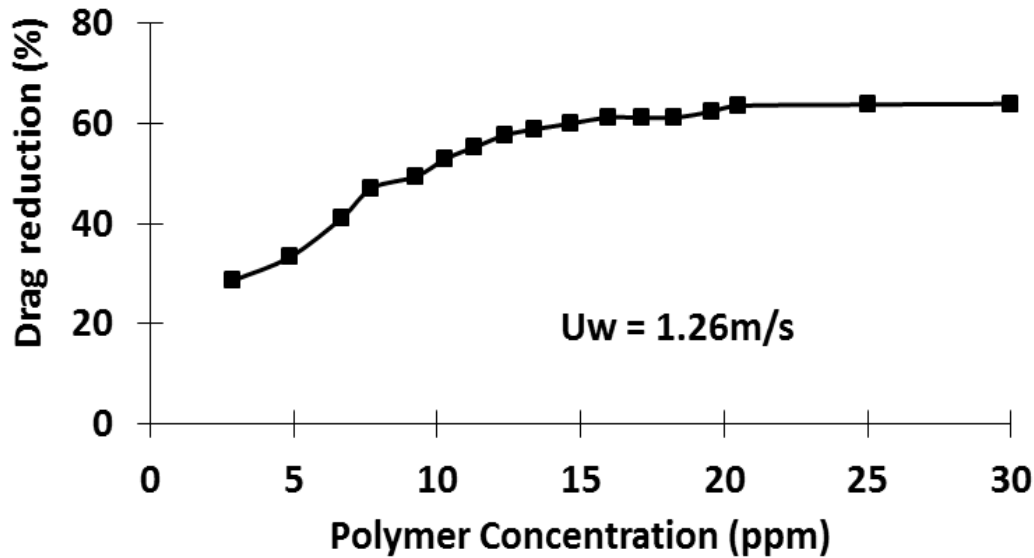
Figure 5-2 Effect of polymer concentration on drag reduction in single phase water flows at velocity of 1.26 m/s

The measurements from HPAM experiments were compared with those from the PEOs alongside the maximum drag reduction asymptote (MDRA; (Virk, 1975), on the Prandtl–Karman (P-K) coordinates in Figure 5-3. The friction factor (*f*) is calculated from the measured pressure drop before and after polymer addition and is given by Equation 4-1. The P-K line is given by Equation 4-2 while the MDRA is given by Equation 5-4 as shown;

$$f = 0.58 \, \mathrm{Re}^{-0.58} \qquad\qquad \textbf{5-4}$$

It was found that compared to HPAM, the addition of 8MPEO in the water phase had similar effects while that of 5MPEO was different, as can be seen from Figure 5-3.

With the addition of polymers to single phase water flow, friction factors significantly decrease for Reynolds numbers above 2000 where flow becomes turbulent. The maximum drag reduction obtained in this work with HPAM was about 80 % for Reynolds numbers over 42000, while with 8MPEO and 5MPEO it was about 70 % and 55 % respectively
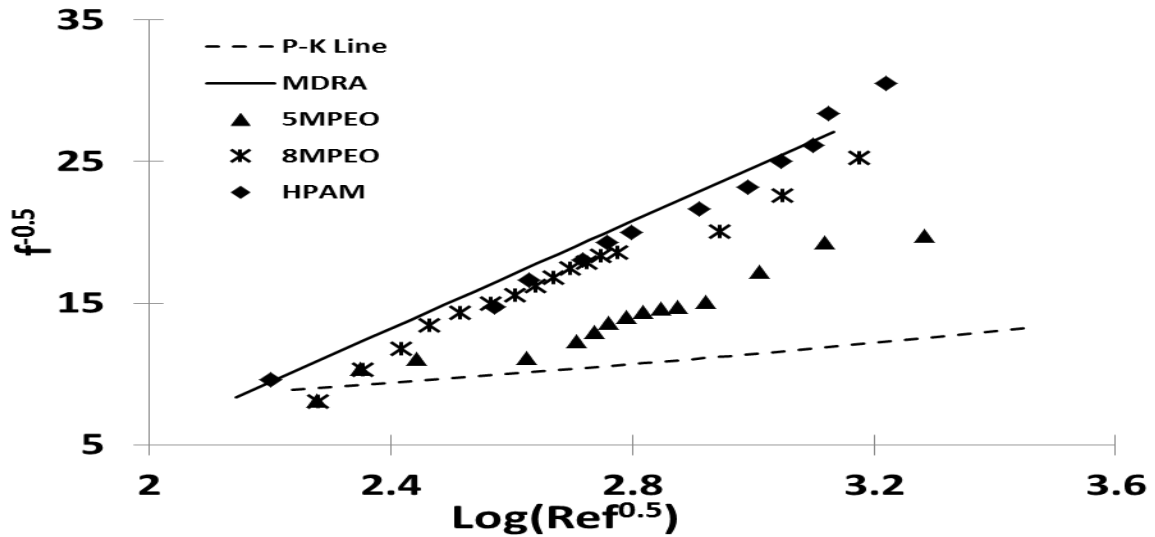
Figure 5-3 Comparison of drag reduction of different polymers (HPAM, 5MPEO & 8MPEO) with Virk's MDRA

Figure 5-3 clearly shows that drag reduction increases with the polymer molecular weight. The polymer ionic structure can also be significant (Abdulbari et al., 2014; Al-Sarkhi, 2010) which may explain the different values of friction factors between solutions of HPAM and 8MPEO particularly at Reynolds numbers above 15000. With PEO polymers the decrease in friction factors becomes less steep at high Reynolds numbers (above 15000) compared to HPAM. PEO polymers are prone to mechanical degradation at high Reynolds numbers (Wei and Willmarth, 1992) while HPAM has a higher resistance (Abubakar et al., 2014a; Den Toonder et al., 1995; Hoyt, 1986).

5.2 Two-Phase Flows

5.2.1 Effect of Polymer on Flow Patterns and Flow Pattern Map

The two-phase flow patterns observed in this study, before and after the addition of the polymer in the water phase can be seen in Figure 5-4. Without any polymer added, the flow patterns were stratified, stratified wavy, dual continuous, rivulet, and dispersed either with water or with oil as the continuous phase. Slug flow appeared in some cases in the region of transition between stratified to dual continuous or dispersed flows but it was not a stable pattern.

Dual continuous; Uso =0.245m/s, Usw=0.51m/s → Stratified flow

Stratified wavy; Uso =0.43m/s, Usw=0.28m/s → Stratified flow

Rivulet flow; Uso =0.30m/s, Usw=0.22m/s → Stratified flow

Dispersed (Do/w); Uso =0.11m/s, Usw=0.676m/s → Dispersed (Do/w) large drops

Dispersed (Dw/o) flow; Uso =0.51m/s, Usw=0.11m/s → Stratified flow
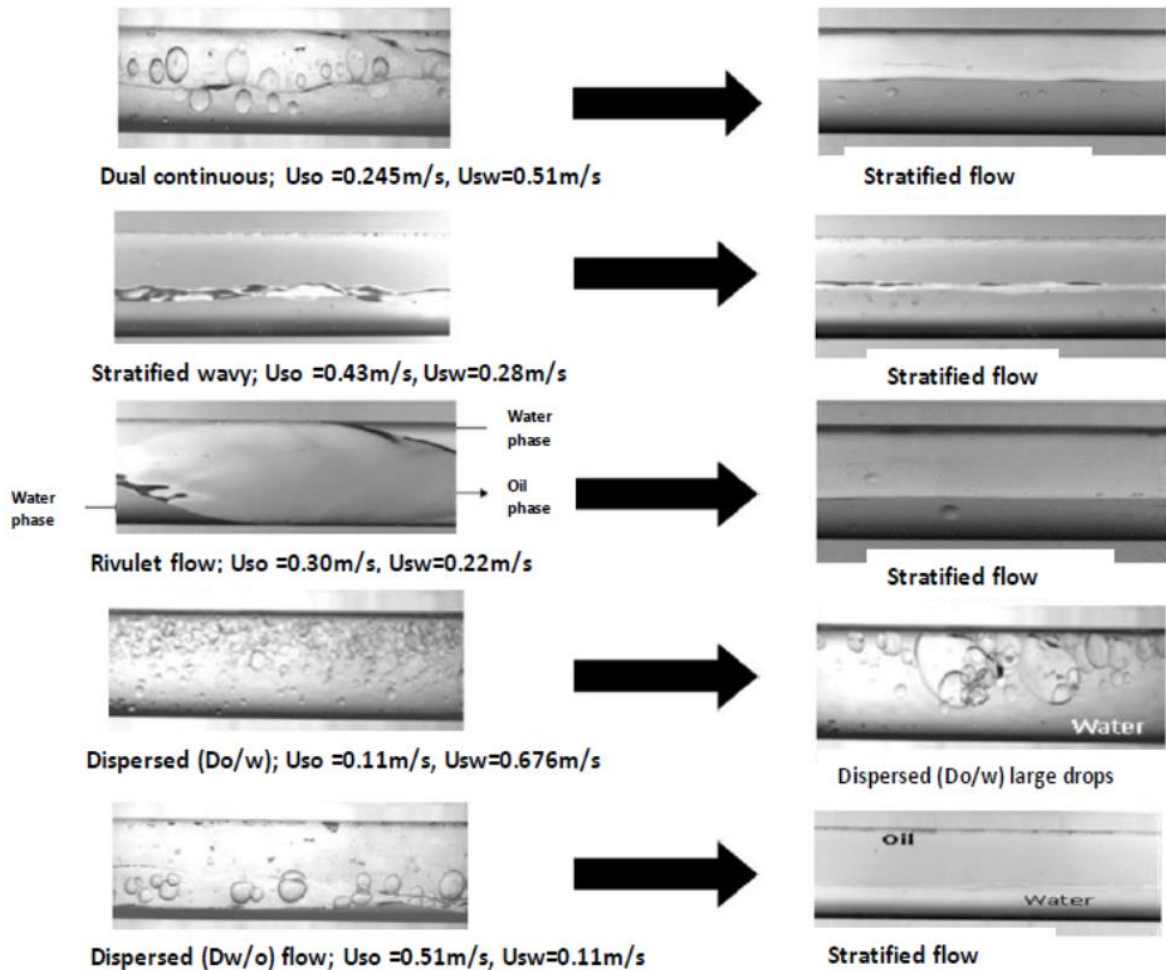
Figure 5-4 Effect of polymer addition on horizontal oil-water flow patterns

The Eötvös number for the system studied was calculated to be 4.78, which suggests that surface tension forces play an important role on the flow pattern characteristics and explain the appearance of the rivulet pattern (Brauner and Moalem, 1992a; Das et al., 2010). In the stratified wavy flows, the amplitude of the waves increased with increasing fluid velocities. In the dispersed patterns, water drops floated near the bottom of the pipe while oil drops floated near the top of the pipe due to gravity (Barral et al., 2013).

When polymer was added in the water phase, the flow pattern characteristics and their transition boundaries changed. This can be seen in Figure 5-4 and Figure 5-5 for polymer concentration in water of 20 ppm. In stratified wavy flows the wave amplitudes reduced. Rivulet flow was not seen and at these conditions stratified flow formed instead. The dual continuous pattern was either changed to stratified or stratified wavy flow at the lower mixture velocities or remained dual continuous but with larger drops. The dispersed flows

(oil in continuous water, Do/w, and water in continuous oil, Dw/o) sometimes changed to dual continuous or to stratified flows. When the dispersed pattern did not change, larger drops with sizes of about 0.3–0.7D were seen after the polymer addition. These changes are a result of the decreased turbulence in the water phase which favours drop coalescence and reduces drop formation from the oil–water interface; larger drops also promote the stratification of the two phases. The findings agree with previous investigations in horizontal oil–water flows by (Al-Wahaibi et al., 2012, 2007) in 25.4 and 14 mmID pipes and (Al-Yaari et al., 2012, 2009) in a 25.4 mmID pipe. However, in these studies the rivulet flow pattern was not seen. The changes in the flow patterns with the addition of polymer are summarised in Table 5-1. The flow pattern transition lines before and after the addition of 20 ppm polymer are shown in Figure 5-5. As can be seen, the region of stratified and stratified wavy flow has been extended with the polymer addition for as much as about 35 %, to superficial velocities of Uso = 0.65 m/s and Usw = 0.80 m/s.
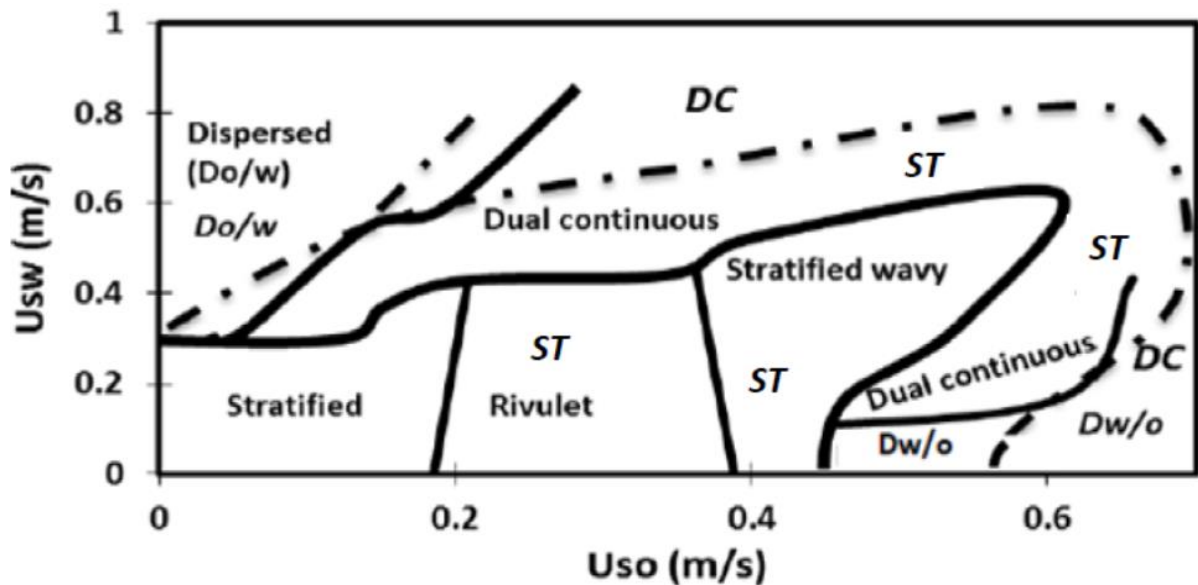
Figure 5-5 Oil–water flow pattern map. Bold lines represent pattern boundaries before polymer addition while broken lines represent pattern boundaries after polymer addition in water. Pattern names in normal font are for flow without polymer; pattern names in italics are for flow with polymer with *ST; stratified, DC; dual continuous, Do/w & Dw/o; dispersed oil-in-water and water-in-oil flow.*

Table 5-1 Flow patterns without and with HPAM in the water phase.

Without polymer	With polymer
Stratified flow	Stratified
Stratified-wavy flow	Stratified, stratified-wavy
Rivulet flow	Stratified
Dual continuous flow	Stratified, stratified-wavy, Dual continuous
Dispersed oil-in-water (Do/w) flow	Stratified, Dual continuous, Dispersed oil-in water (larger drops)
Dispersed water-in-oil (Dw/o) flow	Stratified, Dual continuous

5.2.2 Effect of Polymer Addition on Pressure Drop

It was found that when polymer was added to the water phase the pressure drop of the two-phase flow reduced significantly. The reduction in pressure drop obtained when the polymer concentration in the water phase varied from 10 ppm to 50 ppm can be seen in Figure 5-6 for different superficial oil and water velocities corresponding to stratified/stratified wavy and early stage of dual continuous flows. Drag reduction initially increased with increasing polymer concentration but after about 20 ppm it did not vary significantly, which agrees with the results found in single phase water flow (see Figure 5-2). This concentration reflects a saturation of the region of strong turbulence activity with the polymer, beyond which no further changes in drag reduction are noticeable (Hoyer et al., 1996). The observed optimal polymer concentration of 20 ppm is in agreement with previous reports (Al-Wahaibi et al., 2007) and was used in the rest of the studies of interface characteristics in stratified flows detailed below. From data not shown here it was found that a high drag reduction of about 52 % was obtained when dispersed flow changed to stratified flow.

The effects of superficial oil and water velocities (Uso and Usw) in drag reduction can be seen in Figure 5-7. It can be seen that drag reduction increases with increasing superficial water velocity for all superficial oil velocities. As the superficial water velocity increases, the in-situ water velocity and Rew also increase and enhance turbulence which leads to higher drag reduction (Abubakar et al., 2014a; Al-Sarkhi, 2010; Manfield et al., 1999). With increasing Uso, and constant Usw drag reduction initially increases but then slightly decreases, although the in-situ Rew increases. It is possible that as the oil flowrate increases and oil occupies a larger part of the pipe cross section, its contribution to the two-phase pressure drop is more important to that of the water phase particularly at low water rates because the water wetted perimeter is reduced.
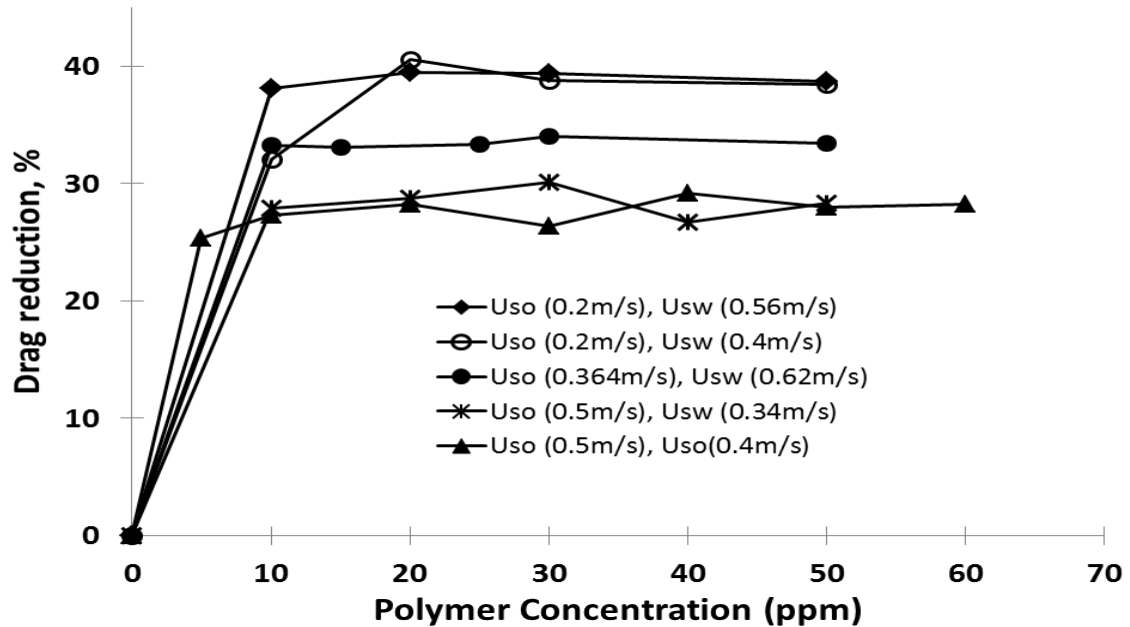
Figure 5-6 Effect of polymer concentration on drag reduction in oil-water flows at different superficial oil and water velocities
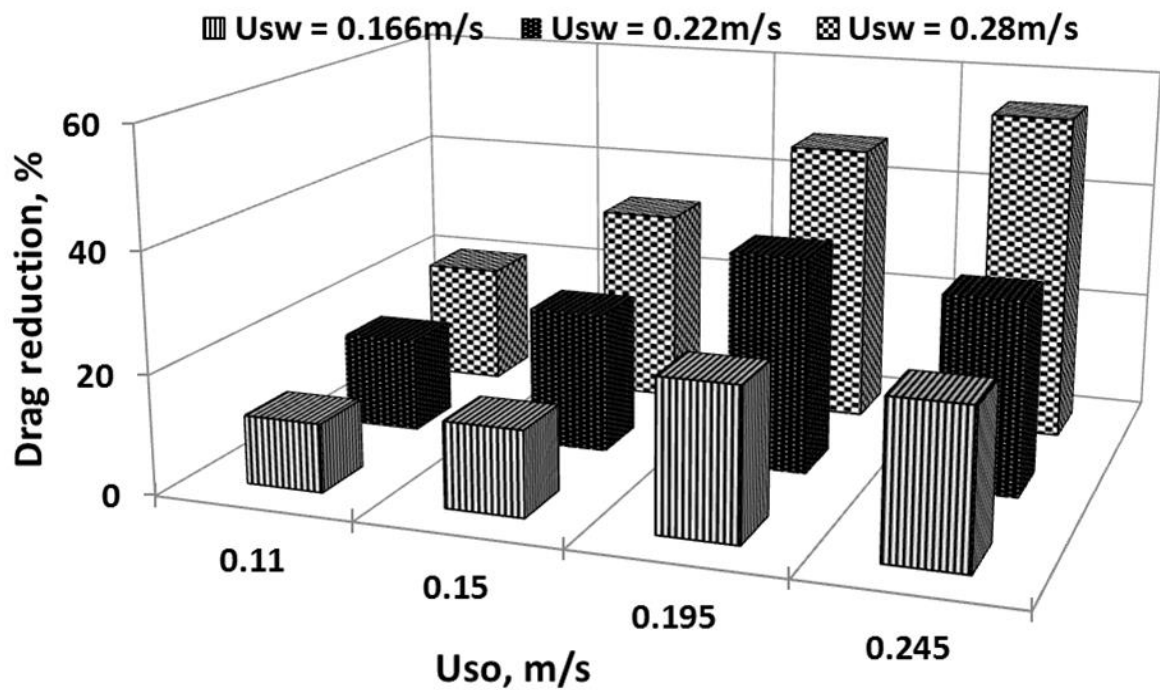
Figure 5-7 Drag reduction (DR, %) for different superficial water (Usw) and superficial oil (Uso) velocities

This observation also agrees with the findings of Abubakar et al. (2015a) who observed a decrease in drag reduction with increasing oil input fraction. They also reported that the addition of water-soluble polymer to oil-water flows resulted in zero and negative drag reduction particularly at very high oil input fraction, while a maximum drag reduction of 64 % was reported for the highest mixture velocity and lowest oil input fraction.

The behaviour of drag reduction with increasing Usw for a fixed Uso may depend on the particular flow pattern prior to the polymer addition. For example, the pattern at Usw = 0.28 m/s and Uso = 0.195 m/s is close to the transition boundary between stratified and rivulet flow where pressure fluctuations are high (Barral et al., 2013); drag reduction is found to be about 42 %. The pattern at Usw = 0.34 m/s is clearly in the region of stratified flows and has drag reduction of about 30 %. Flows at Uso = 0.245 m/s and 0.30 m/s are within the stable flow regions of rivulet and dual continuous flows with less disturbances associated with flow pattern changes particularly near the boundaries. The maximum drag reduction observed in these current experiments was about 52 % when dispersed flows (Dw/o and Do/w) changed to stratified flow.

Figure 5-8 shows the results from the two-fluid model (2FMpol) where the friction factor correlation for drag reduced flow (Equation 5-2) was used for the water wall friction factor. The modified two-fluid model (2FMpol) also included a new correction for interface curvature as discussed in Section 4.3 while the roughness factor was not included because of the dampening effect of the polymer on the interfacial waves. It should be noted that the interface curvature remained after the addition of polymer to the oil-water flows and a new correlation that describes the relationship between the two heights was obtained and used in the 2FMpol model. The new correlation is given as:

$$h_b = 0.7619h_w + 0.0004151 \qquad\qquad \textbf{5-5}$$

Where h_b and h_w are respectively the heights at the middle and wall of the pipe.

The pressure gradient data used in these comparisons are the same as those shown in Figure 5-7. The results of the modified model were also compared with the predictions of the homogeneous model suggested by Al-Sarkhi et al. (2011) using the friction factor correlation found experimentally in drag reduced oil-water flows of Equation 2-12. The drag-reduced pressure drop is calculated as follows:

$$\left(\frac{dp}{dz}\right)_{pol} = \frac{2f_m\rho_m U_m^2}{D}$$
5-6

where f_m, is the friction factor of the oil-water mixture and is given in Equation 2-12, U_m is the mixture velocity calculated from the sum of the superficial water and oil velocities, and the mixture density ρ_m, is given as

$$\rho_m = H_w\rho_w + H_o\rho_o$$
5-7

ρ_o *and* ρ_w, H_o and H_w are the density and hold up of oil and water phase respectively.

With Equation 5-5, the prediction of the drag-reduced pressure drop was about 5.6 % improved over that obtained from using Equation 4-6. It can be observed from Figure 5-8 that the pressure drop data predicted with the modified two-fluid model (2FMpol) lie well within the ±15 % boundary of the experimental data, while the Al-Sarkhi et al. (2011) model under-predicted all the experimental data by as much as 42 % in some cases.
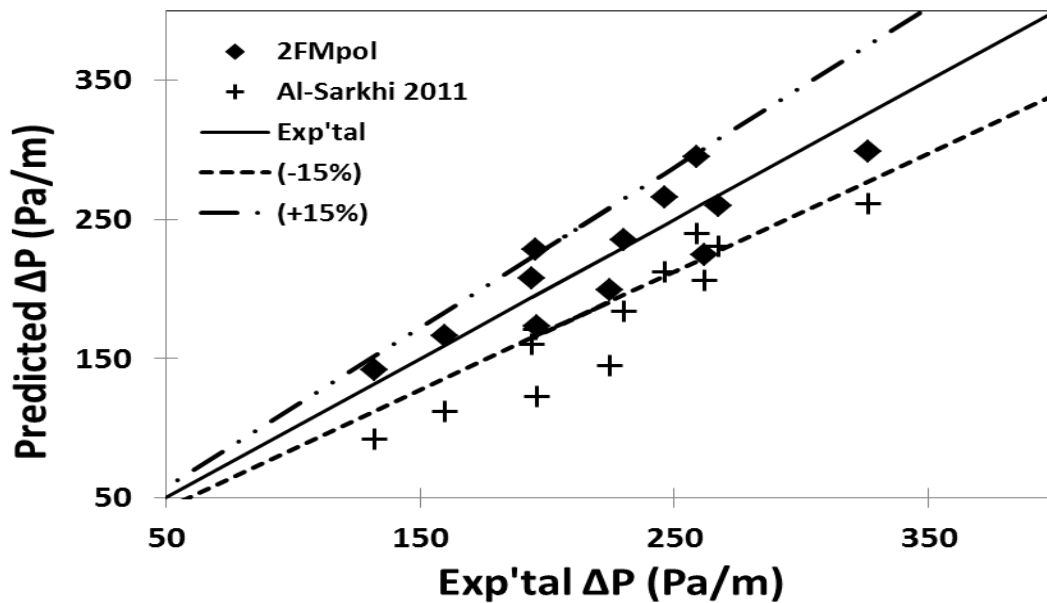
Figure 5-8 Prediction of experimental pressure drop with drag reduction models

The prediction was observed to improve with increasing superficial water velocity (Usw) for a fixed superficial oil velocity (Uso). The under-prediction could be attributed to the homogeneous model used for the pressure drop that is not suitable for stratified flows. Al-Wahaibi et al. (2012) also reported that the model by Al-Sarkhi et al. (2011) under-predicted their experimental data by an average of 32 %.

The two-fluid model with the modified water wall friction factor to account for the presence of the polymer (2FMpol) was also used with the different interfacial shear stress correlations discussed in Section 4.6. It was found that the results from the Hall (1992) and Taitel et al. (1995) model were closer to the experimental data and predictions from 2FMpol while those from (Brauner, 1991) where much higher and over predicted (see Appendix Fig. 7). All four models however had similar trends. .

5.2.3 Effect of Polymer Addition on Interface Height and Wave Celerity in Stratified Flows

The changes in interface height during stratified and stratified wavy flows before and after the addition of polymer to the water phase were captured with the conductance probes, and are compared in Figure 5-9 for a superficial oil velocity of 0.51 m/s.
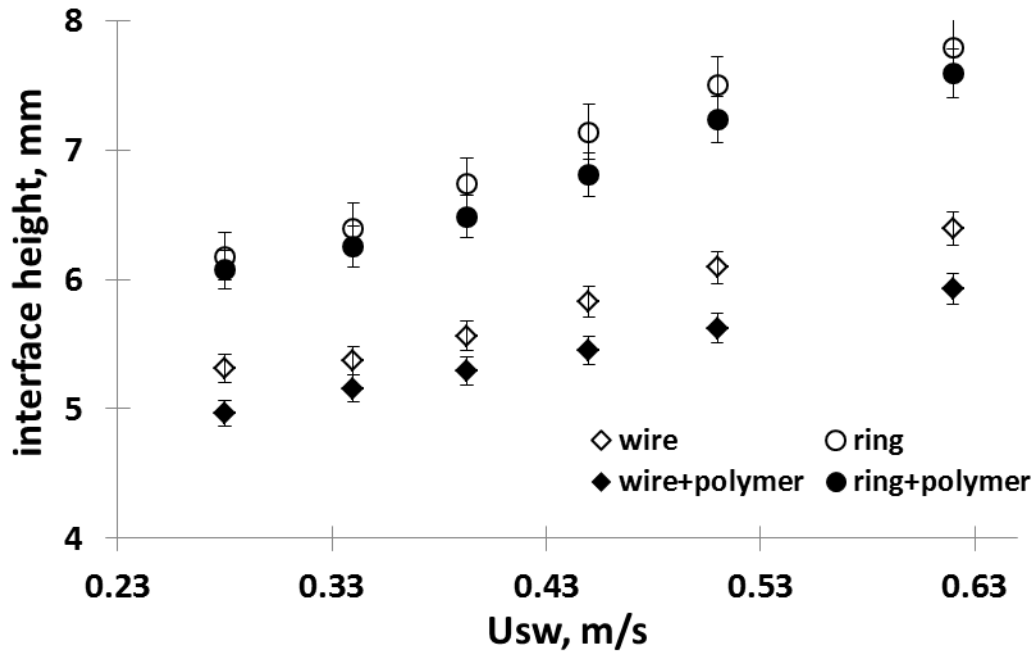
Figure 5-9 Effect of adding 20 ppm polymer in the water phase on the interface height during stratified/stratified wavy oil–water flows for Uso = 0.51 m/s.

There is a difference in interface height between the middle of the pipe (given by the wire probe) and at the wall (given by the ring probe) which suggests that the interface has a concave shape, justified by the low Eötvös number for this system. In all cases, the interface height increased with superficial water velocity as expected. The addition of the polymer resulted in a decrease in average interface height both in the middle of the pipe and at the wall. This can be explained as a result of the reduced frictional resistance of the water flow (drag reduction) that can lead to an increase in its velocity (Al-Yaari et al., 2012). For a

constant water flowrate an increase in velocity would decrease the in-situ water holdup and the interface height, by as much as 10 %. The change in interface height after polymer addition was less (about 5 %) at low water velocities (Usw < 0.40 m/s, Re_w < 7100; Re_w is the in-situ Reynolds number of the water phase) which suggests that the polymer is less effective at low Reynolds number. The onset of drag reduction was observed at in-situ Reynolds number of about 1900 in the water phase.

The observed decrease in interface height does not agree with some of the previous investigations on oil–water flows (Al-Wahaibi et al., 2007; Al-Yaari et al., 2012). Al-Wahaibi et al. (2007) observed an increase in the interface height after polymer addition in water both at low and high oil velocities. There was, however, some uncertainty in these results since interface heights were observed with high speed imaging from outside the pipe and it was not always clear whether the heights measured were at the wall or close to the middle of the pipe. Al-Yaari et al. (2012) used conductivity probes, as in the present work, and found that when polymer was added in the water phase the interface height increased for superficial oil to water velocity ratio greater than 1 while it reduced for ratio less than 1. The authors attributed the increase in interface height to the dampening of interfacial waves and the coalescence of drops which increase the height of the continuous water layer. However, their measurements included dual continuous as well as dispersed (Do/w) flows. In the current work only stratified and stratified wavy patterns were included in the interface height measurements since the conductivity probe data cannot be reliably used to estimate the interface height when drops are present.

A change in the interfacial wave celerity was also found with the addition of the polymer for all conditions studied and an example is shown in for Uso = 0.51 m/s. The celerity of the oil-water flows was measured from using the video images of the flow for the particular flow condition. The procedure involves following the wave at the interface for a chosen time frame and the distance traveled is determined from the ruler inserted in the view box which is captured alongside the flow. It is observed that for a fixed oil velocity, the celerity increases with increasing water velocity before and after the polymer addition as expected. The wave celerity increased by over 10 % when polymer was added. These are in agreement with the increase in average water velocity observed after polymer addition and as discussed above. This is also evident in Table 5-2 where some in-situ velocities before and after polymer addition to the oil-water flows are shown.
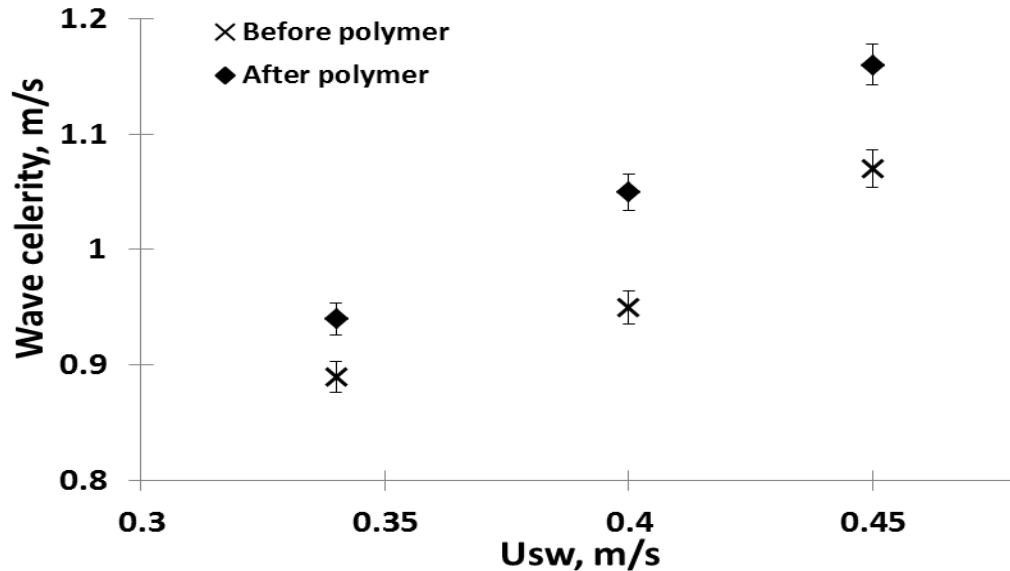
Figure 5-10 Effect of adding 20 ppm polymer in the water phase on the wave celerity during stratified/stratified wavy oil–water flows Uso = 0.51 m/s.

Table 5-2 Effect of HPAM addition on the in-situ oil to water velocity (Slip) ratio

Uso (m/s)	Usw (m/s)	hw (mm)	hw+pol (mm)	Uo (m/s)	Uw (m/s)	Uo+pol (m/s)	Uw+pol (m/s)	S = Uo/Uw	S+pol
0.51	0.28	5.31	4.96	0.78	0.81	0.75	0.88	0.97	0.85
0.51	0.34	5.37	5.16	0.79	0.96	0.77	1.02	0.83	0.75
0.51	0.393	5.56	5.29	0.81	1.05	0.78	1.14	0.77	0.69
0.432	0.11	3.41	3.38	0.53	0.58	0.53	0.59	0.91	0.898
0.432	0.166	4.19	4.17	0.58	0.66	0.576	0.66	0.88	0.87
0.432	0.34	6.03	5.80	0.73	0.83	0.71	0.87	0.89	0.82
0.15	0.22	6.78	6.41	0.29	0.46	0.27	0.49	0.63	0.55
0.15	0.34	9.14	8.63	0.49	0.49	0.42	0.53	0.99	0.799
0.067	0.34	10.37	9.87	0.33	0.43	0.27	0.45	0.77	0.60

"+pol" implies parameter after addition of polymer to flow.

5.2.4 Effect of Polymer Addition on Amplitude, Wavelength and Power Spectrum of Interfacial Waves

Wave amplitudes in the separated flows were determined from the standard deviation of the averaged time series data of the interface height from the wire conductance probe. The addition of polymer was found to decrease the amplitudes of the interfacial waves as can be seen in Figure 5-11 in agreement with the high speed images (see Figure 5-4). The decrease in amplitude depended on the flow conditions; waves at high mixture velocities reduced in amplitude while at low ones they could even be completely eliminated when polymer was added.

a. Change in amplitude with polymer concentration

Without polymer   With 20ppm polymer

b. Wave form at Uso = 0.51 m/s Usw = 0.45 m/s
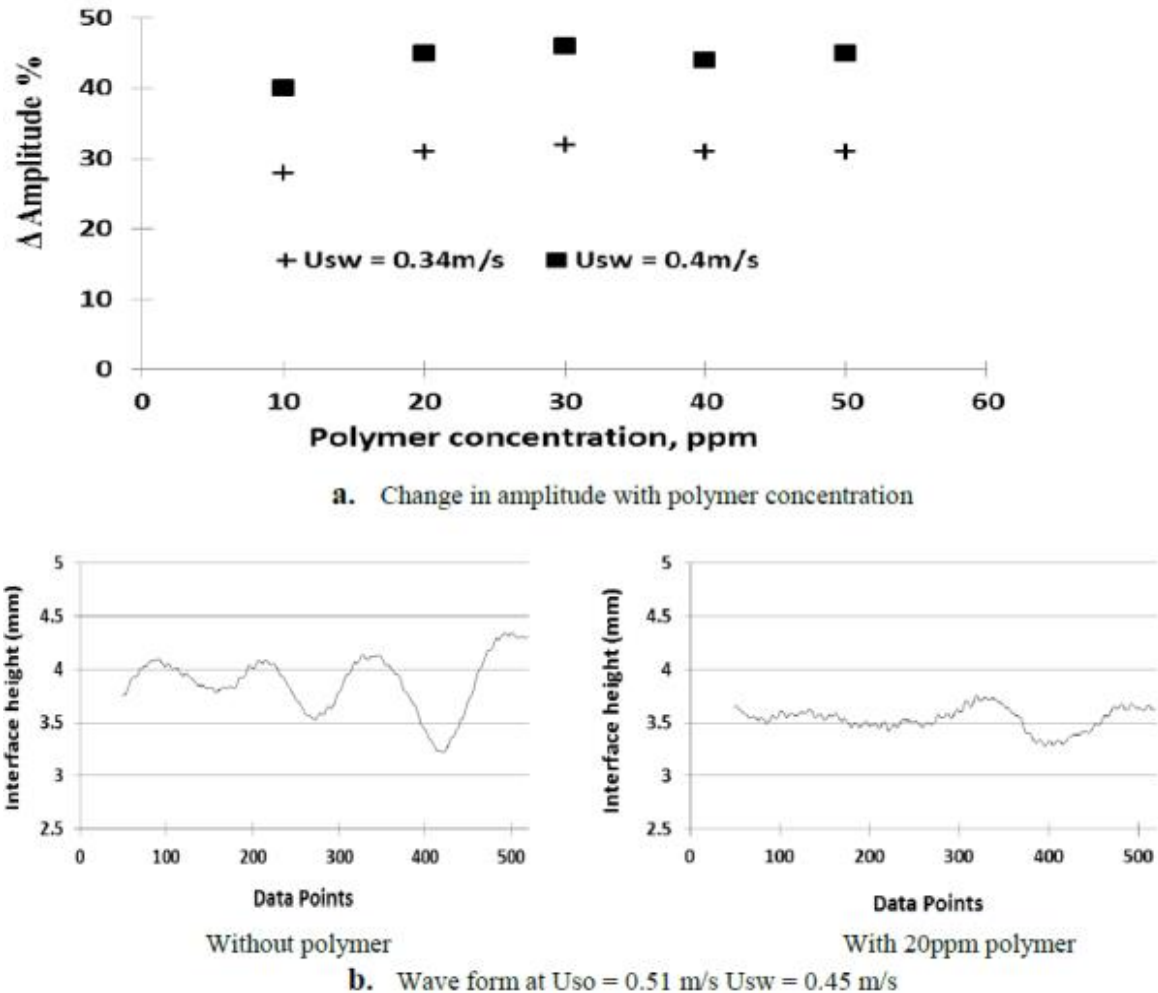
Figure 5-11 Change in wave amplitude with polymer concentration

It is also worth noting that the reduction of the wave amplitude did not change significantly with increase in polymer concentration beyond 20 ppm, which agrees with the observations on drag reduction (see Figure 5-6 and Figure 5-7). Some investigators (Cheung and Street, 1988; Cohen and Hanratty, 1968) have reported that the presence of waves at the interface of air–water flow is evidence of turbulent energy production and transfer of mechanical energy between phases. Generation of turbulence bursts at the wavy interface in oil–water flows has also been discussed (Kumara et al., 2010b). The decrease in wave amplitude could therefore be related to changes in turbulence in water with the addition of the polymer.

Decreased wave amplitudes have been observed in both gas–liquid and liquid–liquid flows (Al-Sarkhi and Soleimani, 2004; Al-Wahaibi et al., 2007; Al-Yaari et al., 2012; Hanratty and Al-Sarkhi, 2001) when polymer is added. Interfacial waves are considered to increase the interfacial shear stresses and hence pressure drop in two phase flows (Andritsos et al.,

2008; Hadžiabdić and Oliemans, 2007; Rodriguez and Baldani, 2012). A reduction in their amplitudes would therefore result in a reduction in the interfacial shear stress and further contribute to the reduced frictional pressure drop observed when polymer is added.

It is worth noting that the dampening of interfacial waves, measured as reduced amplitude, did not seem to be affected by changes in the velocity ratio, *S* (in-situ oil to water velocity) for all conditions studied within the stratified, rivulet and stratified wavy regions (see Figure 5-5). Except at very low velocities in the stratified flow region, waves were dampened after polymer addition at all slip ratios. Table 5-2 shows the changes of the velocity ratio, S, after polymer addition for some selected flow conditions together with the respective in-situ phase velocities. Here hw, S, Uo and Uw represent the interface height, velocity ratio, in-situ oil and water velocities respectively while "pol" denotes that polymer is present. The in-situ velocities were calculated from the input phase flowrates and the measured interface heights from the two conductivity probes. The interface is in many cases curved and its shape and position are found from the measured heights as described in section 4.
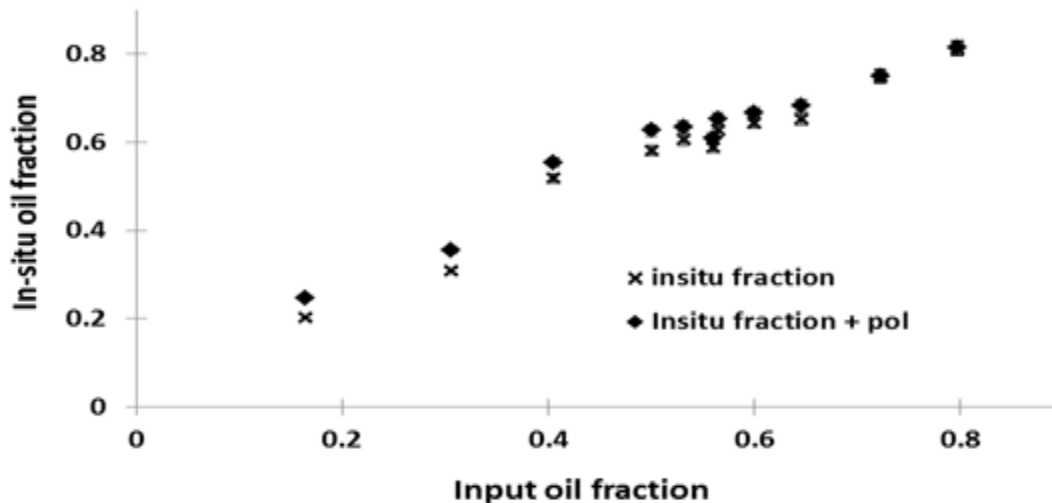
Figure 5-12 Plot of in-situ oil fraction versus input oil fraction for oil–water flows.

In all cases, S was less than 1 before the polymer was added which means that oil has a lower in-situ average velocity than water as it is the more viscous phase (Lovick and Angeli, 2004). With the addition of the polymer and the corresponding increase in water velocity, the slip ratio reduced further to values less than 1. Despite this increase in the relative velocities of the two phases, the waves were still dampened. As can be seen from Figure 5-12, when polymer was added, the in-situ oil fraction increased until about oil fractions equal to 0.70,

above which the change is not significant probably because of the low velocity of the water phase at these conditions and reduced effect of the polymer.

While wave amplitudes decreased (Figure 5-11), wavelengths increased with the addition of polymer, as shown in Figure 5-13. The wavelengths were obtained from the video images of the flow before and after polymer addition. The locations of the crests and troughs of all the well-formed waves were noted. With the help of the ruler inserted in the view box, the distance between a wave crest and a trough was measured from which the wavelengths were calculated. The values presented are averages obtained from this process.

The largest wavelength increase of about 50 % was observed at Usw = 0.40 m/s for Uso = 0.51 m/s; this condition is well within the region of stratified wavy flows with well-developed waves before the addition of polymer to the flow. However, there was no particular trend with water velocity in the cases studied. The increase in wavelength and reduction in wave amplitude after polymer addition is indicative of the stratification of the flow as was visually observed during the experiments (Figure 5-4).
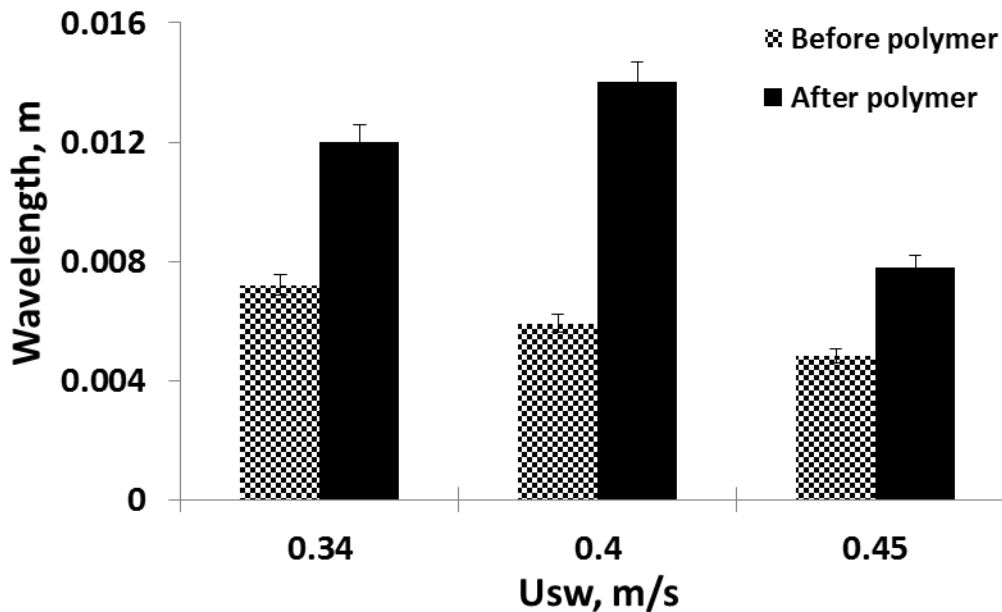
Figure 5-13 Effect of adding 20 ppm polymer in the water phase on wavelengths for Uso = 0.51 m/s

From the times series of the wire conductivity probe signal in the middle of the pipe the power spectrum of the contributing wave frequencies was calculated (for the procedure see (Barral and Angeli, 2013)). This is shown in Figure 5-14 for superficial oil velocity 0.51 m/s

and superficial water velocities 0.34 m/s and 0.40 m/s. As can be seen, the major contributing frequencies are less than 10 Hz for both flow conditions, but with varying intensities. The addition of the HPAM (20 ppm) resulted in over 85 % reduction (calculated from the maximum intensity peaks), in the intensity of the contributing frequencies which is also a reflection of the dampening of interfacial waves.

a. Usw = 0.34 m/s

b. Usw = 0.4 m/s
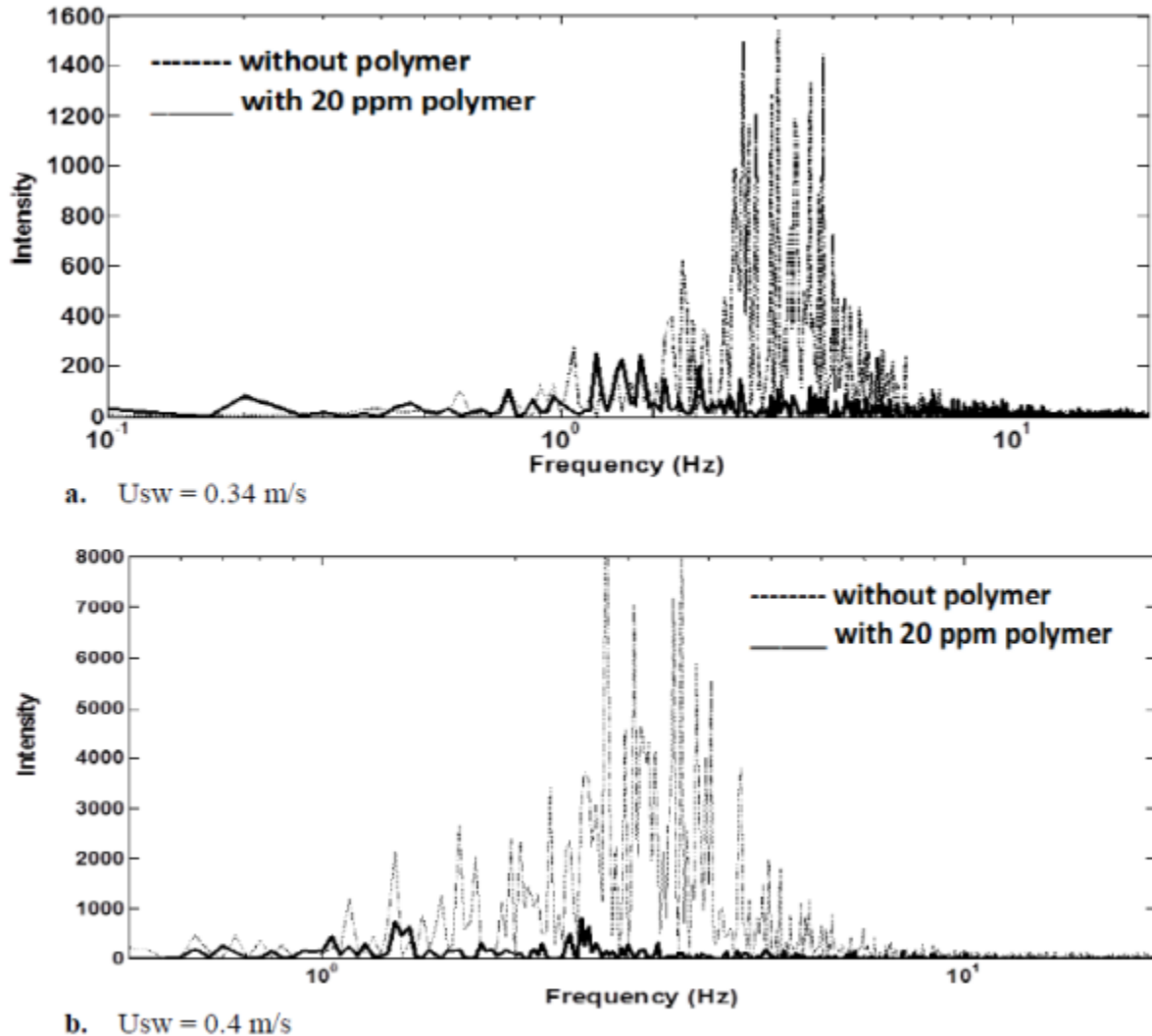
Figure 5-14 Effect of adding 20 ppm polymer in the water phase on the power spectrum of the interface signal in stratified oil–water flows at Uso = 0.51 m/s.

5.3 Conclusions

The effect of a drag reducing polymer on pressure drop and flow patterns in horizontal oil–water flows was studied experimentally and results presented in this chapter. In the stratified

flow regime, in particular, the changes in wave characteristics and water hold up were investigated with the use of conductance probes. In summary, the following were found:

- Addition of the polymer extended the stratified region in the oil–water flow pattern map to higher superficial oil and water velocities. Dispersed, rivulet and dual continuous flows changed to stratified flow, while in the cases where dispersed and dual continuous flows remained, they had larger drops when polymer was added.

- The highest drag reduction of about 52 % was achieved for polymer concentrations as low as 20 ppm when dispersed and stratified wavy flows changed to stratified flows.

- The two-fluid model was modified to account for drag reduction by the inclusion of a correlation for drag-reduced friction factor obtained from single phase measurements and curved interface after polymer addition to oil-water flows. The modified model predicted better the experimental data compared to literature models using drag-reduced friction factor correlations.

- In stratified flows, addition of polymer in the water phase increased the average water velocity and decreased the interface height.

- Addition of polymer to stratified oil–water flows decreased the wave amplitude and increased the wavelength and celerity.

CHAPTER 6

6 PIV MEASUREMENTS IN SINGLE PHASE WATER AND TWO PHASE OIL-WATER FLOWS

In this chapter, results of the application of particle image velocimetry (PIV) in both single phase water as well as oil-water flows are presented and discussed. Also discussed are the changes to the turbulence properties of these flows as a result of the addition of polymeric materials. Different polymeric materials were applied and comparisons between their effects on these flows are discussed. The single phase experiments were performed as a basis for comparison with available reports in the literature and for confidence in the results of the oil-water experiments, and these are shown in Section 6.1. The observation of asymmetry in the velocity profiles of drag-reduced single phase water flow are also presented in this section. Section 6.2 shows results and discussion for oil-water flows. Under this section, polymer effect on mean axial velocity profile is presented in Section 6.2.1, while polymer effects on the components of the axial, radial and Reynolds stresses are respectively presented in Sections 6.2.2, 6.2.3 and 6.2.4. Comparisons between the effectiveness of the different polymers (HPAM & PEOs) are thereafter presented in Section 6.2.5. Conclusions drawn from the chapter are summarized in Section 6.3

6.1 PIV Measurements in Single-Phase Flows

The effect of polymer addition on velocity profiles and turbulence properties during single phase water flows can be seen in Figure 6-1 and Figure 6-2 for average water velocities 0.80 m/s and 1.81 m/s (Re = 11055 and 25400 respectively). The experimental dimensionless velocity profile is plotted in Figure 6-1a and Figure 6-2a together with the profiles for the viscous sublayer, the log-law and the maximum drag reduction asymptote (Sher and Hetsroni, 2008; Virk, 1975).

$U^+ = y^+$ viscous sub-layer **6-1**

$U^+ = 2.5\ln y^+ + 5.5$ log-law layer **6-2**

$U^+ = 11.7\ln y^+ - 17.0$ Maximum drag reduction asymptote (MDRA) **6-3**

where U^+ and y^+ are respectively the dimensionless velocity and distance from the wall. ($U^+ \equiv U/u_f$, where u_f (friction velocity) $\equiv \sqrt{\tau_w/\rho}$; $y^+ \equiv y u_f/\nu$ and $\nu \equiv \mu/\rho$ is the kinematic viscosity). The velocity profile changes with the addition of the polymer and approaches the

MDRA curve. It was also observed that when polymer was present, the shape of the velocity profile (not shown here) becomes more parabolic and has a higher maximum compared to the flows without polymers, which suggests laminarization of the flow. With increased drag reduction from 66 % and 74 %, the Newtonian plug (the region between the Newtonian profile and the drag reduced profile) also increases when Figure 6-1a, and Figure 6-2a, are compared.
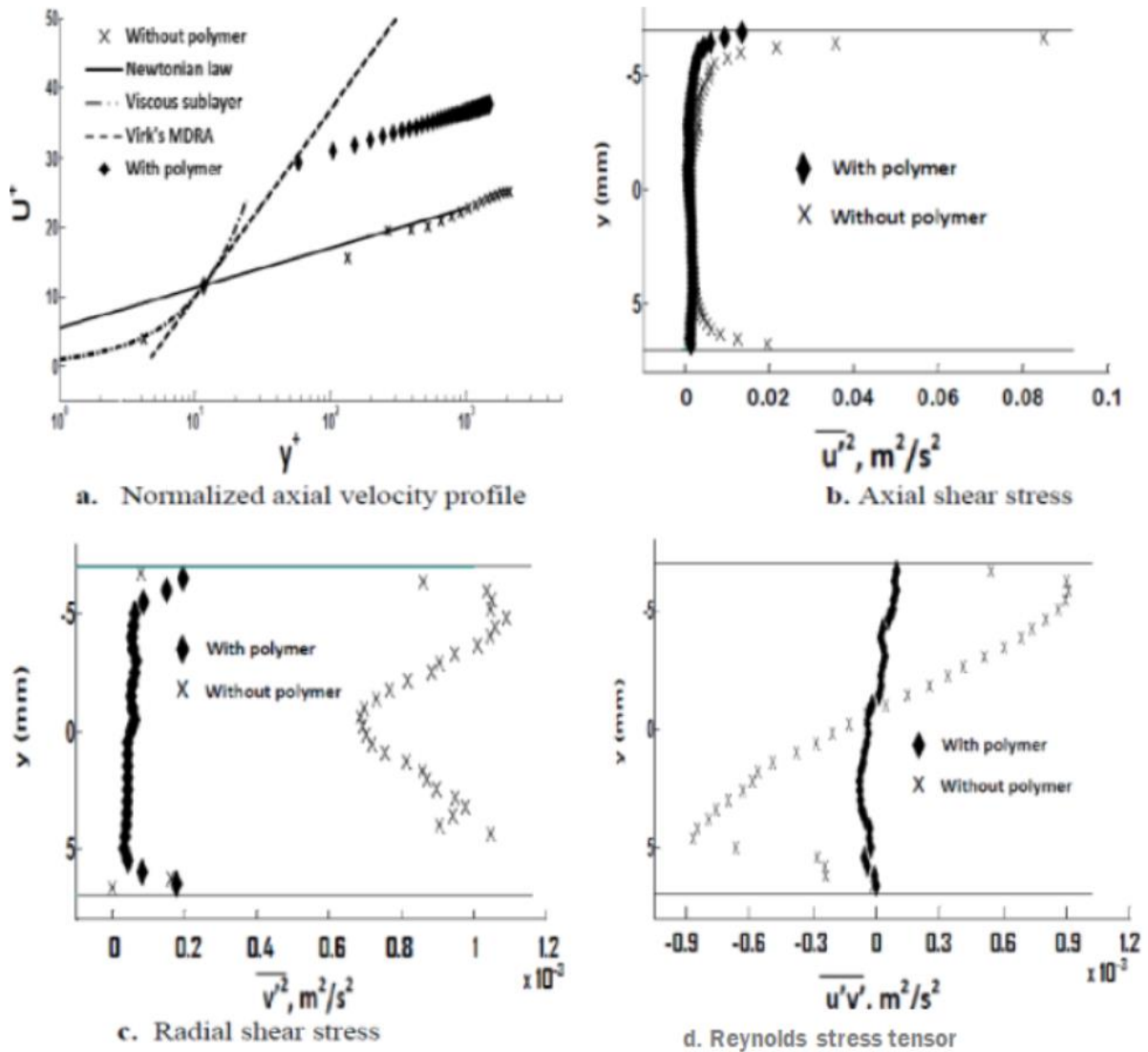
Figure 6-1 Turbulence profiles for drag reduced water flow at U = 0.80 m/s in 14 mmID pipe

This observation is in agreement with the reports by Virk, (1975) and Sher and Hetsroni, (2008) where the Newtonian plug increased with drag reduction and was attributed to increased effectiveness of the polymer based on their model.

a. Normalized axial velocity profile

b. Axial shear stress

c. Radial shear stress

d. Reynolds stress tensor
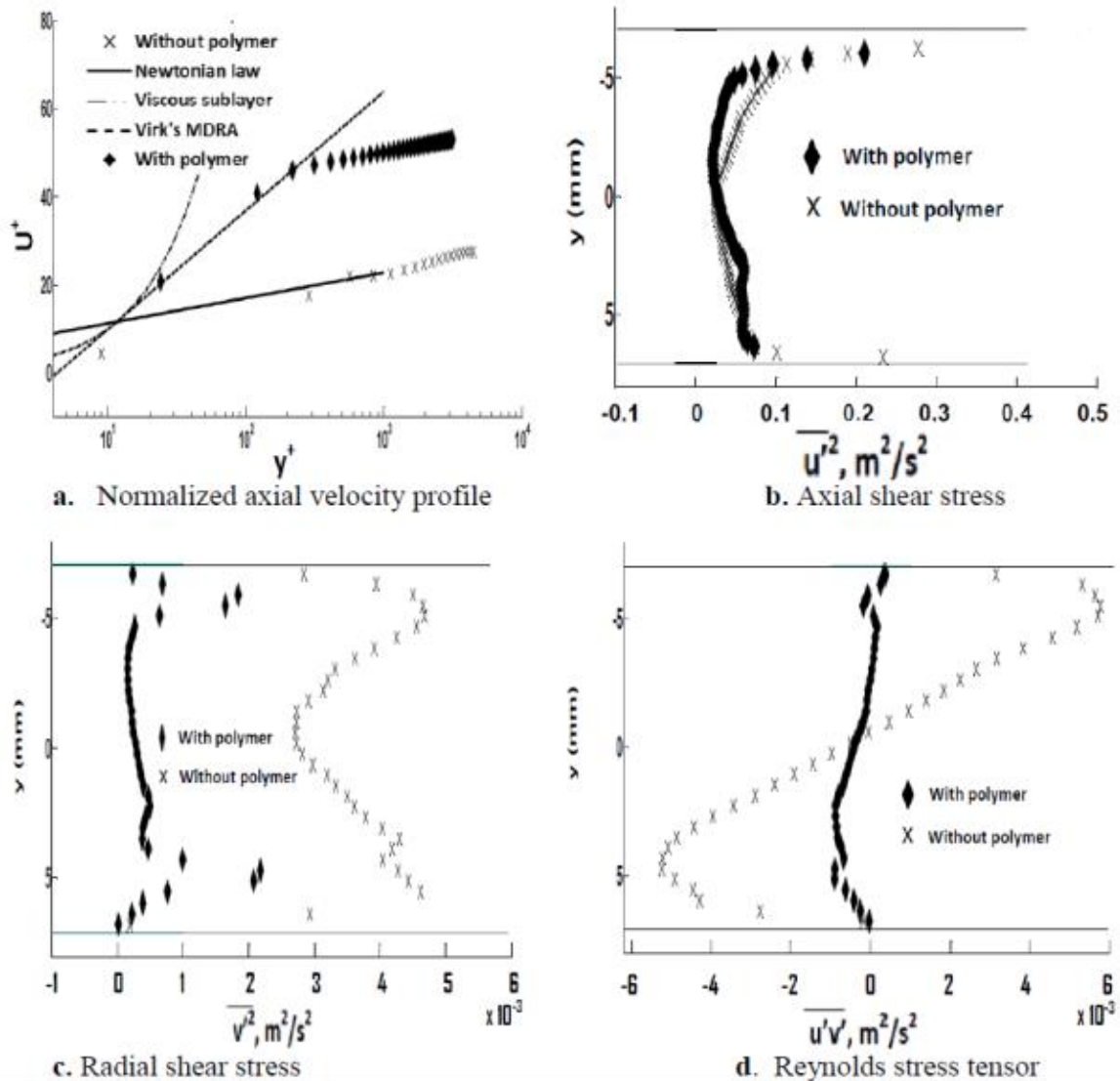
Figure 6-2 Turbulence profiles for drag reduced water flow at U = 1.81 m/s in 14 mm ID pipe

The velocity fluctuations in the axial and radial directions before and after the polymer addition are shown in Figure 6-1(b, c) and Figure 6-2(b, c) for 0.80 m/s and 1.81 m/s velocities respectively. As can be seen, the fluctuating velocities reduced with the addition of polymer. The reduction for the u' was more pronounced close to the wall while for v' occurred at the whole pipe cross section.

In addition, the shear Reynolds stresses (Figure 6-1d and Figure 6-2d) became almost zero when polymer was added. These results agree with previous findings (Warholic et al., 2001, 1999) that addition of polymer reduces the Reynolds stresses although the axial and radial stresses do not necessarily become zero. It should be noted that the small data scattering

seen near the wall is a result of the difficulty in conducting PIV measurements in that area (Den Toonder et al., 1997; Elseth, 2001).

6.1.1 Observations of Asymmetry in Velocity Profiles of Drag-Reduced Water Flows

When the axial velocity profiles of drag-reduced single phase water flows were measured, they were found to be asymmetrical about the flow axis. The observed asymmetry appeared at all Reynolds numbers tested (see Figure 6-3). Similar asymmetry has been reported before by Escudier et al. (2009, 2005) and Esmael and Nouar (2008) who found that it was limited to drag-reduced flows in the transitional flow regimes for Re < 10000. The velocity profiles for flows at Re = 5600, 11200, and 25300 obtained here are shown in Figure 6-3.
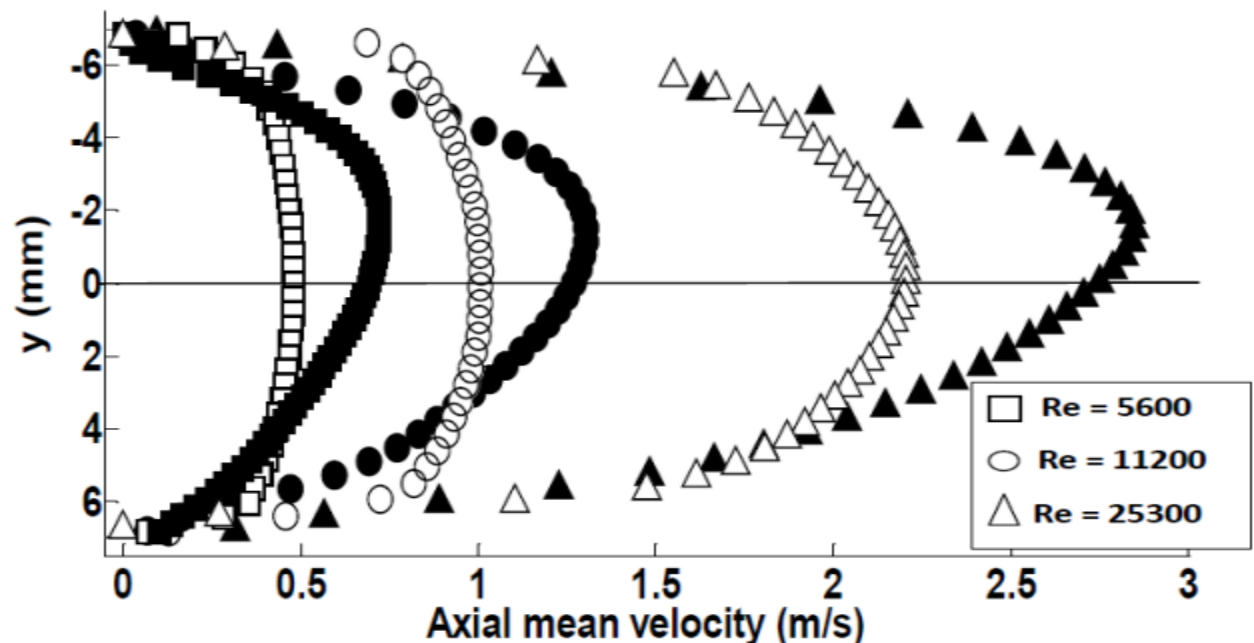
Figure 6-3 Velocity profiles for drag-reduced water flows. Filled symbols are for flows with 20ppm polymer in water while empty symbols are for water only.

The asymmetry seemed to be higher at lower Re. It can be observed from Figure 6-3 that the shape of the velocity profile after polymer addition suggests that the polymer solution is mainly active at the lower region of the pipe implying that it is not well mixed and a concentration gradient may exist. An image of the radial distribution of the velocity magnitude before and after polymer addition (Figure 6-4) confirms the asymmetry in the velocity profile (Figure 6-3) with the peak occurring at the upper part of the pipe.
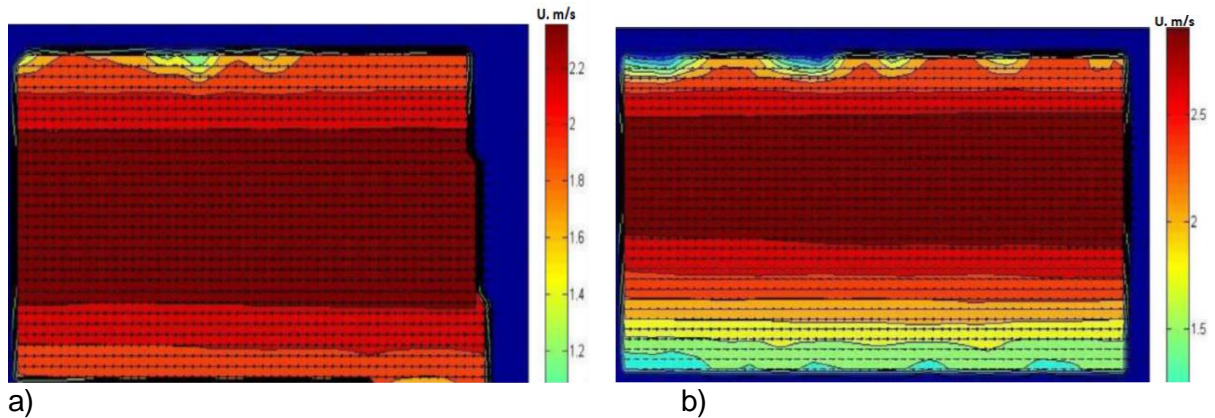
Figure 6-4 PIV Image of axial velocity magnitude for flows at Re = 25300 (U = 1.81m/s) (a) Without polymer, (b) with 20ppm HPAM from 1000ppm master solution.

While the profile is symmetric for only water flows, when polymer is present large velocity gradients appear at the lower part of the pipe compared to the upper one. This region resembles the thickened buffer layer reported by Zadrazil et al., (2012).

Figure 6-5 and Figure 6-6 show some PIV images captured when the polymer master solution was mixed with silver-coated seeding particles before it was injected into the water flow ahead of the inlet section of the pipe. The intention was to trace the mixing pattern of the concentrated polymer solution in the flow using the seeding particles. It can be observed that the particles were well distributed in the flow at all velocities studied while polymer threads with attached particles were observed in most cases. The presence of the polymer threads implies a heterogeneous system and justifies the high drag reduction (65 % for Re = 11200 and 75 % for Re = 25300) observed in these experiments (Hoyer and Gyr, 1998; Vleggaar and Tels, 1973). To evaluate the mixing in the pipe, the second inlet (usually for oil) was used to introduce water without polymer and seeding particles. Similar results and presence of polymer threads were also obtained but drag reduction was less.

To evaluate further whether the asymmetry in the profile was due to insufficient mixing of the polymer, further tests were carried out, as described below:

A. Reduction of the concentration of polymer master solution from 1000 ppm to 500ppm
B. Change of the in-situ polymer concentration from optimal 20 ppm to 5, 10 and 50 ppm.
C. Reduction of the diameter of the polymer injection point.
D. Location of the injection point 1m downstream the previous location and after the inlet section.
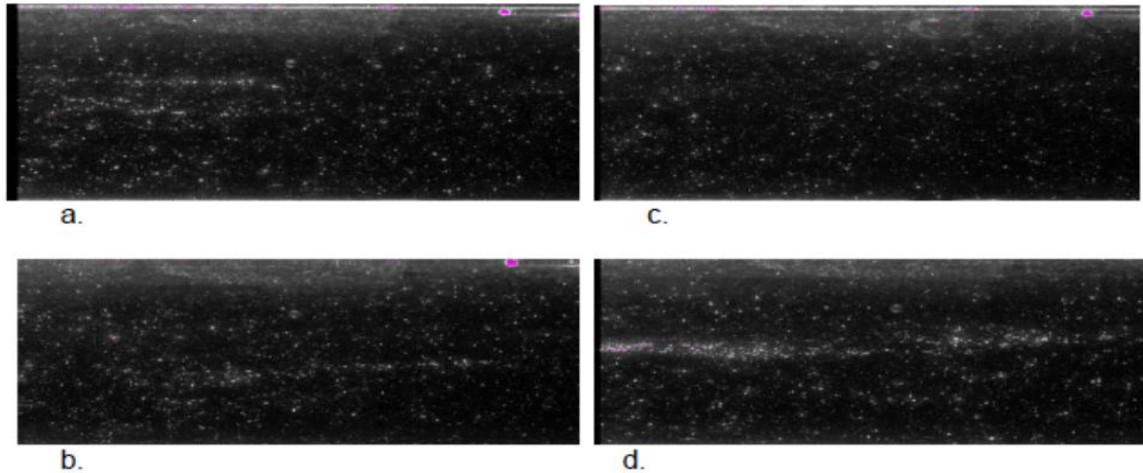
Figure 6-5(a – d) Polymer+tracer particles distribution for single phase water flow at Re = 11200 (U = 0.80m/s)
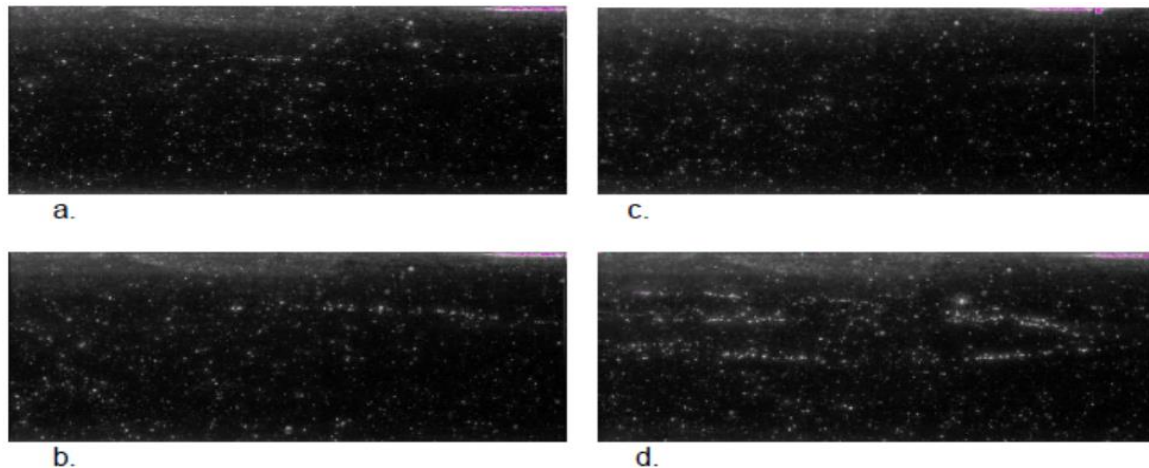
Figure 6-6 (a – d) Polymer+tracer particles distribution for single phase water flow at Re = 25300 (U = 1.81m/s)

E. Location of the polymer injection point to the upper stream line of the inlet section (see figure 3-4). This is to ensure that the polymer solution mixes better with the flow since injection from the lower section may force the polymer to stay at the bottom of the pipe and reduce mixing.

F. Illumination with the laser from the bottom of the pipe as against from the top. This is in the case there are some diffraction effects of the laser sheet

G. Increase the intensity of the laser with reduced camera aperture in case there is laser energy reduction across the pipe section that could affect the profile.

H. Recycle the water phase with the polymer, and later with very small fresh polymer injection

The above changes in the experimental methodology still resulted in flow profile asymmetry.

a) fresh polymer injection without recycle　　b) polymer recycle without fresh injection

c) after 6 recycles without fresh polymer injection
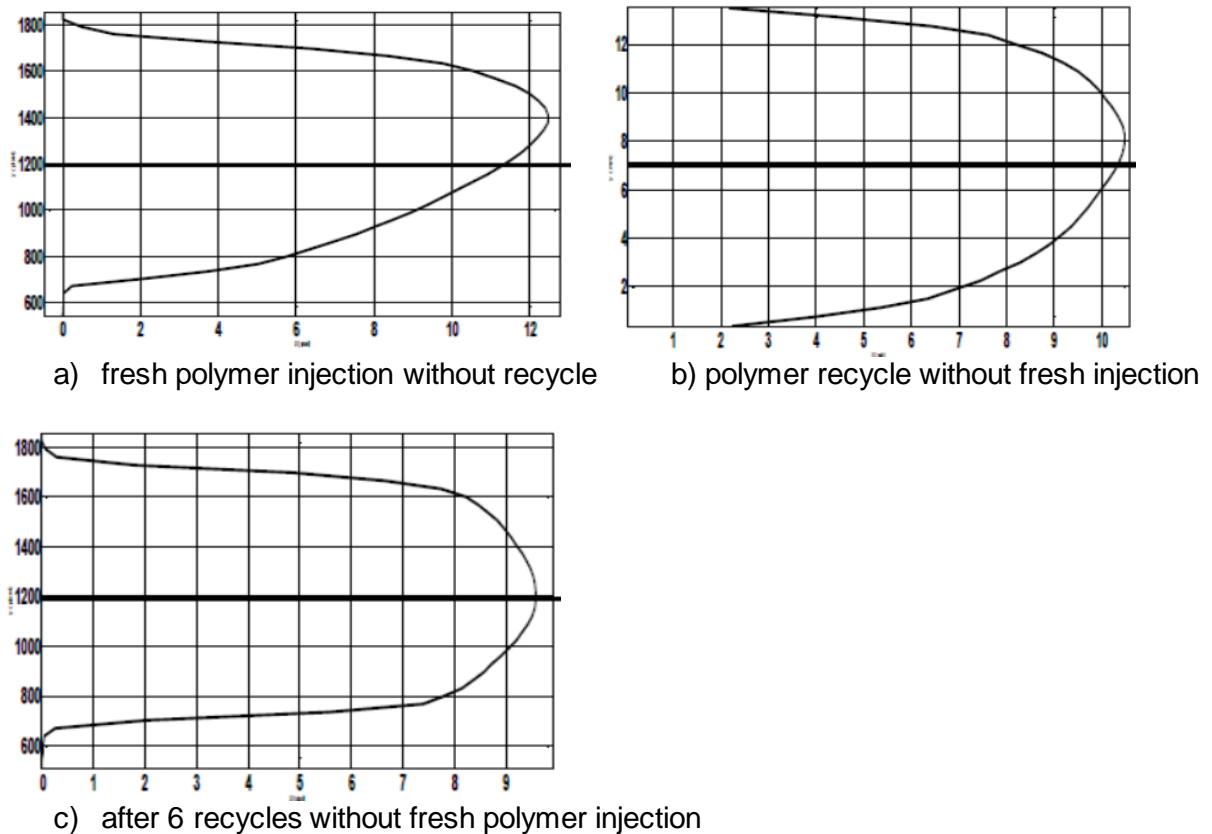
Figure 6-7 Velocity profile of flow at Re = 11200 (U = 0.80m/s)

Only when the polymer solution was recycled and passed through the centrifugal pump, there were changes to the profile with corresponding changes to drag reduction. The profiles obtained are shown in Figure 6-7. As can be seen, when the polymer was recycled once (Figure 6-7b), the degree of asymmetry of the profile reduced compared to flow without recycle (Figure 6-7a) while drag reduction was also reduced to 40 %. The shape of the profile changed while the axial velocity gradient in the lower pipe section increased from the initial value when there was no recycle. Moreover, when the polymer recycle continued without any fresh polymer injection, the measured drag reduction continued to decrease while the velocity profile became more symmetrical until after 6 recycles. At this point, the measured drag reduction was zero and the observed profile was fully symmetrical as in the case of flow without polymer injection (Figure 6-3). However, when 5 ppm from the 1000 ppm master solution of polymer was injected with the recycled flow, drag reduction and profile asymmetry appeared again.

The above shows that the asymmetry in the profile when polymer is added is not caused by the experimental procedure.

Furthermore, the measurement position (view box) was moved upstream to 1m from the polymer injection point and 0.20 m from the mixing point of the two fluid streams. Here, measurements were made for a single stream of water with and without polymer as well as two streams with both branches of the inlets used for water while the polymer solution was injected separately in one of the streams. Both streams contained tracer particles. Images of the flow as well as the profiles are shown in Figure 6-8 to Figure 6-10. Figure 6-8 shows flows at Re = 2330, while Figure 6-9 and Figure 6-10 show flows at Re = 5600 and 11200 respectively. In all cases, single and double streams, the particles were well mixed as can be seen. It can also be seen that with the addition of polymer the maximum velocity increased. It should be noted that the flows are not fully developed at this point of measurement. The asymmetry of the profile after polymer injection is noticeable and increases with fluid velocity. This observation agrees with the profiles obtained at 4m downstream the injection point (Figure 6-3). Also, the percentage increase of the maximum velocity reduces with increasing flowrate. Similar results were obtained when only one inlet was used for water with polymer injection. These results show that the asymmetry in the profile does not depend on axial location in agreement with previous findings (Escudier et al., 2009, 2005).

a. Velocity profile   b. Without polymer   c. With polymer
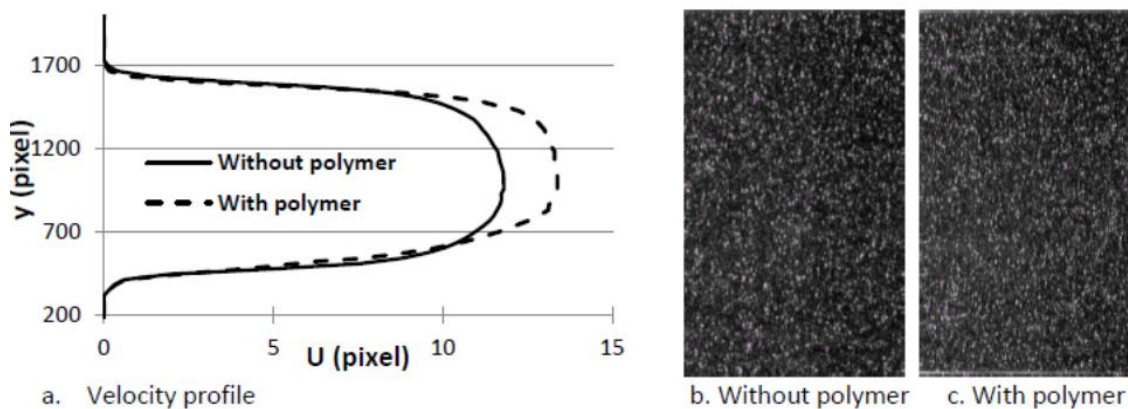
Figure 6-8 Velocity profile and PIV image for U = 0.17m/s (upper and lower water streams)

a. Velocity profile   b. Without polymer   c. With polymer
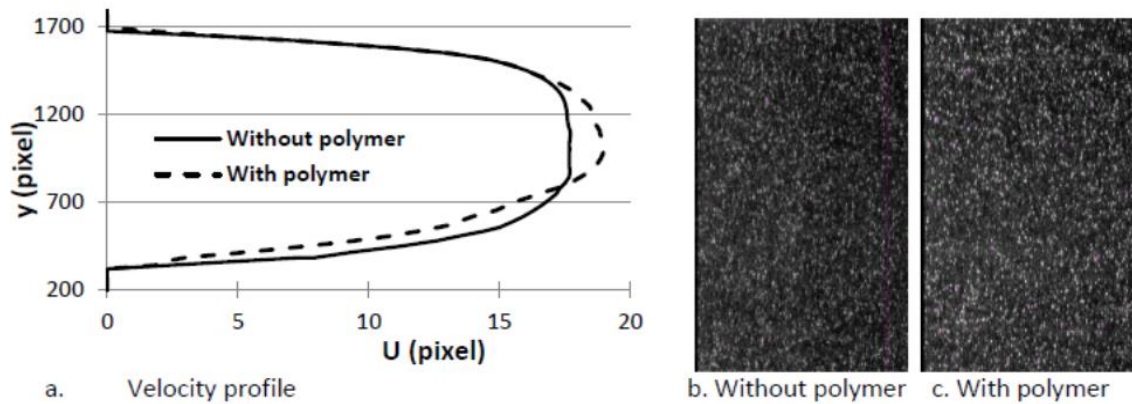
Figure 6-9 Velocity profile and PIV image for U = 0.4m/s (upper and lower water streams)

a. Velocity profile   b. Without polymer   c. With polymer
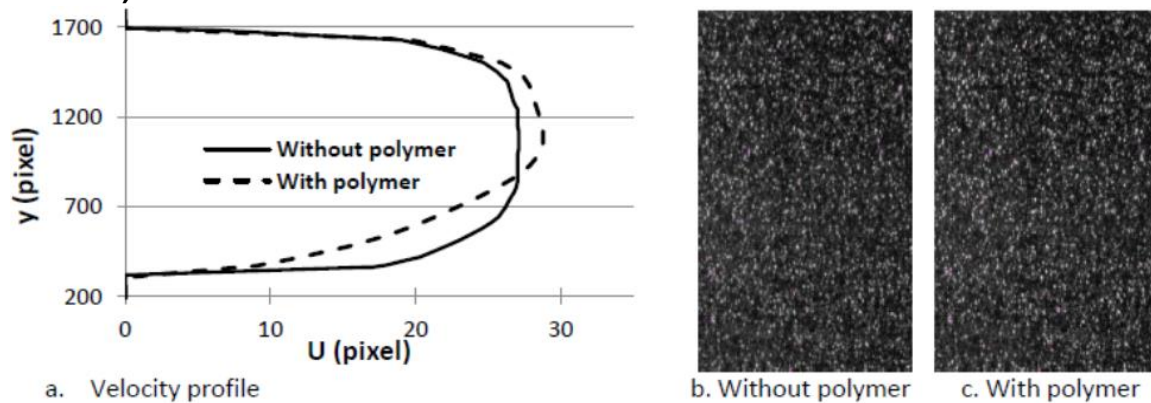
Figure 6-10 Velocity profile and PIV image for U = 0.8m/s (upper and lower water streams)

The polymer preparation method adopted in this study was similar to previous works (Abdullah et al., 2008; Al-Sarkhi and Soleimani, 2004; Den Toonder et al., 1997; Hanratty and Al-Sarkhi, 2001; Nieuwenhuys, 2003; Warholic et al., 1999) and is not considered to cause the observed profile asymmetry.

6.1.1.1 Comparative Experiments with Polyethylene Oxides (PEOs)

To establish whether the profile asymmetry was caused by the type of polymer used (HPAM), some measurements were made with 5MPEO (5 x 10^6 g/mol) and 8MPEO (8 x 10^6 g/mol). The velocity profiles are shown in Figure 6-11 for 20 ppm in-situ polymer concentration from injected 1000 ppm master solution.

As can be seen from Figure 6-11, the profile from 8MPEO is similar to that from HPAM in shape and location of the maximum velocity although with HPAM it is slightly higher at all velocities. The profiles with 5MPEO look different and are closer to flow without polymer. As

already discussed in section 5.1.1 and in Figure 5-3, the higher molecular weight polymers produce higher drag reduction and also increase the asymmetry in the velocity profile.

The densities of 1000 ppm and 20 ppm solutions of these polymers were not different to that of water and gravity is not considered to be the cause of the asymmetry as also concluded by Escudier et al. (2009).
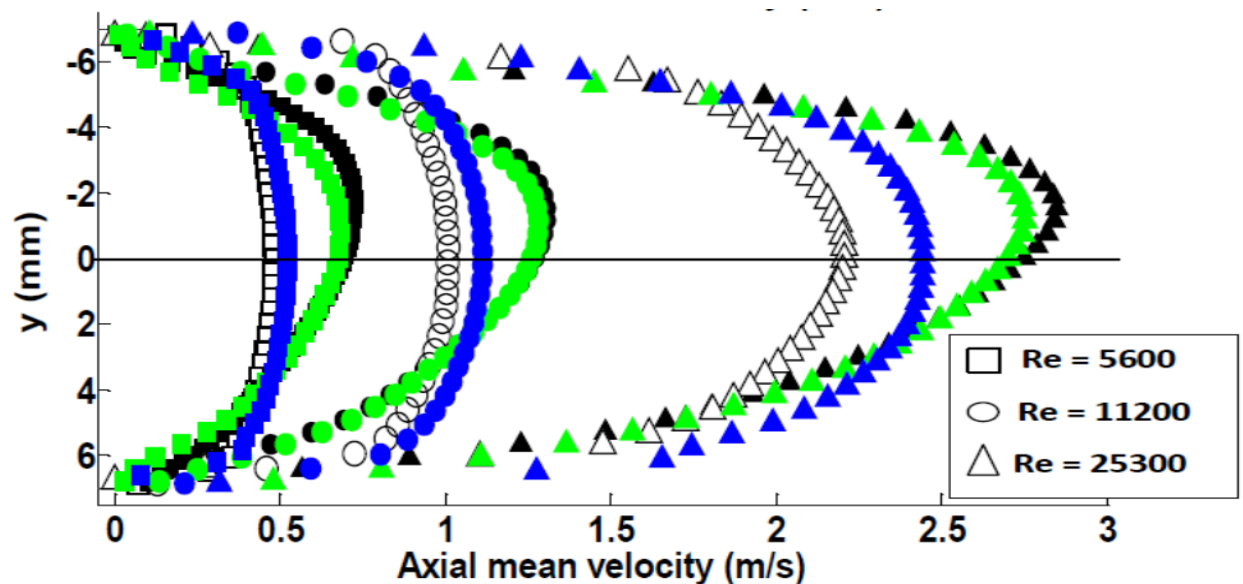
Figure 6-11 Comparative velocity profile for drag-reduced water flows Empty symbols are for water only, while black fill is HPAM, blue 5MPEO, green 8MPEO.

The apparent shear viscosity vs shear rate for the different polymers at concentrations of 1000 ppm, 100 ppm, 50 ppm and 20 ppm are shown in Figure 6-12. As can be seen, the viscosity of the polymers is influenced by their molecular weight and HPAM is more shear thinning than the others. Its viscoelastic nature, and highly flexible molecular and ionic structure impacts on it a high drag reduction capability in comparison to PEOs of similar molecular weight and concentrations (Ebagninin et al., 2009; Escudier et al., 2009; Lewandowska, 2006; Zadrazil et al., 2012).

Concentration can also affect the profile asymmetry. Escudier et al. (2009) used two different polyacrylamide solutions with lower molecular weight than HPAM but higher concentrations (1250 ppm and 300 ppm) and found increased asymmetry with concentration. They however did not report the drag reduction for these concentrations.

The molecular weight and degree of formation of entanglements and aggregates of the polymer fibres are highly indicated as possible causes of the observed profile asymmetry, but some questions remain unanswered.
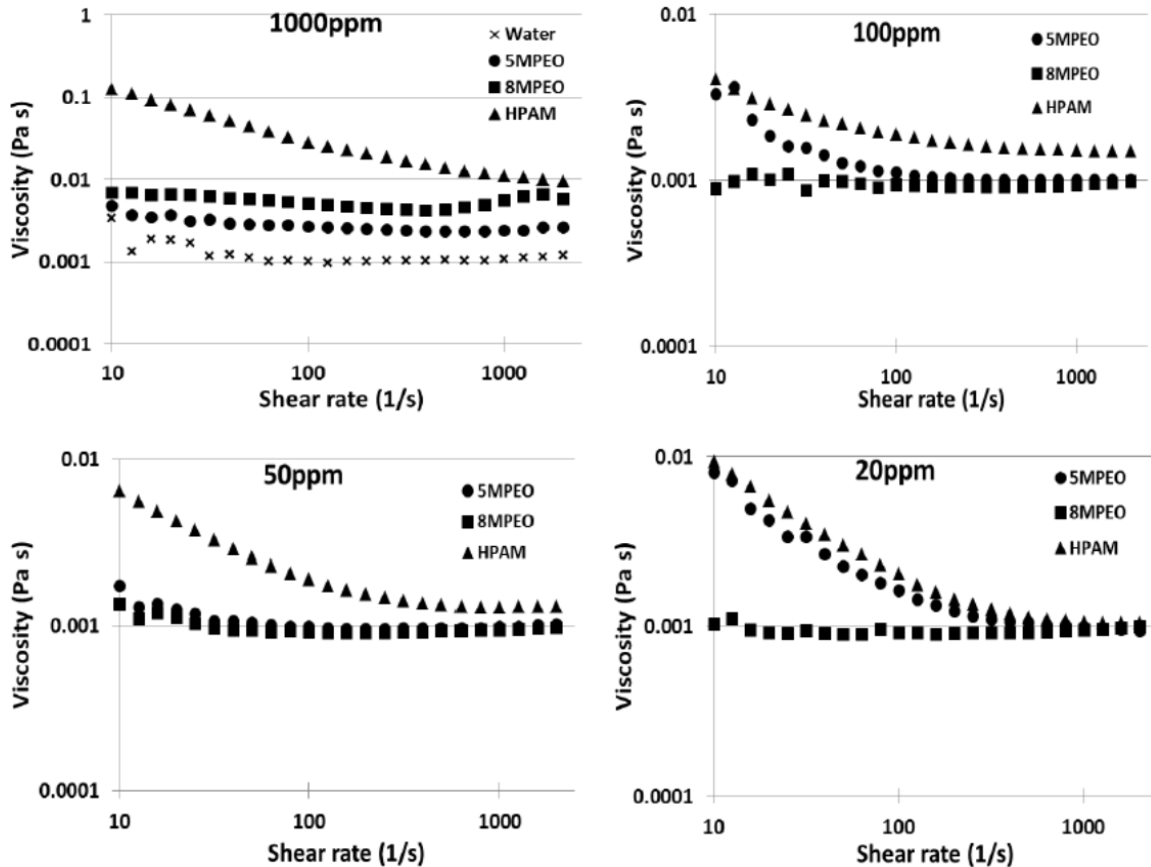
Figure 6-12 Plots of apparent shear viscosity vs shear rate of investigated polymers at different concentrations

6.2 PIV Measurements in Oil-water Flows

In the figures that follow, the 0 mark in the y-axis represents the middle of the 14 mm pipe with 7 mm representing the lower pipe wall and in most cases represented by a dark line.

6.2.1 Influence of Polymer on Mean Axial Velocity

The mean axial velocity profiles in the water phase calculated from the PIV measurements both before and after the addition of polymer are shown in Figure 6-13 for three oil superficial velocities 0.11 m/s, 0.195 m/s and 0.245 m/s and for water superficial velocities equal to 0.166 m/s and 0.22 m/s. In the flow without polymer, the maximum of the axial velocity profiles increases with water velocity. From Table 6-1 and at Uso = 0.11 m/s, the

average in-situ water velocities are in both cases higher than those of the oil (Uo = 0.221 m/s, Uw = 0.331 m/s; Uo = 0.232 m/s, Uw = 0.422 m/s) and the peaks of the velocity profiles are away from the interface. At Uso = 0.195 m/s, the superficial water velocities are in one case lower (Usw = 0. 166 m/s) and in the other higher (Usw = 0.22 m/s) than the oil one. The in-situ water velocities are in both cases higher than those of the oil (Uo = 0.335 m/s, Uw = 0.398 m/s; Uo = 0.352 m/s, Uw = 0.497 m/s) but their difference has decreased compared to the first case and the maximum of the axial velocity profiles has shifted closer to the interface. At Uso = 0.245 m/s even though the superficial oil velocity is higher than both the superficial water velocities, the in-situ oil velocity is again less than the water velocities (Uo = 0.396 m/s, Uw = 0.436; Uo = 0.442 m/s, Uw = 0.498 m/s). The maximum of the velocities is close to the interface. The profiles are similar to those reported by Kumara et al. (2010a, 2010b) where the velocity of the water phase near the interface was found to increase with increasing oil superficial velocity at fixed water superficial velocity.

Table 6-1 Experimental conditions for PIV measurements in oil-water flows

Uso (m/s)	Usw (m/s)	Uo (m/s)	Uw (m/s)	Reo	Rew	$S = \dfrac{Uo}{Uw}$
0.11	0.166	0.221	0.331	465	2837	0.668
	0.22	0.232	0.422	476	3739	0.550
0.15	0.166	0.267	0.379	595	2957	0.704
	0.22	0.293	0.456	624	3828	0.643
	0.28	0.317	0.531	650	4713	0.597
0.195	0.166	0.335	0.398	759	3002	0.842
	0.22	0.352	0.497	780	3933	0.708
	0.28	0.387	0.564	818	4801	0.686
0.245	0.166	0.396	0.436	921	3090.	0.908
	0.22	0.442	0.498	979	3935	0.888
	0.28	0.380	0.790	897	5339	0.481

When polymer is added in water, the velocity profiles acquire a more parabolic shape while the maximum values increase. The profiles are closer to laminar flow although the actual Rew is higher than in the cases without polymer (see also Table 5-2). This change leads to a reduction in the axial velocity gradient (du/dy) in the region close to the wall and indicates

an increase in the thickness of the boundary layer (White and Mungal, 2008; Zadrazil et al., 2012).

The average in-situ velocity in the water phase is higher than in the oil phase at all cases studied and the peaks in the profiles are away from the interface, while they tend to approach the interface as the oil velocity increases. The maximum axial water velocity increased with water and oil superficial velocities and was found to be between 12 % to 30 % higher than in the flow without polymer for all conditions studied.
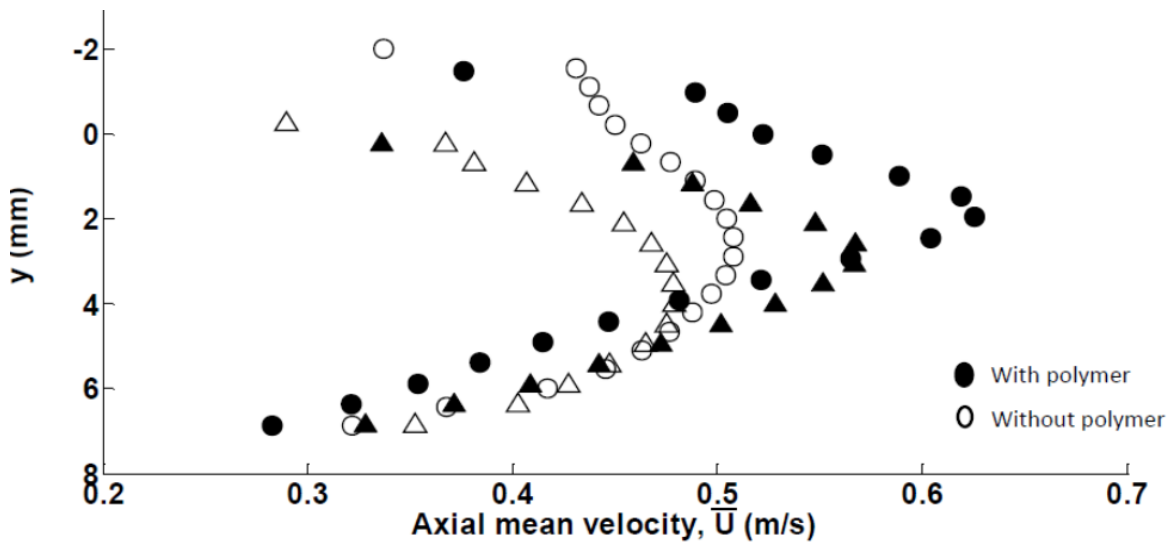
a) Uso = 0.11m/s; Usw = 0.166m/s (triangles) and Usw = 0.22m/s (circles)
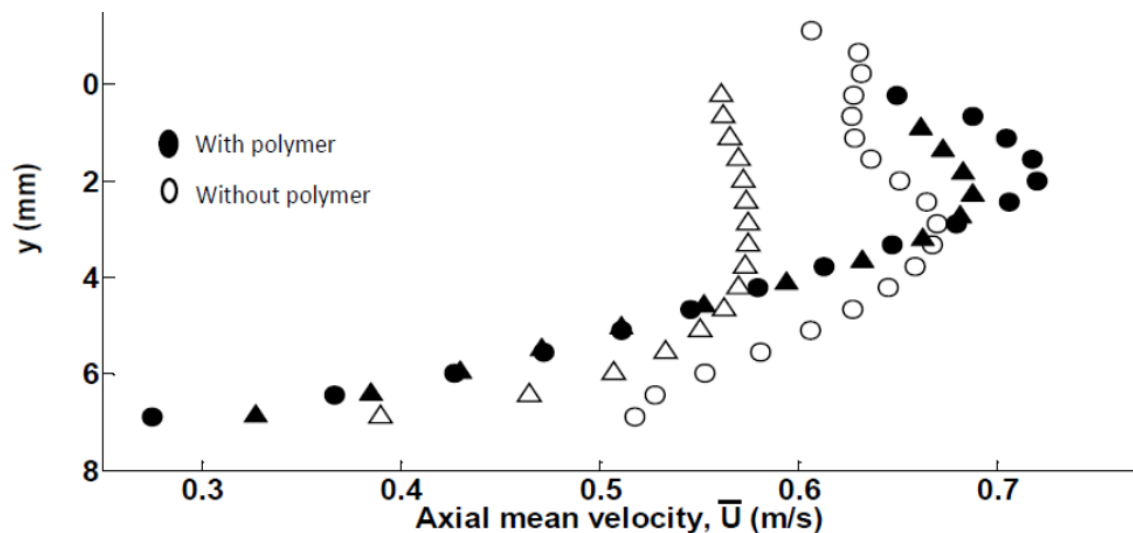
b) Uso = 0.195m/s; Usw = 0.166m/s (triangles) and Usw = 0.22m/s (circles)

c) Uso = 0.245m/s; Usw = 0.166m/s (triangles) and Usw = 0.22m/s (circles)

Figure 6-13 (a-c) Mean axial velocity profiles in the water phase. Open symbols are for flow without polymer while filled symbols are for flow with polymer

6.2.2 Influence of Polymer on Axial Velocity Fluctuations u'

The axial component of velocity fluctuations calculated from Equation 3-5 are shown in Figure 6-14 for the same conditions shown in Figure 6-13.

a) Uso = 0.11m/s, where Usw = 0.166m/s (triangle) and Usw = 0.22m/s (circles)

b) Uso = 0.195m/s, where Usw = 0.166m/s (triangle) and Usw = 0.22m/s (circles)

c) Uso = 0.245m/s, where Usw = 0.166m/s (triangle) and Usw = 0.22m/s (circles)

Figure 6-14 (a-c) Mean axial stress component profiles in the water phase. Open symbols are for flow without polymer while filled symbols are for flow with polymer

For flows without polymer the fluctuations have their highest values in the regions close to the wall and the interfaces (see Figure 6-13 and Figure 6-14). These are regions of high shear rates in single and multiphase flows (Kumara et al., 2009; Schmitt, 2008). The peak of the axial fluctuations in the lower wall region increases with increasing superficial and actual water velocity for a fixed superficial oil velocity. The peak also generally increases for fixed superficial water velocity (but increasing in-situ velocity) and increasing superficial oil

velocity, apart from Uso = 0.245 m/s and Usw = 0.166 m/s (Uo = 0.396 m/s, Uw = 0.436 m/s).

With the addition of polymer, there is a significant reduction of the axial component of velocity fluctuations in the interface and the wall regions where the velocity fluctuations were reduced by as much as 81% compared to the flows without polymer. This implies that the polymer is significantly active in the regions of high shear stresses. In the bulk water flow however, the axial stress component increased (see Figure 6-14) which suggests an increase in momentum transfer in the axial direction. The increase is located in similar radial positions where the minimum values of the fluctuation components were observed in the Newtonian flows (see Figure 6-14). This is also similar to the location where the maximum values of the axial velocity appear (Schmitt, 2008; Zhang et al., 1998). This profile suggests a redistribution of turbulent motion in the axial direction of flow. This profile suggests a redistribution of turbulence in the axial direction of flow. In their reports on drag reduced single phase water flows, Wei and Willmarth, (1992), Warholic et al. (1999) and White et al. (2004) reported an increase in the streamwise turbulence intensity after polymer addition while the peak moves farther away from the wall than in the Newtonian flows. However, Warholic et al. (1999) and White et al. (2004) concluded that the increase was restricted to drag reductions less than 64 % and that at higher drag reductions (close to MDRA), the peak of the profile of the streamwise turbulence intensity reduces to values less than for the Newtonian flows This reduction in the peak of the axial turbulence profile for higher drag reduction was also observed in the single phase results shown in Figure 6-1 and Figure 6-2 where drag reduction were respectively 65 % and 74 %. The reduction of the axial velocity fluctuations particularly in the near wall region helps to reduce the degree of corrosion in pipes used for fluid transport (Kang et al., 1998a; Sedahmed et al., 1999; Sellin et al., 1982).

6.2.3 Influence of Polymer on Radial Velocity Fluctuations, v'

The radial components of velocity fluctuations v'^2, calculated from Equation 3-6, are shown in Figure 6-15. The radial fluctuations are about an order of magnitude less than the axial fluctuations. Unlike the axial component, the maximum value of the radial component of velocity fluctuations is in the bulk flow while in the region close to the pipe wall the values are low (Kumara et al., 2010a, 2010b). The radial stress tensor is also high close to the interface (upper section of the profiles), because of the wavy nature of the interface (Cheung and Street, 1988; Cohen and Hanratty, 1968).

As can be seen the fluctuations do not change significantly with increasing oil superficial velocities at constant water superficial velocities, but increase with water velocity for the same oil velocity. The values of the radial component would be affected by interfacial waviness and Reynolds number. For constant superficial water velocity, when the superficial oil velocity increases the relative in-situ velocity between the two phases decreases (Table 6-1), and this can reduce the interfacial waves which seem to decrease the radial component of velocity fluctuations. Moreover, the oil phase was always laminar with Reynolds numbers typically less than 1000; an increase in the oil flowrate therefore has no significant effect on the radial fluctuations around the interface. With increasing water superficial velocity, Usw, for a fixed oil superficial velocity Uso, the difference in the in-situ velocities of oil and water increases which leads to waves with higher amplitude. In addition, the water phase Rew increases (increased turbulence). These phenomena increase the radial velocity fluctuations in the water phase. For example at Uso = 0.11 m/s and Usw = 0.166 m/s, the relative in-situ velocity between the phases is 0.11 m/s and the Rew = 2837 while at Uso = 0.11 m/s and Usw = 0.22 m/s, it is 0.19 m/s and the Rew = 3739.

The addition of polymer led to a significant reduction of the radial fluctuation component, particularly in the bulk flow, with values of 30 – 70 % less than those in the flow without polymer. At lower water velocity, specifically at Usw = 0.166 m/s and 0.22 m/s, the drag-reduced radial fluctuation profile is similar at all Uso.
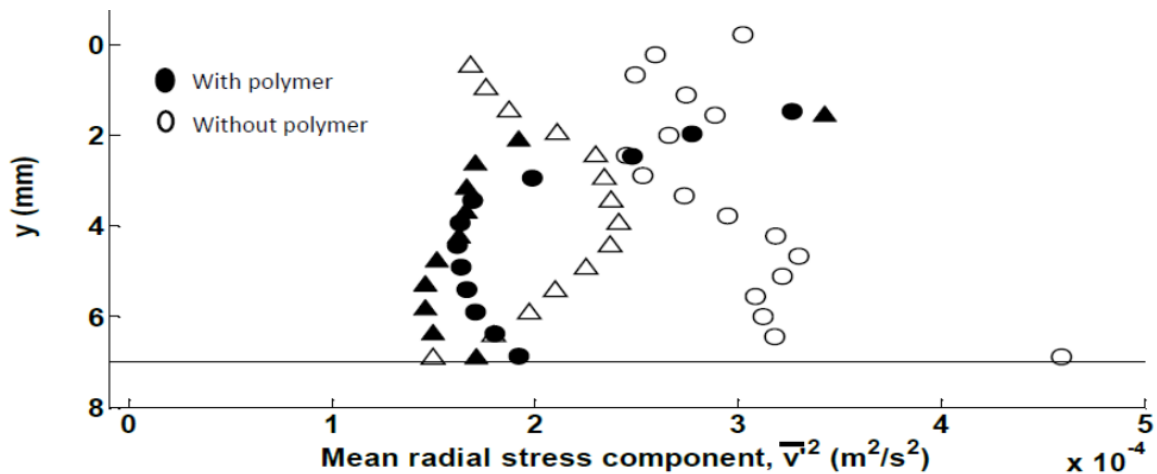
a) Uso = 0.11m/s, where Usw = 0.166m/s (triangle) and Usw = 0.22m/s (circles)
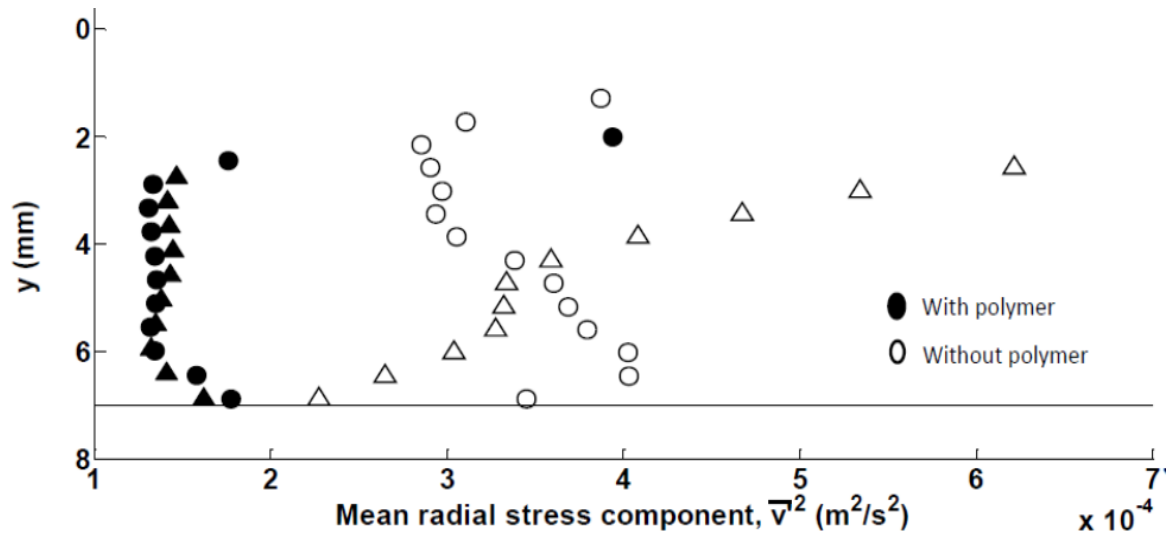
b) Uso = 0.195m/s, where Usw = 0.166m/s (triangle) and Usw = 0.22m/s (circles)
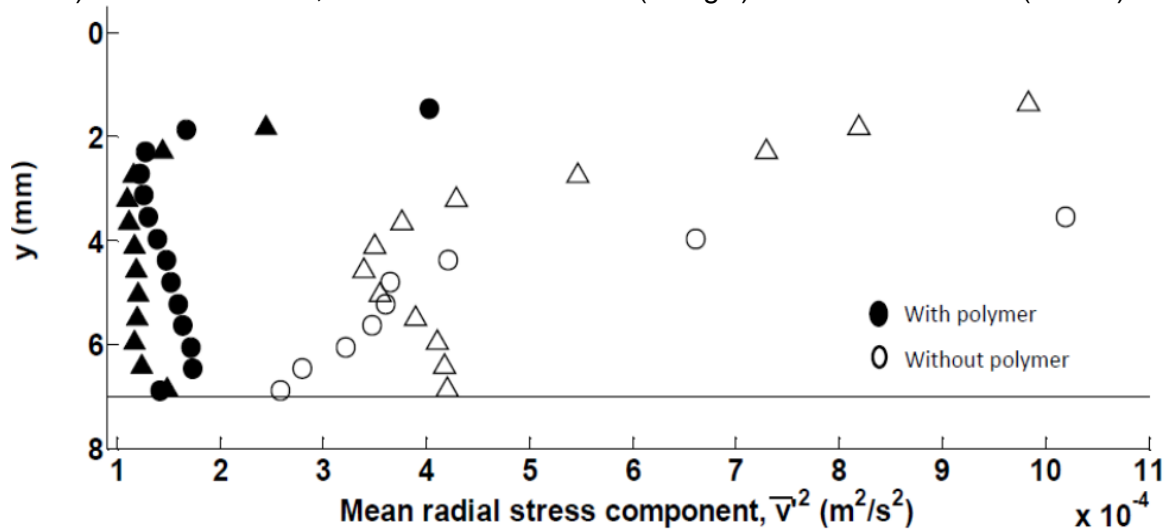
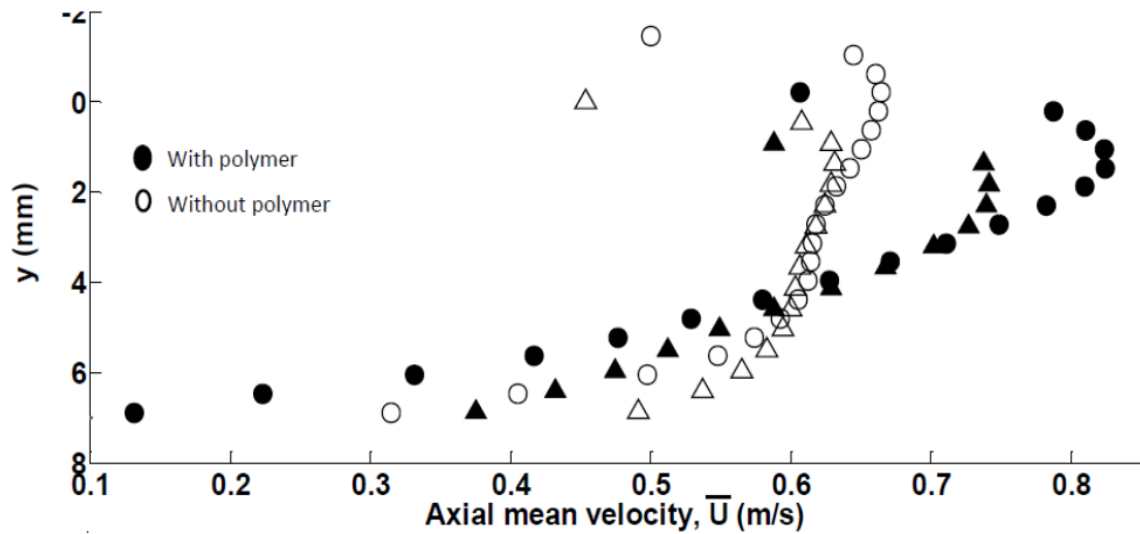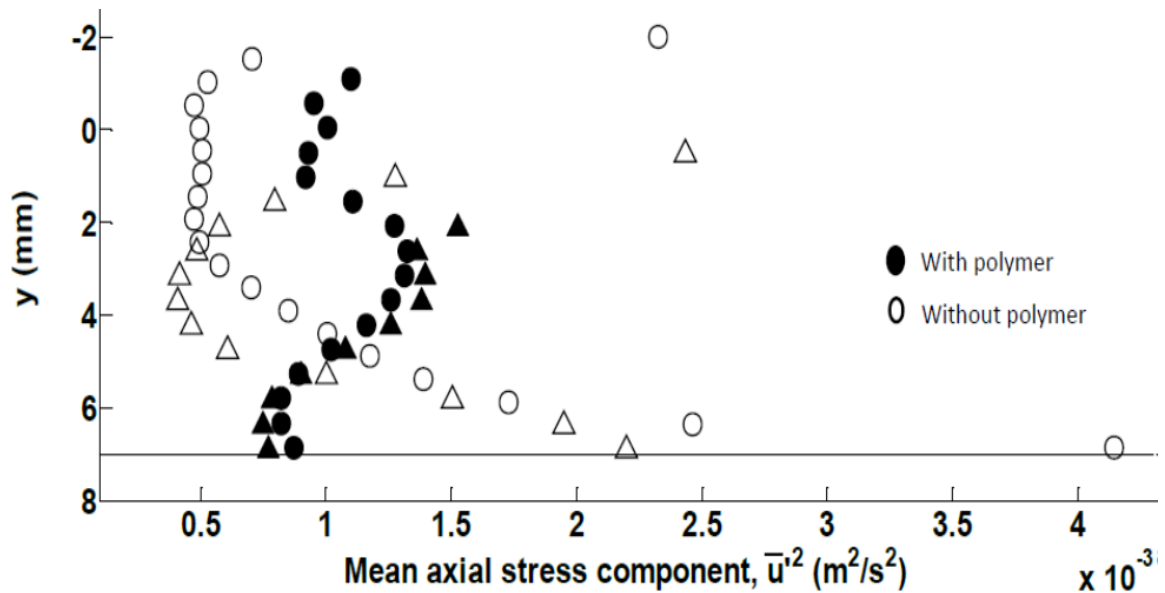c) Uso = 0.245m/s, where Usw = 0.166m/s (triangle) and Usw = 0.22m/s (circles)

Figure 6-15 (a-c) Mean radial stress component profiles in the water phase. Open symbols are for flows without polymer while filled symbols are for flow with polymer

As can be observed, when polymer is added in the flow the radial component of velocity fluctuations is reduced while the axial one is reduced in the near wall and interface regions but increased within the bulk flow. This supports the proposed mechanism that drag reduction is not just a suppression of turbulence but it involves a redistribution of turbulent kinetic energy from the radial to the axial flow direction (Brasseur et al., 2005; Den Toonder et al., 1997; Wei and Willmarth, 1992; White and Mungal, 2008).

6.2.4 Influence of Polymer on Reynolds Stress Component, u'v'

The Reynolds stress component for the oil-water flows calculated from Equation 3-7 are shown in Figure 6-16 and increase with increasing oil or water velocities. The shear Reynolds stress were negative at the lower part of the velocity profile, positive at the upper part and zero at similar radial positions where the maximum of the axial velocity is observed and in agreement with a previous report (Scharnowski et al., 2010). The highest values of the mean Reynolds stress are found in the region near the wall and the interface where also the maximum values of the magnitude of the radial and axial components of velocity fluctuations occur. These observations agree with previous studies in gas-liquid (Birvalski et al., 2013) and liquid-liquid flows (Kumara et al., 2010a, 2010b).

When polymer was added to the flows, the Reynolds stress component reduced everywhere within the flow and more significantly in the near wall and near interface regions. The reduction of the maximum values in the near wall region was as much as 90 % in some cases. The reduction increased with increasing actual water phase Reynolds numbers. A reduction in the mean Reynolds stress indicates a decrease of turbulent momentum transfer in the radial direction (Gyr and Bewersdorff, 1995; Wei and Willmarth, 1992). In Newtonian flows, the high velocity gradients in the near-wall region lead to high production of turbulent eddies which are transported into the bulk flow in the radial direction against the desired axial flow direction. This leads to energy losses and increased pressure drop. The reduction in the radial transport of the turbulent eddies with polymer leads to a decrease in energy losses and a corresponding enhancement of the axial flow (Figure 6-13). This improved energy efficiency is measured as a reduction in the pressure drop (drag reduction) of the system. However, the decrease in Reynolds stress component is not proportional to the measured drag reduction.

In cold regions where pipes are heated to prevent hydrate formation among other things, the reduction in momentum transfer from the wall to the bulk flow can help in conserving the heat thereby reducing operational costs (Vleggaar and Tels, 1973; Wang et al., 2011; Zhang et al., 2013).
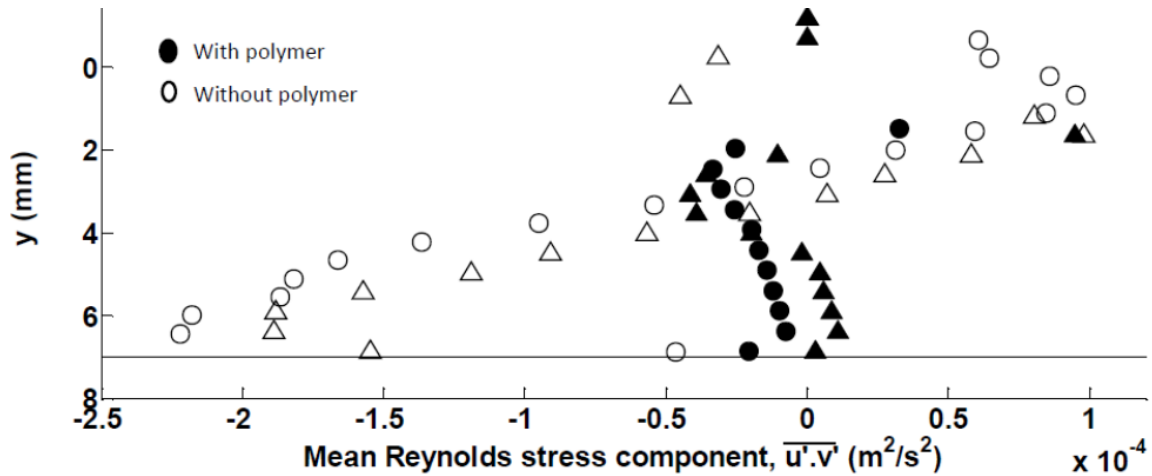
a) Uso = 0.11m/s, where Usw = 0.166m/s (triangle) and Usw = 0.22m/s (circles)
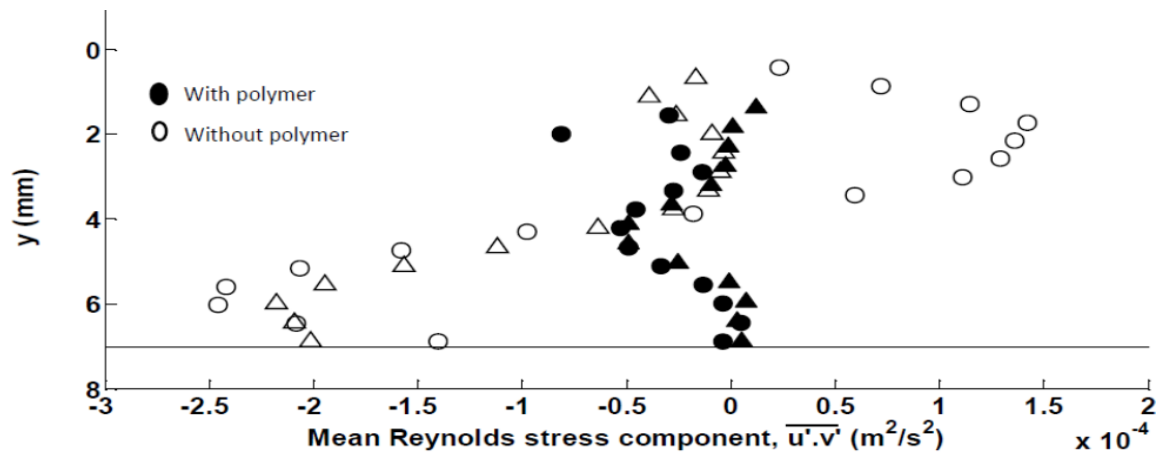
b) Uso = 0.195m/s, where Usw = 0.166m/s (triangle) and Usw = 0.22m/s (circles)
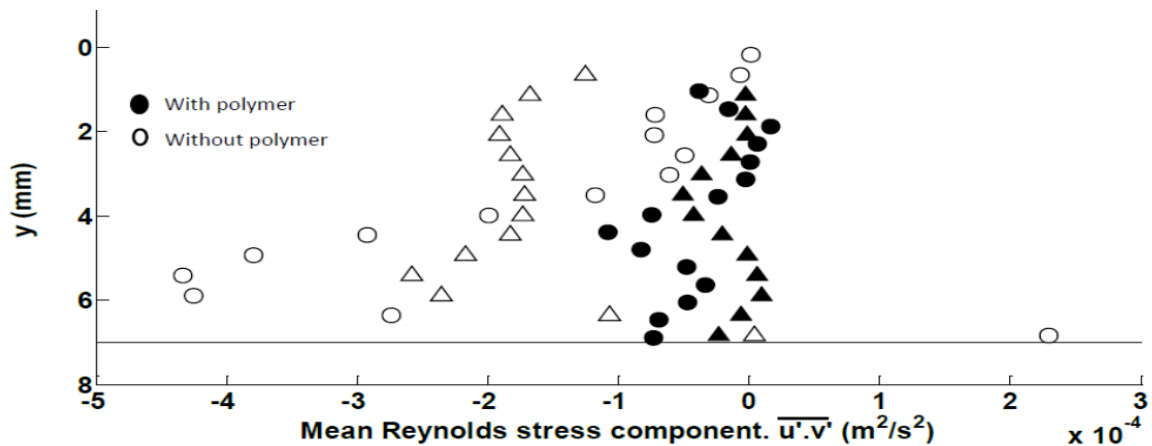
c) Uso = 0.245m/s, where Usw = 0.166m/s (triangle) and Usw = 0.22m/s (circles)
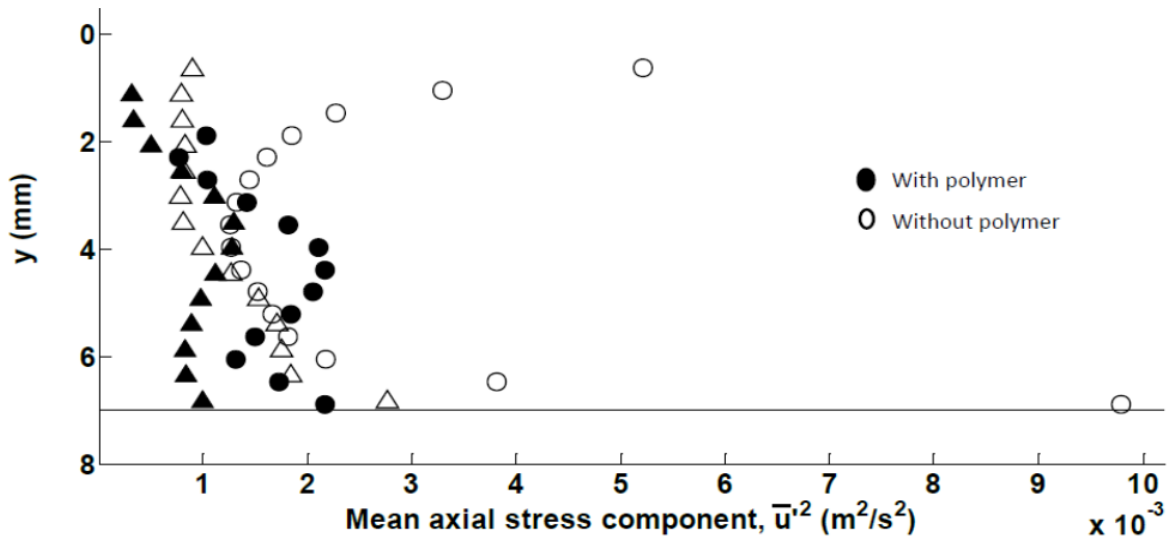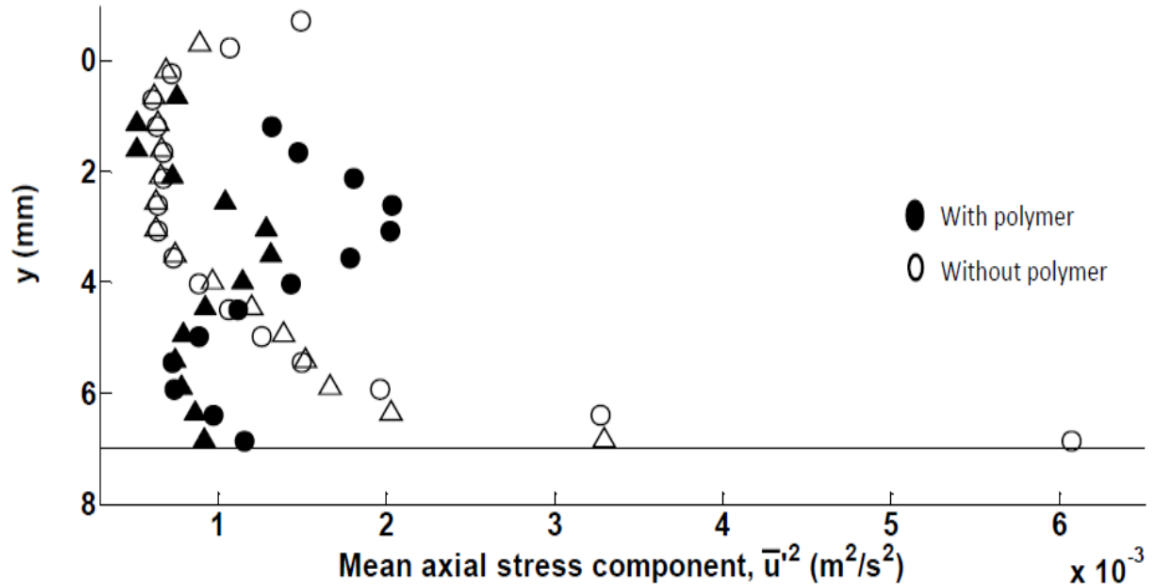
Figure 6-16 (a-c) Mean Reynolds stress component profiles in the water phase. Open symbols are for flow without polymer while filled symbols are for flow with polymer.

6.2.5 Experiments with Polyethylene Oxide (PEO)

It was found that compared to HPAM, the addition of 8MPEO in the water phase had similar effects while that of 5MPEO was different, as can be seen from the friction factor against Reynolds number graphs in Von Karman coordinates as shown in Figure 5-3 and discussed in Section 5.1.1. In the same figure the maximum drag reduction asymptote (MDRA; Virk, 1975) and the Prandtl-Karman (P-K) line for Newtonian flows are also shown.

For the oil-water flow studied here the actual water Re were less than 10000 where the effects of 8MPEO and HPAM were found to be similar. Therefore, only comparisons between HPAM and 5MPEO will be shown. In the following velocity and stress profiles are compared for HPAM and 5MPEO, for Uso = 0.15 m/s and Usw = 0.166 m/s as can be seen in Figure 6-17 to Figure 6-20. When 5MPEO is added to the water phase, the maximum of the velocity increases but the profile does not change shape significantly (see Figure 6-17). In general 5MPEO affects the flow less than HPAM.

With the addition of 5MPEO, the axial and the absolute values of the mean Reynolds stress were increased compared to the flow without polymer, while they were reduced when HPAM was added. The radial component of the velocity fluctuations was slightly reduced with 5MPEO compared to the flow without polymer but not as much as in the case of HPAM. The Reynolds stress and axial component of the velocity fluctuations depend on the axial velocity gradient and are high in areas of large velocity gradient (Scharnowski et al., 2010). The increase in the axial velocity gradient close to the wall after the addition of 5MPEO leads to corresponding increase in the Reynolds stress and axial component of the velocity fluctuations, when compared to flows without polymer. The same trends were seen at the other Uso tested. At higher superficial oil and water velocities, Uso > 0.15 m/s and Usw > 0.25 m/s (not shown here) where the water Reynolds number was greater than 4000, there was some reduction in the axial velocity fluctuations and Reynolds stress in the 5MPEO solution compared to flow without polymer but not as large as with the HPAM. This suggests that with low molecular weight polymers higher Reynolds numbers may be required to initiate drag reduction. Polymers with large molecular weights have high degree of chain entanglement and aggregate formation which enhance drag reduction (Abdulbari et al., 2014; Al-Sarkhi, 2010; Sellin et al., 1982; Virk, 1975; Zadrazil et al., 2012). High molecular weight polymers are also less susceptible to mechanical degradation compared to their lower molecular weight counterparts with the same chemical structure. In addition, ionic

polymers, such as HPAM, are known to be more effective drag reducing agents compared to non-ionic ones, such as the PEOs (Abubakar et al., 2014a).
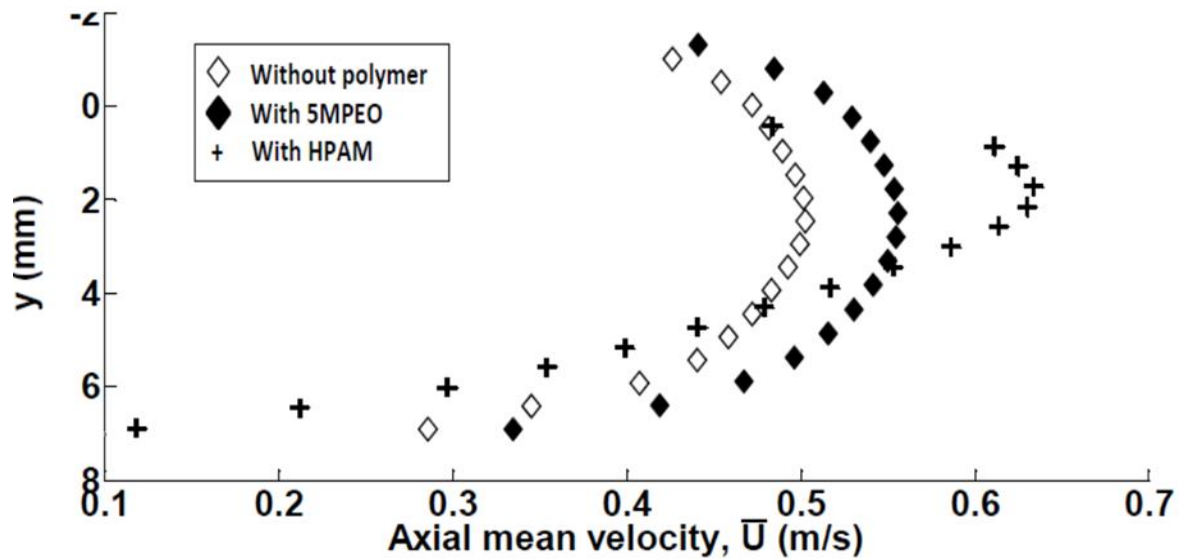
Figure 6-17 Axial velocity profiles for Newtonian and drag-reduced oil-water flows at Uso = 0.15 m/s and Usw = 0.166 m/s
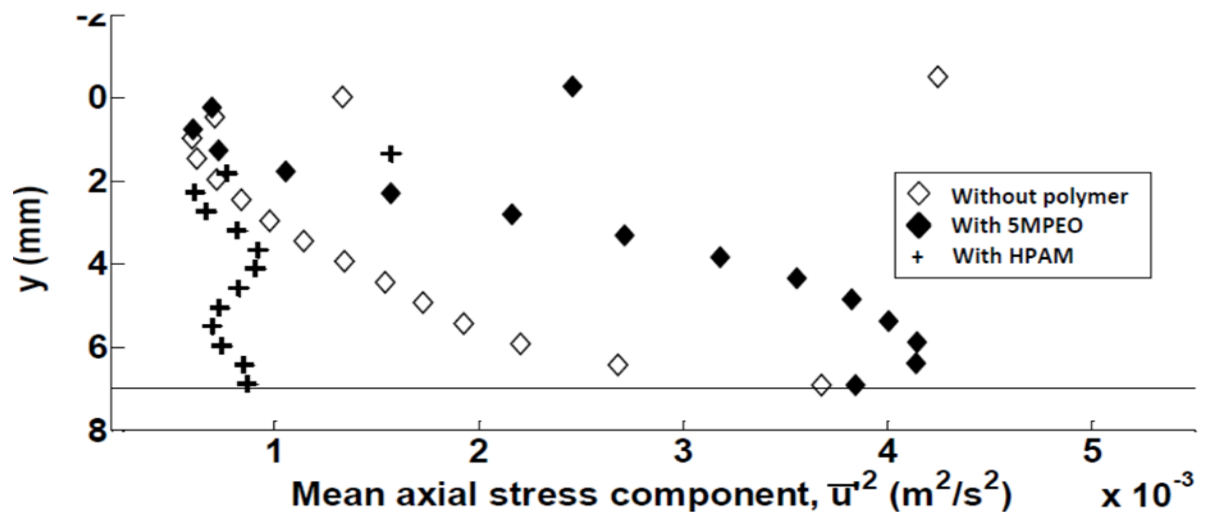
Figure 6-18 Axial stress component for Newtonian and drag-reduced oil-water flows at Uso = 0.15 m/s and Usw = 0.166 m/s
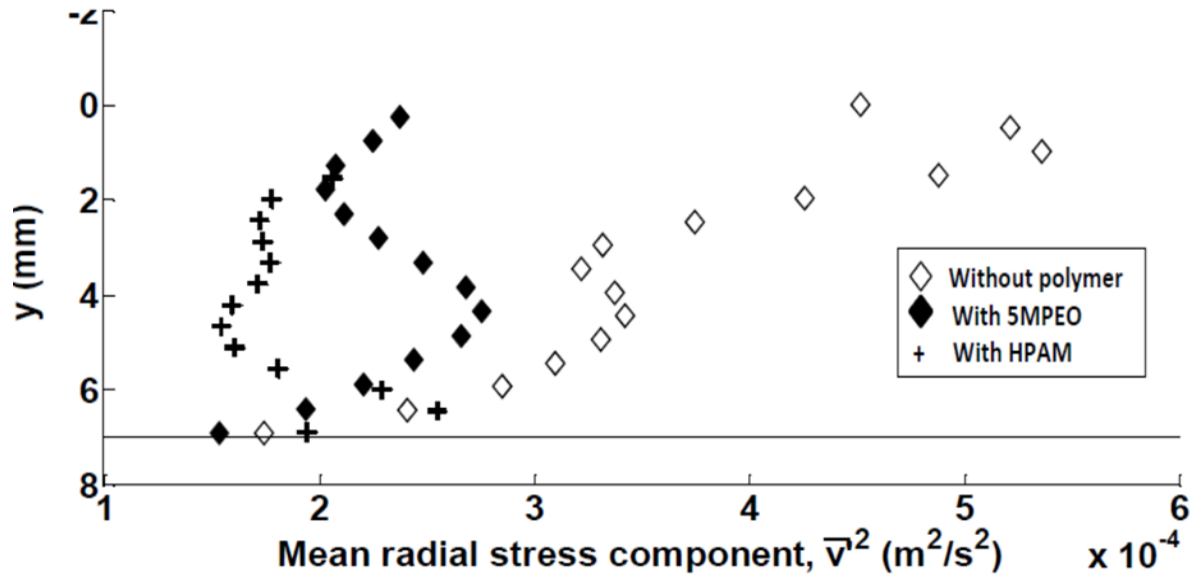
Figure 6-19 Radial stress component for Newtonian and drag-reduced oil-water flows at Uso = 0.15 m/s and Usw = 0.166 m/s
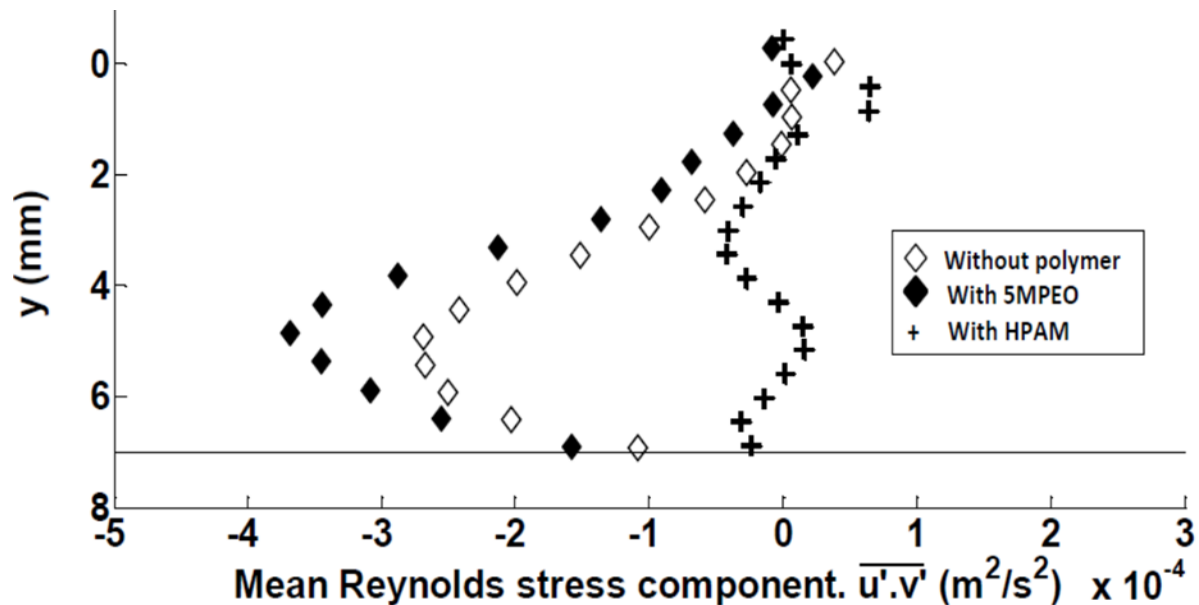
Figure 6-20 Reynolds stress component for Newtonian, and drag reduced oil-water flows at Uso = 0.15 m/s and Usw = 0.166 m/s

6.3 Conclusions

The effects of different polymers on the velocity and turbulence properties of oil-water two-phase flows have been studied using PIV. The polymers used were polyacrylamide (HPAM) and two types of polyethylene oxide (PEO) with different molecular weights. Investigations were carried out in the stratified and stratified wavy flow regimes, where the following were found:

- The degree of asymmetry of the velocity profiles of drag-reduced single phase water flows was found to be influenced by the molecular weight of the polymers used. The cause of the asymmetry is unknown and is attributed to an inherent property of the polymers.

- The addition of polymer to the water phase of oil-water flows increased the average and the maximum velocity in the water phase. The axial velocity profile became more parabolic signifying laminarization of the flow in the water layer.

- Turbulence properties of the flows were significantly affected by the addition of polymer to the water phase; mean Reynolds stress and radial component of velocity fluctuations were reduced throughout the pipe section while the axial component of velocity fluctuations were reduced close to the wall but increased in the bulk flow.

- Drag reduction was affected by the molecular weights of the polymers used and increased with increasing molecular weight. Polymer ionic strength and mechanical degradation at high Reynolds numbers also affected the degree of drag reduction.

CHAPTER 7

7 CONCLUSIONS AND RECOMMENDATIONS

7.1 Conclusions

In this thesis, drag reduction in horizontal two phase oil (Exxsol D140: viscosity 5.5 mPas, density 830 kg/m^3) and water flows has been investigated. The drag reducing polymers used were mixed in the water phase and they include Magnafloc 1011 (hydrolysed copolymer of polyacrylamide and sodium acrylate, HPAM, mol. wt. = 10 x 10^6 g/mol), 5 x 10^6 g/mol and 8 x 10^6 g/mol) and polyethylene oxide (PEO). The investigations were carried out with the aid of a high speed camera, conductance probes and particle image velocimetry (PIV) in a horizontal 14 mmID acrylic test section. Measurements with the conductance probes and particle image velocimetry were carried out in the stratified flow regimes.

Flow patterns and their boundaries were studied with high speed imaging. In the flows without polymers the patterns were found to depend on the superficial oil and water velocities. Stratified and stratified wavy flows appeared at low to moderate superficial oil and water velocities. The amplitude of the interfacial waves increased with velocities until drops of either phase entrained in the opposite phase resulting in dual continuous flows. At some moderate velocities rivulet flow occurred (Usw < 0.34 m/s and Uso > 0.15 m/s) that has a meandering form. This pattern is mainly observed in pipes of small diameters where the Eötvös number is small (4.78 for the current system). At even higher mixture velocities the flow was dispersed with oil (at low water fractions) or water (at high water fractions) as the continuous phase. The sizes of the drop ranged from about 0.1D to 0.3D (D is pipe diameter) and reduced with increasing mixture velocities. Annular flows appeared for a short time during transitions between stratified wavy and dual continuous, dispersed oil in water and dual continuous flows while slug flows also appeared temporarily in the transition from stratified wavy to dispersed oil in water flows. Pressure drop increased with mixture velocity and fluctuated during rivulet flow. Within the stratified and stratified wavy flow regions, the interface height increased with superficial water velocity for a fixed superficial oil velocity.

In stratified flow two types of conductance probes (wire and ring probes) were used to obtain the variation of interface height with time at the wall (ring probe) and at the pipe centre (wire probe) respectively. The results showed that the interface had a concave shape that was described with a correlation between the heights at the wall and the pipe centre. In addition,

from the time signal of the interface height, wave amplitudes were calculated. The interface shape correlation alongside the calculated amplitude of the interfacial waves were implemented in a two-fluid model to account for interface curvature and roughness. The modified model was able to predict the experimental data on pressure drop better than when flat and smooth interface was assumed. The predictions of the interface height were particularly sensitive to interface curvature, while those of pressure drop were affected by both the interface roughness and curvature. Predictions of the two-fluid model with other literature correlations on interfacial shear stress were also improved particularly at low fluid velocities when the interface curvature was included.

When 20 ppm of polymer solution was added to the water phase, drag reduction of 80 % was found in single phase water flows and 52 % in oil-water flows. Drag reduction was found to increase with increasing water and oil velocities and then began to decrease with fixed water and increasing oil superficial velocities. The addition of the polymer extended the stratified flow region to higher superficial oil and water velocities. Stratified wavy, dual continuous, dispersed and rivulet flow patterns changed to stratified flow. Dual continuous flow also changed to stratified wavy or dual continuous flows with larger drops, while dispersed flows sometimes changed to dual continuous flows or dispersed flows with larger drops. The highest drag reduction was obtained when dispersed and stratified wavy flows changed to stratified flow. In addition, the in-situ velocities, interfacial wave celerity and wavelength were found to increase with the addition of polymer while the interface height, wave amplitude and the power spectrum of the interface height (that indicate the interface waviness) decreased. With the addition of the polymer the water phase velocity increased even though the interface height decreased. As a result the oil to water velocity ratio reduced. These changes in the oil-water flows with polymer addition were attributed to the reduction in the turbulence of the water phase, which leads to dampening of the interfacial waves and to increasing drop coalescence. The two-fluid model was modified to account for drag reduction with a correlation for the water friction factor obtained from single phase measurements and curved interface correlation after polymer addition to oil-water flows. The modified model predicted better the experimental data compared to a homogeneous model suggested in the literature that uses a mixture friction factor.

Particle image velocimetry was used to obtain velocity profiles and turbulence properties in the water phase during stratified flows. It was found that with polymer added, the axial velocity profile in the water phase became more parabolic signifying laminarization of the

flow. When polymer was present, the Reynolds stress and radial component of the velocity fluctuations reduced throughout the pipe cross section while the axial component of velocity fluctuations reduced close to the wall but increased in the bulk flow. In addition, when the low molecular weight PEO was added to the flow, it resulted in increased axial velocity gradient as well as increased axial velocity fluctuations and Reynolds stress component particularly at low superficial oil and water velocities compared to the high molecular weight PEO and HPAM. In general, the molecular weight and ionic strength of the polymers used influenced the measured drag reduction, turbulence properties and velocity profiles of both single phase water and oil-water flows.

Finally, the studies in the small scale pipe (14 mmID) help to gain some fundamental understanding of the dynamics of two-phase liquid-liquid flows when polymers are added that can be applicable to large scale pipelines as well.

7.2 Recommendations for Future Works

The two-fluid model developed should be compared against a larger set of data. The experiments were conducted with only one type of oil in a horizontal pipe of intermediate diameter. It will be worthwhile to obtain experimental data from different oils with varying viscosities and in different pipe sizes and inclinations and compare them against the model predictions.

The effects of polymer addition on the interfacial wave characteristics in stratified flows should also be extended to different pipe diameters, inclinations, oil viscosities and polymer types so that a better understanding can be gained. This will enable a more accurate evaluation of the changes in the interfacial wave characteristics and their contribution to drag reduction. The results obtained from the different pipe sizes can be used to develop an algorithm or model which may be used for scale-up purposes to describe or predict the dynamics of both Newtonian and drag-reduced flows in industrial pipe sizes.

These studies should also include combinations of different drag reducing agents such as polymer, fibers, and that may act synergistically. A preliminary study of the combination of polyethylene oxide and polyamide fibers in water was conducted in pipes of different sizes and a synergistic effect in drag reduction was observed. Drag reduction was found to be higher with the combined drag reducing agents than when either PEO or fibers was used alone. The results can be found in Appendix 3.

Drag reduction experiments in liquid-liquid flows have been limited to the addition of polymers to just one of the phases. It is recommended to study the effects on flow patterns and pressure drop when polymers are added to both phases.

The accuracy of the PIV measurements in the near wall and near interface regions can be improved by using fluorescent particles as tracers that minimize errors due to reflections. Fluorescent particles emit light at a different wavelength to that of the laser which can then be filtered out of the image. The internal walls of the visualization section of the pipe can also be painted with a fluorescent dye or paint while other seeding particles can be used as tracers. Additionally, PIV measurements in drag-reduced flows should be extended to other flow patterns apart from the stratified flow investigated in this study. The use of fluorescent particles can help minimize the difficulty posed from reflections on the drops and interface in other flow patterns. Studies should be extended to different pipe sizes and fluid properties for different types of drag reducing additives and their combinations.

BIBLIOGRAPHY

Abdulbari, H.A., Shabirin, A., Abdurrahman, H.N., 2014. Bio-polymers for improving liquid flow in pipelines—A review and future work opportunities. J. Ind. Eng. Chem. 20, 1157–1170.

Abdulbari, H.A., Yunus, R.M., Abdurahman, N.H., Charles, A., 2013. Going against the flow—A review of non-additive means of drag reduction. J. Ind. Eng. Chem. 19, 27–36.

Abdul-hadi, A.A., Khadom, A.A., 2013. Studying the Effect of Some Surfactants on Drag Reduction of Crude Oil Flow. Chinese J. Eng. 2013, 1–6.

Abdullah, M., Odjoji, E., Angeli, P., 2008. The Effect of Polymer Concentration and Hydration Period on Horizontal oil-water, in: 11th International Conference on Multiphase Flow in Industrial Plant (MFIP 2008). Palermo, Italy, pp. 303–310.

Abubakar, A., Al-Hashmi, A.., Al-Wahaibi, T., Al-Wahaibi, Y., Al-Ajmi, A., Eshrati, M., 2014a. Parameters of Drag Reducing Polymers and Drag Reduction Performance in Single-Phase Water Flow. Adv. Mech. Eng. 2014, 1 – 8.

Abubakar, A., Al-Wahaibi, T., Al-Hashmi, A.R., Al-Wahaibi, Y., Al-Ajmi, A., Eshrati, M., 2015a. Influence of drag-reducing polymer on flow patterns, drag reduction and slip velocity ratio of oil–water flow in horizontal pipe. Int. J. Multiph. Flow 73, 1–10.

Abubakar, A., Al-Wahaibi, T., Al-Wahaibi, Y., Al-Hashmi, A.R., Al-Ajmi, A., 2014b. Roles of drag reducing polymers in single- and multi-phase flows. Chem. Eng. Res. Des. 92, 2153–2181.

Abubakar, A., Al-Wahaibi, Y., Al-Wahaibi, T., Al-Hashmi, A., Al-Ajmi, A., Eshrati, M., 2015b. Effect of low interfacial tension on flow patterns, pressure gradients and holdups of medium-viscosity oil/water flow in horizontal pipe. Exp. Therm. Fluid Sci. 68, 58–67.

Adrian, R.J., Westerweel, J., 2011. Particle Image Velocimetry, illustrate. ed. Cambridge University Press.

Ahmed, B.S.K., 2014. A study of gas lift on oil/water flow in vertical risers. Cranfield University.

Al-Sarkhi, A., 2010. Drag reduction with polymers in gas-liquid/liquid-liquid flows in pipes: A literature review. J. Nat. Gas Sci. Eng. 2, 41–48.

Al-Sarkhi, A., 2012. Effect of mixing on frictional loss reduction by drag reducing polymer in annular horizontal two-phase flows. Int. J. Multiph. Flow 39, 186–192.

Al-Sarkhi, A., Abu-Nada, E., Batayneh, M., 2006. Effect of drag reducing polymer on air–water annular flow in an inclined pipe. Int. J. Multiph. Flow 32, 926–934.

Al-Sarkhi, A., Hanratty, T.J., 2001. Effect of pipe diameter on the performance of drag-reducing polymers in annular gas-liquid flows. Trans IChemE 79.

Al-Sarkhi, A., Nakla, M. El, Ahmed, W.H., 2011. Friction factor correlations for gas-liquid/liquid-liquid flows with drag-reducing polymers in horizontal pipes. Int. J. Multiph. Flow 37, 501–506.

Al-Sarkhi, A., Soleimani, A., 2004. Effect of drag reducing polymers on two-phase gas – liquid flows in a horizontal pipe. Chem. Eng. Res. Des. 82, 1583–1588.

Al-Wahaibi, T., Angeli, P., 2007. Transition between stratified and non-stratified horizontal oil–water flows. Part I: Stability analysis. Chem. Eng. Sci. 62, 2915–2928.

Al-Wahaibi, T., Angeli, P., 2008. Droplet size and velocity in dual continuous horizontal oil–water flows. Chem. Eng. Res. Des. 86, 83–93.

Al-Wahaibi, T., Angeli, P., 2009. Predictive model of the entrained fraction in horizontal oil–water flows. Chem. Eng. Sci. 64, 2817–2825.

Al-Wahaibi, T., Smith, M., Angeli, P., 2007. Effect of drag-reducing polymers on horizontal oil–water flows. J. Pet. Sci. Eng. 57, 334–346.

Al-Wahaibi, T., Yusuf, N., Al-Wahaibi, Y., Al-Ajmi, A., Al-Hashmi, A.R., Olawale, A.S., Mohammed, I.A., 2012. Experimental study on the effect of drag reducing polymer on flow patterns and drag reduction in a horizontal oil–water flow. Int. J. Heat Fluid Flow 37, 74–80.

Al-Wahaibi, T.K., 2006. Investigations on the transition between stratified to non-stratified horizontal oil-water flows. University College London.

Al-Yaari, M., Al-Sarkhi, A., Abu-Sharkh, B., 2012. Effect of drag reducing polymers on water holdup in an oil–water horizontal flow. Int. J. Multiph. Flow 44, 29–33.

Al-Yaari, M., Soleimani, A., Abu-Sharkh, B., Al-Mubaiyedh, U., Al-Sarkhi, A., 2009. Effect of drag reducing polymers on oil–water flow in a horizontal pipe. Int. J. Multiph. Flow 35, 516–524.

Andritsos, T., Tzotzi, C., Hanratty, T.J., 2008. Interfacial shear stress in wavy stratified Gas-Liquid two-phase flow, in: 5th European Thermal-Sciences Conference. The Netherlands, pp. 0–7.

Andritsos, T.., Hanratty, T.., 1987. Influence of interfacial waves in stratified gas-liquid flows. AIChE J. 33, 444–454.

Arashiro, E.Y., Demarquette, N.R., 1999. Use of the Pendant Drop Method to Measure Interfacial Tension between Molten Polymers. Mater. Res. 2, 23–32.

Arirachakaran, S., Oglesby, K.D., Shoulam, O., Brill, J.P., 1989. An analysis of oil water flow phenomena in horizontal pipes., in: SPE Proceeding: Production Operation Symposium. SPE, pp. 155–167.

Baik, S., Hanratty, T.J., 2003. Effects of a drag reducing polymer on stratified gas–liquid flow in a large diameter horizontal pipe. Int. J. Multiph. Flow 29, 1749–1757.

Baik, S., Vlachogiannis, M., Hanratty, T.J., 2005. Use of particle image velocimetry to study heterogeneous drag reduction. Exp. Fluids 39, 637–650.

Barral, A.H., 2014. Stratified Wavy Oil-Water Flows. University College London (UCL).

Barral, A.H., Angeli, P., 2013. Interfacial characteristics of stratified liquid-liquid flows using a conductance probe. Exp. Fluids 54, 1604:1–15.

Barral, A.H., Edomwonyi-Otu, L.C., Angeli, P., 2013. Flow patterns and interfacial characteristics in stratified oil-water flows In pipes of different diameter, in: Experimental Methods in Multiphase Flows. Jeju, South Korea, pp. 1–6.

Bewersdorff, H.W., Gyr, A., Hoyer, K., Tsinober, A., 1993. An investigation of possible mechanisms of heterogeneous drag reduction in pipe and channel flows. Rheol. Acta 32, 140–149.

Birvalski, M., Tummers, M.J., Delfos, R., Henkes, R.A.W.M., 2013. PIV measurements of waves and turbulence in stratified horizontal two-phase pipe flow, in: The 16th International Conference on Multiphase Production Technology. BHR Group, Cannes, France, pp. 337 – 351.

Birvalski, M., Tummers, M.J., Delfos, R., Henkes, R.A.W.M., 2014. PIV measurements of waves and turbulence in stratified horizontal two-phase pipe flow. Int. J. Multiph. Flow 62, 161–173.

Brasseur, J.G., Robert, A., Collins, L.R., Vaithianathan, T., 2005. Fundamental Physics Underlying Polymer Drag Reduction , from Homogeneous DNS Turbulence with the FENE-P Model 23–26.

Brauner, N., 1991. Two-phase liquid-liquid Annula flow. Int. J. Multiph. Flow 17, 59–76.

Brauner, N., 2002. Modelling and Control of Two-Phase Phenomena : Liquid-Liquid Two-Phase Flow Systems, in: Modeling and Control of Two-Phase Flow Phenomena. CISM, Udine, Italy.

Brauner, N., Moalem, D., 1992a. Flow pattern transitions in two-phase liquid-liquid flow in horizontal tubes. Int. J. Multiph. flow 18, 123–140.

Brauner, N., Moalem, D.., 1992b. Identification of the range of small diameter conduits, regarding two-phase flow pattern transistions. Int. Commun. heat mass Transf. 19, 29–39.

Brauner, N., Moalem, M.., Rovinsky, J., 1998. A two-fluid model for stratified flows with curved interfaces. Int. J. Multiph. Flow 24, 975–1004.

Brauner, N., Moalem, M.D., 1993. The Role of Interfacial Shear Modelling in Predicting The stability of stratified Two-Phase. Chem. Eng. Sci. 48, 2867–2879.

Brennen, C.E., 2005. Fundamentals of Multiphase Flows, Technology. Cambridge University Press. doi:10.1007/s11214-006-9083-0

Chakrabarti, D.P., Das, G., 2006. The Transition from Water Continuous to Oil Continuous Flow Pattern. AIChE J. 52.

Chaouki, J., Faıcal, L., Milorad, P.., 1997. Noninvasive Tomographic and Velocimetric Monitoring of Multiphase Flows. Ind. Eng. Chem. Res 36, 4476–4503.

Cheung, T.K., Street, R.L., 1988. The turbulent layer in the water at an air—water interface. J. Fluid Mech. 194, 133–151.

Cohen, L.S., Hanratty, T.J., 1968. Effect of waves at a gas-liquid interface on a turbulent air flow. J. Fluid Mech. 31, 467–479.

Colombo, L.P.M., Guilizzoni, M., Sotgia, G., 2014. A detailed characterization of viscous oil-water flows downward sudden contractions in horizontal pipes. J. Phys. Conf. Ser. 547, 012025. doi:10.1088/1742-6596/547/1/012025

Das, G., De, B., Mandal, T.K., 2010. The rivulet flow pattern during oil–water horizontal flow through a 12mm pipe. Exp. Therm. Fluid Sci. 34, 625–632.

De Castro, M.S., Pereira, C.C., dos Santos, J.N., Rodriguez, O.M.H., 2012. Geometrical and kinematic properties of interfacial waves in stratified oil–water flow in inclined pipe. Exp. Therm. Fluid Sci. 37, 171–178.

Delfos, R., Hoving, J., Boersma, B., 2011. Experiments on drag reduction by fibres in turbulent pipe flow Background, in: Euromech Meeting 513. Udine, Italy, pp. 1–27.

Den Toonder, J.M.J., Draad, a. a., Kuiken, G.D.C., Nieuwstadt, F.T.M., 1995. Degradation effects of dilute polymer solutions on turbulent drag reduction in pipe flows. Appl. Sci. Res. 55, 63–82.

Den Toonder, J.M.J., Hulsen, M.A., Kuiken, G.D.C., Nieuwstadt, F.T.M., 1997. Drag reduction by polymer additives in a turbulent pipe flow: numerical and laboratory experiments. J. Fluid Mech. 337, 193–231.

Deslouis, C., 2003. Microscopic aspects of surfactants action on flow induced corrosion. Electrochim. Acta 48, 3279–3288.

Dore, V., Tsaoulidis, D., Angeli, P., 2012. Mixing patterns in water plugs during water/ionic liquid segmented flow in microchannels. Chem. Eng. Sci. 80, 334–341. doi:10.1016/j.ces.2012.06.030

Doulah, M.S., 1981. Mechanism of drag reduction in turbulent pipe flow by the addition of fibers. Ind. Eng. Chem. Fundam. 20, 101–102.

Drelich, J., Fang, C., White, C.L., 2002. Measurement of Interfacial Tension in Fluid-Fluid Systems. Encycl. Surf. Colloid Sci.

Dubief, Y., White, C.M., Terrapon, V.E., Shaqfeh, E.S.G., Moin, P., Lele, S.K., 2004. On the coherent drag-reducing and turbulence-enhancing behaviour of polymers in wall flows. J. Fluid Mech. 514, 271–280.

Dunlop, E.H., Cox, L.R., 1977. Influence of molecular aggregates on drag reduction. Phys. Fluids 20, S203.

Ebagninin, K.W., Benchabane, A., Bekkour, K., 2009. Rheological characterization of poly(ethylene oxide) solutions of different molecular weights. J. Colloid Interface Sci. 336, 360–7.

Elseth, G., 2001. An Experimental Study of Oil-Water Flows in Horizontal Pipes. PhD Thesis. Telemark University College.

Escudier, M.P., Poole, R.J., Presti, F., Dales, C., Nouar, C., Desaubry, C., Graham, L., Pullum, L., 2005. Observations of asymmetrical flow behaviour in transitional pipe flow of yield-stress and other shear-thinning liquids. J. Nonnewton. Fluid Mech. 127, 143–155.

Escudier, M.P., Rosa, S., Poole, R.J., 2009. Asymmetry in transitional pipe flow of drag-reducing polymer solutions. J. Nonnewton. Fluid Mech. 161, 19–29.

Esmael, A., Nouar, C., 2008. Transitional flow of a yield-stress fluid in a pipe: Evidence of a robust coherent structure. Phys. Rev. E 77, 057302.

Fabre, J., Line, A., 2010. Slug flow [WWW Document]. 10.1615/AtoZ.s.slug_flow.

Fadhl, H.F., 2011. Silica Powder as Drag Reducing Agent in Gas-Oil Flowing in Pipeline System, in: First Scientific Conference on Modern Technologies in Oil & Gas Refinery. pp. 1–14.

Fernandes, R.L.J., Fleck, B.A., Heidrick, T.R., Torres, L., Rodriguez, M.G., 2009. Experimental Study of DRA for Vertical Two-Phase Annular Flow. J. Energy Resour. Technol. 131, 023002.

Gómez Cuenca, F., Gómez Marín, M., Folgueras Díaz, M.B., 2008. Energy-savings modeling of oil pipelines that use drag-reducing additives. Energy and Fuels 22, 3293–3298.

Gyr, A., Bewersdorff, H.W., 1995. Drag reduction of turbulent flows with additives. The Netherlands Kluwer Academic Publishers, Dordrecht.

Gyr, A., Tsinober, A., 1997. On the rheological nature of drag reduction phenomena. J. Nonnewton. Fluid Mech. 73, 153–162.

Hadri, F., Guillou, S., 2010. Drag reduction by surfactant in closed turbulent flow. Int. J. Eng. Sci. Tecnol. 2, 6876–6879.

Hadžiabdić, M., Oliemans, R.V.A., 2007. Parametric study of a model for determining the liquid flow-rates from the pressure drop and water hold-up in oil–water flows. Int. J. Multiph. Flow 33, 1365–1394.

Hall, A.R.W., 1992. Multiphase Flow of Oil, Water and Gas in Horizontal Pipes. University of London.

Hanratty, T.J., Al-Sarkhi, A., 2001. Effect of drag-reducing polymers on annular gas - liquid ¯ flow in a horizontal pipe. Int. J. Multiph. Flow 27, 1151–1162.

Hong, C.H., Choi, H.J., Zhang, K., Renou, F., Grisel, M., 2015. Effect of salt on turbulent drag reduction of xanthan gum. Carbohydr. Polym. 121, 342–7.

Hoyer, K., Gyr, A., 1998. Heterogeneous drag reduction concepts and consequences. J. Fluids Eng. 120, 818–823.

Hoyer, K., Gyr, A., Tsinober, A., 1996. On the mechanism of drag reduction in dilute polymer solutions. Appl. Sci. Res. 55, 289–295.

Hoyt, J.W., 1986. Drag Reduction, in: Mark HF et Al (eds) Encyclopedia of Polymer Science and Engineering. John Wiley & Sons, New York, USA, pp. 129–151.

Jahanmiri, M., 2011. Particle Image Velocimetry: Fundamentals and Its Applications. Chalmers University of Technology, Goteborg, Sweden.

Janes, N., Muzychka, Y.S., Guy, B., Walsh, E.J., Walsh, P., 2010. Heat transfer in gas-liquid and liquid-liquid two phase plug flow systems, in: 2010 12th IEEE Intersociety Conference on Thermal and Thermomechanical Phenomena in Electronic Systems. Ieee, pp. 1–11.

Jin, N., Zhao, A., Zhai, L., Gao, Z., 2013. Liquid holdup measurement in horizontal oil-water two-phase flow by using concave capacitance sensor, in: International Conference on Multiphase Flows (ICMF). Jeju, South Korea, pp. 1–8.

Jubran, B., Zurigat, Y., Goosen, M., 2005. Drag Reducing Agents in Multiphase Flow Pipelines: Recent Trends and Future Needs. Pet. Sci. Technol. 23, 1403–1424.

Kale, D., Metzner, A., 1976. Turbulent Drag Reduction in Dilute Fiber Suspensions : Mechanistic Considerations. AIChE J. 22, 669–674.

Kale, D.D., Metzner, A.B., 1974. Turbulent Drag Reduction in Fiber-Pol ymer Systems: Specificity Considerations. AIChE J. 20, 1971–1972.

Kang, C., Jepson, W.P., Gopal, M., 1998a. The Effect of Drag Reducing Agents on Corrosion in Multiphase Flow, in: Corrosion' 98. pp. 54:1–11.

Kang, C., Vancko, R.M., Green, A.S., Kerr, H., Jepson, W.P., 1998b. Effect of Drag-Reducing Agents in Multiphase Flow Pipelines. J. Energy Res. Technol. 120, 15.

Karami, H.R., Mowla, D., 2012. Investigation of the effects of various parameters on pressure drop reduction in crude oil pipelines by drag reducing agents. J. Nonnewton. Fluid Mech. 177-178, 37–45.

Kataoka, I., Serizawa, A., 2010. Bubble Flow.

Katepalli, R.S., Christopher, M.W., 2000. The onset of drag reduction by dilute polymer additives, and the maximum drag reduction asymptote. J. Fluid Mech. 409, 149–164.

Kim, K., Sirviente, A.I., 2005. Turbulence structure of polymer turbulent channel flow with and without macromolecular polymer structures. Exp. Fluids 38, 739–749.

Kim, S.-M., Mudawar, I., 2012. Universal approach to predicting two-phase frictional pressure drop for adiabatic and condensing mini/micro-channel flows. Int. J. Heat Mass Transf. 55, 3246–3261.

Kulicke, W., Kotter, M., Grager, H., 1989. Drag Reduction Phenomenon with Special Emphasis on Homogeneous Polymer Solutions. Adv. Polym. Sci. 89, 1–68.

Kumara, W.A.S., Elseth, G., Halvorsen, B.M., Melaaen, M.C., 2010a. Comparison of Particle Image Velocimetry and Laser Doppler Anemometry measurement methods applied to the oil–water flow in horizontal pipe. Flow Meas. Instrum. 21, 105–117.

Kumara, W.A.S., Halvorsen, B.., Melaaen, M.., 2009. Velocity and turbulence measurements of oil- water flow in horizontal and slightly inclined pipes using PIV 1–16.

Kumara, W.A.S., Halvorsen, B.M., Melaaen, M.C., 2010b. Particle image velocimetry for characterizing the flow structure of oil–water flow in horizontal and slightly inclined pipes. Chem. Eng. Sci. 65, 4332–4349.

Langsholt, M., 2012. An experimental study on polymeric type DRA used in single- and multiphase flow with emphasis on degradation , diameter scaling and the effects in three-phase oil-water-gas flow, in: DRA, Corrosion and Erosion; In 8th North American Conference on Multiphase Technology. BHR Group, Banff, Canada, pp. 1–15.

Lee, C.., Lee, S.., 2008. Pressure drop of two-phase plug flow in round mini-channels: Influence of surface wettability. Exp. Therm. Fluid Sci. 32, 1716–1722.

Lewandowska, K., 2006. Comparative Studies of Rheological Properties of Polyacrylamide and Partially Hydrolyzed Polyacrylamide Solutions. J. Appl. Polym. Sci. 103, 2235–2241.

Li, F.., Kawaguchi, Y., Yu, B., Wei, J., Hishida, K., 2008. Experimental study of drag-reduction mechanism for a dilute surfactant solution flow. Int. J. Heat Mass Transf. 51, 835–843.

Liberatore, M.W., Baik, S., McHugh, A.J., Hanratty, T.J., 2004. Turbulent drag reduction of polyacrylamide solutions: effect of degradation on molecular weight distribution. J. Nonnewton. Fluid Mech. 123, 175–183.

Lovick, J., Angeli, P., 2004. Droplet size and velocity profiles in liquid–liquid horizontal flows. Chem. Eng. Sci. 59, 3105–3115.

Lumley, J.L., 1973. Drag Reduction in Turbulent Flow by Polymer Additives. J. Polym. Sci. Macromol. Rev. 7, 263–290.

Manfield, C.J., Lawrence, C., Hewitt, G., 1999. Drag-reduction with additive in multiphase flow: a literature survey. Multiph. Sci. Technol. 11, 197–221.

Mansour, A., Salem, A., Sylvester, N.D., 1998. The Effect of Heterogeneous Dra Reducing Surfactant In Drag and Heat Transfer Reduction in Crude Oil Systems. Chem. Eng. Commun. 168, 229–242.

Metzner, A.B., 1977. Polymer solution and fiber suspension rheology and their relationship to turbulent drag reduction. Phys. Fluids 20, S145.

Min, T., Yul Yoo, J., Choi, H., Joseph, D.D., 2003. Drag reduction by polymer additives in a turbulent channel flow. J. Fluid Mech. 486, 213–238.

Moore, B., 2013. Gas-Liquid Flow in Adsorbent Microchannels. MSc Thesis. Georgia Institute of Technology.

Morgan, R.., Markides, C.., Hale, C.., Hewitt, G.F., 2012. Horizontal liquid–liquid flow characteristics at low superficial velocities using laser-induced fluorescence. Int. J. Multiph. Flow 43, 101–117.

Morgan, R.., Markides, C.., Zadrazil, I., Hewitt, G.F., 2013. Characteristics of horizontal liquid–liquid flows in a circular pipe using simultaneous high-speed laser-induced fluorescence and particle velocimetry. Int. J. Multiph. Flow 49, 99–118.

Mowla, D., Naderi, A., 2006. Experimental study of drag reduction by a polymeric additive in slug two-phase flow of crude oil and air in horizontal pipes. Chem. Eng. Sci. 61, 1549–1554.

Neogi, S., Lee, A., Jepson, W.P., 1994. A Model for Multiphase (Gas-Water-Oil) Stratified Flow in Horizontal Pipelines. Proc. SPE Asia Pacific Oil Gas Conf. 553–562.

Ngan, K.., 2010. Phase Inversion in dispersed liquid-liquid pipe flow Kwun Ho Ngan. Chem. Eng. University College London.

Ngan, K.H., Ioannou, K., Rhyne, L.D., Wang, W., Angeli, P., 2009. A methodology for predicting phase inversion during liquid–liquid dispersed pipeline flow. Chem. Eng. Res. Des. 87, 318–324.

Nieuwenhuys, G.M.., 2003. Effect of Drag-Reducing Polymers on a Vertical Multiphase Flow by G . M . H . MEAH : 230. MEAH 230 1–51.

Ogata, S., Numakawa, T., Kubo, T., 2011. Drag Reduction of Bacterial Cellulose Suspensions. Adv. Mech. Eng. 2011, 1–6.

Otten, L., Fayed, A.., 1976. Pressure drop and drag-reduction in two-phase non-Newtonian slug flow. Can. J. Chem. Eng. 54, 111–114.

Panton, R.L., Barajas, A.., 1993. The effect of contact angle in two-phase flow in capilary tubes. Internatioanl J. Multiph. Flow 19, 337–346.

Parimal, P.M., Cheolho, K., Alvaro, A., 2008. IPC2008-64336 The Performance of Drag Reducing Agents in Multiphase Flow, in: IPC2008, Seventh International Pipeline Conference. Calgary, Canada, pp. 1–9.

Paschkewitz, J.., Dubief, Y., Shaqfeh, E.S.G., 2005. The dynamic mechanism for turbulent drag reduction using rigid fibers based on Lagrangian conditional statistics. Phys. Fluids 17, 063102.

Pietro, A., 2007. Multiphase Flows : Basic Physics and Engineering Modeling, MSc Course series, The University of Illinois, USA.

Pollert, J., Sellin, R.H.., 1989. Mechanical degradation of drag reducing polymer and surfactant additives: a review ,in: R.H.J. Sellin, R.T. Moses (Eds.), Drag Reduction in Fluid Flows: Techniques for Friction Control, in: Fourth International Conference on Drag Reduction. Davos, Switzerland, p. 179.

Rodriguez, O.M.., Bannwart, A.., 2006. Experimental study on interfacial waves in vertical core flow. J. Pet. Sci. Eng. 54, 140–148.

Rodriguez, O.M.H., Baldani, L.S., 2012. Prediction of pressure gradient and holdup in wavy stratified liquid–liquid inclined pipe flow. J. Pet. Sci. Eng. 96-97, 140–151.

Rosehart, R.G., Scott, D., Rhodes, E., 1972. Gas–liquid slug flow with drag reducing polymer solutions. AIChE J. 18, 744–750.

Roy, A., Larson, R., 2005. A mean flow model for polymer and fiber turbulent drag reduction. Appl. Rheol. 15, 370–389.

Saether, G., Kubberud, K., Nuland, S., Lingelem, M.., 1989. Drag reduction in two phase flow, in: Fourth International Conference on Multiphase Flow. American Institute of Chemical Engineers, France, pp. 171–184.

Scharnowski, S., Hain, R., Kähler, C.J., 2010. Estimation of Reynolds Stresses from PIV Measurements with Single-Pixel Resolution, in: 15th Int Symp on Applications of Laser Techniques to Fluid Mechanics. Lisbon, pp. 5–8.

Schmitt, F.G., 2008. About Boussinesq's turbulent viscosity hypothesis : historical remarks and a direct evaluation of its validity. Comptes Rendus Mec. Elsevier 335, 617–627.

Sedahmed, G.H., Abdo, M.S.E., Amer, M., El-Latif, G.A., 1999. Effect of drag reducing polymers on the rate of mass transfer controlled corrosion in pipelines under developing turbulent flow. Int. Commun. heat mass Transf. 26, 531–538.

Sellin, R.H.J., Hoyt, J.W., Scrivener, O., 1982. The effect of drag-reducing additives on fluid flows and their industrial applications. Part 1: Basic aspects. J. Hydraul. Res. 20, 29–68.

Sharma, R.., Seshadri, V., Malhotra, R.C., 1978. Turbulent Drag Reduction by Injection of Fibers. J. Rheol. (N. Y. N. Y). 22, 643.

Sharma, R.S., Seshadri, V., Malhotra, R.., 1979. Drag Reduction in Dilute Fibre Suspensions: Some Mechanistic Aspects. Chem. Eng. Sci. 34, 703–713.

Sher, I., Hetsroni, G., 2008. A mechanistic model of turbulent drag reduction by additives. Chem. Eng. Sci. 63, 1771–1778.

Sifferman, T.R., Greenkorn, R.A., 1981. Drag Reduction in Three Distinctly Different Fluid Systems. Soc. Pet. Eng. J. 663 – 669.

Tabor, M., De Gennes, P.G., 1986. A Cascade Theory of Drag Reduction . Europhys. Lett. 2, 519–522.

Taitel, Y., Barnea, D., Brill, J.P., 1995. Stratified three phase flow in pipes. Int. J. Multiph. Flow 21, 53–60.

Taitel, Y., Duckler, A.E., 1976. Model for Predicting Flow Regimes transitions in Horizontal and Near horizontal Gas-liquid Flow. AIChE J. 22, 47–55.

Taitel, Y., Dukler, A.E., 1976. A model for predicting flow regime transitions in horizontal and near horizontal gas–liquid flow. AIChE J. 22, 47–55.

Tamano, S., Kitao, T., Morinishi, Y., 2014. Turbulent drag reduction of boundary layer flow with non-ionic surfactant injection. J. Fluid Mech. 749, 367–403. doi:10.1017/jfm.2014.225

Tiu, C., Moussa, T., Sridhar, T., 1993. Effect of solvent on polymer in turbulent flow. Science (80-.). 48, 261–284.

Toms, B., 1948. Some observations on the flow of linear polymer solutions through straight tubes at large Reynolds numbers., in: International Congress on Rheology. North Holland publication company, Amsterdam, pp. 135–141.

Tropea, C., Yarin, A., Foss, J., 2007. Springer Handbook of Experimental Fluid Mechanics. Springer.

Tsaoulidis, D., Dore, V., Angeli, P., Plechkova, N. V., Seddon, K.R., 2013. Dioxouranium(VI) extraction in microchannels using ionic liquids. Chem. Eng. J. 227, 151–157.

Virk, P.S., 1975. Drag Reduction Fundamentals. AIChE J. 21, 625–656.

Vlachogiannis, M., Hanratty, T.J., 2004. Influence of wavy structured surfaces and large scale polymer structures on drag reduction. Exp. Fluids 36, 685–700.

Vlachogiannis, M., Liberatore, M.W., McHugh, A.J., Hanratty, T.J., 2003. Effectiveness of a drag reducing polymer: Relation to molecular weight distribution and structuring. Phys. Fluids 15, 3786.

Vleggaar, J., Tels, M., 1973. Heat transfer in a heterogeneous drag reduction system. Int. J. Heat Mass Transf. 16, 1629–1631.

Wang, Y., Yu, B., Zakin, J.L., Shi, H., 2011. Review on Drag Reduction and Its Heat Transfer by Additives. Adv. Mech. Eng. 2011, 1–17.

Warholic, M.D., Heist, D.K., Katcher, M., Hanratty, T.J., 2001. A study with particle-image velocimetry of the influence of drag-reducing polymers on the structure of turbulence. Exp. Fluids 31, 474–483.

Warholic, M.D., Massah, H., Hanratty, T.J., 1999. Influence of drag-reducing polymers on turbulence: effects of Reynolds number, concentration and mixing. Exp. Fluids 27, 461–472.

Wei, T., Willmarth, W.W., 1992. Modifying turbulent structure with drag-reducing polymer additives in turbulent channel flows. J. Fluid Mech. 245, 619 – 641.

Westerweel, J., 1997. Fundamentals of digital particle image velocimetry. Meas. Sci. Technol. 8, 1379–1392.

White, C., Mungal, M.G., 2008. Mechanics and Prediction of Turbulent Drag Reduction with Polymer Additives. Annu. Rev. Fluid Mech. 40, 235–256.

White, C.M., Somandepalli, V.S.R., Mungal, M.G., 2004. The turbulence structure of drag-reduced boundary layer flow. Exp. Fluids 36, 62–69.

Xu, M., Xiong, R.H., Li, Y.F., Yang, J.M., Luo, X., Yu, Y.B., Zhao, T.Z., 2010. Pattern transition and holdup behaviors of horizontal oil-water pipe flow.pdf, in: 7th International Conference on Multiphase Flow. Tampa, Florida, USA, pp. 1–6.

Yu, B., Li, F., Kawaguchi, Y., 2004. Numerical and experimental investigation of turbulent characteristics in a drag-reducing flow with surfactant additives. Int. J. Heat Fluid Flow 25, 961–974.

Yusuf, N., Al-Wahaibi, T., Al-Wahaibi, Y., Al-Ajmi, A., Olawale, A.S., Mohammed, I.A., Al-Hashmi, A., 2011. Effect of pipe diameter on the efficiency of drag reducing polymer in horizontal oil-water flows, in: 15th BHR Group Multiphase Production Technology International Conference. Elsevier B.V, Cannes, France, pp. 71–85.

Zadrazil, I., Bismarck, A., Hewitt, G.F., Markides, C.N., 2012. Shear layers in the turbulent pipe flow of drag reducing polymer solutions. Chem. Eng. Sci. 72, 142–154.

Zakin, J.., Lu, B., Bewersdorff, H.W., 1998. Surfactants drag reduction. Rev. Chem. Eng. 14, 253–320.

Zhang, J., Childress, S., Libchaber, A., 1998. Non-Boussinesq effect: Asymmetric velocity profiles in thermal convection. Phys. Fluids 10, 1534.

Zhang, X., Liu, L., Cheng, L., Guo, Q., Zhang, N., 2013. Experimental study on heat transfer and pressure drop characteristics of air-water two-phase flow with the effect of polyacrylamide additive in a horizontal circular tube. Int. J. Heat Mass Transf. 58, 427–440.

Zhou, X., Doup, B., Sun, X., 2013. Measurements of liquid-phase turbulence in gas–liquid two-phase flows using particle image velocimetry. Meas. Sci. Technol. 24, 125303.

APPENDICES

Appendix 1 Calibration of Flowmeters

To calibrate each flowmeter, the respective fluid was run at different flowrates and was collected. The volume collected over a certain time was measured and plotted against the indicators in the flowmeter. The calibration curves for the oil and water flowmeters are shown in Appendix Fig. 1. The same procedure was repeated for the bigger flowmeters.

Calibration curves with axes Flowrate (l/min) vs Rotameter value.

Water, Qw (l/min): $y = 0.0022x^2 + 0.1975x + 0.6003$, $R^2 = 0.9998$

Oil, Qo (l/min): $y = 0.0026x^2 + 0.1715x - 0.0431$, $R^2 = 0.9998$
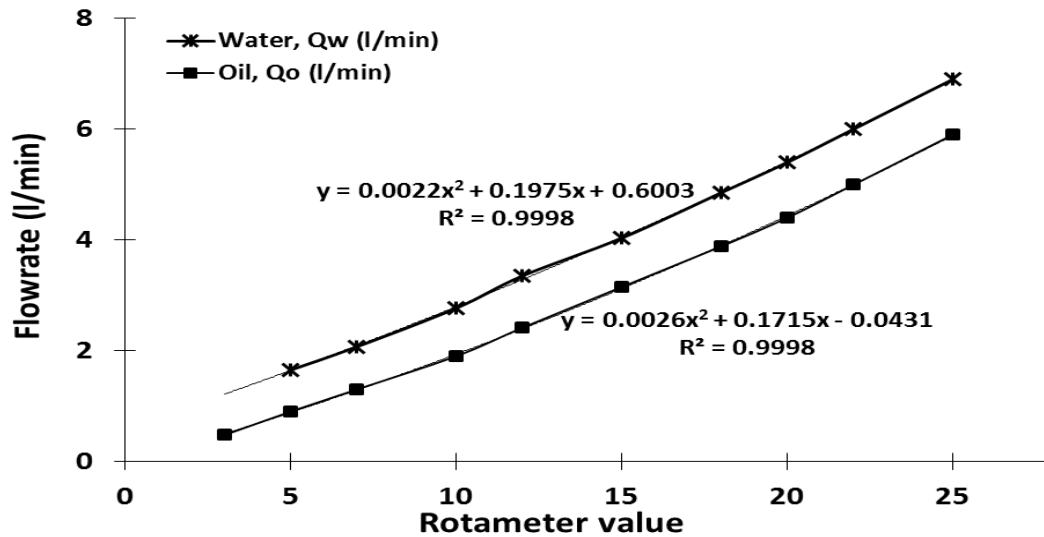
Appendix Fig. 1 Calibration curves for oil and water flow rotameters

Appendix 2 Comparing predictions of Rodriguez and Baldani, (2012)
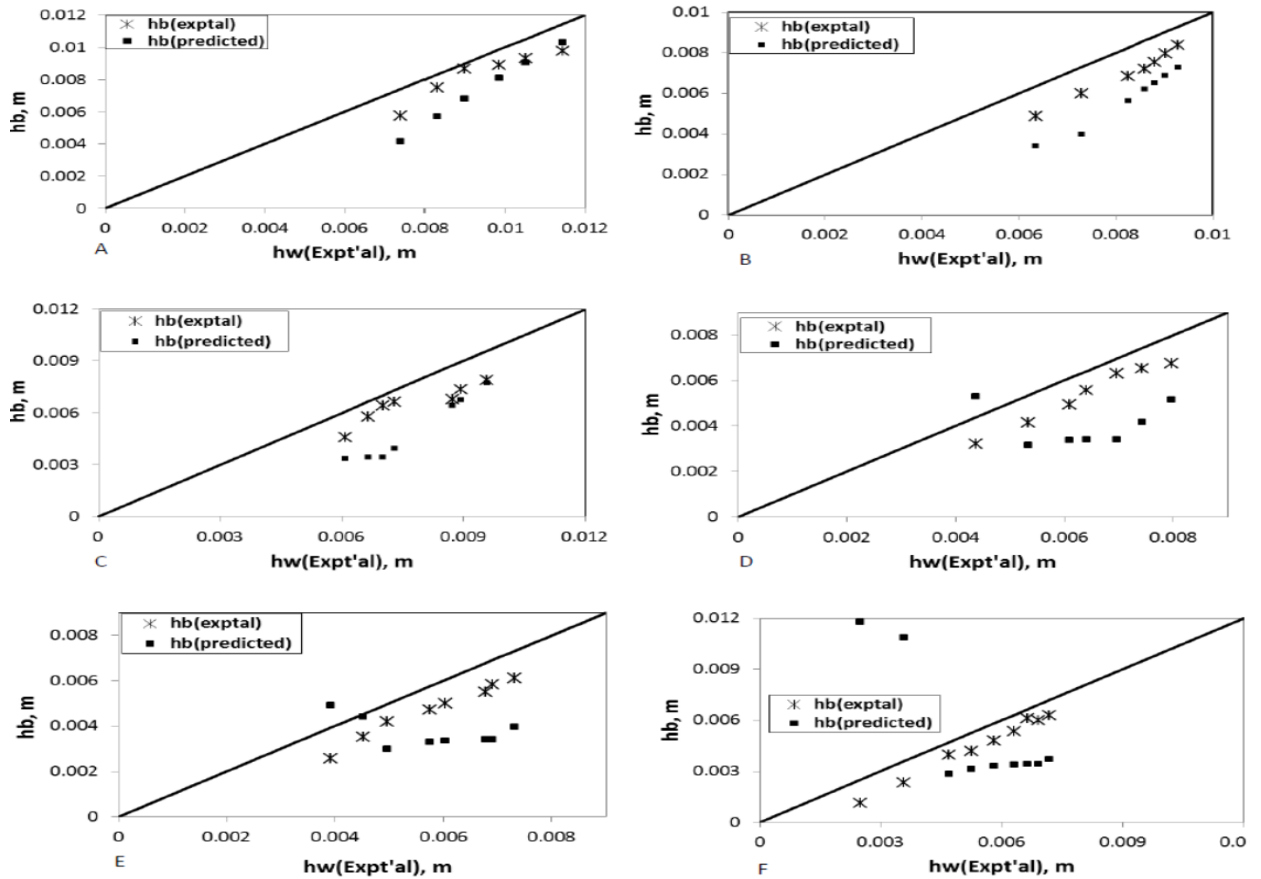
Iso = 0.022, 0.067, 0.11, 0.195, 0.30 and 0.432 for A to F respectively. Data points below the thick middle line (hw) represents points with a concave curvature while those above represents points with a convex curvature.
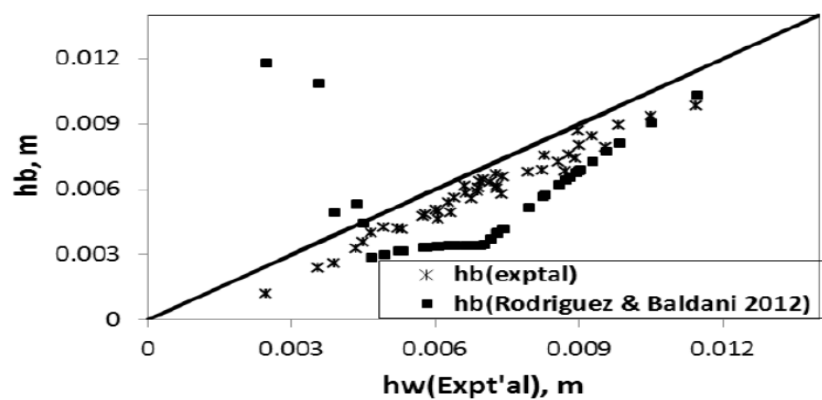
Combined A to F above

Appendix Fig. 2 Results of the comparison of experimental interface height with the prediction of Rodriguez and Baldani, (2012)
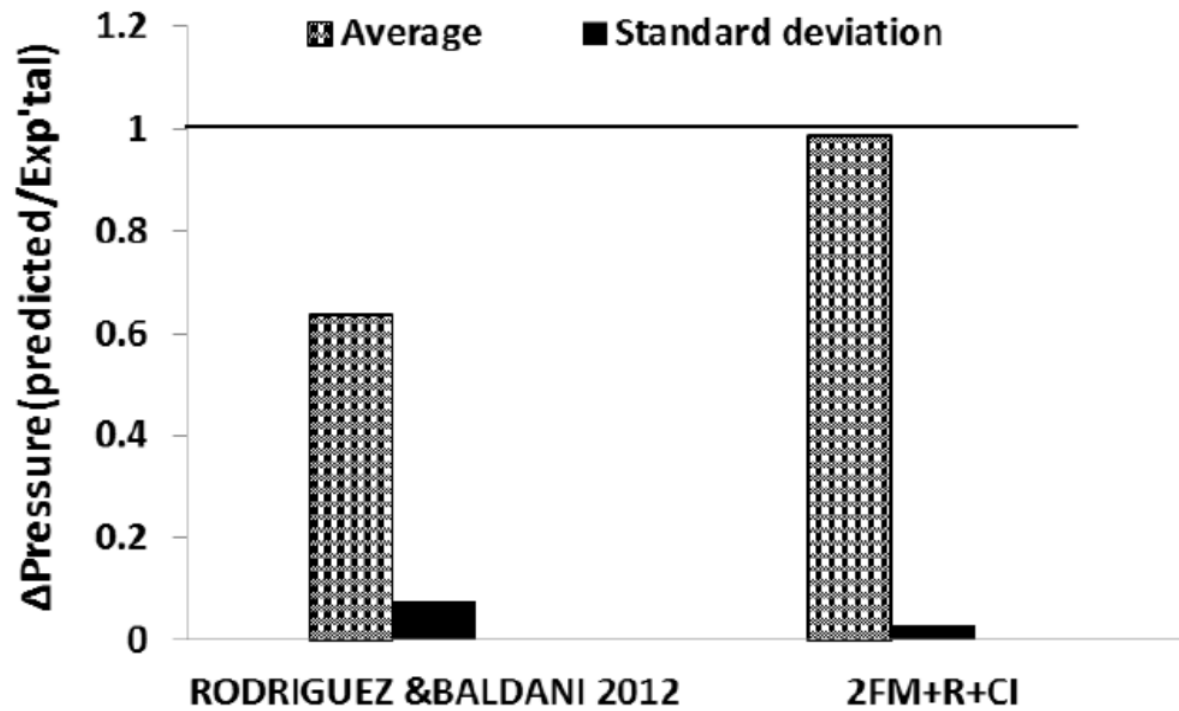
Appendix Fig. 3 Comparison of pressure drop prediction by Rodriguez and Baldani, (2012) **model with the modified two fluid model (2FM+R+CI**

Appendix Table 1 Pressure gradient (Pa/m) for oil-water flow obtained in the 14 mmID acrylic pipe

Usw (m/s)	Uso (m/s)										
	0.008	0.022	0.047	0.067	0.11	0.15	0.195	0.30	0.432	0.51	0.584
0.052	20	40	60	70	100	130	120	360	440	500	700
0.11	40	60	80	90	140	180	180	300	480	540	700
0.166	60	80	100	110	180	200	220	370	540	580	740
0.222	100	110	120	150	210	260	280	480	620	680	780
0.28	120	140	150	180	250	290	320	500	720	800	840
0.336	160	180	200	240	300	340	380	570	740	840	980
0.393	200	220	240	290	350	380	460	640	820	920	1080
0.45	260	280	300	340	410	450	500	720	920	1020	1120
0.51	320	340	360	400	490	500	580	820	1040	1160	1280
0.563	370	400	430	460	560	540	640	920	1160	1280	1440
0.62	430	480	500	540	640	620	680	1040	1220	1380	1540
0.676	500	550	570	600	720	740	760	1120	1360	1500	1720
0.733	580	600	640	700	810	840	840	1220	1480	1640	1820
0.797	660	680	730	800	900	980	960	1340	1600	1780	2000

Appendix 3 Polymer-Fiber Laden Flows in Large Diameter Pipes

The results of the comparison of the polymer drag reduced flows with the MDRA and P-K line are shown in Appendix Fig. 4(a-d). As can be seen, there is a very good agreement between Newtonian flows with the P-K line in all tested Reynolds numbers.
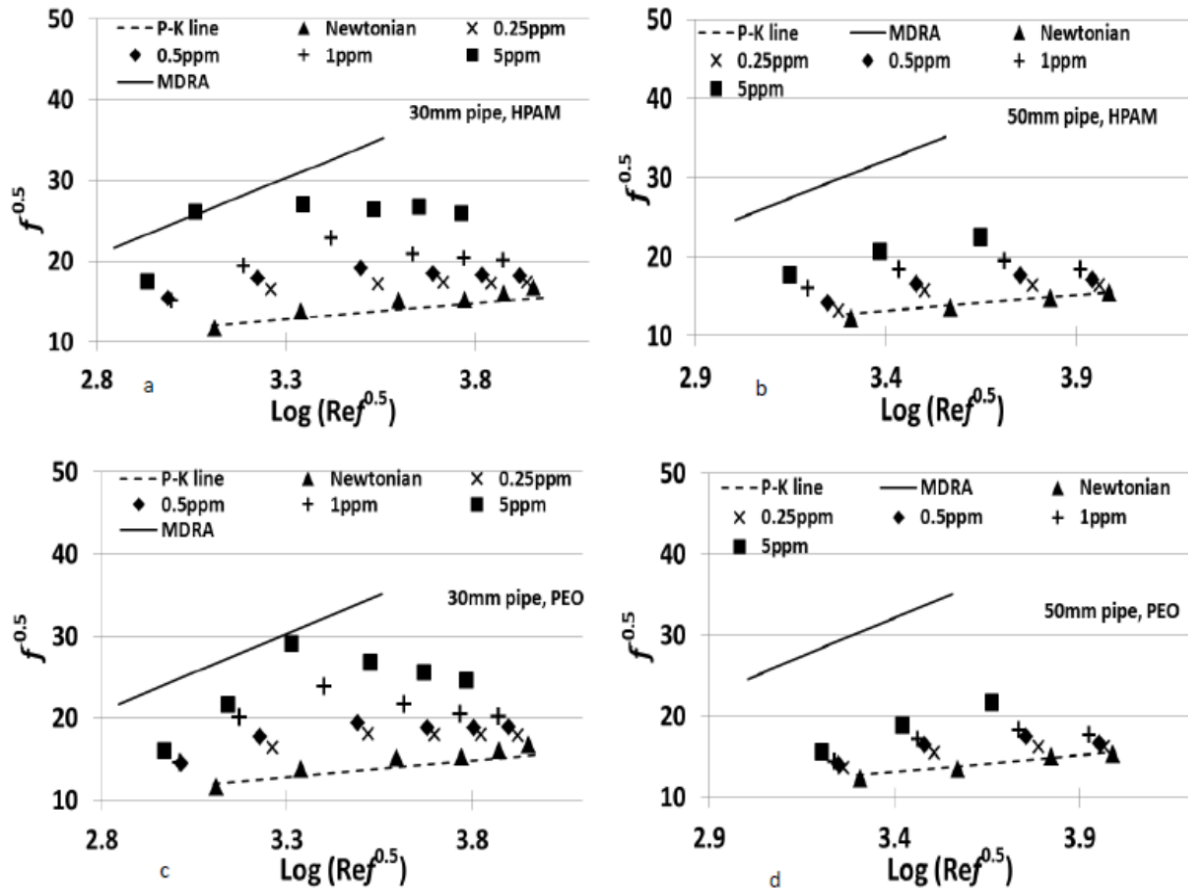
Appendix Fig. 4 Plots of friction factors vs Reynolds number for 8MPEO and HPAM in 30mm and 50mm pipes at different polymer concentrations.

It can also be observed that for both polymers, drag reduction increased with increasing polymer concentration and approached the MDRA. Owing to instrument limitations higher polymer concentrations could not be tested in order to determine the optimum polymer concentration for these polymers and that at which the MDRA can be attained. Drag reduction also increased with increasing Reynolds number until it reached a peak at a Reynolds number of 60000 and 100000 for 30 mm and 50 mm pipes respectively corresponding to a velocity of 2 m/s. Again the behaviour could not be tested at 5 ppm for Re = 150000 to see if it follows the same trend. It is possible that at high Reynolds number, the polymer threads and aggregates breakup at these low concentrations. This is different to

previous findings though in most cases higher polymer concentrations up to 200 ppm were used with an optimum of 10 ppm for PEO and 20 ppm for HPAM and polyisobutylene (PIB) (Abdulbari et al., 2014; Abubakar et al., 2014a; Al-Wahaibi et al., 2012).

Appendix Fig. 4(a & c, b & d) shows the comparison of drag reduction in both pipe sizes for both polymers. It can be observed that higher drag reduction was obtained in smaller pipe diameter (30 mm) for the same polymer concentration and MDRA was attained with just 5 ppm in the 30 mm pipe. This could be attributed to the fact that any condition that favours increased friction factor and low eddy generation will enhance drag reduction, and this is characteristic of smaller pipe diameters (Al-Sarkhi and Hanratty, 2001; Karami and Mowla, 2012; Virk, 1975).

When the drag reduction effectiveness of the two polymers was compared, it was found that HPAM performed better than PEO. Although the differences were not significant, HPAM has been found to be a better drag reducer than PEO because of its higher resistance to mechanical degradation and its ionic nature that increases the higher hydrodynamic volume compared to PEO of similar molecular weight (Abubakar et al., 2014a; Den Toonder et al., 1995; Hoyt, 1986). The mechanical resistance of PEO and HPAM was briefly tested in a 100 ppm (from 2000 ppm master solution) homogenous system and Re = 30000 and 60000 in the 30 mm pipe. Both systems were pumped through a centrifugal pump in a once-through experiment. While the PEO gave zero drag reduction on both cases, the HPAM gave 27 % and 55 % respectively, showing higher resistance to the shearing action of the pump, compared to the PEO solution.

Appendix Fig. 5 and Appendix Fig. 6 shows the additional drag reduction when fibers are added to the polymer solution.
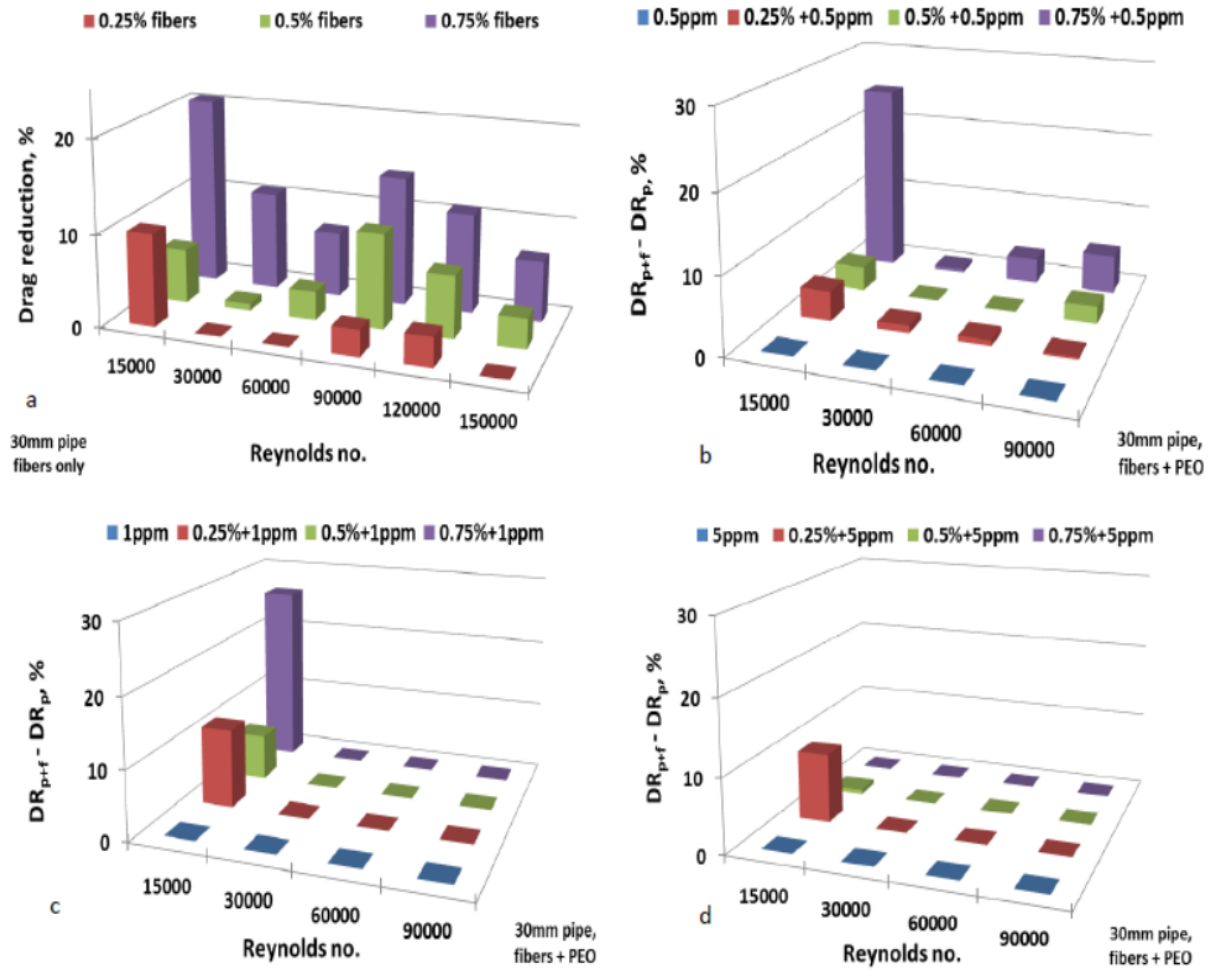
Appendix Fig. 5 Drag reduction by fibers vs Reynolds no. in 30mm pipe for different polymer concentrations.
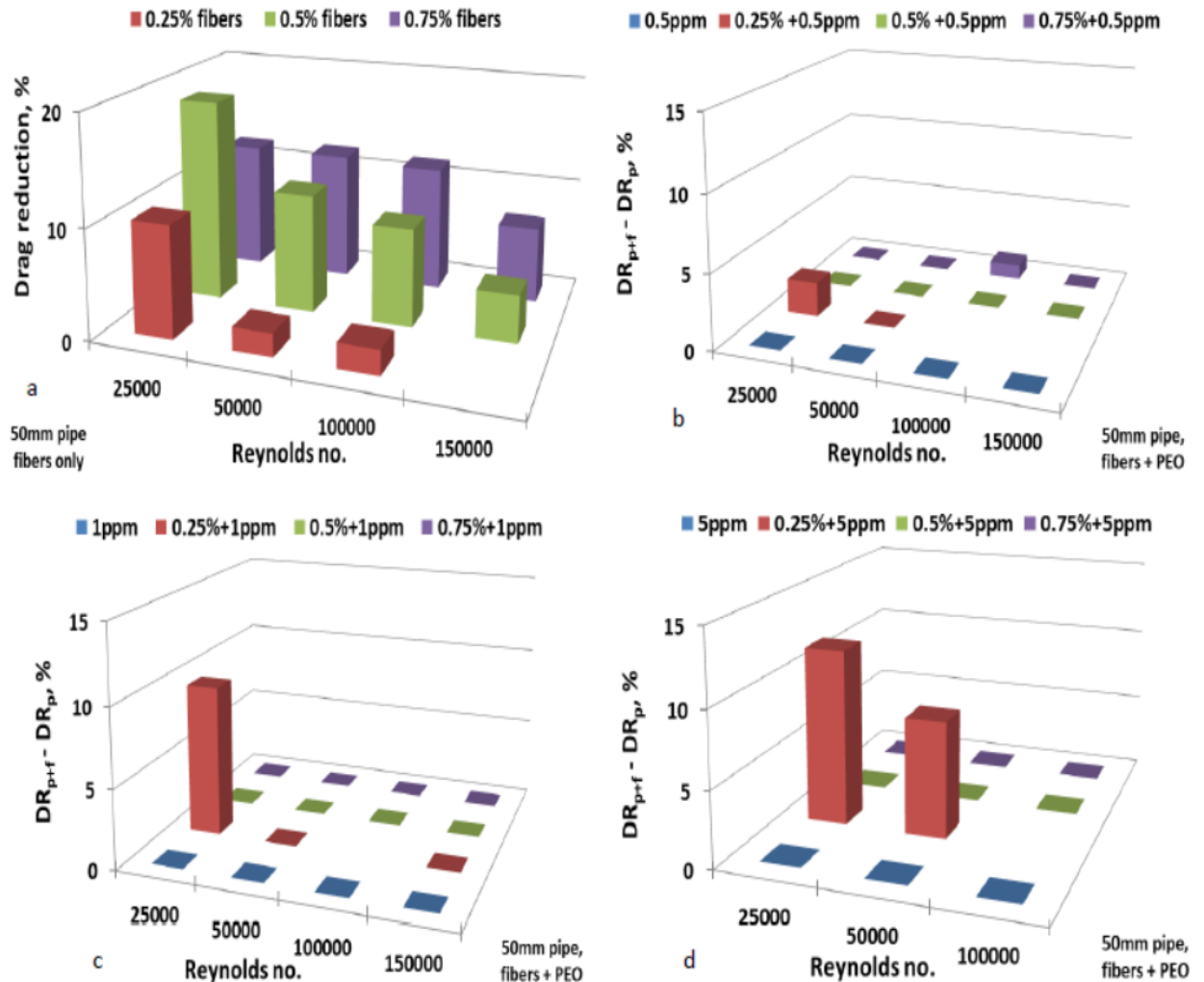
Appendix Fig. 6 Drag reduction by fibers vs Reynolds no. in 50mm pipe for different polymer concentrations.

As can be seen in Appendix Fig. 5a and Appendix Fig. 6a, that the fibers produced drag reduction but not at the same degree as polymers. Drag reduction in the 50 mm pipe is seen to reduce with increased Reynolds number for fixed fiber concentration, particularly at Re = 150000. The trend observed in the 30 mm pipe was not consistent as can be seen in Appendix Fig. 5a. The reduction in % DR with increasing in Reynolds number may be due to collisions of fibers in turbulent flows leading to energy losses (Doulah, 1981). In addition, at high Reynolds numbers, the fiber entanglements straighten out under inertia effects in the axial flow direction thereby limiting fiber-fluid interactions. Drag reduction as high as 10 % was found in some cases. This is not as high as the values reported by Kale and Metzner, (1976, 1974; Metzner, 1977) who used asbestos as well as nylon fibers but at different

concentrations (Nylon fibers; 0.08 wt%, asbestos; 0.05, 0.1 and 0.25 wt%) from those in this study.

The effects of combined fibers + polymers are shown in Appendix Fig. 5b - d and Appendix Fig. 6b – d. in these cases, 0 values mean that the addition of fibers to polymer solution did not produce additional drag reduction compared to polymer alone. It can be observed that for both pipe sizes, few cases exists where the combination of fibers and polymer resulted in an increase in drag reduction particularly for fiber concentration of 0.25 % and at Reynolds numbers of 15000 and 25000 for the 30 mm and 50 mm pipes respectively, corresponding to a velocity of 0.5 m/s. These results at the lower Reynolds number agree with the effect of fibers only shown Appendix Fig. 5a and Appendix Fig. 6a. Clearly, the combination of fibers and polymer solution increases drag reduction at low Reynolds numbers and low fiber concentrations particularly in the 50mm pipe, while higher fiber concentrations give higher drag reduction in the fibers-only systems. The drag reduction results obtained are not as high as those reported for asbestos (L/D 350) + polymer combinations (Kale and Metzner, 1974; Metzner, 1977). Metzner, (1977) studied asbestos and PEO (150 ppm) solutions as well as nylon fibers (L/D 100) and PEO solutions, and reported an increase in drag reduction. Drag reduction increased with increasing asbestos concentrations (200 wppm to 800 wppm) at fixed polymer concentration (150 ppm).

The results shown in this brief study are promising and more work needs to be done to establish the optimum conditions for the combinations of fibers with polymers in drag reduction.
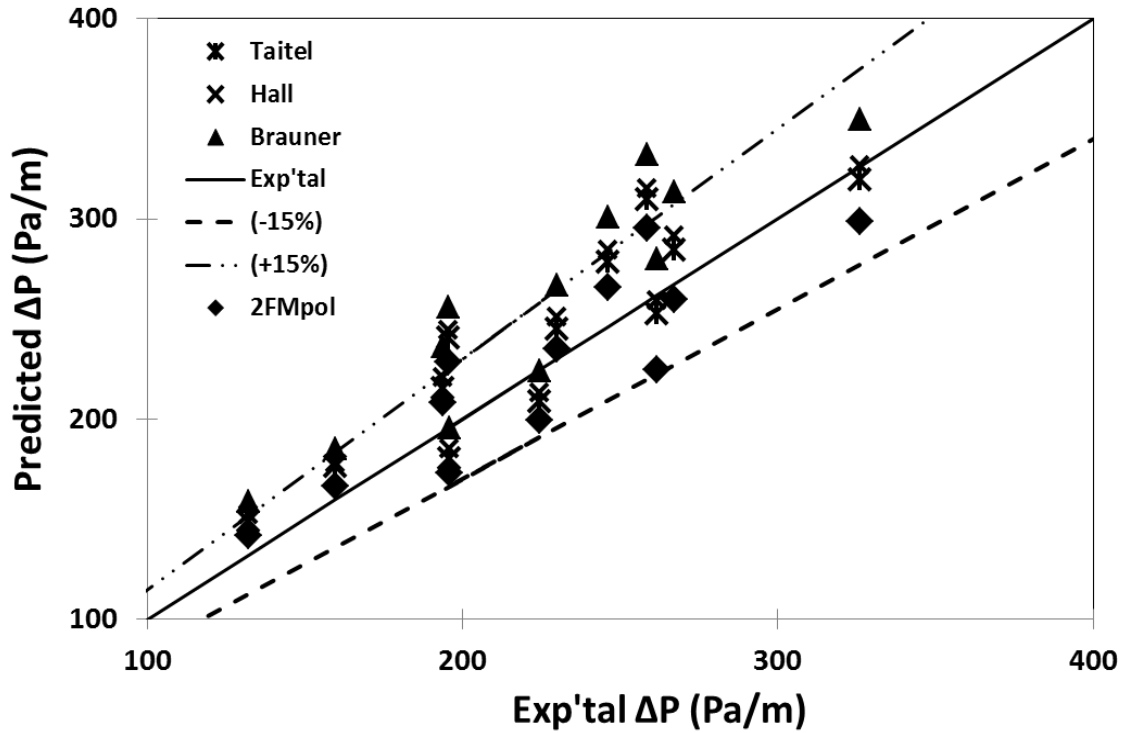
Appendix Fig. 7 Comparison of drag-reduced pressure drop prediction using modified friction factor and different interfacial shear stress correlations in the two-fluid model

Appendix 4 Matlab Codes

Appendix 4a Codes for Two-Fluid Model (as written in Matlab)

```
clear all
close all
clc

format longG


hw=(0:0.00001:0.014); %height of water
D=0.014; %pipe diameter
A=pi*D^2/4; %cross sectional area of pipe
Rho=828; % density of oil
Muo=0.0055; %viscosity of oil
Rhw=1000; %density of water
Muw=0.001; % viscosity of water


Uso=(0.11); %initial values of Uso

Usw=(0.166);   %initial values of Usw

Y=(2*hw./D)-1;
Si=D*(1-Y.^2).^0.5;  % interfacial lenght
So=D*acos(Y); % wall perimeter of oil phase
Sw=pi*D-So; % wall perimeter of water phase
Ao=D*(So-Si.*Y)./4; % area of oil phase
Aw=A-Ao; % area of water phase
Ho=Ao./A; % oil hold up
Hw=Aw./A; % water hold up

Uo=Uso./Ho; % in-situ oil velocity

Uw=Usw./Hw; % in-situ water velocity
Dw=zeros(1,length(hw)); % equivalent hydraulic diameter of water phase
Do=zeros(1,length(hw)); % equivlent hydraulic diameter of oil phase


for i=1:length(hw),
   if Uo(i)<Uw(i),
      Dw(i)=4*Aw(i)/(Sw(i)+Si(i));
      Do(i)=4*Ao(i)/So(i);
   elseif Uo(i) > Uw(i),
      Dw(i)=4*Aw(i)/Sw(i);
      Do(i)=4*Ao(i)/(So(i)+Si(i));
   elseif 0.98<=(Uo(i)/Uw(i))<=1.05;
      Dw(i)=4*Aw(i)/Sw(i);
      Do(i)=4*Ao(i)/So(i);
```

```
    end
end

NRew=Dw.*Uw.*Rhw./Muw;
NReo=Do.*Uo.*Rho./Muo;

for i=1:length(hw),
   if Uw(i)>Uo(i),
      Rhi=Rhw;
      Mui=Muw;
      Ui=Uw;
   elseif Uw(i)<Uo(i),
      Rhi=Rho;
      Mui=Muo;
      Ui=Uo;
   end
end

NRei = ((Si./pi).*(Ui.*Rhi./Mui));


for i=1:length(hw),
   if Dw(i)*Uw(i)*Rhw/Muw>2100,
      n=0.25;
      m=0.0792;
   elseif Dw(i)*Uw(i)*Rhw/Muw<2100,
      n=1.0;
      m=16.0;
    end
   Fw=(m*(NRew).^(-n));
end

for i=1:length(hw),
  if Do(i)*Uo(i)*Rho/Muo>2100,
      n=0.25;
      m=0.0792;
   elseif Do(i)*Uo(i)*Rho/Muo<2100,
      n=1.0;
      m=16.0;
   end
   Fo=(m*(NReo).^(-n));
end


 %.*(1+20*(0.0004/0.014)); % frictionn factor of oil phase
%Fi=m*(NRei).^(-n); % interfacial friction factor

for i=1:length(hw),
   if Uw(i)>Uo(i),
      Fi=Fw.*(1+20*(0.00045/0.0501)); %from Rodriguez and Baldani (2012)
```

```
   elseif Uw(i)<Uo(i),
       Fi=Fo.*(1+20*(0.00045/0.0501));
   end
end


tw=Fw.*Uw.^2.*Rhw/2; % shear stress for water phase
to=Fo.*Uo.^2.*Rho/2;  % shear stress for oil phase
ti=(Fi.*Rhi.*(Uo-Uw).*abs(Uo-Uw))./2;


   Dpo=((to.*So)+(ti.*Si))./(-Ao);
   Dpw=((tw.*Sw)-(ti.*Si))./(-Aw);
%
equal_p=zeros(1,length(hw));
for i=1:length(hw),
   equal_p(i)=Dpo(i)-Dpw(i);
   if equal_p(i)==0,
    fprintf('i= %d \n',i);
   end

end


for i=1:length(hw)-1,
   if(hw(1,i)<=0.014 && Si(1,i)>=0),
    if equal_p(i)>0 && equal_p(i+1)<0,
      fprintf('hw( %d )= %f \n',i,hw(i));
       fprintf('hw( %d )= %f \n',i+1,hw(i+1));
       x_zero=-1*equal_p(i+1)*(hw(i)-hw(i+1))/(equal_p(i)-equal_p(i+1))+hw(i+1);
       fprintf('x_zero= %f \n',x_zero);
       fprintf('Dpo bef= %f \n',Dpo(i));
       fprintf('Dpo aft= %f \n',Dpo(i+1));
       Dpo_zero=-1*equal_p(i+1)*(Dpo(i)-Dpo(i+1))/(equal_p(i)-equal_p(i+1))+Dpo(i+1);
       fprintf('Dpo_zero= %f \n',Dpo_zero);
       fprintf('Si bef= %f \n',Si(i));
       fprintf('Si aft= %f \n',Si(i+1));
       Si_zero=-1*equal_p(i+1)*(Si(i)-Si(i+1))/(equal_p(i)-equal_p(i+1))+Si(i+1);
       fprintf('Si_zero= %f \n',Si_zero);

    end
   end
end
```

Appendix 4b Codes for Two-Fluid Model with curved interface (as written in Matlab)

```
clear all
close all
clc
```

```matlab
format longG
%Parameters/constants
hw=0.00536; %(0:0.00001:0.014); %height of water
D=0.014; %pipe diameter
A=pi*D^2/4; %cross sectional area of pipe
Rho=828; % density of oil
Muo=0.0055; %viscosity of oil
Rhw=1000; %density of water
Muw=0.001; % viscosity of water

Uso=(0.245); %initial values of Uso

Usw=(0.28);   %initial values of Usw

Y=(2*hw./D)-1;
hb=1.065*hw-0.0009;
x=(hw.*D-hw.^2).^0.5;

z=hw-hb;

T=2*atan(x./z);
B=2.*pi-2.*T;
R=x./(sin(B./2));
Si=B.*R; % interfacial lenght 0.0114744; %
So=D*acos(Y); % wall perimeter of oil phase
Sw=pi*D-So; % wall perimeter of water phase
Ao=(Si.*R./2)-(sin(B).*(R.^2)./2)+(D.*So./4)-(x.*(2.*hw-D)./2); % area of oil phase
Aw=A-Ao; % area of water phase
Ho=Ao./A; % oil hold up
Hw=Aw./A; % water hold up

Uo=Uso./Ho; % in-situ oil velocity
Uw=Usw./Hw; % in-situ water velocity

Dw=zeros(1,length(hw)); % equivalent hydraulic diameter of water phase
Do=zeros(1,length(hw)); % equivlent hydraulic diameter of oil phase

for i=1:length(hw),
    if Uo(i)<Uw(i),
        Dw(i)=4*Aw(i)/(Sw(i)+Si(i));
        Do(i)=4*Ao(i)/So(i);
    elseif Uo(i) > Uw(i),
        Dw(i)=4*Aw(i)/Sw(i);
        Do(i)=4*Ao(i)/(So(i)+Si(i));
    elseif 0.98<=(Uo(i)/Uw(i))<=1.05;
        Dw(i)=4*Aw(i)/Sw(i);
        Do(i)=4*Ao(i)/So(i);
    end
end
```

```matlab
NRew=Dw.*Uw.*Rhw./Muw;
NReo=Do.*Uo.*Rho./Muo;

for i=1:length(hw),
   if Dw(i)*Uw(i)*Rhw/Muw>2100,
     n=0.25;
     m=0.0792;
   elseif Dw(i)*Uw(i)*Rhw/Muw<2100,
     n=1.0;
     m=16.0;
   end
   Fw=(m*(NRew).^(-n));
end
for i=1:length(hw),
  if Do(i)*Uo(i)*Rho/Muo>2100,
     n=0.25;
     m=0.0792;
   elseif Do(i)*Uo(i)*Rho/Muo<2100,
     n=1.0;
     m=16.0;
   end
   Fo=(m*(NReo).^(-n));
end

for i=1:length(hw),
   if Uw(i)>Uo(i),
      Fi=Fw.*(1+20*(0.00045/0.0501)); %from Rodriguez and Baldani (2012)
   elseif Uw(i)<Uo(i),
      Fi=Fo.*(1+20*(0.00045/0.0501));
   end
end
tw=Fw.*Uw.^2.*Rhw/2; % shear stress for water phase
to=Fo.*Uo.^2.*Rho/2;  % shear stress for oil phase

ti=((Aw.*to.*So)-(Ao.*tw.*Sw))./(Si.*(Ao+Aw)); % interfacial shear stress

Dpo=((to.*So)+(ti.*Si))./(-Ao);
Dpw=((tw.*Sw)-(ti.*Si))./(-Aw);

equal_p=zeros(1,length(hw));
for i=1:length(hw),
   equal_p(i)=Dpo(i)-Dpw(i);
   if equal_p(i)==0,
     fprintf('i= %d \n',i);
   end

end
%find zero
for i=1:length(hw)-1,
```

```
  if equal_p(i)>0 && equal_p(i+1)<0,
    fprintf('hw(i)= %f \n',hw(i));
    fprintf('hw(i+1)= %f \n',hw(i+1));
    x_zero=-1*equal_p(i+1)*(hw(i)-hw(i+1))/(equal_p(i)-equal_p(i+1))+hw(i+1);
    fprintf('x_zero= %f \n',x_zero);
    fprintf('Dpo bef= %f \n',Dpo(i));
    fprintf('Dpo aft= %f \n',Dpo(i+1));
    Dpo_zero=-1*equal_p(i+1)*(Dpo(i)-Dpo(i+1))/(equal_p(i)-equal_p(i+1))+Dpo(i+1);
    fprintf('Dpo_zero= %f \n',Dpo_zero);
    fprintf('Si bef= %f \n',Si(i));
    fprintf('Si aft= %f \n',Si(i+1));
    Si_zero=-1*equal_p(i+1)*(Si(i)-Si(i+1))/(equal_p(i)-equal_p(i+1))+Si(i+1);
    fprintf('Si_zero= %f \n',Si_zero);
    fprintf('hb bef= %f \n',hb(i));
    fprintf('hb aft= %f \n',hb(i+1));
    hb_zero=-1*equal_p(i+1)*(hb(i)-hb(i+1))/(equal_p(i)-equal_p(i+1))+hb(i+1);
    fprintf('hb_zero= %f \n',hb_zero);
  end

end
```

Appendix 5 Codes for PIV Profile Generation

FROM POINT VEC. TO POINT MAT FILE

```
%%%%%%%         mfile to read Insight3g vectors         %%%%%%%
%%%%%%%%%%%%%%%%%%%%%%%%%%%%%%%%%%%%%%%%%%%%%%%%%
%%%%%%%%%%%%%%%%%%%%%%%%%%%%%%%
%%%%%%%                 read / .vec                 %%%%%%%
%%%%%%%                ----> .fig + .mat            %%%%%%%
%%%%%%%                                    %%%%%%%
%%%%%%%%%%%%%%%%%%%%%%%%%%%%%%%%%%%%%%%%%%%%%%%%%%
%%%%%%%%%%%%%%%%%%%%%%%%%%%%%%

clear all

close all

%ouverture du fichier .vec----------------------------------------------

[fnom,fchemin]=uigetfile('*.vec','fichier vec'); %selectionner un champs pour donner le
chemin du répertoire contenant les .txt

        cd(fchemin);
        rep=dir(['*.vec']);
        fin=size(rep);
%----------------------------------------------------------------------
UU_cumul=[];
VV_cumul=[];
```

```
pas=1;

for k=1:pas:fin; % Boucle sur les fichiers .tif

    fichier=rep(k).name;
    Str1 = ['Treating file : ', rep(k).name];
    disp(Str1);
    fid=fopen(num2str(fichier),'r');
    F = fread(fid);
    fclose(fid);

    F=strrep(F,',','. '); %changement des virgules en points
    C = textscan(F, '%f %f %f %f %f %f %f %f %f', 'delimiter', ',','MultipleDelimsAsOne', 1,
'HeaderLines', 1);

    X=C{1};
    Y=C{2};
    U=C{3};
    V=C{4};

    %reconstruction of the 2D map----------------------------------------

    test1=abs(diff(X));
    maillage=min(test1);
    M1=max(X); m1=min(X); M2=max(Y); m2=min(Y);
    [ta,to]=find(X==M1);
    c1=ta(1);
    [dim11,dim22]=size(Y);
    c2=dim11/c1;

    x=X(1:c1);
    y=linspace(m2,M2,c2);
    [XX,YY]=meshgrid(x,y);
    [xx,yy]=meshgrid(1:c1,1:c2);

    UU=[];
    VV=[];

    for toto1=1:c1
        for toto2=1:c2
            UU(toto1,toto2)=U(toto1 + (toto2-1).*c1);
            VV(toto1,toto2)=V(toto1 + (toto2-1).*c1);
        end
    end

%    figure(1)
%    quiver(XX,YY,UU',VV',6,'r')
%    axis([m1 M1 m2 M2])

    %filtering------------------------------------------------------------
```

```
v=sqrt(UU.*UU+VV.*VV);

%filtering by median filter
Xf=x(1:length(x)-1);
Yf=y(1:length(y)-1);
us=filter2(1/5*[0 1 0; 1 1 1; 0 1 0],UU,'valid');
vs=filter2(1/5*[0 1 0; 1 1 1; 0 1 0],VV,'valid');
Us(2:length(x)-1,2:length(y)-1)=us;
Vs(2:length(x)-1,2:length(y)-1)=vs;
v1=sqrt(Us.*Us+Vs.*Vs);

%creation of temporal matrix------------------------------------------
UU_cumul(:,:,k)=UU(:,:);
VV_cumul(:,:,k)=VV(:,:);
Us_temp(:,:,k)=Us;
Vs_temp(:,:,k)=Vs;

%Visualization------------------------------------------------------
figure(2)
color=10;
surf(Xf,Yf,v1)
shading 'interp';
colormap('jet');
colorbar;
axis([min(Xf) max(Xf) min(Yf) max(Yf) 0 color])
caxis([0 color])
view(90,90)
title('Vectors velocity field');
xlabel('distance');
ylabel('distance');

end

newnamex=strcat('Vel_temp');
save(newnamex,'UU_cumul','VV_cumul','Us_temp','Vs_temp','Xf','Yf');
```

Appendix 5b FROM GENERATED POINT MAT TO FIGURES/PROFILES

```
%%%%%%%          mfile to read Insight3g vectors          %%%%%%%
%%%%%%%%%%%%%%%%%%%%%%%%%%%%%%%%%%%%%%%%%%%%%%%%%%%
%%%%%%%%%%%%%%%%%%%%%%%%%%%%%%%%%
%%%%%%%                read / .mat                %%%%%%%
%%%%%%%                ----> .fig                %%%%%%%
%%%%%%%%%%%%%%%%%%%%%%%%%%%%%%%%%%%%%%%%%%%%%%%%%%%%%
%%%%%%%%%%%%%%%%%%%%%%%%%%%%%%%%%

clear all
% close all
```

```
%load interface motion (.mat)--------------------------------------------
[fnom1,fchemin1]=uigetfile('*.mat','fichier mat');
fspec1=[fchemin1 fnom1];
load(fspec1);

%calibration factors-------------------------------------------------

Upipe=92;Lpipe=1148;Dpx=Lpipe-Upipe;
Imx=2048;Imy=2048;%size of raw image (Pixel)
Dm=0.014;%Internal diameter (m)
calib_spa=Dm/Dpx;%spatial calibration ration (m/Pixel)
Maillage_PIV=31;%correlation  box size(Pixel)
Y0=Upipe + fix(Dpx/2);
%parameters of PIV field---------------------------------------------

[dim1,dim2,dim3]=size(UU_cumul);
X_Pixel=Maillage_PIV:Maillage_PIV:Maillage_PIV*dim1;
Y_Pixel=Maillage_PIV:Maillage_PIV:Maillage_PIV*dim2;
Xs_Pixel=Maillage_PIV:Maillage_PIV:Maillage_PIV*(dim1-1);
Ys_Pixel=Maillage_PIV:Maillage_PIV:Maillage_PIV*(dim2-1);

%mean velocity computation---------------------------------------------

UUtest=mean(Us_temp,3);
VVtest=mean(Vs_temp,3);
Yc_Pixel=Y_Pixel-Y0;Ysc_Pixel=Ys_Pixel-Y0;

figure(1)
color=15;
surf(Ysc_Pixel,Xs_Pixel,Us_temp(:,:,10))
shading 'interp';
colormap('jet');
colorbar;
axis([min(Ysc_Pixel) max(Ysc_Pixel) min(Xs_Pixel) max(Xs_Pixel) 0 color])
caxis([0 color])
view(90,90)
title('Vectors velocity field');
xlabel('distance (Pixels)');
ylabel('distance (Pixels)');
[x1,y1]=ginput(2);% select graphically the upper and the lower boundaries on y axis of the
calculation area

Bi=fix(y1(1)./Maillage_PIV);
Bs=fix(y1(2)./Maillage_PIV);
New_UUtest=UUtest(Bi:Bs,:);
New_VVtest=VVtest(Bi:Bs,:);
U_bar_prof=mean(New_UUtest,1);
V_bar_prof=mean(New_VVtest,1);
```

```
[idx1,idx2]=find(Ysc_Pixel*calib_spa < (Lpipe-Y0)*calib_spa & Ysc_Pixel*calib_spa >
(Upipe-Y0)*calib_spa);
Y_test=Ysc_Pixel(idx2)*calib_spa;
U_test=U_bar_prof(idx2);

%Figures---------------------------------------------------------------

figure(2)
hold on,
plot(U_test,Y_test,'o');
title('Axial mean velocity profile');
ylabel('Distance (m)');
xlabel('Axial mean velocity (m/s)');
line(0.01*(-10:10),(Upipe-Y0)*calib_spa*ones(21))
line(0.01*(-10:10),(Lpipe-Y0)*calib_spa*ones(21))
set(gca,'YDir','reverse')

figure(3)
hold on,
plot(V_bar_prof(idx2),Y_test,'o');
title('Radial mean velocity profile');
ylabel('Distance (m)');
xlabel('Radial mean velocity (m/s)');
line(0.1*(-5:5),(Upipe-Y0)*calib_spa*ones(11))
line(0.1*(-5:5),(Lpipe-Y0)*calib_spa*ones(11))
set(gca,'YDir','reverse')

%velocity fluctuation computation----------------------------------------

for toto=1:dim3
    UUftest(:,:,toto)=Us_temp(Bi:Bs,:,toto)-New_UUtest(:,:);
    VVftest(:,:,toto)=Vs_temp(Bi:Bs,:,toto)-New_VVtest(:,:);
end

U2temp=mean((UUftest).^2,3);
U2prof=mean(U2temp,1);
V2temp=mean((VVftest).^2,3);
V2prof=mean(V2temp,1);
UVtemp=mean(VVftest.*UUftest,3);
UVprof=mean(UVtemp,1);

%Figures---------------------------------------------------------------

figure(4)
hold on
plot(U2prof(idx2),Y_test,'o');
title('Mean u^2 Reynolds stress component');
ylabel('Distance (m)');
xlabel('mean u^2 (m^2.s^(-2))');
line(0.01*(-5:5),(Upipe-Y0)*calib_spa*ones(11))
```

```
line(0.01*(-5:5),(Lpipe-Y0)*calib_spa*ones(11))
set(gca,'YDir','reverse')

figure(5)
hold on
plot(V2prof(idx2),Y_test,'o');
title('Mean v^2  Reynolds stress component');
ylabel('Distance (m)');
xlabel('mean v^2 (m^2.s^(-2)');
line(0.01*(-5:5),(Upipe-Y0)*calib_spa*ones(11))
line(0.01*(-5:5),(Lpipe-Y0)*calib_spa*ones(11))
set(gca,'YDir','reverse')

figure(6)
hold on
plot(UVprof(idx2),Y_test,'o');
title('Mean u.v Reynolds stress component');
ylabel('Distance (m)');
xlabel('mean u.v (m^2.s^(-2)');
line(0.01*(-5:5),(Upipe-Y0)*calib_spa*ones(11))
line(0.01*(-5:5),(Lpipe-Y0)*calib_spa*ones(11))
set(gca,'YDir','reverse')

%Viscous sublayer detection%-------------------------------------------

%        %%-------------linear fit of friction velocity--------------------
%        length_fit=2;
%        xxfit=Y_test(length(Y_test)-length_fit:length(Y_test));
%        yyfit=U_test(length(Y_test)-length_fit:length(Y_test));
%        [curve, goodness, output] = fit(xxfit',yyfit','Poly1');
%        outpout_curve=fit(yyfit',xxfit','Poly1');
%        U_wall=curve((Lpipe-Y0)*calib_spa);

    %%-------------friction velocity by Blasius law--------------------

    mu=10^(-6);%cinematic viscosity
    rho=1000;%density
    Tho_wall=0.03955*rho*mean(U_test)^(7/4)*mu^(1/4)*(Dm)^(-1/4);
    U_wall=sqrt(Tho_wall/rho);

[idx3,idx4]=find(Y_test<0);%detecte la patie superieure du profil

Ydim11=Y_test(idx4)-(Upipe-Y0)*calib_spa;
Udim11=U_test(idx4);
Ydim1=(U_wall/mu).*Ydim11;
Udim1=Udim11./U_wall;

[idx5,idx6]=find(Y_test>0);%detecte la patie inferieure du profil

Ydim22=Y_test(idx6)+(Upipe-Y0)*calib_spa;
```

```
Udim22=U_test(idx6);

for toto=1:length(Ydim22)
    Ydim2(toto)=-(U_wall/mu).*Ydim22(-toto+1+length(Ydim22));
    Udim2(toto)=Udim22(-toto+1+length(Ydim22))./U_wall;
end

%Figures----------------------------------------------------------------

Xf=0.1:0.1:1000;
Yf=2.5*log(Xf)+5.5;%log law for Newtonian flow
Zf=11.7*log(Xf)-17.0;  %MDRA

figure(7)
hold on
semilogx(Ydim1,Udim1,'o');
hold on , semilogx(Xf,Yf) %plot of Newtonian law of the wall
hold on , semilogx(Xf,Xf) %Plot of viscous sublayer
hold on , semilogx(Xf,Zf) %Plot of maximum drag reduction asymptote

title('Normalized Axial mean velocity for the upper profile part');
ylabel('U+');
xlabel('y+');

figure(8)
hold on
semilogx(Ydim2,Udim2,'o');
hold on , semilogx(Xf,Yf) %plot of Newtonian law of the wall
hold on , semilogx(Xf,Xf) %Plot of viscous sublayer
hold on , semilogx(Xf,Zf) %Plot of maximum drag reduction asymptote

title('Normalized Axial mean velocity for the lower profile part');
ylabel('U+');
xlabel('y+');

Ydim2=Ydim2.';
Udim2=Udim2.';
Yf=Yf.';
Xf=Xf.';
Zf=Zf.';

atvisz=[Xf Yf];
% Col={'y1','y2'};
filename = 'C:\Users\Lawrence\Documents\converted.xls';
xlRange = 'A2';
xlswrite(filename,atvisz,'sheet4');

atvisz1=[Xf Zf];
% Col={'y1','y2'};
filename = 'C:\Users\Lawrence\Documents\converted.xls';
```

```matlab
xlRange = 'A2';
xlswrite(filename,atvisz1,'sheet5');

atvisz2=[Ydim2 Udim2];
% Col={'y1','y2'};
filename = 'C:\Users\Lawrence\Documents\converted.xls';
xlRange = 'A2';
xlswrite(filename,atvisz2,'sheet6');
```